CANADIAN THESES

THÈSES CANADIENNES

NOTICE

The quality of this microfiche is heavily dependent upon the quality of the original thesis submitted for microfilming. Every effort has been made to ensure the highest quality of reproduction possible.

If pages are missing, contact the university which granted the degree.

Some pages may have indistinct print especially if the original pages were typed with a poor typewriter ribbon or if the university sent us an inferior photocopy.

Previously copyrighted materials (journal articles, published tests, etc.) are not filmed.

Reproduction in full or in part of this film is governed by the Canadian Copyright Act, R.S.C. 1970, c. C-30.

AVIS

La qualité de cette microfiche dépend grandement de la qualité de la thèse soumise au microfilmage. Nous avons tout fait pour assurer une qualité supérieure de reproduction.

S'il manque des pages, veuillez communiquer avec l'université qui a conféré le grade.

La qualité d'impression de certaines pages peut laisser à désirer, surtout si les pages originales ont été dactylographiées à l'aide d'un ruban usé ou si l'université nous a fait parvenir une photocopie de qualité inférieure.

Les documents qui font déjà l'objet d'un droit d'auteur (articles de revue, examens publiés, etc.) ne sont pas microfilmés.

La reproduction, même partielle, de ce microfilm est soumise à la Loi canadienne sur le droit d'auteur, SRC 1970, c. C-30.

THIS DISSERTATION
HAS BEEN MICROFILMED
EXACTLY AS RECEIVED

LA THÈSE A ÉTÉ
MICROFILMÉE TELLE QUE
NOUS L'AVONS REÇUE

ISBN 0-315-30976-8

To my parents

Table of Contents

Acknowledgments

I wish to express my sincere appreciation to my supervisor Dr. H. Teitelbaum for his encouragement during the course of this study and particularly for giving direction to many key aspects of the study.

I would like to give special thanks to all the members and staff of the department of chemistry for their help and their advice, and to the computer centre for its generous grant of computer time.

I would especially like to thank Dr. George Burns for supplying us with the shock tube, Elizabeth Sullivan for help in computer programming, Eva Szabo for her careful drawing of my graphs, Diana Hall for her patience and accurate typing and to my colleague, Chris Carruthers for his computer help and proofreading.

My sincere thanks to my parents for their moral support and encouragement throughout my study and to my friends in Ottawa for their understanding and their good company.

And finally, all praise to God!

Key to symbols

a = Sound velocity

a = Laser beam radius

$\overline{A^2}$ = Vibrational amplitude coefficient

b = Amplitude of a sound wave

b = Constant associated with the repulsive part of the interaction potential

C, C_V, $C_{V\infty}$ = Heat capacities

d = Range of intermolecular potential

D = Distance from the center of the shock tube to the photodiode

E = Vibrational energy

ΔE = Energy gap

g = Degeneracy

g_{ii} = Spectroscopic constant

g = Reduced second order rate constant

G = Gain of the amplifier

h = Enthalpy

h = Planck's constant

I = Reaction cross section

I = Moment of inertia

J = Rotational quantum number

k = Boltzmann constant

k_{ij}, k_{lk}^{ji} = Rate constant

l = Internal dimension of the test section

l = Length of a 1-D box

L = Cell dimension

m = Mass of a particle or an atom

M = Foreign gas

n = Reduced specific heat

n = Translational quantum number

N = Total number of molecules

N_i = Population of molecules having vibrational quantum number

P = Transition probability

p = Light power of the laser

P = Pressure

P_s = Steric factor

Q_{10} = Dipole matrix element

Q_{01} = Quadrupole matrix element

r = Internuclear distance

r_c = Intermolecular separation at the classical turning point

r_i = Load resistor

R = Gas constant

s_i = Sensitivity of the photodiode

Δ = Deflection of the laser beam at the photodiode

S = Slope of LnV vs t_1

t = Time

T = Temperature

u = Relative velocity

U = Shock wave velocity

$\mathcal{U}$ = Interaction potential

v = Vibrational quantum number

v = Volume

ϑ = Reduced perturbation factor

V^{i-j} = Matrix coupling element for vibrational state i and j

V = Voltage

W = Molecular weight

x_{ij} = Spectroscopic constant

X = Mole fraction

y = Coordinate of the laser beam in the shock tube

Z = Collision frequency (Sec^{-1})

Z_{10} = Number of collisions per transition

α = The reciprocal of the range of intermolecular forces (1/d)

β = Specific refractivity

γ = Relative efficiency of V-V to V-T

δ = Degree of excitation

ϵ = Attractive potential

ζ = Reduced critical kinetic energy of collision

η = Refractive index

θ = Deflection angle

λ = Energy gap constant

μ = Reduced mass

ν = Oscillation frequency

ξ = Coordinate of the laser beam at the photodiode

ρ = Density

r = Intermolecular separation at zero energy

σ = Collision diameter

τ_c = Duration of collision

τ^* = Relaxation time in laboratory coordinates

τ' = Experimentally observed relaxation time

τ = Theoretically expected relaxation time

ϕ = Relative efficiency of M to relaxer AB

φ = Phase shift

χ_e = Anharmonicity constant

ω = Angular sound frequency

List of Tables

List of Figures

Abstract

Vibrational relaxation times of pure N_2O, C_2H_2 and mixtures of C_2H_2 in Ar have been measured behind incident shock waves in order to test the validity of the Bethe-Teller law. It is shown that the phenomenological relaxation time, τ', is not a time independent constant and therefore the Bethe-Teller law can not be applied to polyatomic molecules.

While the vibrational relaxation time of C_2H_2 increases continuously with time and does not exhibit any sign of equlibrium or near equilibrium under our experimental conditions (T=613-1184 K and Zt=50-274), the vibrational relaxation time of N_2O increases with time below 1300 K and decreases with time above 1200 K under our experimental conditions (T=450-1893 K and Zt=49-3703) where Z is the collision frequency and t the laboratory time. The many disparate results of N_2O in the literature are reconciled in terms of a mechanism whereby the step $(0,0,0) \longrightarrow (0,1,0)$ is rate determining at low temperatures when the ν_3 mode is not involved, and the parallel step $(1,0,0)+(0,0,0) \longrightarrow (0,2,0)+(0,1,0)$ takes over at high temperatures close to equilibrium.

From measurements in C_2H_2-Ar mixtures, the linear mixture rule, $k=X_1k_1 + X_2k_2$ where $k_i=1/P\tau_i$, is found to fail, with deviations being most severe at high temperatures and far from equilibrium.

The relaxation process was simulated by solving the master equation numerically. All energy levels up to 4067 cm^{-1} for N_2O and 4670 cm^{-1} for C_2H_2 have been included. All possible V-T and

inter-and intramolecular V-V processes were also included, subject to the restriction that the energy gap, $|\Delta E| \leq 700\ cm^{-1}$. Microscopic rate coefficients, scaled according to $\exp(-\lambda|\Delta E|)$, were assigned, reducing the problem to one of three parameters; λ (for V-T processes), λ_{VV} (for V-V processes), and k_{10}^{01}/k_{01} where k_{10}^{01} is the constant for the V-V process:

$$(0,1,0) + (0,0,0) \longrightarrow (0,0,0) + (0,1,0)$$

and k_{10} is the rate constant for the V-T process :

$$(0,1,0) + (0,0,0) \longrightarrow (0,0,0) + (0,0,0)$$

Detailed comparisons between the result of shock-induced and laser-induced relaxations are made. They are interpreted in terms of the three parameters, i.e. in terms of the importance of intra-and intermolecular intermode exchange processes and V-T processes. It was found that intermolecular V-V processes are responsible for the time-dependence of τ, and that the increasing density of states accessible at longer times at higher temperatures is responsible for a change in mechanism. Good qualitative agreement with the experimental results is reached for the temperature dependence, the time dependence of the vibrational relaxation time and for failure of the mixture rule. However, because of the arbitrary choice of relaxation parameters, it was difficult to reach a quantitative agreement with the experimental results.

CHAPTER 1: INTRODUCTION

1.1 Theory of molecular energy transfer

The internal energy of a molecule can be divided into rotational, vibrational and electronic energy. In addition, real molecules are constantly in motion, and an additional translational energy is ascribed to the molecules. A set of quantum numbers is associated with these different types of energy. Since quanta associated with translational and rotational energy are small, these degrees of freedom can often be treated classically; on the other hand, quanta associated with vibrational and electronic energy are large enough so that a quantum mechanical treatment is required for them.

1.1.1 Conditions for energy transfer

In accordance with the uncertainty principle, during a collision, energy levels of the molecule are broadened by an amount $\bar{h}/\tau_c$, where $\bar{h}=h/2\pi$ and τ_c is the duration of the collision. If the energy broadening is smaller than the energy level separation between two adjacent levels $h\nu$, where ν is the frequency of oscillation, the collision will be inefficient in that it does not lead to a change of vibrational energy and it is called an adiabatic collision. An adiabatic collision is a collision whose duration is long compared to the period of vibration ($\tau_c > \frac{2\pi}{\nu}$) (1).

If we replace τ_c by $d/\bar{u}$ where d is the range of the repulsive part of the intermolecular potential and $\bar{u}$ is the relative velocity of approach, the condition for efficient collision becomes:

$$\frac{d}{\bar{u}} < \frac{\bar{n}}{h\nu} \qquad (1.1)$$

By replacing $\bar{u}$ with its value $\sqrt{8kT/\pi\mu}$, the condition for efficient collision becomes:

$$\nu < \frac{1}{2\pi d}\sqrt{\frac{8kT}{\pi\mu}} \qquad (1.2)$$

where μ is the reduced mass of the colliding species, T is the temperature and k is the Boltzmann constant. One can see that the conditions for efficient collisions are:

1 - small mass of collision partner

2 - high temperature

3 - steeper intermolecular potential - small d

4 - low frequency of oscillation

1.1.2 Types of molecular energy transfer

Energy transfer from translational to translational (T-T), translational to rotational (T-R) and translational to vibrational degrees of freedom (T-V) are common; moreover processes involving an intermolecular energy transfer between these different kinds of energy, e.g. (V-R), (V-V) are also possible but less well understood. It is of interest to consider at least qualitatively the efficiency of these different kinds of energy transfer.

Translational to translational energy transfer (T-T) is the most efficient because energy level spacing is extremely small and is given by:

$$\Delta E = nh^2/(4m\ell^2) \qquad (1.3)$$

for a particle in a box of length ℓ, where n is the principal

quantum number and m is the mass of the particle.

Translational to rotational energy transfer (T-R) is also efficient. Rotational energy levels for a rigid diatomic molecule are given by:

$$E_J = J(J+1)\frac{\hbar^2}{2I} \qquad (1.4)$$

and

$$\Delta E = E_J - E_{J-1} = \frac{-J\hbar^2}{I} \qquad (1.5)$$

where I is the moment of inertia ($I=\mu r^2$ and where r is the internuclear distance) and J is the rotational quantum number. Since rotational energy level separation is generally small, of the order of 150 cm^{-1} or less, T-R is an efficient process for all molecules except for H_2, D_2 and HD, which do not fulfill the condition for efficient collision (eq. 1.2) because of the small value of their moment of inertia. In view of the linear relation between the rotational quantum number J and rotational energy level separation (eq.1.5) the efficiency of R-T energy transfer decreases with increasing J.

Translational to vibrational energy transfer (T-V) is a relatively inefficient process since vibrational energy level spacings, ΔE_V, are large compared to rotational and translational spacings; for a Morse oscillator, they are approximated by:

$$\Delta E_V = h\nu(1-2\chi_e v) \qquad (1-6)$$

where v is the vibrational quantum number and χ_e is the anharmonicity constant. Since vibrational level spacing

decreases markedly with increasing vibrational quantum number v, T-V energy transfer becomes more efficient at high vibrational quantum number.

Translational to electronic energy transfer (T-E) is the most improbable of all the kinds of energy transfer discussed above. Since the first excited electronic state is typically some 14000 cm^{-1} above the ground state, the condition for efficient collision is not fulfilled for this case.

Up to now, only translational to translational, rotational, vibrational and electronic energy transfer were considered. It has been shown that certain energy transfer processes such as T-E and T-V, could be very inefficient. However, intermolecular energy transfer processes such as E-V, V-V and R-V, could be efficient if the rotational or vibrational motion of one partner is faster than the relative translational motion and/or if the energy level separation between the two degrees of freedom of interest is small. Molecules containing hydrogen are known to have high vibrational and rotational frequencies; consequently these molecules can transfer vibrational or rotational energy to relaxing molecules (by R-V or V-V processes respectively) without the need for strong collisions which would otherwise be necessary.

Vibrational to vibrational intermolecular energy transfer (V-V) depends mainly on the difference between the initial and final vibrational energies of the colliding molecules. According to the adiabatic principle, the smaller this difference is, the more likely it is for the V-V process to occur, and in the limit

where collision occurs between two identical harmonic oscillator molecules, this difference is zero and V-V should have in this case a maximum efficiency.

Electronic to vibrational intermolecular energy transfer (E-V) may populate high vibrational levels. e.g. electronically excited iodine may be excited up to $v = 2$ upon collision with HCl and up to $v = 3$ and 4 upon collision with HBr and NO respectively (3). Since E-V energy transfer populates high vibrational levels, E-V is usually followed by subsequent intermolecular or intramolecular V-V or V-T processes.

1.1.3 Bethe-Teller law

Bethe and Teller (4) derived a law for the rate of change of vibrational energy of a diatomic molecule. They used a harmonic oscillator as their model and assumed that the only transitions possible are those corresponding to a change in vibrational quantum number of unity ($\Delta v = \pm 1$), in other words, only transitions between neighbouring energy levels are allowed. They also used a scaling law relating every transition rate constant $k_{v,v+1}$ between two adjacent levels v & $v+1$, to the quantum number of the upper level.

$$k_{v,v+1} \propto (v+1) \qquad (1.7)$$

After considerable algebra in simpliying the differential rate equations, Bethe and Teller arrived at an expression for the variation of vibrational energy with time:

$$\frac{dE}{dt} = -\frac{1}{\tau}(E - E_\infty) \qquad (1.8)$$

where E is the vibrational energy at time t, E_∞ is the

vibrational energy at the equilibrium temperature T. τ is the vibrational relaxation time. It is the reciprocal of the vibrational relaxation rate constant difference $(k_{10} - k_{01})$, where k_{10} is the rate constant for the transition from the first vibrational level to the ground level and k_{01} is the rate constant for the reverse process. According to microscopic reversibility, k_{01} is related to k_{10} by:

$$k_{01} = k_{10}(g_1/g_0)\exp(-h\nu/kT)$$

where g is the degeneracy, the vibrational relaxation rate constant can be written as:

$$k_{10} - k_{01} = k_{10}[1-(g_1/g_0)\exp(-h\nu/kT)] \qquad (1.9)$$

Since k_{10} is the product of the collision frequency Z and the transition probability P_{10}: $k_{10} = Z P_{10}$, the final expression for the vibrational relaxation rate constant is:

$$1/\tau = Z P_{10}[1-g_1/g_0\exp(-h\nu/kT)] \qquad (1.10)$$

1.1.4 Temperature dependence of interstate rate constants (T-V Processes)

Landau and Teller (5) developed an expression relating the transition probability to the temperature. They used an exponential interaction potential in their model. Since the collision efficiency depends on the duration of a collision as well as on the period of vibration, Landau and Teller concluded that the transition probability depends on and increases with the ratio of these two factors, and it is an exponential function of this ratio. According to their treatment, only short range forces are effective in producing excitation so that only the repulsive part of the interaction potential is important. The

long range attractive part of the interaction potential can be neglected. After assuming a Maxwell-Boltzmann distribution of relative velocities and averaging over all possible velocities, the transition probability is given by:

$$P_{10} \propto T^{-1/6} \exp(-b/T^{-1/3} + h\nu/2kT) \qquad (1.11)$$

where b is characteristic constant associated with the repulsive part of the interaction potential. The factor $\exp(-bT^{-1/3})$ is the dominant one. Since the collision frequency for a single molecule is directly proportional to the pressure P for a binary collision, most of the experimental results on vibrational relaxation are represented by a plot of log $P\tau$ vs $T^{-1/3}$.

1.1.5 Theoretical studies of vibrational energy transfer

In this section, a summary of the theoretical studies on vibrational energy transfer of a diatomic molecule will be given. Briefly, three theoretical approaches have been used to study vibrational energy transfer: classical, semi-classical and quantum mechanical approaches.

In the classical treatment the trajectory of the colliding atoms and the diatomic molecules are treated classically. The assumption made in this treatment is that only head-on collisions between an atom A and atom B of a harmonic diatomic oscillator BC occur. A one dimensional collinear coordinate system is used. Consequently rotations are not considered (2,5,6,7,8,9,10,11,12). If an exponential interaction potential, is used $U = U_0 \exp(-\alpha r) - \epsilon$, (where α is the reciprocal of the range of the intermolecular forces (1/d) and ϵ is the attractive potential); then the amount of energy transfered during the collision is (8,9,12):

$$\langle \Delta E \rangle = \frac{8\pi^4 \mu^2 \nu^2 G^2}{\mu' \alpha^2} \operatorname{csch}^2 \left(\frac{2\pi^2 \nu}{\alpha u} \right) \quad (1.12)$$

where m_A, m_B and m_C are respectively the mass of A, B and C, μ' is the reduced mass of the diatomic molecule BC, μ is the reduced mass of the system A and BC, $G = m_C/(m_B+m_C)$, u is the relative velocity of A and BC, ν is the frequency of oscillation of the diatomic molecule BC and csch is the hyperbolic cosecant.

In the semi-classical calculation the vibration of the diatomic molecule is treated quantum mechanically with discrete energy levels and the motion of the incident atom is treated classically. Then the probability of transition from a vibrational state i to vibrational state i+1, $P_{i,i+1}$, is calculated (1,2,13,14,15). It is given by:

$$P_{i,i+1} = \frac{8\pi^4 \mu^2 \nu G^2}{h \mu' \alpha^2} \operatorname{csch}^2 \left(\frac{2\pi^2 \nu}{\alpha u} \right)^{(i+1)} \quad (1.13)$$

If the energy transfer by collision in the semi-classical treatment is equal to $\langle \Delta E \rangle = P_{0,1}\, h\nu$, both semi-classical and classical treatment are seen to be identical.

In the pure quantum mechanical treatment, a beam of particles represented by a plane wave is scattered by a stationary harmonic oscillator. The details of calculations are given by Mott and Jackson (16), and the final result for $P_{i,j}$ is:

$$P_{i,j} = |V^{i-j}|^2 \pi^4/4 \, (q_i^2 - q_j^2)^2 \, \frac{\sinh(\pi q_i) \sinh(\pi q_j)}{(\cosh(\pi q_i) - \cosh(\pi q_j))^2} \quad (1.14)$$

where $q_i = 4\pi^2 \mu u_i/\alpha$, $q_j = 4\pi^2 \mu u_j/\alpha$, u_i is the relative velocity

of approach before the collision and u_j is the relative velocity of recession after the collision, sinh is the hyperbolic sine function, cosh is the hyperbolic cosine function and $V_{ij}=\int \psi_i^* U \psi_j dr$ is the overlap factor. $|V^{i-j}|^2$ represent the coupling between state i and state j. It is equal to the square of the matrix element for the transition between the two vibrational states:

$$[V^{i-i}]^2 = 1$$
$$[V^{(i+1)-i}]^2 = [V^{i-(i+1)}]^2 = \alpha^2(\overline{A^2})(i+1)/2\,H$$
$$[V^{(i+2)-i}]^2 = [V^{i-(i+2)}]^2 = \alpha^4(\overline{A^4})(i+1)(i+2)/16\,H^2$$

where $H=4\pi^2\nu/h$ and $(\overline{A^2})$ is the vibrational amplitude coefficient which is the "Cartesian displacement of an atom for unit change of the normal coordinate of a given vibration" (17).

All three approaches agree in the limit of validity of the approximation that the de Broglie wave length is smaller than the range of interaction. If the symmetrized velocity (i.e. the average of approach and recession velocities) is used and if the velocity sufficiently exceeds the threshold velocity necessary for the transition to occur, then the three approaches give similar results.

1.1.6 Polyatomic molecules

For polyatomic molecules several vibrational modes are available, and they might relax separately with different relaxation times. However, the majority of polyatomic molecules exhibit a single relaxation time (6,17). This is thought to be due to rapid V-V energy transfer which maintains a continuous

equilibrium between the upper vibrational levels, followed by V-T relaxation involving transition from the first excited state to the ground state. In fact, for the majority of polyatomic molecules energy gaps between some upper vibrational levels are much smaller then energy gaps for the lowest vibrational levels leading to rapid V-V processes among higher levels followed by a slower V-T energy transfer; nevertheless, a few molecules such as SO_2 have large energy gaps between upper vibrational levels which are comparable to the lowest vibrational levels (18). Such molecules exhibit more than one vibrational relaxation time, and relax via 2 parallel mechanisms with 2 rate constants of the same order of magnitude.

An equation for the probability $\mathcal{P}^{i-j(a)}_{k-l(b)}$ that a transition from vibrational state i to vibrational state j of a vibrational mode (a) of one molecule will occur simultaneously with a transition from vibrational state k to vibrational state l of a vibrational mode (b) of another molecule has been developed by Schwartz, Slawsky and Herzfeld, (SSH theory) (19,29) and improved by Tanczos (21) (SSH-Tanczos theory).

Since polyatomic molecules are not spherically symmetric, and since the collision might not occur in the most favorable orientation, steric factors $P_o(a)$ and $P_o(b)$ are introduced. The transition probability is then:

$$\mathcal{P}^{i-j(a)}_{k-l(b)} = P_o(a)\,P_o(b)\,[V^{ij}(a)]^2\,[V^{kl}(b)]^2 \times \times (4\mu/kT)\exp[-\epsilon/kT]\left(\frac{8\pi^3\mu\Delta E}{h^2}\right)^2 \int_0^\infty f(\bar{u}_i)\,d\bar{u}_i$$

where

$$f(\bar{u}) = \frac{\bar{u}_i^3}{\alpha^4}\cdot\left(\frac{r_c}{\sigma}\right)^2 \exp\left[-\frac{\mu\bar{u}_i^2}{2kT}\right]\left\{\frac{\exp[L-L']}{(1-\exp[L-L'])^2}\right\}, \qquad (1.15)$$

$$L = \frac{4\pi^2\mu}{\alpha h}\cdot\bar{u}_i \text{ and } L' = \frac{4\pi^2\mu}{\alpha h}\cdot\bar{u}_j$$

where μ is the reduced mass of the colliding pair. α, ϵ, u_i and u_j have already been identified, r_c is the intermolecular separation at the classical turning point and ∇ is the separation at zero energy. ΔE is the amount of energy exchanged during the collision.

$$\Delta E = h\nu_a(i-j) + h\nu_b(k-l) = (\bar{u}_i^2 - \bar{u}_j^2)\mu/2 \qquad (1.16)$$

This equation is applied to energy transfer for $\Delta E \leq 50$ cm^{-1}.

For large ΔE Tanczos (21) derived a simpler expression for the transition probability. He found:

$$P_{k\to l(b)}^{i\to j(a)} = P_0(a)P_0(b)\left(\frac{r_c^*}{\sigma}\right)^2 [V''(a)]^2 [V''(b)]^2 8\left(\frac{\pi}{3}\right)^{\frac{1}{2}} \times$$
$$\times \left[\frac{8\pi^3\mu\Delta E}{\alpha^{*2}h^2}\right]^2 \zeta^{\frac{1}{2}} \exp\left[-3\zeta + \frac{\Delta E}{2kT} + \frac{\epsilon}{kT}\right] \qquad (1.17)$$

where

$$\zeta = \frac{\mu u^{*2}}{2kT} = \left(\frac{\Delta E^2 \mu\pi^2}{2\alpha^{*2}h^2 kT}\right)^{\frac{1}{3}}.$$

and α^* and r^* are the values of α and r at the velocity giving the highest contribution to the thermal transition probability. This equation is an extension of the SSH equation. It is known as the SSH-Tanczos equation and it is applicable for $\Delta E \geq 200$ cm^{-1}. The steric factors introduced to account for the collision orientation are usually taken as 1/3 for diatomic and linear polyatomic molecules, and 2/3 for non-linear polyatomics and for the bending mode of linear molecules.

In the SSH-Tanczos equation, (eq. 1.17), the exponential factor controls the temperature dependence of $P_{k-l\ (b)}^{i-j\ (a)}$ since the pre-exponential factor of this equation depends relatively weakly on the temperature. Among the three terms of the exponential

factor, the term 3ζ is the dominant one. It predicts a linear relation between $\log \mathcal{P}^{i-j}_{k-l}\binom{(a)}{(b)}$ and $T^{-1/3}$ as in the Landau-Teller expression (1.11). Nevertheless, if the attractive potential, ϵ, is relatively large (which can easily happen when ΔE is near zero), the third term of the exponential will dominate the temperature dependence of $\mathcal{P}^{i-j}_{k-l}\binom{(a)}{(b)}$. In that case, $\log \mathcal{P}^{i-j}_{k-l}\binom{(a)}{(b)}$ will be a linear function of T^{-1}, consequently, SSH-Tanczos theory predicts the curvature actually observed in Landau-Teller plots ($\log P\tau$ vs $T^{-1/3}$) of strongly polar molecules, as well as the curvature at low temperature for all other molecules. (Some examples which show this behavior will be presented in the next section).

1.1.7 **Temperature dependence of V-V processes**

In the Landau-Teller theory and in the SSH theory discussed earlier, the vibrational transitions are supposed to occur via short range repulsive forces. Both theories are very successful in predicting the temperature dependence of the vibrational relaxation rates of a wide variety of molecules. In both theories, the reaction cross section, I, (which is related to the transition probability by: $I = \mathcal{P}(\pi\lambda^2)$ where $(\pi\lambda^2)$ is the gas kinetic collision cross section) increases with temperature. However, these theories are unable to explain the behaviour of several energy transfer processes such as near-resonant V-V energy transfer process, where the reaction cross section has a strong negative temperature dependence. For example, laser induced fluorescence experiments (22) and shock wave techniques (23) indicate that the cross section of the near resonant V-V

energy transfer process

$$CO_2\ (001) + N_2\ (0) \longrightarrow CO_2\ (000) + N_2\ (1) \qquad \Delta E$$

has a negative temperature dependence below 1000 K. Sharma and Brau (24,25) have explained this behaviour in terms of weak long range forces which couple the N_2 quadrupole moment with the CO_2 dipole moment.

Under conditions where ΔE and the dipole quadrupole spherical potential are both small compared to the kinetic energy at infinite separation, and the de Broglie wave length is small compared to the collision diameter, Sharma and Brau calculated the reaction cross section for V-V energy transfer semi-classically:

$$I(T) = 8\pi\left(\frac{kT}{\mu}\right)^2 \int u\, I(u) \exp\left(-\frac{\mu u^2}{2kT}\right) d\vec{u}$$
$$= 3\pi^3 \mu |Q'_{10} Q_{01}|^2 / 64\hbar^2 \sigma^4 kT \qquad (1.18)$$

where μ is the reduced mass of the CO_2 and N_2 molecules, $Q'_{10} = \langle 000 | Q' | 001 \rangle$ is the dipole matrix element between (000) and (001) states of CO_2 ($Q'_{ij} = \int \psi_i Q' \psi_j dr$), $Q_{01} = \langle 1 | Q | 0 \rangle$ is the quadrupole matrix element between the states i=1 and j=0 of N_2O ($Q_{ij} = \int \psi_i Q \psi_j dr$) and σ is the collision diameter.

The above expressions clearly indicate a negative temperature dependence of the collision cross section of near resonant V-V processes.

1.1.8 Lambert-Salter plot

The relationship between the number of collision per transition, Z_{10}, at room temperature and the frequency of the lowest vibrational mode ν_{min} for polyatomic molecules has been

examined by Lambert and Salter (26,27). A plot of $\log Z_{10}$ vs ν_{min} shows that molecules fall in two distinct classes. (fig 1.1): Non-hydrogen-containing molecules and hydrogen-containing molecules. In both cases the plot is linear and $P_{10} = 1/Z_{10} = N \exp(-\lambda \Delta E_{min})$, where N is a constant and $\Delta E_{min} = h\nu_{min}$. The values of λ are:

$\lambda = 8.3 \times 10^{-3}$ cm for the hydrogen-containing molecules

$\lambda = 17 \times 10^{-3}$ cm for the non-hydrogen-containing molecules.

Some molecules show lower values of Z_{10} than expected by the Lambert-Salter plot, such as SO_2 and NH_3. These two molecules are strongly polar so that the dipole-dipole attraction dominates the relaxation process. CH_3Cl, CH_3Br and CH_3I are also strongly polar but they conform closely to the Lambert-Salter plot. The difference between the CH_3-halogen molecules and molecules such as NH_3 or SO_2 is that in the former the dimerization energy, ΔE_{dim}, is much lower than that for SO_2 or NH_3 (ΔE_{dim} for CH_3Cl = 860 cal. mol^{-1} and ΔE_{dim} for NH_3 = 4660 cal. mol^{-1} (27a)). It appears that the dimerization energy rather than just the dipole moment is the important factor which produces a deviation from the Lambert-Salter plot.

1.1.9 Polanyi-Woodall law

Polanyi and Woodall (28) studied the rotational relaxation of excited HCl produced in the chemiluminescence reaction:

$$H + Cl_2 \longrightarrow HCl^{\uparrow} + Cl$$

The transition probability from higher state j to lower state i

Figure 1.1 Lambert-Salter plot.

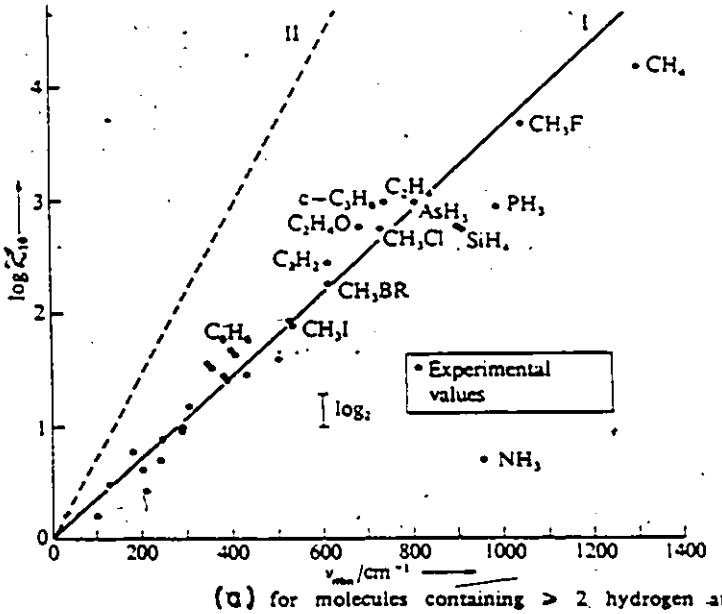

(a) for molecules containing > 2 hydrogen atoms.

From ref. 17

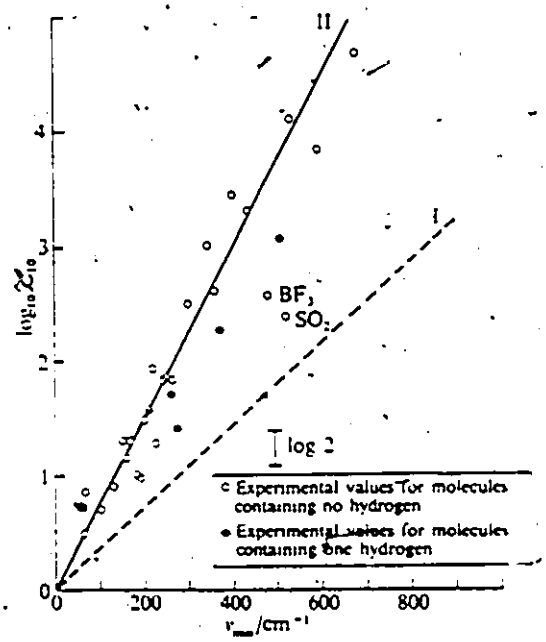

(b) for molecules containing < 1 hydrogen atom

From ref. 17

was found to be given by:

$$P_{j-i} = N' \exp(\lambda' \Delta E) \qquad (1.19)$$

where N' and λ' are constants, ΔE is the energy difference between j and i. Polanyi and Woodall found that at 230 K, the value of λ' is 8.5×10^{-3} cm which is nearly the same as the value of λ found in the Lambert-Salter plot for hydrogen-containing molecules. This is surprising because the former deals with rotational and the latter with vibrational energy changes. We shall later see that the SSH theory also produces a similar value, indicating a universal nature for λ or λ'. This "Energy gap law" is supported by several theoretical calculations (28a, 28b) and has been used by Polanyi to interpret experimental results (28c-28e) and theoretical calculations (28f-28h). On the other hand, Pritchard et al (28i, 28j) have suggested that a "power gap law" ($P = N''(\Delta E)^{-\lambda''}$, where N'' and λ'' are constants) gives a better representation of the transition probability for rotational energy transfer than the exponential gap law does. The power law has had considerable success for a large number of diatomic molecules. Moreover, several theoretical calculations show that the transition probability for rotational energy transfer is best represented by a "power gap law" (28k). Although some methods for direct calculation of the parameters N's and λ's exist (28l-28m), the most reasonable values of those parameters to use are simply empirical ones. It should be noted that within experimental error it is usually not possible to distinguish between the two laws, and each one adequately describes experimental laws.

1.2 Rules for vibrational energy transfer in polyatomic molecules

In polyatomic molecules, the large number of vibrational modes and their combinations makes interpretation of vibrational relaxation times difficult. A few general rules based on a large number of experimental observations and theoretical assumptions are formulated. These rules appear to be useful for making a prediction of certain energy transfer processes.

1. The first of these rules is based on the Bethe-Teller law which has been discussed in section 1.1.3. In this section more details will be added. According to the Bethe-Teller law, the rate of vibrational relaxation of any vibrational mode which relaxes independently of the others is given by:

$$dE/dt = -(E-E_\infty)/\tau$$

where τ is related to the activation and k_{01} and k_{10} by:

$$1/(N\tau) = k_{10}-k_{01}$$

where N is the total number of molecules.

It is worth noting that a few experimental and theoretical studies show that rotation affects the vibrational relaxation of hydrogen containing molecules. For example, Berend et al (28o) studied the vibrational relaxation of HF-HF theoretically. They showed that increasing rotation tends to decrease the orientation effect and thus decrease the vibrational relaxation cross section by a factor of three for J=3 compared to J=0. In another example, Lengel et al (28p) have shown that rotation of electronically excited OH affects the vibrational relaxation cross section. Thirdly, while experimental vibrational

relaxation rate constants for CH_4 are higher than those for CD_4, SSH theory actually predicts the contrary. This discrepancy has been attributed by Jolicard et al (28s) to the rotational effects which are neglected in SSH theory. By calculating the vibrational probabilities for CH_4 molecules using first order perturbation theory, Jolicard et al (28s) showed that rotation has a strong effect on vibrational energy transfer. Actually therefore k_{10} is an average over the initial rotational state and a sum over the final rotational states. Since the rotational sublevels equilibrate within a few collisions, one tends to ignore the fine structure. Therefore, strictly speaking, the notation T for translation should be interpreted as R,T where R represents rotation. This means that if vibrational energy is transfered to rotation, this subsequently is quickly transformed into translation.

The above expression for vibrational energy transfer is valid only when the relaxation proceeds from a Boltzmann distribution to another Boltzmann distribution independently of the size of the perturbation (i.e. temperature change). However, it is not applicable when the initial distribution is not Boltzmann such as in laser-induced perturbation experiments. In such a case different rate laws may be appropriate (29,30).

The following rules deal with V-V energy transfer in polyatomic molecules.

2. If 2 first excited vibrational levels in each of 2 different modes i and j are similar in energy, there will be a rapid intramolecular V-V intermode coupling and the 2 modes will relax

simultaneously with a vibrational relaxation time = $(\sum_j C_j/C_i)\tau_i$ where τ_i is the vibrational relaxation time of the lower mode, and where C_i and C_j are respectively the heat capacity of the lower and the higher vibrational mode (6). This rule can also be applied when several modes are similar in energy: in this case i always represents the mode of lowest energy and j represents all other modes. If the energy levels are not similar, then V-V coupling is not efficient and one can observe two or more relaxation zones with different rate constants corresponding to each of the relaxing modes. This is called multiple relaxation (6).

The following propensity rules formulated by Flynn (31) appear to be valid for molecules with less than 50 vibrational levels below 3000 cm^{-1} under conditions of low to moderate vibrational excitation. They do not apply to molecules with low frequency torsional modes and molecules undergoing sticky collisions, i.e. when the collision partners remain in close proximity to each other for times much longer than the vibrational periods.

3. "Up-the-ladder" V-V intramode exchange

$$A(v) + A(1) \rightleftharpoons A(v+1) + A(0) \quad \Delta E \qquad (1.20)$$

is very efficient. This is due to the near-resonant energy transfer at low vibrational quantum number v. At high vibrational quantum number the anharmonicity becomes important and ΔE for the above process becomes of the order of kT. Consequently this efficiency is expected to drop off. However, since the square of the matrix element increases with increasing

v, the drop-off begins to be important when v is sufficiently high.

4. V-V intermode intramolecular energy transfer is judged efficient if the energy gap between the vibrational levels exchanging energy is less than kT. This rule is illustrated by the following equation:

$$A(i) + M \rightleftharpoons A(j) + M \quad \Delta E \qquad (1.21)$$

If $\Delta E \leq kT$, this process will be efficient, and this efficiency will be increased if there is at least one hydrogen or one deuterium atom in the molecule (6).

1.3 Vibrational relaxation of N_2O

N_2O is a linear asymmetric molecule. It has four normal vibrational modes, a doubly degenerate bending mode (0,1,0) at 589.2 cm^{-1}, a symmetric stretching mode (1,0,0) at 1276.5 cm^{-1} and an asymmetric stretching mode (0,0,1) at 2223.7 cm^{-1} (fig. 1.2). A combination of these modes is also possible. A vibrational energy level diagram for N_2O is represented in fig.1.3. This diagram includes the vibrational modes and the degeneracy of each of the vibrational levels. (See chapter 4 for details of the calculation of the energies.)

The vibrational relaxation of N_2O has been studied by a large number of workers (32-70). The results can be classified into two groups depending on the technique used. In the gas compression technique, a gas undergoes a sudden increase in pressure. Initially the whole energy is in the translational and rotational degrees of freedom. Then a rapid T-R or T-V energy transfer establishes an equilibrium between the three degrees of

Figure 1.2 Vibrational modes of N_2O.

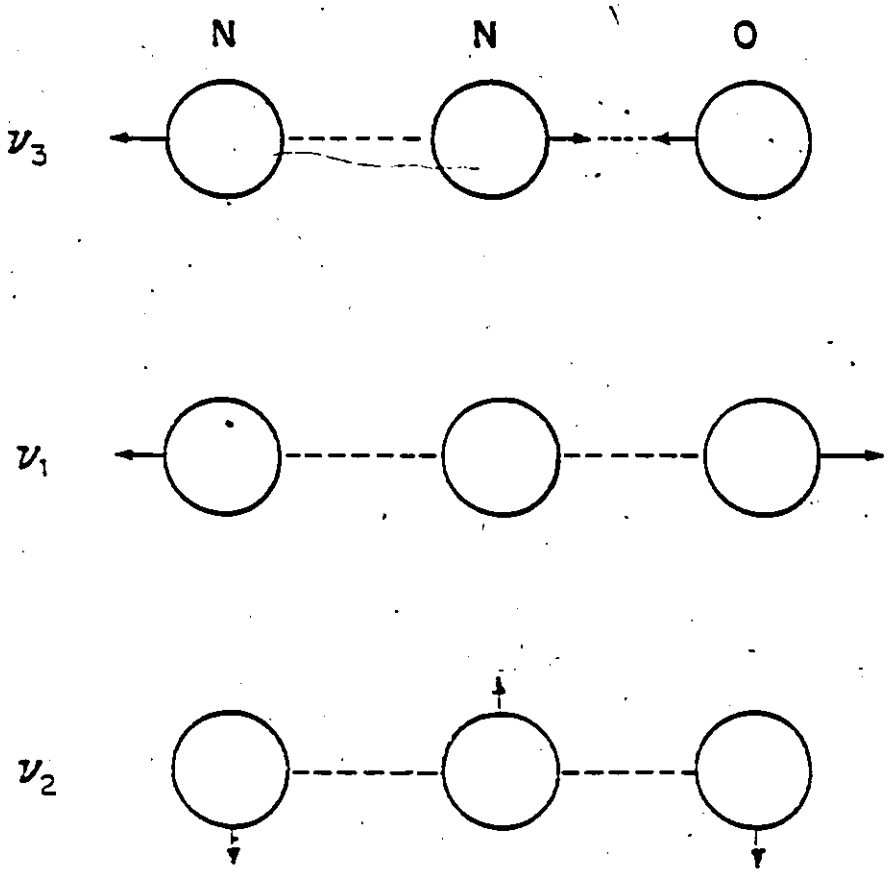

Figure 1.3 Energy level diagram of N_2O.

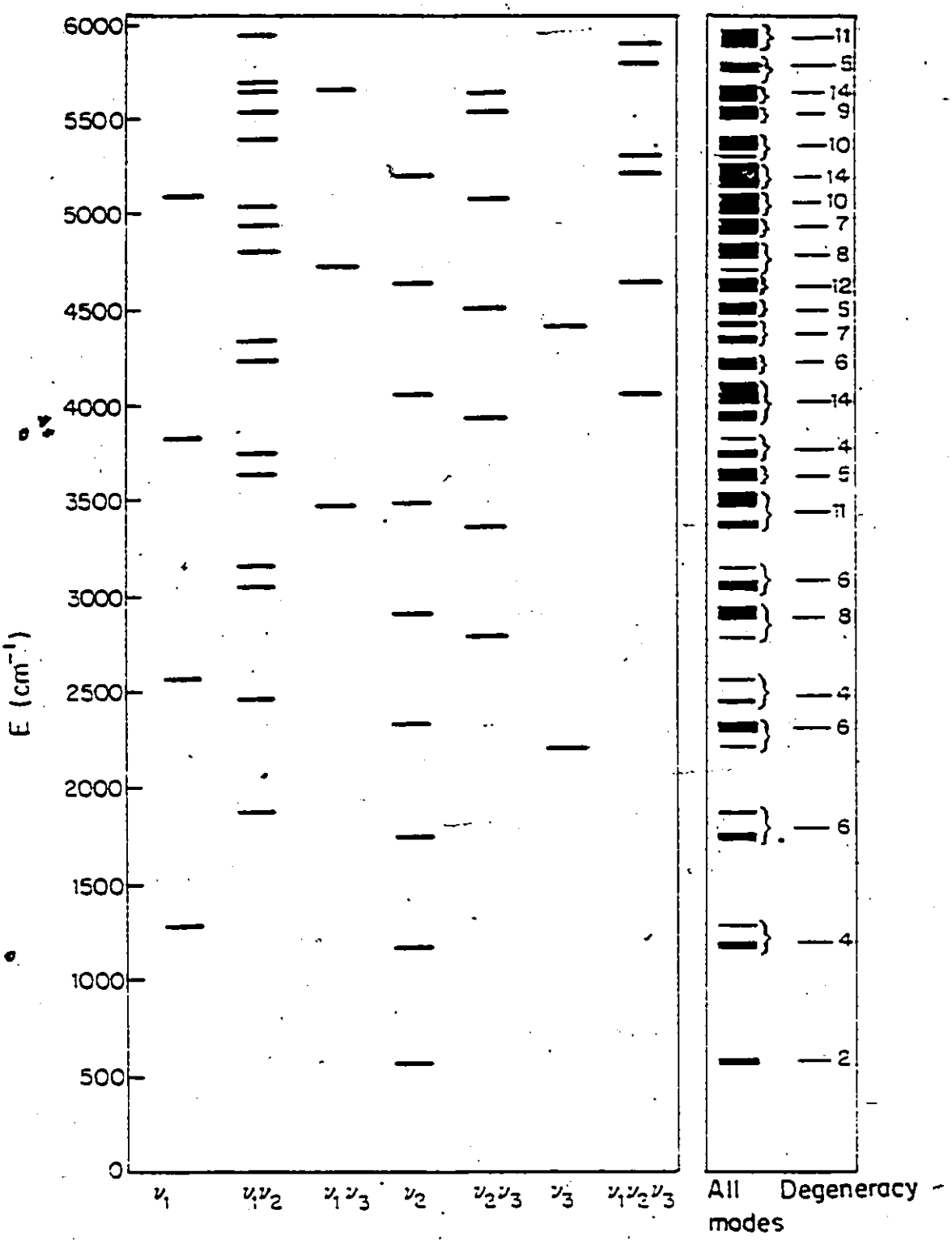

freedom. The measured relaxation time is thought to correspond to T-V processes. It is called the T-V relaxation time. Such rapid compression can be produced by shock wave, impact tube and ultrasonic waves. In the second group of experiments, selected vibrational or rotational modes are excited. This results in an increase of E_{Vib} or E_{Rot}. Relaxation towards equilibrium via V-T or R-T energy transfer can be monitored by following either the decrease of E_{Vib} or E_{Rot}, or by following the corresponding increase in E_T. The measured relaxation time is thought to correspond to V-T processes. It is called the V-T relaxation time. This group of experiments includes infrared excitation, Raman excitation, and infrared chemiluminescence. Within each group, precision of the results is good to excellent. Nevertheless, a large discrepancy may arise when comparing the results of the two different groups of experiments. In this section, the results of each individual technique will be presented separately and a comparison of all known results on the vibrational relaxation of N_2O will be presented at the end.

Shock tube: (see chap. 2 for details about experimental techniques and calculations). The first shock tube study of the vibrational relaxation of N_2O was performed by Griffith et al (32) in 1955, by following the density change behind a shock wave with an interferometer. By comparing the experimental density ratio across the shock wave to the theoretical one calculated by assuming that: (i) all modes are excited, (ii) only bending modes are excited, he concluded that only the bending mode was excited. The two stretching modes were unexcited under their experimental

conditions. The variation of the vibrational relaxation time obtained by Griffith et al with temperature is shown in fig. 1.4. In the observation time available to them, they did not find any evidence for multiple relaxation times. Later, Bhangu (33) investigated the vibrational relaxation of N_2O using a Mach-Zehnder interferometer. Vibrational relaxation times observed by Bhangu are in accord with those found by Griffith et al (fig. 1.4). Nevertheless, Bhangu concluded that the vibrational relaxation time depends not only on temperature but also on the regime of relaxation. Simpson et al (34) also measured the vibrational relaxation time of N_2O using a Mach-Zehnder interferometer. Measurements made up to 1700 K showed that neither the symmetric nor the antisymmetric modes have longer relaxation times than the bending modes. Their results differ markedly from those obtained by Griffith and by Banghu (fig. 1.4). Simpson et al (35,36) also measured the vibrational relaxation times of pure N_2O and of mixtures of N_2O with Ar, ^3He, ^4H_e, D_2, HD and p-H_2 from 350 to 1400 K using a laser Schlieren system. In all cases, it was possible to represent the vibrational relaxation time vs temperature by a Landau-Teller plot (fig. 1.4). For pure N_2O,

$$\ln P\tau = 10.8T^{-1/3} - 1.62$$

where T is the temperature in K and $P\tau$ is the vibrational relaxation time in μsec.atm. These results disagree significantly with those obtained by Simpson et al (34) above 600 K using the interferometer, as is shown in fig.1.4. Simpson attributed this discrepancy to the poorer time resolution of the

Figure 1.4 Landau-Teller plot for V-T (de)activation of pure N_2O (literature results).

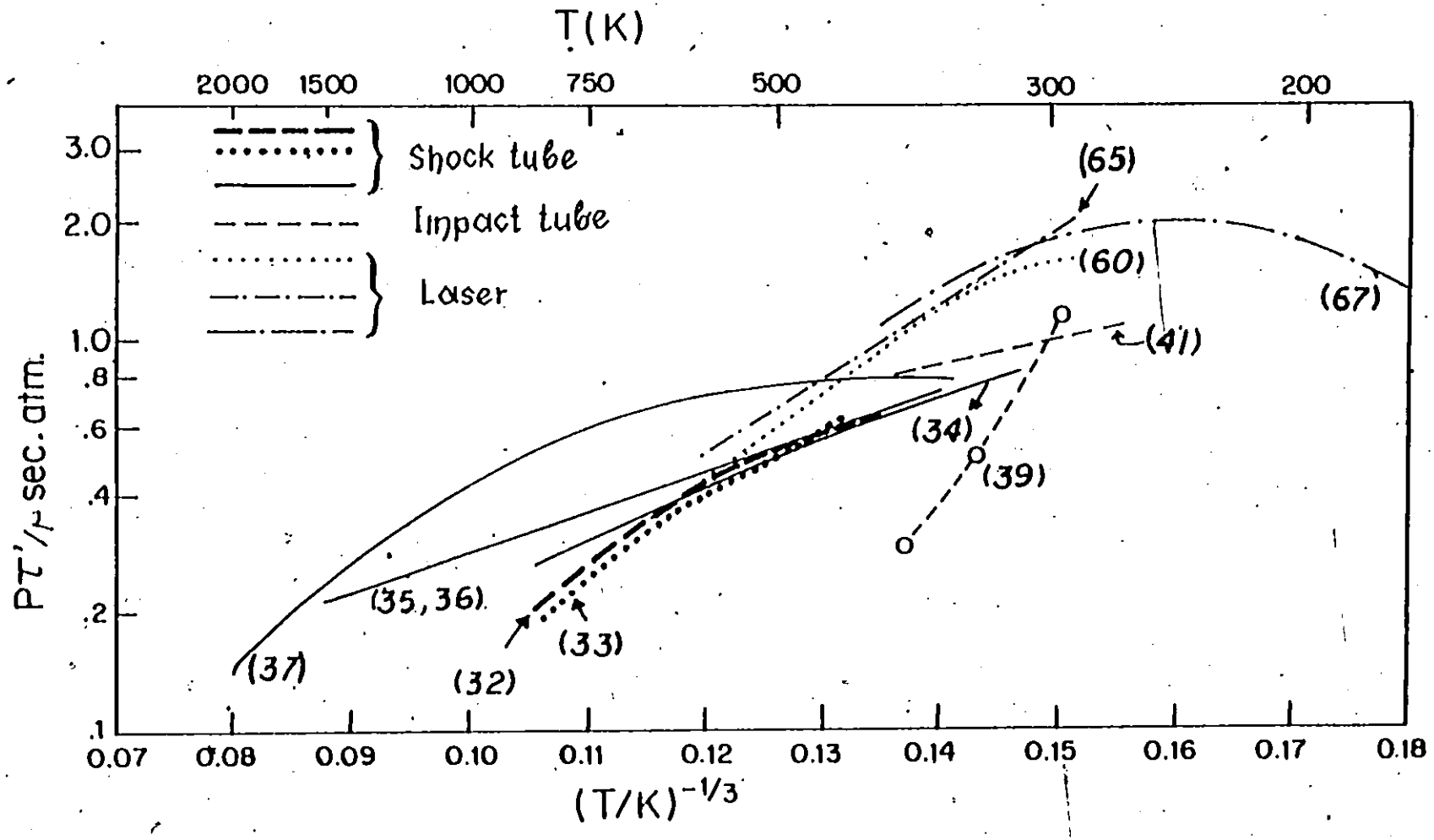

interferometer than that of the laser Schlieren system. For this reason he prefered the new data obtained by the latter method. By using the same technique as in ref. (35,36), Dove et al (37) measured the vibrational relaxation time of pure N_2O between 450 K and 2370 K and of N_2O-Ar mixtures between 800 and 2370 K. The results of Dove et al are in disagreement with all other shock tube results (see fig. 1.4). Dove et al did not observe any indication of multiple relaxation processes. They made two separate analyses: in the first analysis (i) they assumed that the asymmetric stretching mode is slower than the two other modes and relaxes separately. In the second analysis (ii) they assumed that all four vibrational modes relax together. Their experimental results agree with the second analysis in which all four modes relax with the same apparent time constant. However in this as in all other studies, only short time regimes (one to two natural lifetimes) were probed. The fundamental question on the constancy of the phenomenological relaxation time has yet to be satisfactorily answered.

Impact tube: In impact tube experiments, a gas in a reservoir at equilibrium with pressure P_o, temperature T_o and uniform velocity U_o, is allowed to expand isentropically through a nozzle, then adiabatically compressed at the nose of an impact tube. At the stagnation point, the gas is characterized by a pressure P_f, a temperature T_f and a velocity $U_f = 0$; and in the reservoir by a pressure P_g, temperature T_g and velocity $U_g = 0$. If the compression occurs very slowly, the energy and the entropy at the stagnation point will return to their initial values in

the reservoir and the pressure P_g will be equal to the pressure P_o. However, if the compression time is short, the gas energy will depart from its equilibrium energy and the transfer of energy will occur by an irreversible process along with an increase of entropy.

The relationship between the vibrational relaxation time and the variation of pressure is very complicated. For more details on the experimental technique and the data reduction the reader is referred to refs. 6 and 38.

In contrast to the shock tube technique where the temperature varies between 350 K and several thousands of degrees, most of the measurements of vibrational relaxation times using impact tubes are reported at room temperature to 400 K.

Vibrational relaxation times of N_2O have been measured by several workers using impact tubes (39-41). Griffith (39) measured the vibrational relaxation time of N_2O between 290 and 400 K. He found that the vibrational relaxation time decreases with increasing temperature (fig. 1.4), supporting the theory that fast collisions are most important. He reported a value of 1.12 μsec.atm. at 290 K. Huetz et al (40) measured the vibrational relaxation time of pure N_2O and mixtures of N_2O with He, Ne, Ar and N_2 at 300 K. The vibrational relaxation time of the pure N_2O was found to be 1.12 μsec.atm. and the vibrational relaxation times of N_2O colliding with He, Ne, Ar and N_2 are 0.135, 2.2, 6.0 and 1.5 μsec.atm. respectively. Huetz et al (41) also studied the vibrational relaxation time of N_2O as a function of temperature between 290K and 380K. They found Landau-Teller

behaviour for the vibrational relaxation time:

$$\ln P\tau = -16.25 + 16.49\ T^{-1/3}$$

At 300 K one finds: $P\tau = 1.03$ μsec.atm.

In contrast to the shock tube measurements where the vibrational relaxation times are in disagreement with each other over a large temperature range, the vibrational relaxation times measured with impact tubes are self-consistent at room temperature; they vary between 1.03 to 1.12 μsec.atm. This agreement is probably due to the fact that at room temperature only the process (0,0,0) $\rightleftharpoons$ (0,1,0) contributes significantly. In shock tube experiments, the situation is much more complicated at higher temperatures and many processes are involved. This will be discussed later.

Ultrasonic techniques: This method is generally used to measure vibrational and rotational relaxation near room temperature. This technique is well described in standard text books (6,42). A brief description will be given in this section.

When a sound wave passes through a gas, a rapid alternating compression and rarefaction wave occurs. The variation of sound velocity α with the angular sound frequency ω is given by:

$$\alpha^2 = \frac{RT}{W}\left[1 + \frac{R(C_{V_o} + C_{V_\infty}\omega^2\tau^2)}{(C_{V_o}^2 + C_{V_\infty}^2\omega^2\tau^2)}\right] \qquad (1.22)$$

where W is the molecular weight of the gas, C_{V_o} is the heat capacity at constant volume at the lower frequency and $C_{V_\infty} = C_{V_o} - C_{V_1}$ at the higher frequency where the relaxation mode ceases entirely to make its contribution C_{V_1} to the effective heat capacity. The inflection point in the above dispersion

equation corresponds to $\omega\tau=1$.

The variation of the absorption coefficient per wavelength, with the frequency gives similar information. The maximum absorption corresponds to $\omega\tau=1$. Consequently, the vibrational relaxation time can be obtained either by measurement of sound velocity or sound absorption per unit wavelength as a function of frequency. Since the vibrational relaxation time is inversely proportional to the pressure, it is usually more convenient to make measurements by varying the pressure while keeping the frequency constant.

Vibrational relaxation times of pure N_2O measured by ultrasonic techniques at room temperature are in excellent agreement with each other. They vary between 0.89 and 0.99 μsec.atm. (43-47). As for the impact tube techniques, this agreement is probably due to the fact that at room temperature, only the bending mode (0,1,0) is excited, so that the relaxation time of the process (0,0,0) $\rightleftharpoons$ (0,1,0) is measured.

Opto-acoustic effect (Spectrophone): This method provides direct measurement of energy transfer rates provided that excited modes are IR active. In this method, the gas sample is enclosed in a constant volume cell and irradiated with a pulsed beam of IR radiation. Filters or lasers are used to select wavelengths in order to excite a given vibrational level. The excited molecules may lose their vibrational energy by induced emission, spontaneous emission of radiation or by transfer of vibrational energy to relative translational energy by means of inelastic collisions. This latter effect produces a periodic change in the

gas temperature. Since the cell volume is constant, a periodic change of the pressure will be produced leading to the production of a sound wave which can be detected by a suitable microphone. The time lag between the absorption of vibrational energy and its degradation to translational energy determines a phase shift φ between the incident radiation and the emitted sound wave. This phase shift can be directly related to the V-T relaxation time by (6):

$$\tan (\pi/2 - \varphi) = \omega\tau C_{V\infty}/C_{Vo} \qquad (1.23)$$

The amplitude, b, of the sound wave can also be related to the V-T relaxation time by (6):

$$b = \frac{B}{C_{V_o}(1+\omega^2\tau^3(C_{V\infty}/C_{Vo})^{-1}\chi^2} \qquad (1.24)$$

where B is a constant. Consequently, vibrational relaxation times can be determined either by a phase shift measurement or by an amplitude measurement.

Read et al (48-50) measured V-T relaxation times of N_2O at 290 K by monitoring the phase shift. At high energy (4.5μ) only the antisymmetric stretching mode (0,0,1) was excited and the corresponding V-T relaxation time was 1.6 μsec.atm. At low energy (7.8μ), only the symmetric stretching mode (1,0,0) is excited and the V-T relaxation time for this vibrational level is 1.1 μsec.atm. Slobodskaya et al (51) measured V-T relaxation times for N_2O at different energies. The antisymmetric stretching mode (0,0,1) has the larger V-T relaxation time, 1.8 μsec.atm. The symmetric mode (1,0,0) has a V-T relaxation time of 1.13

μsec.atm. Finally De Vasconcelos et al (52) measured V-T relaxation times of the symmetric and the antisymmetric stretching modes of pure N_2O and in mixtures with He, Ne, Ar and Kr at 288 K by using the amplitude method. The V-T relaxation time of the symmetric stretching mode (1,0,0) was found to be 0.87 ± 0.06 μsec.atm. for pure N_2O and 0.14, 1.38, 6.8, 17.7 μsec.atm. in collision with He, Ne, Ar, and Kr respectively. According to De Vasconcelos, two deactivation paths from (1,0,0) are possible. The first one is a direct deactivation by V-T energy transfer. The second one involves Intramolecular V-V energy transfer through the second level of the bending mode (0,2,0). Since the energy difference between (1,0,0) and (0,2,0) is small, a rapid equilibrium will be established between (1,0,0) and (0,2,0). As a consequence, the deactivation of (1,0,0) will occur through the (0,2,0) energy level and the transition (0,2,0) $\longrightarrow$ (0,1,0) $\longrightarrow$ (0,0,0) is therefore the rate determining route. The V-T relaxation time of the (0,0,1) energy level (at 4.5μ) is found to be 1.84 μsec.atm. for pure N_2O and 3.8, 6.8, 12.6 and 23.0 μsec.atm. in collision with He, Ne, Ar and Kr respectively.

Laser induced fluorescence: With the development of lasers, which are convenient sources for vibrational excitations, many molecules have been studied by this method resulting in a large data base of rates of vibrational energy transfer between like molecules and different molecules. This method has also been used to study the vibrational relaxation of pure N_2O and N_2O mixed with foreign gases.

In this technique, the gas sample is irradiated by a pulsed

IR laser. After the laser excitation, the decay of the vibrational fluorescence is monitored with time. The radiative lifetime of the vibrationally excited states is large compared to collisional deactivation, thus the fluorescence signal can be used as a measure of the emitting level's population. The intensity of the fluorescence signal is proportional to the population of the excited emitting levels and apparently decays exponentially with time. The V-T relaxation times are deduced from the slope of the semi-log-plot of the fluorescence intensity with time.

Yardley (53,54), studied the rates of deactivation of pure N_2O (0,0,1) and of N_2O and in mixtures with He, Ne, Ar, Kr, H_2, D_2 and N_2 (v=1) at 298 K by IR fluorescence. A Q-switched N_2O laser was used to excite N_2O into the (0,0,1) level. By plotting the logarithm of the fluorescence intensity transmitted by a 4.5μ filter as a function of time, the V-T relaxation time of the $(0,0,1) \rightleftharpoons (0,0,0)$ deactivation was found to be 1.74 μsec.atm. in the pressure range 5 to 50 torr. Using the relation

$$(P\tau_{obs})^{-1} = X_{N_2O}(P\tau_{N_2O-N_2O})^{-1} + (1-X_{N_2O})(P\tau_{N_2O-M})^{-1}$$

where M is a foreign gas, and X is the mole fraction. The V-T relaxation time of N_2O in collision with the foreign gases was found to be 5.05, 13.6, 12.8, 24.4, 0.236 and 1.21 μsec.atm. for deactivation by He, Ne, Ar, Kr, H_2 and D_2 respectively. In the N_2O-N_2 mixture, a solution of the differential equations for the disappearance of N_2O (0,0,1) predicts a double exponential decay, the rapid decay corresponding to the equilibration of N_2O (0,0,1) with N_2 (v=1), and the slow decay corresponding to the V-T

deactivation of N_2O (0,0,1) and N_2 ($v = 1$) together. From the observation of the fluorescence signals, the V-T relaxation times of these two processes are found to be 0.26 and 21.7 μsec.atm. respectively. By comparing the experimental results of N_2O-rare gas mixtures with the results of CO_2-rare gas mixtures and by assuming that the mechanism of deactivation of N_2O with rare gases is similar to the corresponding (but better known) mechanism for CO_2 colliding with rare gases (54), Yardley concluded that the principal path for intramolecular deactivation of N_2O (0,0,1) by rare gases is through the (1,1,0) level. Finally, Yardley concluded by comparing the calculated rate constants for N_2O-N_2 and CO_2-N_2 that long-range dipole-quadrupole forces are responsible for the vibrational energy exchange between N_2O and N_2. Flynn et al (55) measured the V-T relaxation time of the (0,0,1) vibrational level of pure N_2O at 296 K. A Q-switched N_2O-He-Ne laser was used to excite N_2O molecules. The decay of the (0,0,1) vibrational level was monitored by observing the fluorescence intensity through a 4.5 μ filter. 20 experiments were performed between 1 to 40 torr of N_2O. Each individual experiment showed an exponential decay within the experimental error. The V-T relaxation time of N_2O was found to be 1.96 μsec.atm. which is in good agreement with the V-T relaxation time found by Yardley. Flynn et al suggested that the deactivation of the (0,0,1) level of N_2O occurs via intramolecular V-V energy transfer to the nearby bending mode (0,2,0) as has been suggested for the CO_2 molecule (56,57). Doyennette et al measured the V-T relaxation time of the (0,0,1) vibrational level of N_2O at room

temperature (58,59) and as a function of temperature between 300 and 1000 K (60). In the room temperature measurements, a Q-switched N_2O-He-Ne laser was used to excite the N_2O molecules. The fluorescence intensity of the (0,0,1) vibrational level was monitored as a function of time. The curve representing the variation of the deactivation rate constant with pressure is shown in fig. 1.5. Although, pressures up to 5 torr are shown in fig. 1.5, experiments with pressures up to 50 torr were performed. At low pressure the deactivation rate constant decreases with increasing pressure. This is due to the fact that at low pressure, the diffusion of excited molecules to the wall is very important. Therefore, the wall deactivation is the dominant process in the deactivation of N_2O molecules and its importance decreases with increasing pressure as is usual for diffusion processes (61). However, at high pressure, the deactivation due to quenching collisions becomes dominant and the rate coefficient decreases linearly with the pressure. From the slope of the curve in fig. 1.5 in the high pressure regime, the V-T relaxation times were found to be 1.74 μsec.atm. (58) and 1.77 μsec.atm. (59) which are in good agreement with the results reported by Yardley and Flynn. The variation of the V-T relaxation time of the (0,0,1) vibrational level with temperature, between 400 K and 1000 K (60), is shown in fig. 1.4. Doyennette et al observed that below 400 K, the V-T relaxation time increases less rapidly than expected by the Landau-Teller law. They attributed this behaviour to the long range attractive forces which become more important at low temperature.

Figure 1.5 Variation of the relaxation rate constant with pressure for different cell dimensions $\mathcal{L}$.

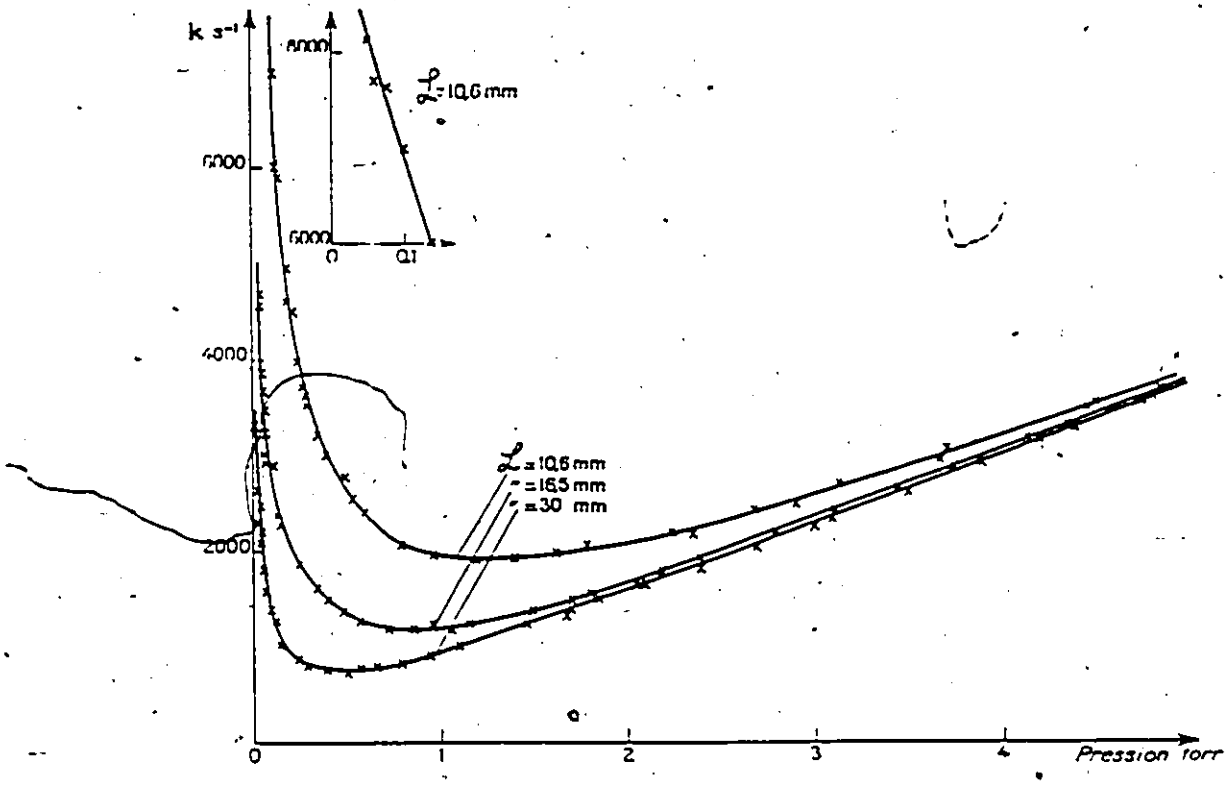

From ref. 58

Henry et al, studied V-V energy transfer between the (0,0,1) vibrational level of N_2O and other molecules at room temperature (62), and as a function of temperature (63-64). The experimental procedure is similar to the one described above. As was discussed by Yardley (53), the fluorescence signal from N_2O (0,0,1) deactivation is the sum of two exponential decays, the rapid decay being due to intermolecular V-V energy transfer, and the slow one due to the V-T energy transfer. Henry et al calculated V-V relaxation times by using the semi-classical method developed by Sharma (24) (eq. 1.18, section 1.1.7). By assuming that V-V energy transfer is due to a long-range interaction, the calculated relaxation times for N_2O-N_2 mixtures agree well with the experimental ones. However, for mixtures with HCl, HBr, and HI, the calculated relaxation times are 2-4 orders of magnitude larger than the experimental "ones". Henry et al attributed this difference to the formation of hydrogen bonding or to V-R energy transfer which is very important in molecules containing hydrogen atoms. The effect of temperature on the rate of V-V energy transfer has been studied by measuring the V-V relaxation time of the N_2O-N_2 and N_2O-CO mixtures between 300 and 1000 K (63-64). Curves representing V-V relaxation times vs temperature are shown in fig. 1.6. These curves show a maximum which appears clearly for the N_2O-N_2 mixture. The maximum extends over a wide range of temperatures. For near resonant V-V energy transfer, the increase of the relaxation time with temperature in the low temperature regime can be attributed to the long-range attractive multipolar forces and the decrease

Figure 1.6 Landau-Teller plot for intermolecular V-V energy transfer in N_2O by collision with N_2O and with foreign gases (literature results).

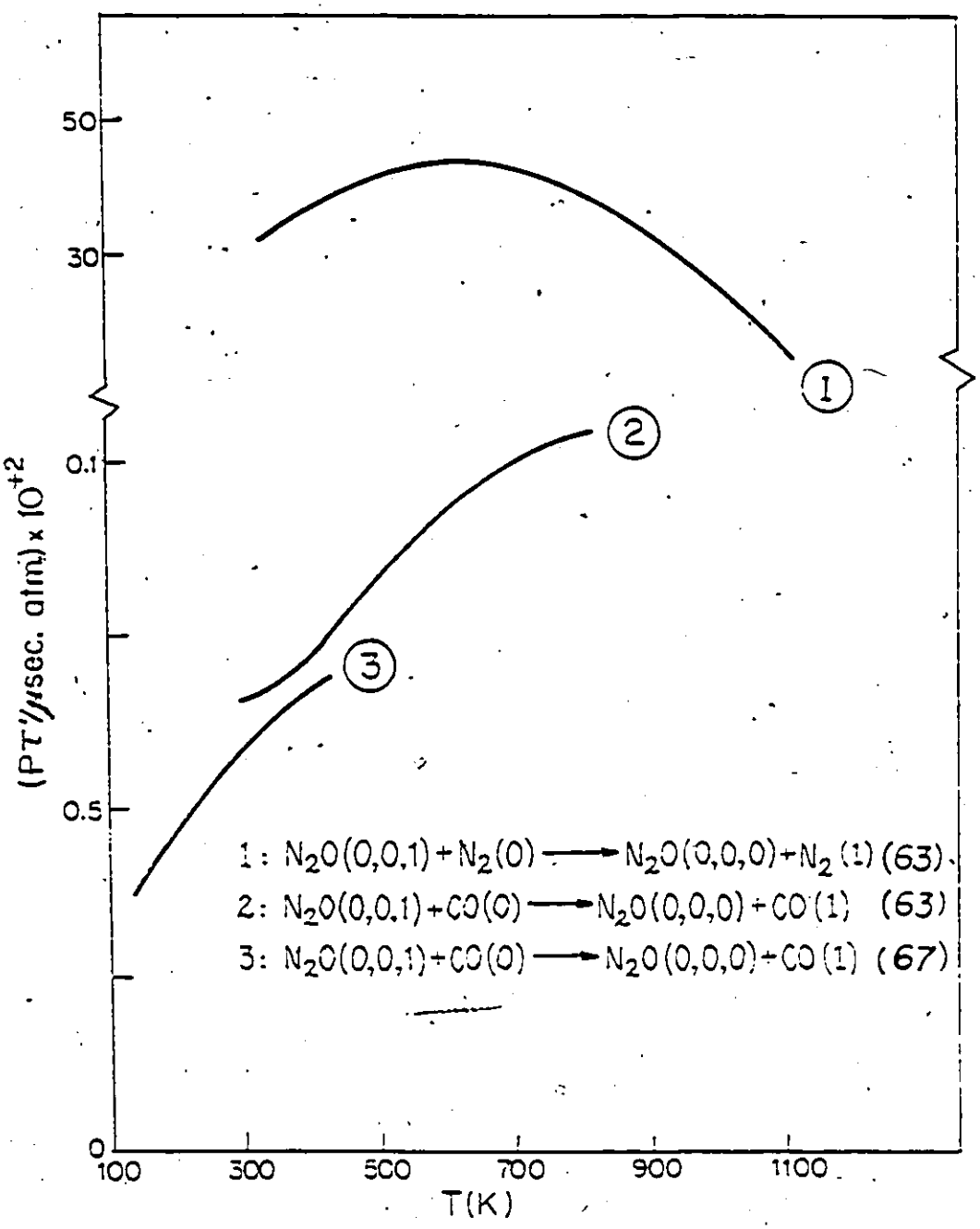

of the relaxation time with increasing temperature in the high temperature regime cannot be interpreted. Henry et al compared the theoretical rate constant to the experimental one. For N_2O-CO mixtures, they concluded that assuming long-range attractive dipole-dipole forces gives better agreement with the experimental results than assuming a dipole-quadrupole interaction. Nevertheless, for the N_2O-N_2 mixture, the dipole-quadrupole interaction explains the experimental results better than the dipole-dipole interaction. Stephenson and Moore (65) measured the rate of V-V energy exchange from the asymmetric stretching mode of CO_2 (0,0,1) to $^{13}CO_2$, N_2O, CO and $^{15}N_2$ as a function of temperature. The technique involves pumping CO_2 (0,0,1) using a CO_2 laser, followed by V-V energy transfer to N_2O, $^{13}CO_2$ ...etc. From the exponential decay of the CO_2 (0,0,1) and/or the N_2O (0,0,1) fluorescence signal, the V-T relaxation time of N_2O by collision with N_2O and CO_2 were found. They are shown on fig. 1.4 and fig. 1.7 respectively. By comparing their experimental data with the available theoretical calculations, Stephenson and Moore reached the conclusion that the vibrational energy transfer is due to multipole moment interactions. Starr and Hancock measured the intermolecular V-V energy transfer between N_2O (0,0,1) and CO as well as the V-T rate of deactivation of N_2O (0,0,1) by collision with N_2O, CO, and Ar at 296 K (66), and as a function of the temperature (67). N_2O was excited by collisions with CO ($v = 1$) which had been directly excited by a frequency-doubled CO_2 laser. A cell filled with CO was used as a filter in order to absorb all CO (1->0) emission; thus the time-resolved

Figure 1.7 Landau-Teller plot for V-T (de)activation of N_2O by collision with foreign gases (literature results).

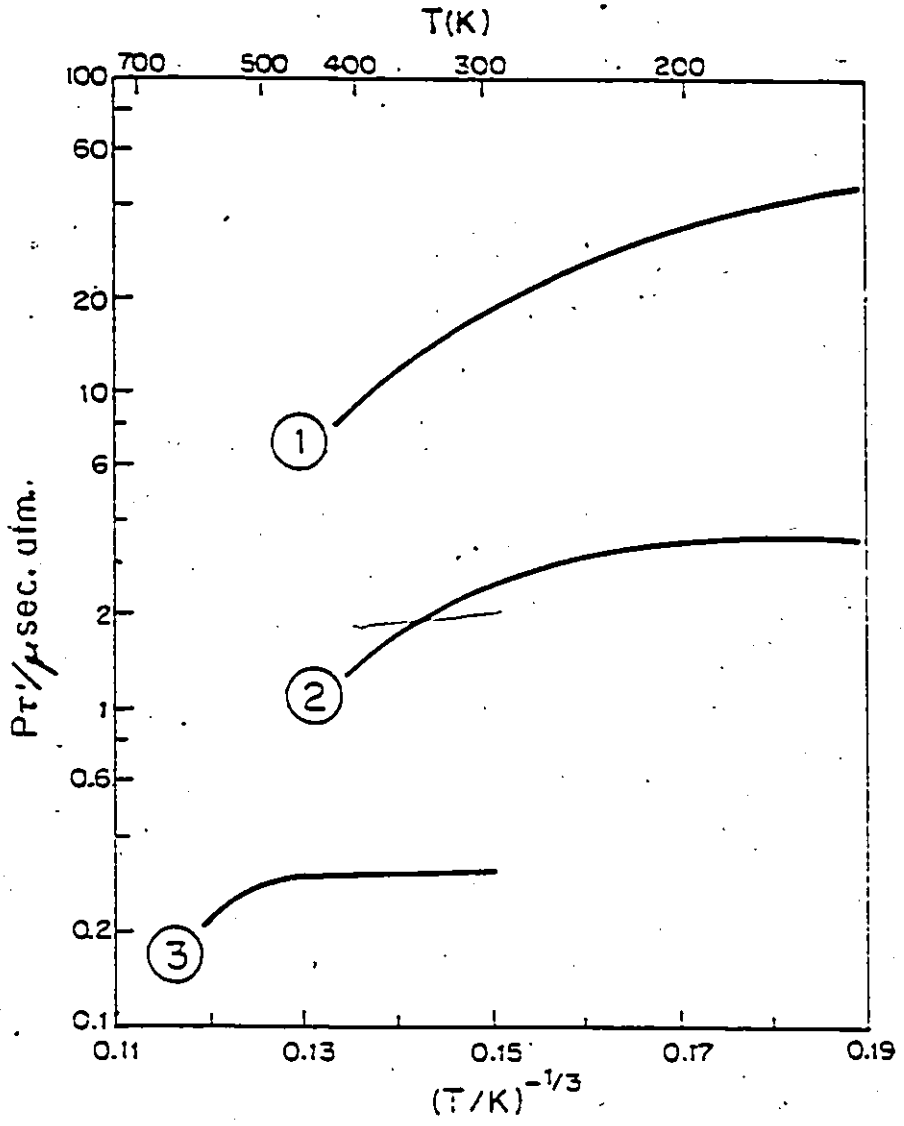

1 : $N_2O(0,0,1) + Ar \longrightarrow N_2O(m,n,0) + Ar$ (67)

2 : $N_2O(0,0,1) + CO \longrightarrow N_2O(m,n,0) + CO$ (67)

3 : $N_2O(0,0,1) + CO_2 \longrightarrow N_2O(m,n,0) + CO_2$ (65)

population of the N_2O (0,0,1) level could be directly monitored. By monitoring the N_2O (0,0,1) fluorescence signal, a fast and a slow relaxation could be measured, as was mentioned earlier. The V-V relaxation time of N_2O by collision with CO at room temperature was found to be 5.85×10^{-3} μ sec.atm. which is in good agreement with the value found by Henry et al. The relaxation time for V-T deactivation by collision with N_2O, CO and Ar are respectively: 1.74, 2.71, and 10.9 μ sec.atm. The dependence of the V-V relaxation time of N_2O (0,0,1) upon collision with CO vs temperature is shown in fig. 1.6. The dependence of the V-T relaxation time of N_2O upon collision with N_2O, CO and Ar on temperature are shown in fig. 1.4 and fig. 1.7. The slopes of the temperature dependence of the V-T relaxation time upon collision with CO and Ar (fig. 1.7) are similar at high temperature. The probability of (V-V) energy transfer between N_2O (0,0,1) and CO, was calculated by the authors using the Sharma-Brau theory (24). In this model, dipole-dipole intermolecular forces were responsible for the energy exchange. These calculations succesfully predict the negative temperature dependence of the deactivation probability in the low temperature regime as was observed experimentally. However, as was discussed above, theoretical calculations fail to give any explanation for the increase in the probability with temperature in the high temperature regime. Picard-Bersellini et al (68) studied the decay of the (0,0,1) vibrational level of N_2O previously excited by activated N_2. They found that intramolecular V-V energy transfer between (0,0,1) and (0,3,0)

was responsible for this decay and the relaxation time of this process was found to be 1.64 μsec.atm.

Up to now, only the laser induced fluorescence measurements involving the antisymmetric stretching mode (0,0,1) of N_2O have been discussed. V-T relaxation times were directly related to this level. The symmetric stretching mode (1,0,0) has received little attention in contrast to the antisymmetric stretching mode. The first vibrational relaxation measurement involving the (1,0,0) mode at room temperature was due to Kung (69). The excitation of the (1,0,0) mode was performed by an overtone activation using a DF laser. From the (1,0,0) fluorescence signal, Kung measured two relaxation times - a short relaxation time equal to 0.062 μsec.atm. which corresponds to the intramolecular V-V energy transfer between (1,0,0) and (0,2,0) and a long relaxation time equal to 1.3 μsec.atm. which corresponds to the V-T deactivation of (0,1,0). From the (0,0,1) fluorescence signal, a single relaxation time equal to 2.11 μsec.atm. was determined. It corresponds to the (0,0,1) $\rightleftharpoons$ (1,0,0)/(0,2,0) process. Kung (70) also measured the intramolecular V-V relaxation time between the (1,0,0) and (0,2,0) levels and the V-T relaxation time of the (0,1,0) mode of N_2O upon collision with Ar, N_2, H_2O and NO. He found values of 0.38, 0.26 and 3×10^{-3} μsec.atm. for (1,0,0) $\rightleftharpoons$ (0,2,0) V-V relaxation for collisions of N_2O with Ar, N_2 and H_2O respectively, and values of 12.1, 1.75, 9.4×10^{-3} and 0.062 μsec.atm. for V-T relaxation for collisions of N_2O (0,1,0) with Ar, N_2, H_2O and NO respectively. It is found that H_2O is very

efficient relaxer. This is probably due to the acid-base type interaction between N_2O and H_2O.

Comparison: Tables 1.1, 1.2 and 1.3 and figures 1.4, 1.6, and 1.7 include the most important published results on the vibrational energy transfer of pure N_2O and of N_2O-foreign gases mixtures. Several important points can be concluded from these results.

In Table 1.1, vibrational relaxation times of pure N_2O measured at room temperature are summarized. Two groups of vibrational relaxation times were measured depending on the technique used. In the gas compression technique, relaxation times of the order of 1 μsec.atm. were measured. Among these the impact tube and the ultrasonic experiments were actually performed for room temperature; whereas the shock tube measurements were performed at higher temperatures, but the relaxation time reported for room temperature was obtained by a short extrapolation. Except for the results of Dove et al (37) and Griffith (32), they are in excellent agreement. This agreement is probably due to the fact that at room temperature, only the bending mode is excited. Even if the stretching mode is somewhat excited, the rapid V-V energy transfer between (1,0,0) and (0,1,0) or (0,2,0) establishes a rapid equilibrium between these two modes, so that the relaxation time of the (0,0,0) $\rightleftharpoons$ (0,1,0) process is measured. In the second group of experiments, (spectrophone and laser induced fluorescence), the symmetric and/or the antisymmetric stretching mode were excited. In this group of experiments the measured relaxation times are in very

Table 1.1 Vibrational relaxation times (μsec.atm) of pure N_2O at room temperature (literature results).

(1,0,0) or (0,1,0)	(0,0,1)	Experimental Techniques	Authors and references
1.0		S.T.	Simpson (35,36)
1.0		S.T.	Simpson (34)
1.2		S.T.	Bhangu (33)
1.3		S.T.	Griffith (32)
0.72		S.T.	Dove (37)
1.12		I.T.	Griffith (39)
1.12		I.T.	Huetz (40)
1.03		I.T.	Huetz (41)
0.92		U.S.	Eucken (43)
0.89		U.S.	Eucken (44)
0.99		U.S.	McCoubrey (45)
0.97 and 0.94		U.S.	Holmes (46)
0.99		U.S.	Decius (47)
1.1	1.6	S.	Read (48)
1.13	1.8	S.	Slobodoskaya (51)
0.87	1.84	S.	DeVasconcelos (52)
	1.74	L.	Yardley (53)
	1.96	L.	Flynn (55)
	1.74	L.	Doyennette (58)
	1.77	L.	Doyennette (59)
	1.74	L.	Hancock (66)
	1.64	L.	Picard (68)
1.3	2.11	L.	Kung (69,70)

S.T. - Shock Tube
I.T. - Impact Tube
U.S. - Ultrasonic
S. - Spectrophone
L. - Laser

good agreement. However, the relaxation times obtained by Kung (69,70) are slightly higher than those obtained by other workers.

In Table 1.2 the V-T relaxation times of the (1,0,0) or (0,1,0), and (0,0,1) modes of N_2O by collision with foreign gases at room temperature are summarized. Not many results have been published on the deactivation of N_2O by foreign gases. For this reason it is difficult to draw a general conclusion. Agreement between these results is not as good as in the case of pure N_2O. In some cases agreement is very good such as for the deactivation of N_2O (0,0,1) by Ar, where relaxation times are 12.6, 10.9 and 12.8 μsec.atm. or for N_2O (1,0,0) deactivated by He, where relaxation times are 0.135 and 0.14 μsec.atm. In all other cases the agreement is poorer.

Table 1.3 summarizes the results of V-V relaxation for collision of N_2O with N_2O and with foreign gases. Again here, the lack of experimental data makes the comparison very difficult. However, good agreement between these results appears in some cases. For example, the intermolecular V-V relaxation times for exchange between N_2O (0,0,1) and N_2 obtained by Yardley (53) and Henry (62) are very close; moreover the intermolecular V-V relaxation times for exchange between N_2O (0,0,1) and CO as obtained by Hancock (66) and by Henry (62) are again in good agreement. In all other cases it was impossible to reach any conclusion.

In fig. 1.4 the dependence of the vibrational relaxation times of pure N_2O on temperature is shown. Experiments performed in shock tubes are somewhat in disagreement with each other.

Table 1.2 Vibrational relaxation times (μsec.atm.) for the deactivation of N_2O by collision with foreign gases at room temperature (literature results).

Collision Partner	(1,0,0) or (0,1,0) excited			(0,0,1) excited		
	Huetz (40)	De Vasconceles (52)	Kung (70)	DeVasconceles (52)	Hancock (66)	Yardley (53)
He	0.135	0.14		3.8		5.05
Ne	2.2	1.38		6.8		13.6
Ar	6.0	6.8	12.1	12.6	10.9	12.8
Kr		17.7		23.0		24.4
N_2	1.5		1.75			21.7
NO			0.062			
CO					2.71	
H_2O			.00094			
H_2						0.236
D_2						1.21

Table 1.3 V-V relaxation times (μsec.atm) for deactivation of N_2O by collision with N_2O and with foreign gases at room temperature (literature results).

Collision Partner	Intramolecular V-V (1,0,0) --> (0,1,0)	Intermolecular V-V ; (0,0,1) excited		
	Kung (69,70)	Hancock (66)	Yardley (53)	Henry (62)
N_2O	0.062			
Ar	0.38			
N_2	0.26		0.26	0.294
CO		5.85×10^{-3}		6.57×10^{-3}
CO_2				2.31×10^{-2}
HCl				
HBr				1.51×10^{-1}
HI				6.56×10^{-3}
H_2O	3×10^{-3}			

Simpson et al, for example, measured the vibrational relaxation time of pure N_2O in a shock tube using an interferometer in one case (34) and a laser schlieren system (35,36) in another case. The results obtained by these two techniques are different. Simpson et al attributed this difference to the measurement system. However Dove et al (37) used a laser Schlieren system and their results are also in disagreement with all other shock tube results. Consequently, the disagreement is not due to the measurement system, but rather may reflect a fundamental difficulty in experiments involving large perturbations. Vibrational relaxation times obtained by impact tube techniques are also in serious disagreement with each other. In contrast to the gas compression techniques, laser induced fluorescence data are seemingly satisfactory. This is due to the fact that only the vibrational mode (0,0,1) is initially excited. However, the Landau-Teller plots in this case appear to be steeper than the Landau-Teller plot obtained for the gas compression data. It appears also that at low temperatures there is a deviation of the Landau-Teller plot from linearity. Indeed, the V-T relaxation time at low temperature decreases with decreasing temperature.

The dependence of the V-V relaxation time for deactivation of N_2O by collision with foreign gases on temperature is shown in fig.1.6. The results of the N_2O and CO system obtained by Henry (63) and Hancock (67) seem to match each other. In the N_2O - N_2 system the decrease of the V-V relaxation time with decreasing temperature is evident.

Fig. 1.7 shows the variation of the V-T relaxation time for

N_2O by collision with foreign gases. Because of the lack of results, it is impossible to make a comparison between the different techniques used and between the results of different authors. However, it appears that at high temperatures the curves representing $P\tau$ vs $T^{-1/3}$ are parallel and increase with decreasing temperature finally tending to a constant value.

1.4 Vibrational relaxation of C_2H_2

C_2H_2 is a linear symmetrical molecule. It has three stretching modes; two symmetric: (1,0,0,0,0) at 3373.7 cm^{-1} and (0,1,0,0,0) at 1973.8 cm^{-1} respectively, one antisymmetric: (0,0,1,0,0) at 3281.9 cm^{-1} and two doubly degenerate bending modes: (0,0,0,1,0) at 611.6 cm^{-1} and (0,0,0,0,1) at 729.3 cm^{-1} (fig. 1.8). Combinations of these modes are also possible.

The vibrational level diagram of C_2H_2 is illustrated in fig. 1.9. On this figure, the vibrational modes and the degeneracy of each vibrational level are illustrated.

Not as many data have been published on the vibrational relaxation of C_2H_2 as on that of N_2O. The relaxation time of C_2H_2 is known to be very short (71-76) because of the hydrogen atoms, and its measurement is thus much more difficult than that of N_2O. Moreover, C_2H_2 has 7 vibrational modes (including 2 degenerate sets) compared to 4 for N_2O. Consequently, its energy level diagram is significantly more complicated, and the analysis of the different deactivation pathways of C_2H_2 is more difficult than the corresponding one for N_2O.

The first measurement of the vibrational relaxation time of C_2H_2 is due to Edmonds and Lamb (71). They extracted the

Figure 1.8 Vibrational modes of C_2H_2.

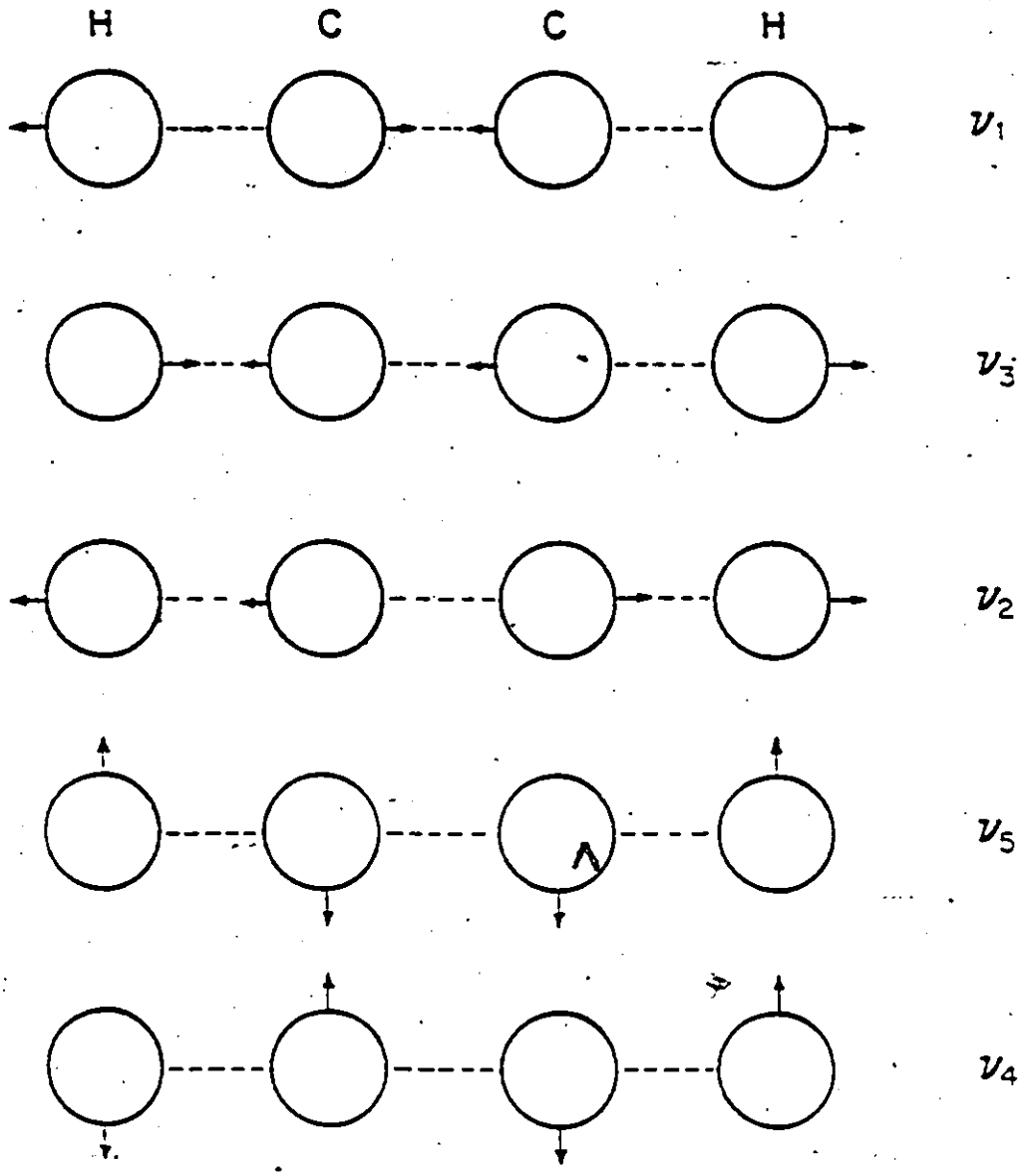

Figure 1.9 Energy level diagram of C_2H_2.

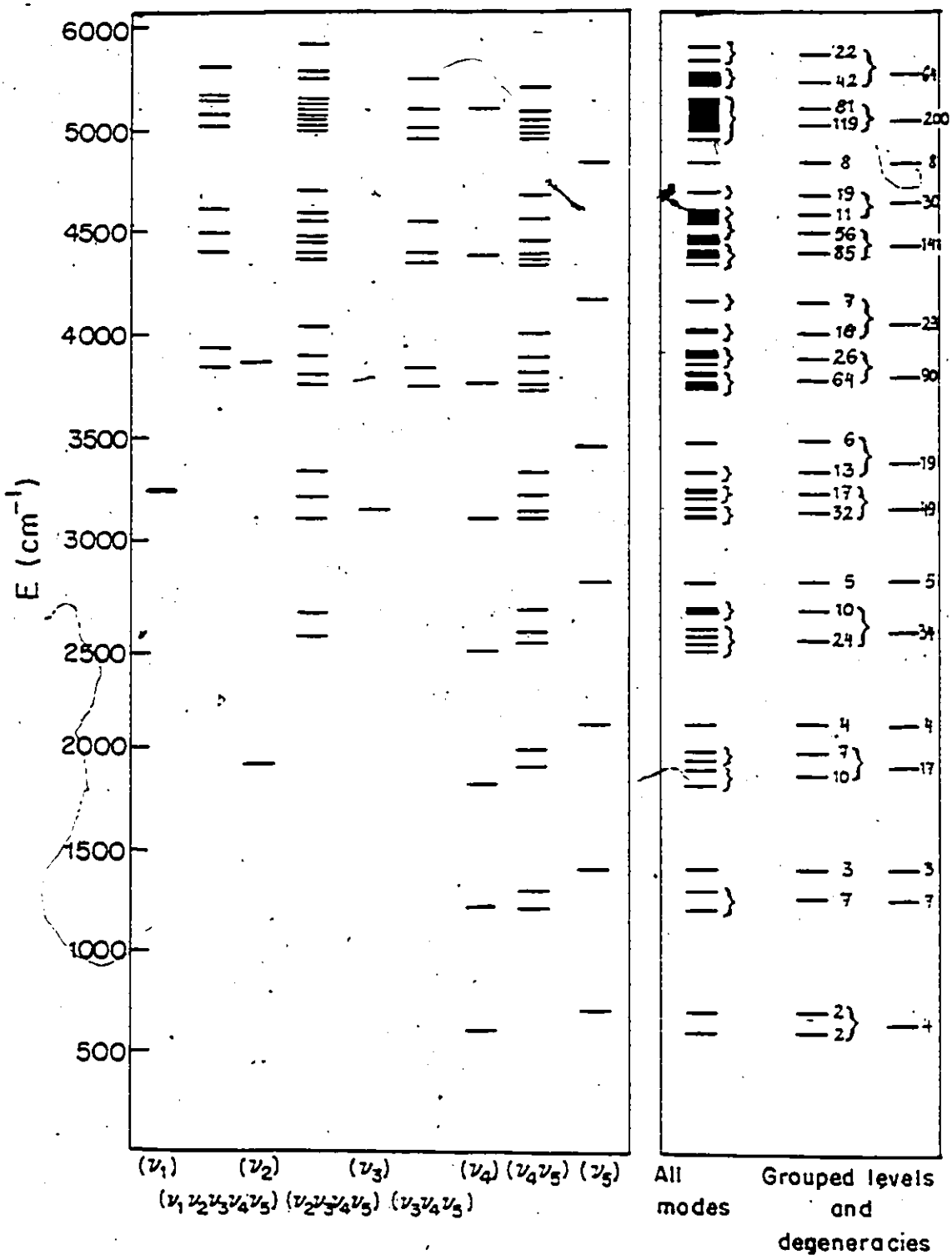

vibrational relaxation time of a number of polyatomic gases at 298 K from measurements of acoustic absorption. They obtained a vibrational relaxation time of 0.11 μsec.atm. for pure C_2H_2. Later, several authors measured the vibrational relaxation time of C_2H_2 using ultrasonic techniques. Lambert et al (72) measured a vibrational relaxation time of 0.0728 μsec.atm. at 298 K. Stretton (73) obtained a value of 0.082 μsec.atm. Springer et al (74), measured the vibrational relaxation time of C_2H_2, CH_4, C_2H_4, and C_6H_6 between 300 and 900 K. In all cases the vibrational relaxation times were found to vary with temperature according to the Landau-Teller law. For C_2H_2 the vibrational relaxation time is given by (74):

$$\log P\tau = 9.682T^{-1/3} - 8.577$$

This is represented graphically in fig. 1.10.

Häger et al (75) studied vibrational relaxation of C_2H_2 and C_2H_2-rare gas mixtures at room temperature using the laser induced fluorescence technique. Laser pulses from a parametric oscillator were used to excite (0,0,1,0,0) and/or (0,1,0,1,1) at 3300 cm^{-1}. Time dependent fluorescence signals from (0,1,0,0,0) and (0,0,0,0,1) were observed at 8 μ and 13.7 μ respectively. The fluorescence signal at 13.7 μ may be due to

$$(0,0,0,0,1) \longrightarrow (0,0,0,0,0)$$

$$(0,0,0,0,2) \longrightarrow (0,0,0,0,1)$$

$$\text{or } (0,0,0,1,1) \longrightarrow (0,0,0,0,1)$$

However, an absorption cell filled with C_2H_2 essentially in the ground state, interposed between the fluorescence cell and the I.R. detector, blocked 90% of the fluorescence signal proving

Figure 1.10 Landau-Teller plot for V-T (de)activation of pure C_2H_2 (literature results).

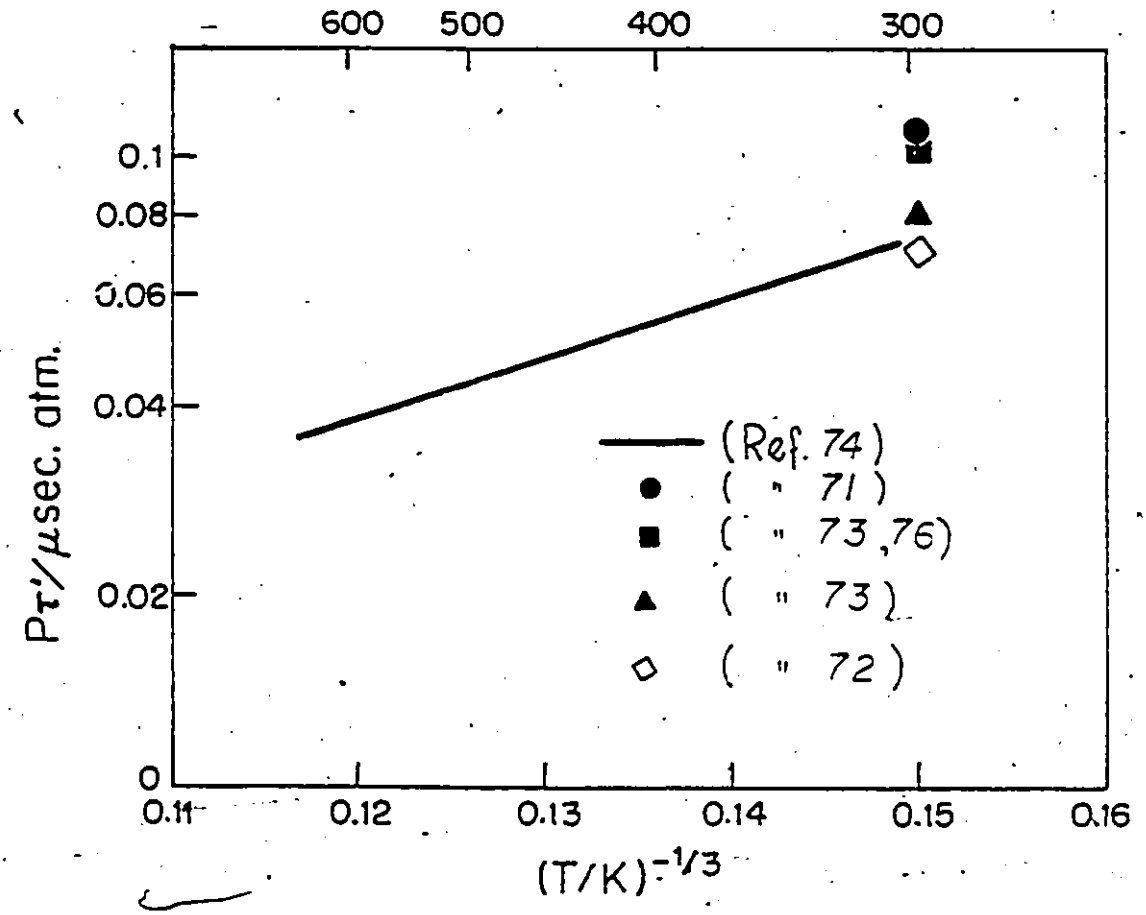

that the fluorescence signal at 13.7μ was mainly due to the (0,0,0,0,1) $\longrightarrow$ (0,0,0,0,0) transition. The fluorescence signal observed at 8μ was attributed by Hager et al to the

(0,1,0,0,0) $\longrightarrow$ (0,0,0,0,1)

transition. The results for (0,1,0,0,0) and (0,0,0,0,1) deactivation including gas kinetic collision numbers are summarized in table 1.4.

It is known (75) that following V-V intermolecular processes:

$C_2H_2(0,1,0,1,1) + C_2H_2(0,0,0,0,0) \longrightarrow C_2H_2(0,1,0,0,0) + C_2H_2(0,0,0,1,1)$

and

$C_2H_2(0,0,0,1,1) + C_2H_2(0,0,0,0,0) \longrightarrow C_2H_2(0,0,0,1,0) + C_2H_2(0,0,0,0,1)$

are very rapid. The depopulation of (0,1,0,0,0) cannot occur by a simple V $\longrightarrow$ T/R energy transfer step, since ΔE for such a process is -2000 cm^{-1}. The expected number of collisions per deactivation, according to the Lambert-Salter plot (fig. 1.1) is several orders of magnitude larger than the actual experimental one of 650. Consequently, the experimentally observed deactivation of (0,1,0,0,0) can only be interpreted as a pure V-V energy exchange to the neighboring combination of levels of lower fundamental frequencies. The combination modes (0,0,0,1,2), (0,0,0,2,1), and (0,0,0,3,0) are within KT of the energy of (0,1,0,0,0), thus V-V energy transfer to these modes is expected to be relatively rapid according to the propensity rules of Flynn, mentioned in Ch.1. Since the experimental deactivation of (0,1,0,0,0) is nevertheless slow, the authors assume that for

Table 1.4 Vibrational relaxation times (μsec.atm) and collision numbers for the deactivation of C_2H_2 by collision with C_2H_2 and with foreign gases at room temperature (75,76).

Collision Partner	(0,0,0,0,1) deactivation	Collision number	(0,1,0,0,0) deactivation	Collision number
C_2H_2	0.104	1090	0.0618	650
Ne	2.86	22100	2.09	16300
Ar	1.99	15600	1.69	13100
Kr	1.96	14400	1.41	10400
Xe	2.31	1800	1.71	13400
N_2	0.953	8000	1.31	11000
CO	0.550	4500	0.645	5300
H_2	0.0156	280	0.0424	700
HBr	0.0465	300	0.626	4100

C_2H_2, the usual rules for vibration relaxation in polyatomic molecules discussed in section 1.2 are not applicable and that the C-C stretching mode (0,1,0,0,0) seems to be isolated from the other vibrational modes and can store its energy for a long time.

The depopulation of (0,0,0,0,1) occurs after about 1100 collisions. Since (0,0,0,1,0) and (0,0,0,0,1) are very close in energy, a rapid equilibrium between these two vibrational levels will be established and the deactivation of (0,0,0,0,1) will take place through the (0,0,0,1,0) mode, (which is of lower energy).

Vibrational relaxation times and collision numbers for deactivation of (0,1,0,0,0) and (0,0,0,0,1) by collision with rare gases are also presented in Table 1.4. Collision numbers are 13 to 25 times larger than those for the self-relaxation of C_2H_2. This is due to the fact that rare gases cannot take up internal energy so that rare gases are less efficient in deactivating C_2H_2 than C_2H_2 itself.

Deactivation of C_2H_2 by H_2, HBr, N_2 and CO was also studied at room temperature by Hager et al (76) using the same technique as for pure C_2H_2 and the C_2H_2-rare gas mixtures. Results are summarized in Table 1.4. Deactivation of (0,0,0,0,1) by H_2 and HBr seem to be very rapid. Only roughly 300 collisions are required to deactivate (0,0,0,0,1). This type of behaviour also was observed with N_2O. These results are surprising; while the low collision number for deactivation of C_2H_2 by H_2 is expected, deactivation of C_2H_2 by collision with HBr is assumed to be less efficient and a higher collision number is expected. The low collision number observed experimentally for deactivation of

(0,0,0,0,1) by HBr was attributed by Hager et al to an attractive interaction between HBr and C_2H_2 or even to an incipient chemical reaction. N_2 and CO seem to slow down the deactivation of both (0,1,0,0,0) and (0,0,0,0,1), as was the case for rare gases. However N_2 and CO are more efficient than the rare gases; this is due to the additional possibility of V-V energy transfer processes which are rather efficient

$$C_2H_2(0,1,0,0,0) + N_2(v=0) \longrightarrow C_2H_2(0,0,0,0,0) + N_2(v=1) \quad \Delta E = 357 \text{ cm}^{-1} \qquad (1.25\text{ (a)})$$

$$C_2H_2(0,1,0,0,0) + CO(v=0) \longrightarrow C_2H_2(0,0,0,0,0) + CO(v=1) \quad \Delta E = 164 \text{ cm}^{-1} \qquad (1.25\text{ (b)})$$

Table 1.5 and figure 1.10 summarize most of the known results on the vibrational relaxation of C_2H_2. Relaxation times measured at room temperature are in good agreement. However, not many results have been published on the deactivation of C_2H_2 by collision with foreign gases nor on the dependence of the vibrational relaxation time on temperature. Therefore we cannot make any judgement on these results, as we did for N_2O.

1.5 Linear mixture rule

The linear mixture rule has been widely used to separate contributions to the rate constant from two or more collision partners. This rule states that if k_1 is the rate constant of the process $A + M_1 \longrightarrow B + M_1$ and k_2 is the rate constant of the process $A + M_2 \longrightarrow B + M_2$, where M_1 and M_2 are neutral species, then the rate constant k for the overall process A--> B is a linear function of k_1, and k_2:

$$k = X_1 k_1 + X_2 k_2 \qquad (1.26)$$

Table 1.5 Vibrational relaxation times (μsec.atm) of pure C_2H_2 at room temperature (literature results).

(0,0,0,0,1) or (0,0,0,1,0) deactivation	(0,1,0,0,0) deactivation	Experimental Technique	Authors and References
0.11		Acoustic	Edmonds and Lamb (71)
0.0728		U.S.*	Lambert and Salter (72)
0.082		U.S.	Stretton (73)
0.0754		U.S.	Wang (74)
0.104	0.0618	L.**	Hager (75,76)

* Ultrasonic technique

** Laser technique

where X_1 and X_2 are respectively the mole fractions of collisional partners M_1 and M_2. The linear mixture rule is used in vibrational relaxation , diatomic dissociation, unimolecular decomposition or isomerization at the low pressure limit. It can be represented graphically by a linear plot of the overall rate constant as a function of the mole fraction of one of the collision partners (fig. 1.11). In the case of vibrational relaxation of A (M_1=A), the intercept at X_1=1 gives the rate constant for the deactivation of A by itself and the intercept at X_1 = 0 gives the rate constant for the deactivation of A by M_2.

It has been seen in the previous two sections that several authors have used the linear mixture rule to extract the rate constant for the deactivation of N_2O and C_2H_2 by collision with foreign gases. In these examples the validity of the linear mixture rule has not been discussed by the authors. In this section, the validity of the linear mixture rule will be discussed in detail. The reason for the non-linearity as pointed out by several authors will be discussed.

It has been shown theoretically that the linear mixture rule does hold under very limited conditions. Pritchard et al (77) have pointed out that under conditions where V-V and/or R-R energy transfer are very important, a marked deviation from the linear mixture rule for dissociation will be observed. This was shown by direct integration of the master equation for dissociation of a non dilute diatomic gas. Linear mixture rules for dissociation hold in the limit of infinite dilution (78) otherwise, the disappearence of A, which is evidently one of the

Figure 1.11 Linear mixture rule.

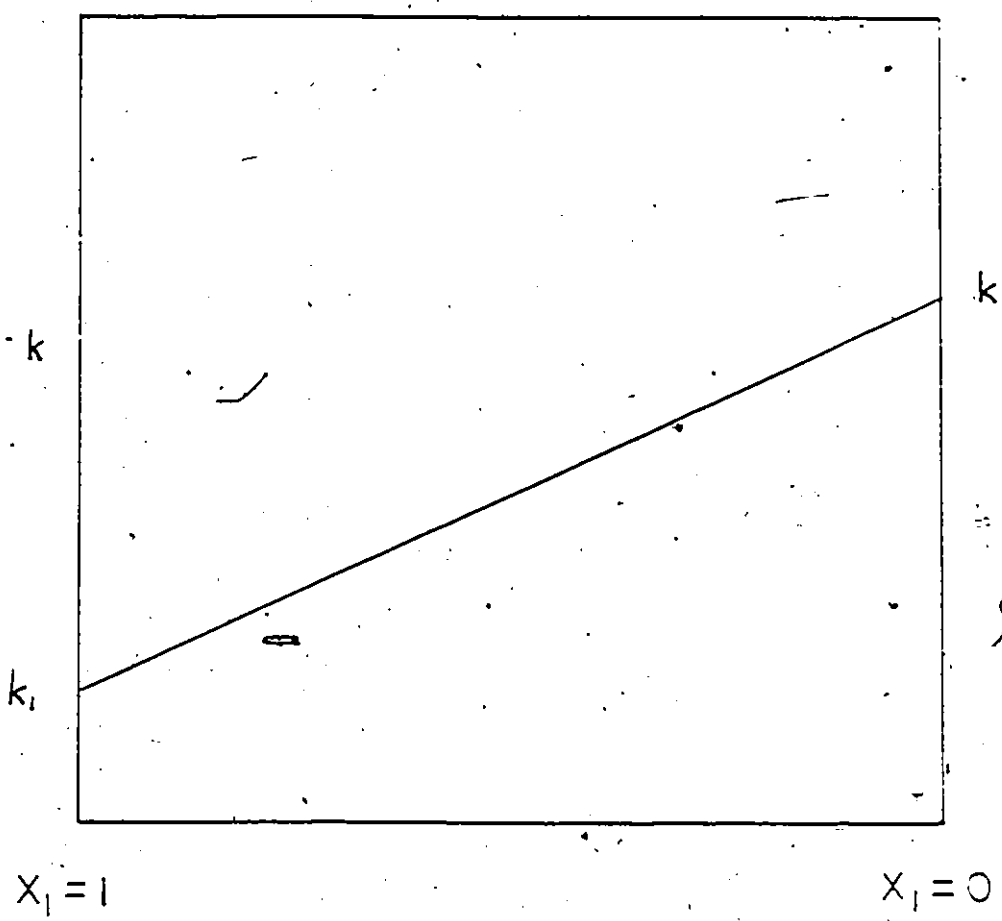

collision partners will be given by:

$$\frac{d[A]}{dt} = -k_1[A]^2 - k_2[M_2][A] \qquad (1.27)$$

This rate equation leads to a break-down of the linear mixture rule. Schlag and Valance (79) have shown that necessary conditions for the linear mixture rule to hold are: a) the process is out of the incubation or transient period and b) the reactants are in thermal equilibrium below the critical energy. If the equilibrium is disturbed during the reaction the linear mixture rule will break down, so that deviation from linearity is an indication of non-equilibrium processes. The linear mixture rule will hold only if the reverse reaction can be ignored i.e. if the products of dissociation do not recombine. In this way second order kinetics is avoided.

Two trivial conditions for the linear mixture rule to hold (78) for A $\longrightarrow$ B are: a) there is one level in A and a product state B; b) there are many levels in A but the microscopic rate constants for deactivation by collision with M_1 and M_2 are related by a constant factor. These conditions can not be absolutely satisfied in a real system and therefore the linear mixture rule can not be obeyed in general.

Troe (80) has given a theoretical treatment for polyatomic dissociation under non-equilibrium conditions. He concluded that the deviation from the linear mixture rule is within experimental error. Dove and Raynor (81) have shown that under conditions where vibrational and rotational energy distributions are not in equilibrium, contributions of collision partners to the

vibrational relaxation and to the dissociation rate constants cannot be added linearly. However, in both studies (80,81), the reactant is infinitely diluted in an inert gas, so that the effect of intermolecular V-V energy transfer can be neglected.

In a recent paper, Dove et al (82) solved the master equation for the vibrational relaxation of highly diluted mixtures of a molecule in two inert gases, by the eigenvalue method (matrix method). They reached the following conclusions:

a) the linear mixture rule is obeyed under very limited conditions: i) relaxation is near equilibrium, ii) relaxation proceeds by one single step, iii) the collisional pattern of the two inert species are similar.

b) deviations from linearity are always positive and vary from a few percent to a factor of two.

c) deviations from linearity are large when the difference between the collisional pattern for the two inert species is large.

d) great curvature in mixture plots occurs when a highly efficient collider is added to a mixture containing a collider of low efficiency.

Teitelbaum (29,78) studied the vibrational relaxation of a mixture of a diatomic molecule, AB, with an inert gas, M, by solving the detailed master equation for vibrational relaxation. V-V energy transfer and anharmonicity were explicitly considered and conditions for the validity of the linear mixture rule were examined. Only transitions between neighboring levels were allowed, $\Delta V = \pm 1$, and the Landau-Teller scaling law was used to

scale the rate constants. The general rate law was found to be;

$$\frac{dE}{dt} = -\frac{(\bar{E}-\bar{E}_\infty)}{\tau} - N_{AB}\, k^{2,0}_{1,1}\chi_e \left[\frac{2\bar{E}^2}{h\nu} + \bar{E} - \frac{\overline{E^2}}{h\nu} \right]_o$$

$$\exp - \left(\frac{N_{AB}\, k^{2,0}_{1,1}}{1-\chi_e} + \frac{2}{\tau}\right) t \qquad (1.28)$$

In this equation $k^{2,0}_{1,1}$ is the rate constant for the process

$AB(1) + AB(1) \longrightarrow AB(2) + AB(0)$.

$$1/\tau = X_{AB}(k^{AB}_{1,0} - k^{AB}_{0,1}) + X_M(k^M_{1,0} - k^M_{0,1}),$$

where $k^{AB}_{1,0}$ is the rate constant for the process

$$AB(1) + AB(0) \longrightarrow AB(0) + AB(0)$$

and $k^M_{1,0}$ is the rate constant for the process

$$AB(1) + M \longrightarrow AB(0) + M$$

E, E_∞, have been identified in section 1.1.3, N_{AB} is the total number of diatomic molecules, and χ_e is the Morse spectroscopic anharmonicity constant. The above rate law differs from the Bethe-Teller rate law (eq. 1.8) by an additional term due to V-V processes. The V-V contribution decays much faster than the V-T contribution if it can be assumed (as is usually the case) that $k^{2,0}_{1,1} >> k_{1,0}$. However, despite the small amount of energy change associated with V-V processes, for sufficient quantities of AB, $N_{AB}\, k^{2,0}_{1,1}$ can be much larger than $1/\tau$ and the amplitude of the V-V contribution may exceed that of V-T, particularily when the initial distribution is not Boltzmann. From eq. 1.28, it is clear that the vibrational relaxation time is not constant.

Only under conditions where the V-V term is negligible such as when $N_{AB} \longrightarrow 0$, or $k^{2,0}_{1,1} \longrightarrow 0$ or $\chi_e \longrightarrow 0$ or

$$[2\overline{E}^2/(h\nu) + \overline{E} - \overline{E^2}/(h\nu)]_o \longrightarrow 0,$$

can the vibrational relaxation time be constant. In the general cases where the initial population is not Boltzmann such as in laser excitation experiments or in chemical activation experiments, the rate of relaxation is not purely exponential and does not obey the Bethe-Teller law so that the vibrational relaxation time is not expected to be a constant. It is important in these cases to realize that a phenomenological rate "constant" is time dependent. This has been defined e.g. (29,78) by:

$$1/\tau'' = \frac{-d}{dt} (\ln dE/dt) \qquad (1.29)$$

and $1/P\tau''$ or $1/N\tau''$ can be written as a function of X_{AB} and depends on five additional parameters:

a) $\gamma = k^{2,0}_{1,1}/(k^{AB}_{1,0} - k^{AB}_{0,1})$: this represents the relative importance of V-V and V-T rate constants.

b) $\phi_M = (k^{M}_{1,0} - k^{M}_{0,1})/(k^{AB}_{1,0} - k^{AB}_{0,1})$: this is the relative V-T efficiency of M and AB.

c) $\vartheta = (\overline{E}_o - \overline{E}_{\infty,e})/\{ h\nu\chi_e[2/(\overline{E}/h\nu)^2 + (\overline{E}/h\nu) - \overline{E^2}/(h\nu)^2]_o\}$: this represents the deviation from equilibrium.

d) $\eta = C_{AB}/k$: this represents how classical the oscillating molecule is.

e) χ_e which is the anharmonicity constant.

Fig 1.12 shows the variation of the effective second order rate coefficient, ϑ, with the mole fraction X_{AB} at constant

Figure 1.12 Variation of the vibrational relaxation rate constant for a diatomic molecule as a function of mole fraction (Test of the linear mixture rule).*

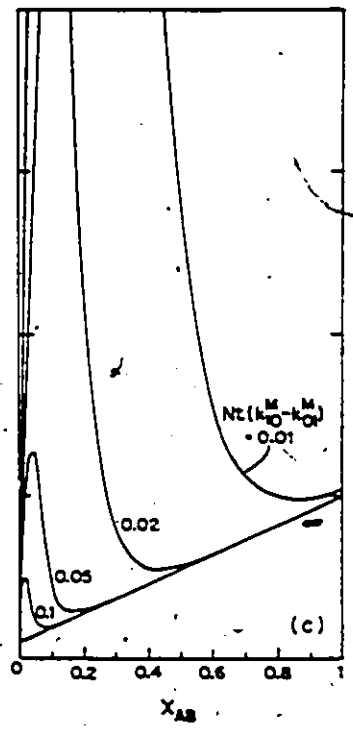

* Typical conditions used here are $\gamma = 100$, $\delta = 10$, $\chi_e = 0.01$, $\lambda = 4.5$, and $\phi_M = 0.1$.

From ref. 78

Nt $(k^M_{1,0} - k^M_{0,1})$ which is the most likely experimental situation. At early time, the non-linearity is evident. The deviation from linearity is always positive and exhibits a maximum. This maximum appears at low X_{AB}. It is due to the fact that even though at low X_{AB}, the V-V amplitude becomes smaller, its decay time becomes longer. These two properties of the V-V contribution compete and give a maximum at low X_{AB}. The linear mixture rule is observed only at equilibrium i.e. after several natural lifetimes from the begining of the relaxation process. At this time the rapid V-V rate has decayed leaving only the V-T rate, which is a linear function of the molar fraction. Consequently, from a limited range of X_{AB}, a linear extrapolation to $X_{AB}=0$ or $X_{AB}=1$ leads to false estimates of the limiting rate constants unless measurements are performed at equilibrium.

The effect of temperature on the linearity of the mixture rule is not straightforward. Teitelbaum (78) predicted that the non-linearity of the mixture rule for diatomics will be more pronounced at high temperatures, as has been observed experimentally (83) for polyatomics.

Rao and Mallu calculated the vibrational relaxation times of SO_2-Ar and CH_4-Ar mixtures between 300 K and 2000 K (84) as well as of CH_4-O_2 mixtures between 300 K and 1400 K (85) by using the SSH-Tanczos method (21). The reciprocal relaxation times were plotted as a function of the mole fraction at different temperatures. Their results show non-linearity in the mixture rule which becomes more pronounced at high temperatures, (fig. 1.13 (a), (b) and (c)). Rao suggested that V-V intermolecular

Figure 1.13 Variation of the vibrational relaxation times calculated by SSH-Tanczos method as a funtion of mole fraction (Test of the linear mixture rule).

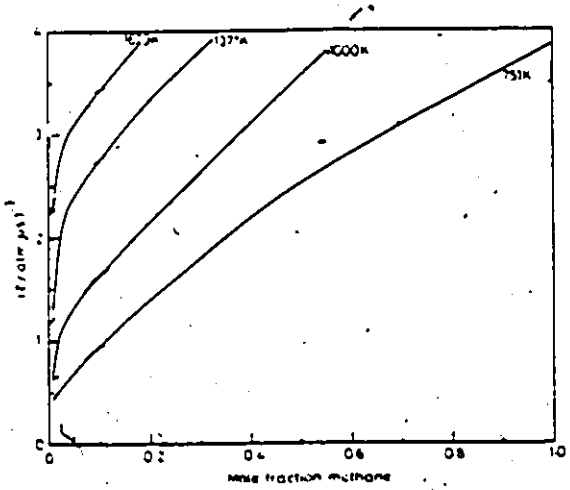

(a) Vibrational relaxation times in CH_4–Ar mixtures at different temperatures.

From ref. 84

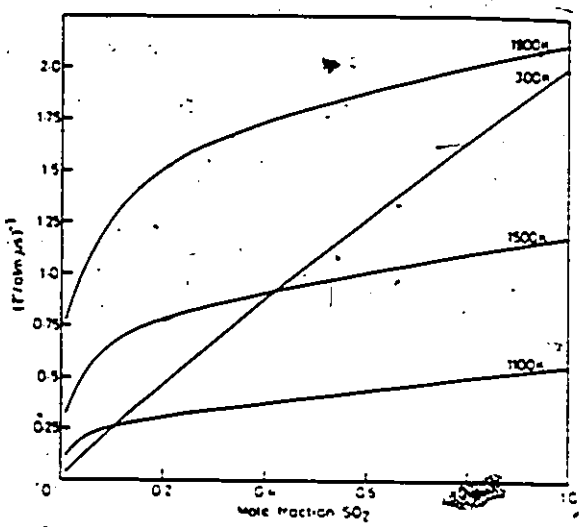

(b) Vibrational relaxation times in SO_2–Ar mixtures at different temperatures.

From ref. 84 ?

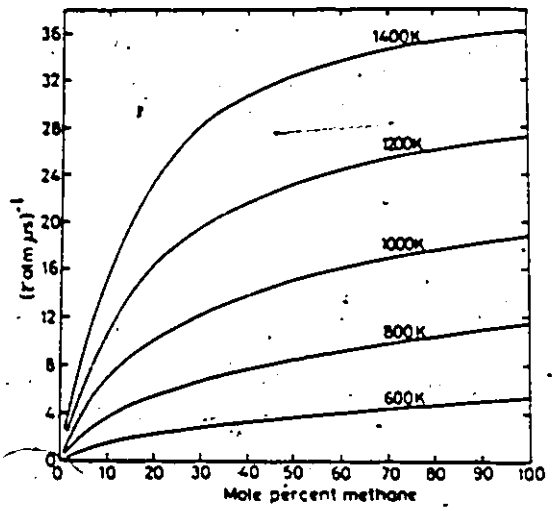

(c) Vibrational relaxation times in CH_4–O_2 mixtures at different temperatures.

From ref. 84

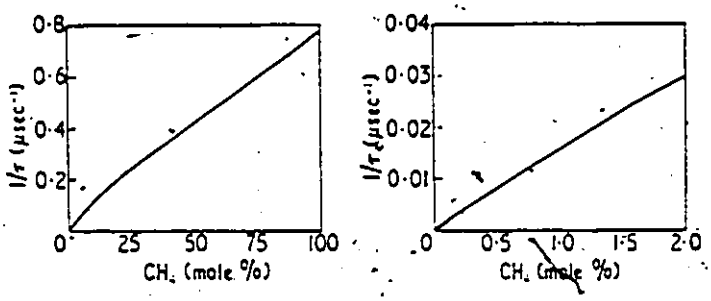

(d) Reciprocal effective relaxation time for O_2–CH_4 mixtures.

From ref. 86

exchanges are responsible for the non-linearity. Stretton et al (86) calculated the rate of vibrational relaxation for mixtures of O_2 with CH_4, CD_4, C_2H_4, H_2O, D_2O and HDO using the SSH-Tanczos method. A plot of the reciprocal relaxation time vs mole fraction of O_2 shows clear non-linearity in fig. 1.13 (d).

Up to now, the conditions for the validity of the linear mixture rule has been discussed. Some theoretical calculations which clearly indicate an expectation of non-linearity has been presented. Now some experimental results on this subject concentrating on three categories of experimental results will be presented.

In the first category, the mixture rule is found to be linear within experimental error (41, 67, 70, 87-93). However, the possibility of non-linearity cannot be excluded. In fact, the experimental error does not allow us to confirm the presence or the absence of linearity. Since there is no evidence for non-linearity in this category of experimental data, the linear mixture rule is explicitly or implicitly assumed by the authors to be valid! Several examples show this kind of behaviour. Hancock et al (87), measured the vibrational relaxation times of DF-Ar mixtures between 198 K and 296 K using the laser fluorescence technique. At 264 K and 296 K, the reciprocal of the vibrational relaxation time was found to be linear with mole fraction (fig. 1.14 (a)) However, at 232 K, deviation from linearity was apparent (fig. 1.14 (b)). This behaviour is probably due to the dimerization of DF. The rate of vibrational relaxation of HF-Ar mixtures has also been studied by Hancock et

Figure 1.14 Examples where the linear mixture rule seems to be obeyed.

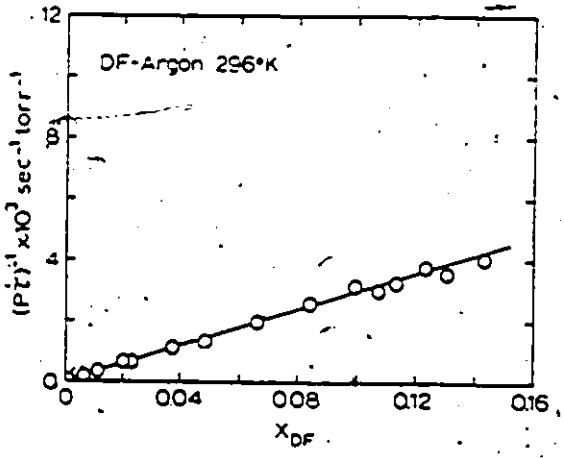

(a) Observed DF excitation and quenching rates as a function of DF molefraction in argon at 296 °K.

From ref. 87

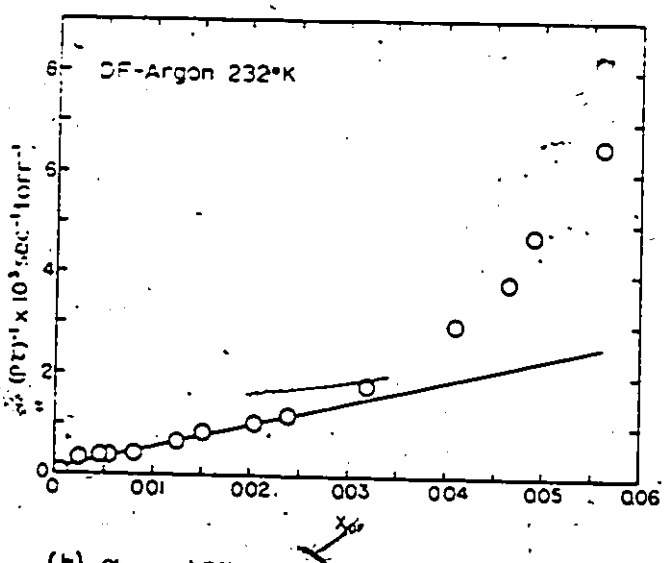

(b) Observed DF excitation and quenching rates as a function of DF molefraction argon at 232 °K.

From ref. 87

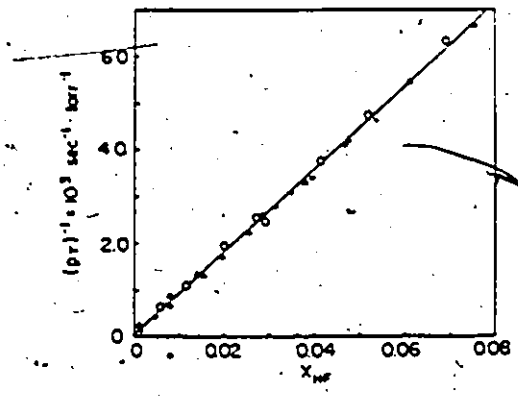

(c) Vibrational relaxation rates in HF–Ar mixtures as a function of HF mole fraction. The intercept is $k_{HFAr} = 60 \pm 30$ sec^{-1}-torr^{-1}, and the slope $(k_{HFHF} - k_{HFAr}) = (8.74 \pm 0.06) \times 10^6$ sec^{-1}-torr^{-1}. Data were taken at fixed argon pressures: + at 81.4 torr, O at 49.9 torr, and △ at 41.4 torr.

From ref. 88

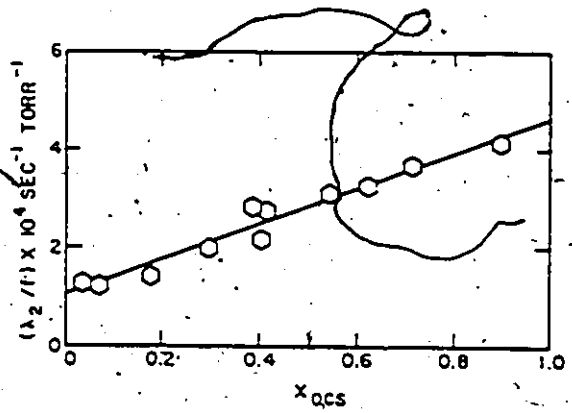

(d) Vibrational relaxation rates in OCS–CO mixtures. Experimental relaxation times varied between 3.8 – 126 μsec for OCS and CO partial pressures in the range 0.41–7.6 torr and 0.19–17.0 torr, respectively.

From ref. 66

Continued

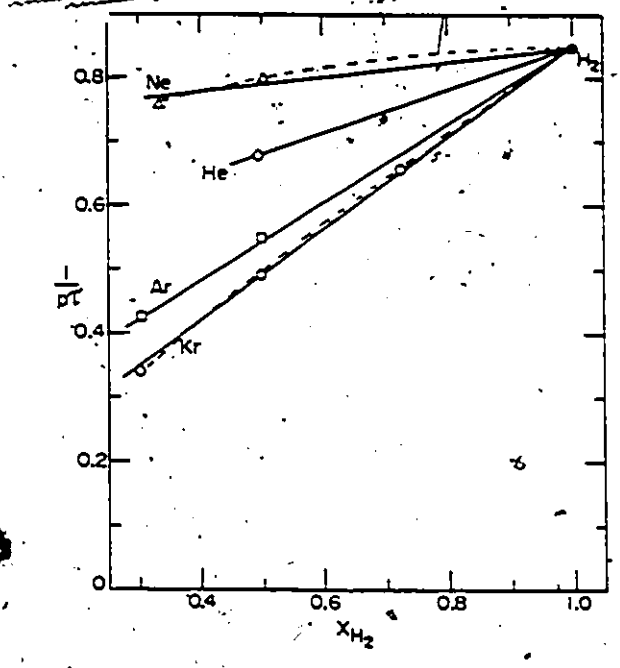

From ref. 94

(e). Graph showing test of linear mixture rule. Plot of inverse standard relaxation times of experimental mixtures at 2000 K, as a function of mole fraction of H_2. The mixture points were obtained from fits of the experimental points to Landau–Teller expressions. For the ternary mixtures, the relatively small effect of Kr has been subtracted, so that x_{H_2} and pr for these cases are effective values. The straight lines have been drawn to pass through the point for pure H_2

From ref. 95

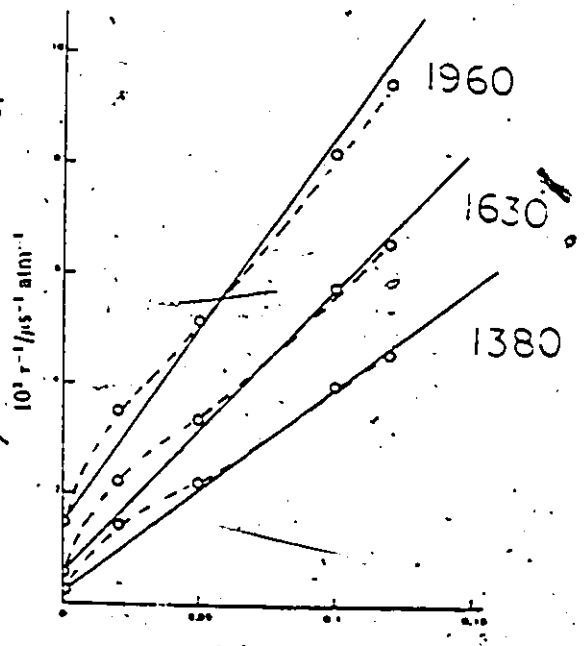

(f)—Plot of reciprocal experimental relaxation time against mole fraction for mixtures of CO with HCl at three temperatures. Values of T/K given against the curves.

al (88) using the laser fluorescence technique. Mixtures with mole fractions down to 0.001 of HF were measured. The plot of $1/P\tau$ vs X_{HF} seems to be perfectly linear between X_{HF} = 0.001 and 0.08 mole (fig. 1.14 (c)). However, linear extrapolation up to X_{HF}=1 gives results which differ markedly from the results of pure HF, thus indirectly indicating non-linearity. Hancock et al (66) measured the vibrational relaxation of OCS(0,0,1)-CO mixtures between X_{OCS}=0,02 and X_{OCS}=0.9. Despite the large enough range of mole fraction we cannot see any evidence for nonlinearity (fig. 1.14 (d)). In many cases, the plots of the reciprocal of the relaxation time vs mole fraction seem to be linear within experimental error. However, the range of the mole fraction is not large enough to allow us to decide on this conclusively.

In the second category of experimental data, the linear mixture rule was assumed to hold within experimental error. However, non-linearity can be easily observed. Several examples show that non-linear plots give a better representation of the mixture rule than linear ones. Dove et al (94) measured the vibrational relaxation of H_2 in several inert species. Their results are represented in fig. 14(e): It seems that a curve gives better representation of their $1/P\tau$ vs X_{H_2} data. Borrel et al (95) measured the vibrational relaxation of HCl-CO mixtures in a shock tube. Their results are shown in fig. 1.14(f). Again here, a curve gives a better fit to the experimental data. This also may indicate a break-down of the linear mixture rule. Several other examples show that a curve gives much better fit to

experimental data than a straight line (96-101). This leaves some doubt about the validity of the linear mixture rule in the examples mentioned in category one.

In the third category of experimental data, the linear mixture rule clearly breaks down. Several examples in the literature exhibit a nonlinearity in the plot of the reciprocal vibrational relaxation time vs mole fraction (50,83,102-105). Fig. 1.15 shows two examples of such a plot (taken from ref. 105). In this figure, the mixture rule for CH_4-Ar and N_2O-Ar vibrational relaxation are presented at different temperatures. Distortion from linearity is most evident at mole fractions <0.02, and is most pronounced at high temperatures.

In summary, non-linearity arises when experimentalists force a fit of the data to a first order rate law, whereas mixed first and second order kinetics might be a better representation of the data. Second order V-V processes are very important at the beginning of the relaxation; they are responsible for the deviation from linearity which arises from pure first order kinetics. Non-linearity becomes very important at high temperatures. Non-linearity arises for dissociation reactions also when the reactants are not in thermal equilibrium below the critical energy. And finally, several experimental data show that the linear mixture rule is not generally valid.

1.6 Justification for the present study

Previous results on the vibrational relaxation of polyatomic molecules seemed ambigious and at best inconclusive. For example, literature data on the vibrational relaxation of N_2O are

Figure 1.15 Examples showing failure of the linear mixture rule.

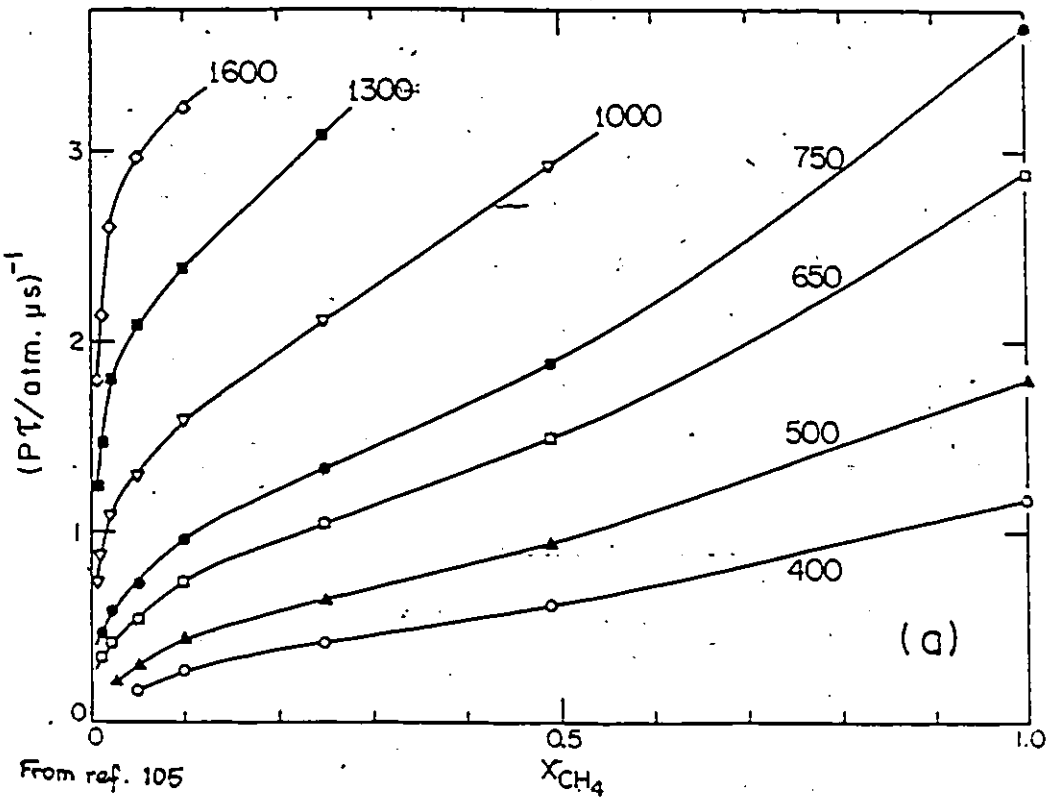

From ref. 105

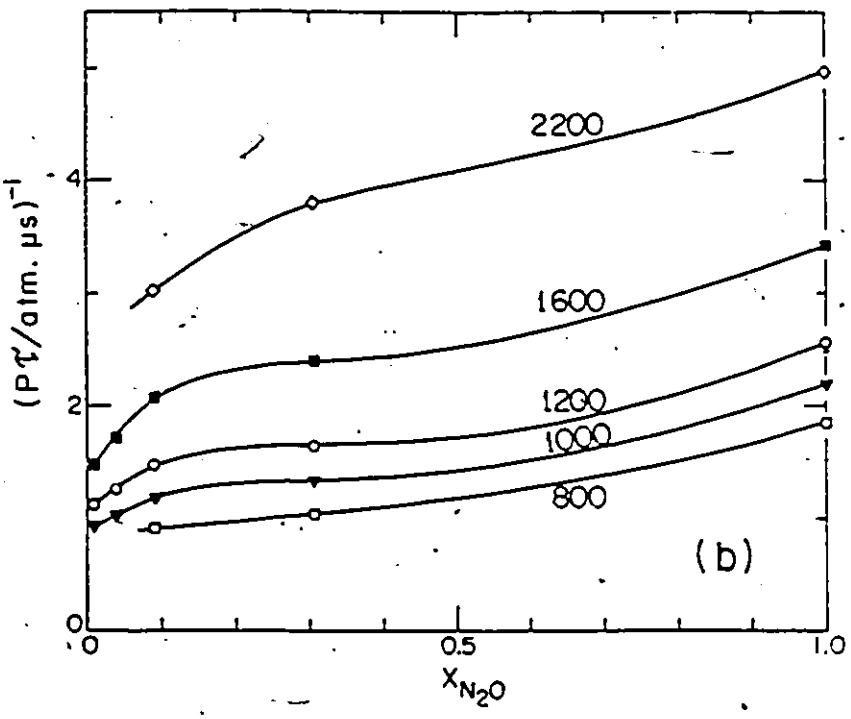

From ref. 105

in conflict with each other. Furthermore, while most of the theoretical studies on the linear mixture rule predict the failure of this rule, many experimental results show that the linear mixture rule is obeyed (within experimental error). For these reasons we have decided to study the vibrational relaxation of polyatomic molecules in some detail in order to understand the mechanism of the relaxation and see why most of the data on polyatomic molecules are in conflict. We chose N_2O for such study as a model compound because this molecule has been widely tested and the reported data are in contradiction. On the other hand acetylene is less known, it relaxes extremely fast (~20 times faster than N_2O), its structure (i.e. vibrational level diagram, symmetrization, number of atoms per molecule) is different from N_2O. Acetylene will therefore provide additional information on the structure - relaxation relationships.

CHAPTER 2: EXPERIMENT

A shock wave technique has been used to measure the vibrational relaxation time of N_2O, C_2H_2, and C_2H_2-Ar mixtures. The shock tube has been widely used over the last 30 years to study vibrational energy transfer, combustion, isomerization, dissociation, ionization ...etc. It is a very valuable tool for the study of physical and chemical processes at high temperatures, because, not only working temperature, pressure and gas compositions can be varied over a wide range, but also because the shock generated process can be monitored by a variety of instrumental methods.

2.1 Sound waves and shock waves

The ideal sound wave is a reversibly, isentropic, adiabatic process. It is propagated through the gas by collision between molecules, and there is no net flow of the gas molecules in the direction of the propagation of the wave. It can be shown that the propagation velocity, of a sound wave is:

$$a = \sqrt{(C_p/C_v)P/\rho} = \sqrt{(C_p/C_v)RT/W} \qquad (2.1)$$

where W and ρ are respectively the molecular weight and the density of the gas.

A shock wave is produced when a disturbance is forced through a gas with a velocity greater than the velocity of the sound wave. When a shock wave is produced, a sudden increase in the pressure, the temperature and the density of the gas occurs, and the molecules will be set in motion in the same direction as the shock wave. Unlike the sound wave, the shock wave is an irreversible with positive entropy change process.

2.2 Formation of the shock wave

A shock wave is produced in the laboratory by a shock tube. A shock tube consists basically of two sections separated by a thin diaphragm which can be burst when required (fig 2.1 (a)); One section is filled with a high pressure gas (the driver section), and the other section is filled with a relatively low pressure test gas (the test section). When the diaphragm is burst (by mechanical means or under the high pressure of the driver gas), a shock wave is formed. This rapidly moves at a supersonic velocity and rushes out to compress the test gas. Within a short time, the gas flow becomes steady, and a sharp, planar boundary (the shock front) separating the unheated test gas from the heated gas is formed. Behind the shock front, the contact surface separating the driver gas from the heated gas moves at lower velocity than the shock front (fig. 2.1 (d)). Simultaneously, an expansion wave or a rarefaction wave moves back into the driver section at the speed of sound. This wave is characterized by a falling temperature.

The variations of the pressure and the temperature along the shock tube are shown in fig.2.1 (b) and (c). The pressure and temperature rise sharply from T_0 and P_0 in the unshocked gas to T_1 and P_1 at the shock front, and remain constant (if no chemical or physical changes to the hot gas result) until the contact surface. Behind the contact surface, in the driver gas, the temperature falls down below the room temperature T_0 then rises slowly in the rarefaction zone to reach T_0. The pressure rises slowly in the rarefaction zone to reach the initial pressure P_3

in the driver section.

The thermodynamic states are determined by the initial conditions of the unshocked gas, the shock wave velocity and the conservation laws of fluid mechanics. This will be discussed later in section 2.6. At the shock front, the kinetic energy of the gas entering the shock front reaches equilibrium in only a few collisions. For most polyatomic molecules, rotational equilibrium is essentially reached in less than 10 collisions. However, the vibrational energy requires typically several thousands of collisions to reach equilibrium. The temperature profile for translational, rotational and vibrational "temperatures" of the shock front are shown in fig. 2.2(a). Initially translational degree of freedom is excited, this causes the translational temperature to increase. Energy is transferred from translational to rotational and then to vibrational degrees of freedom. This causes the translational and rotational temperatures to fall and the vibrational temperature to increase in the shock wave. The density is inversely proportional to the temperature and varies as shown in fig. 2.2(b). The variation of the temperature and the density behind the shock front can be directly related to the chemical and physical processes occuring behind the shock front. In section 2.7 we shall discuss this in terms of vibrational relaxation.

2.3 Shock Tube

The nickel coated steel shock tube used in our laboratory is schematically represented in fig. 2.3. The low pressure section (internal dimensions 6.8 cm X 6.8 cm) is 319 cm long. The high

Figure 2.1 The shock tube (showing pressure and temperature variation).

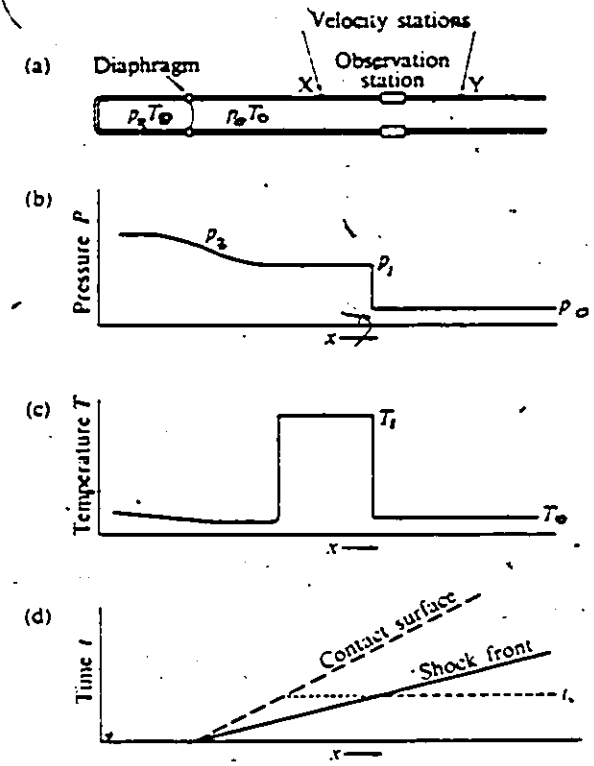

From ref. 17

Figure 2.2 Relaxation behind a shock front.

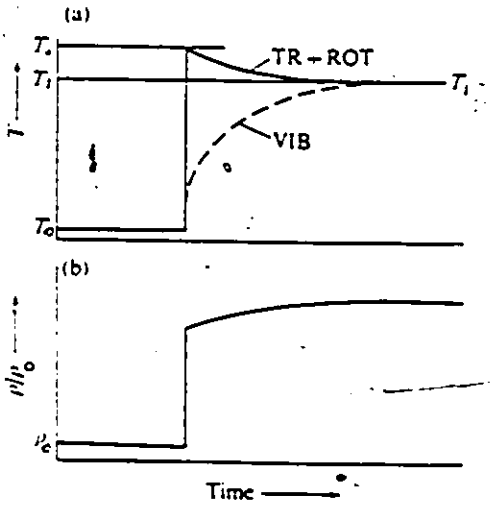

From ref. 17

Figure 2.3 Shock tube and gas handling system

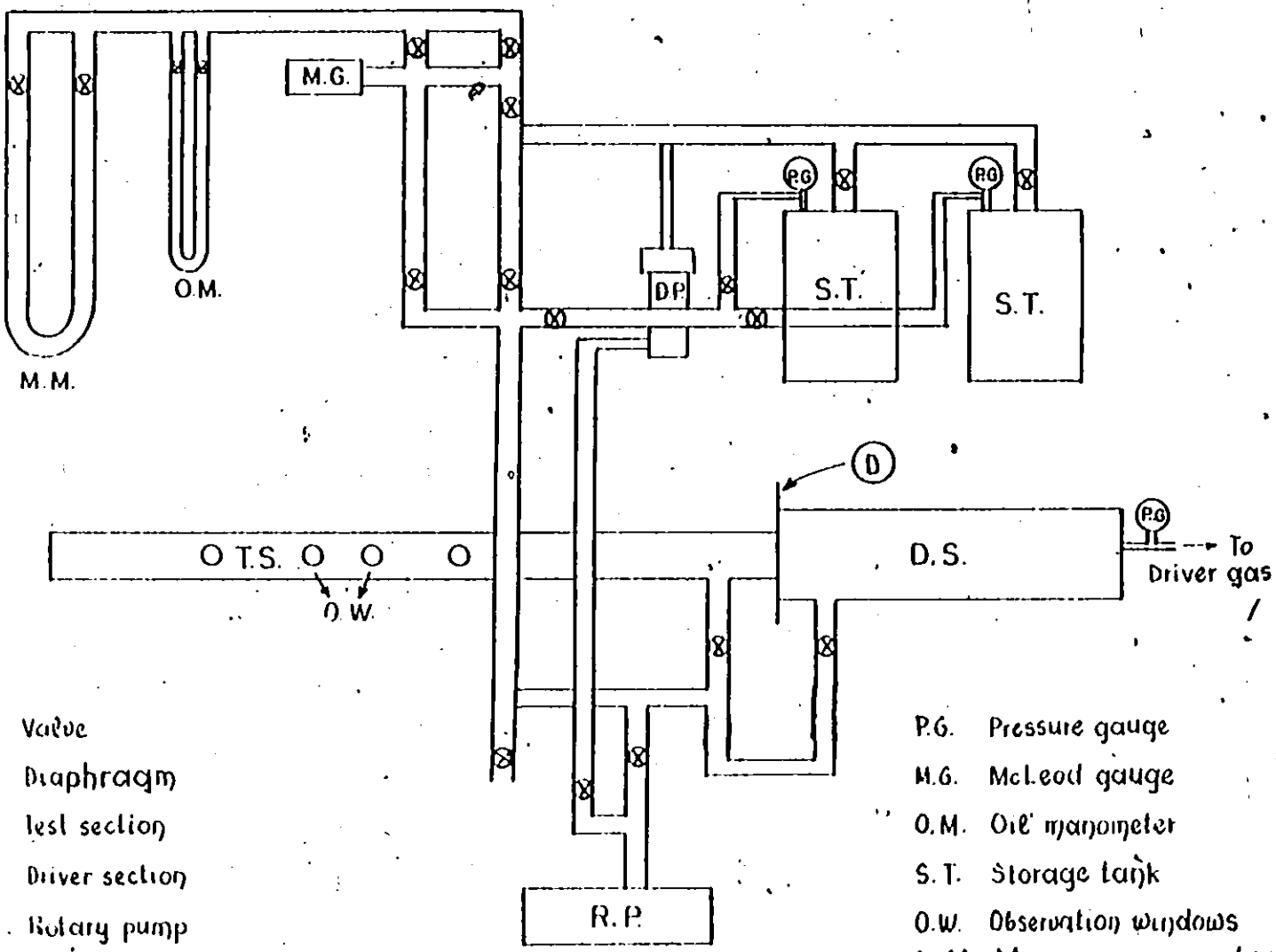

pressure section (9.5 cm internal diameter) is 123 cm long. These two sections are separated by an aluminum foil diaphragm of varying thickness.

The pressure of the test gas varies from 0.5 to 20 torr, and the pressure of the driver gas (He) required to burst the diaphragm depends on the strength of the aluminum foil - in our case:

90-130 torr for Alcan regular household aluminum foil (~0.02 mm thickness)

110-160 torr for Reynolds household aluminum foil (~0.02 mm thickness)

190-250 torr for Reynolds aluminum foil (heavy duty) (~0.04 mm thickness)

250-600 torr for extra thick Alcan Aluminum foil (~0.1 mm thickness)

The latter foils were scratched diagonally with a pencil or a screw driver in order to create a controllable variety of diaphragm strengths.

2.4 Gas handling system and gas mixtures

Steel storage tanks of 235 l capacity were used to prepare the gas mixtures. They were evacuated to a pressure of less than 10^{-2} torr by a rotary pump (EDWARDS EDM 12) and down to approximately 10^{-5} torr by an oil diffusion pump (SPEEDIVAC EDWARDS HIGH VACUUM LTD). Acetylene (99.6% pure from Matheson) was distilled twice and then acetylene-Argon mixtures were prepared at least 24 hours before use. Mass spectrometric analysis showed no impurities in the mixtures. Nitrous oxide (99.99% pure from Matheson) and Ultra-high purity Argon (>99.99% purity from Matheson) were used directly from the cylinder

without any further purification.

Gases were introduced into the test section from the mixture storage tanks for C_2H_2 and C_2H_2-Ar mixtures and directly from the cylinder for N_2O. Pressures in the test section could be measured, using a calibrated McLeod gauge for pressures less than 1.5 torr or by a calibrated oil manometer for pressures between 1.5 and 5 torr or by a calibrated mercury manometer for pressures higher than 5 torr. The driver gas, He, (99.995% pure from Air Products) was introduced directly from the cylinder into the driver section until the diaphragm burst spontaneously.

Leaks in the shock tube and in the tanks were tested routinely using a He-Ne mass spectrometer leak detector (VARIAN 925-40). The outgassing rate in the shock tube varied between 10^{-3} and 10^{-4} torr per minute and the time between the filling of the shock tube and the initiation of the shock wave was kept to less than one minute.

2.5 Measurement of shock wave velocity

The shock wave velocity can be measured by determining the time taken by the shock wave to travel between successive laser beams crossing the shock tube perpendicularly at several positions roughly 40 cm apart (fig. 2.4). A He-Ne laser (6328 Å) (SPECTRA PHYSICS 120) was used for this purpose. The laser is split into two beams of equivalent intensity with a beam splitter. One beam is used for the quantatative laser schlieren system and the other part for the shock wave velocity determination system, which also makes use of the Schlieren effect (see section 2.7 for details of the laser Schlieren

Figure 2.4 Observation section.

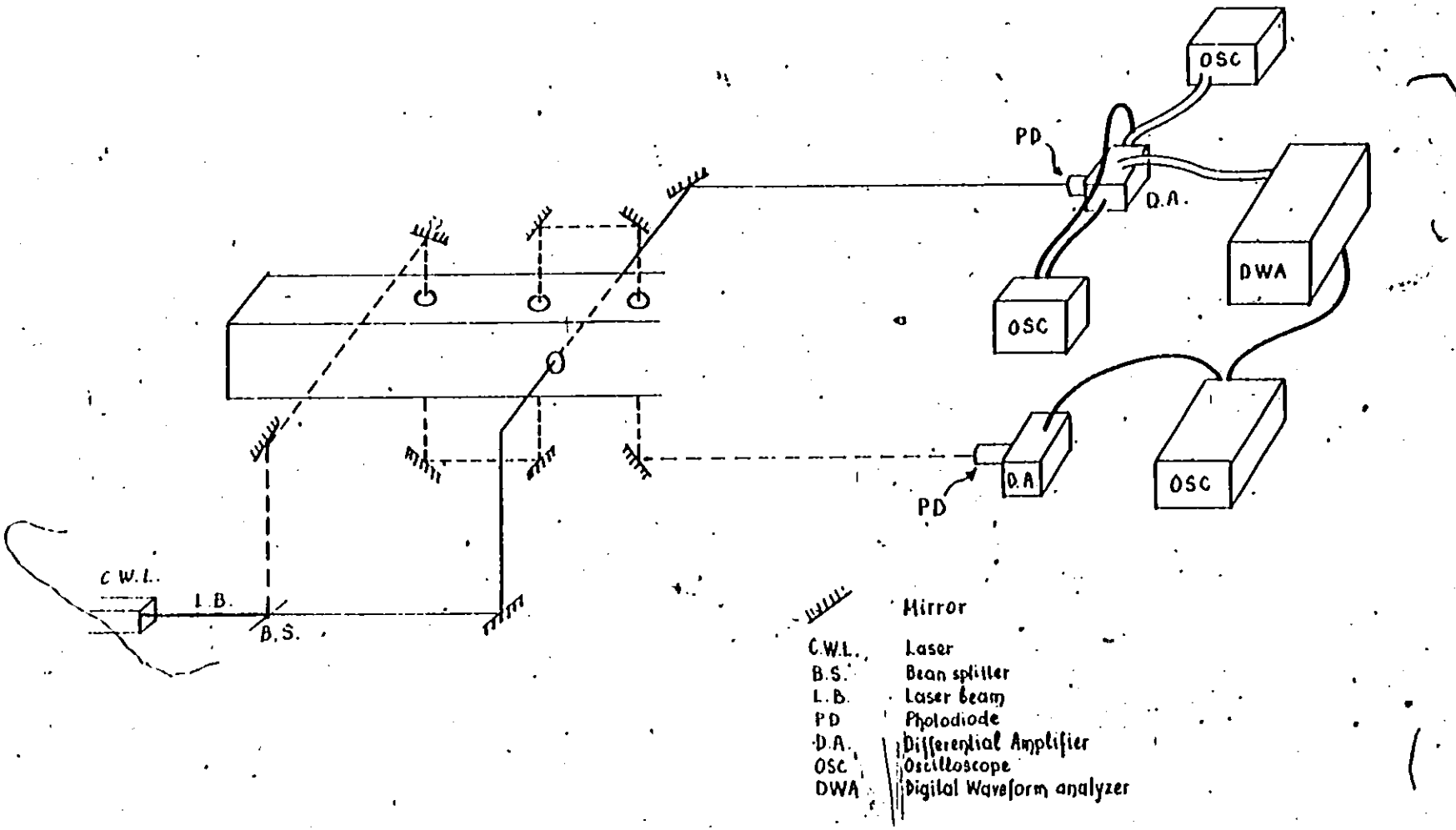

effect). This latter beam crosses the shock tube perpendicularly at three different positions by means of 4 mirrors through flush fitting sets of windows. The windows are of Schlieren quality (flat to 1/20 of a wave length). The deflection of the laser beam by the shock wave at any of the 3 positions can be detected by a four quadrant-connected photodiode (see section 2.8 for more details). The signal due to the deflection of the laser beam was amplified using sets of summing and differential amplifiers constructed in our laboratory (see section 2.8). The signal was displayed and stored on a digital oscilloscope (NICOLET 290-111). Knowing the distances between the laser beams and the time taken by the shock wave to travel between two successive positions (one sees a series of alternating positive and negative spikes, one for each interaction), the shock wave velocity can then be measured with an accuracy better than 1%.

2.6 Shock wave parameters

Shock wave parameters can be calculated by solving the Rankine-Hugoniot equations for shock flow (13, 105, 107) and by using thermochemical data (108) and the measured shock velocity. Under the assumption of no heat exchange in the shock wave, no chemical reactions, no radiation and that the test gas is initially at rest, the Rankine-Hugoniot equations for a real gas can be reduced to:

$$\rho_o U_o = \rho_e U_e \qquad \text{for mass conservation} \qquad (2.2\ (a))$$

$$P_o + \rho_o U_o^2 = P_e + \rho_e U_e^2 \qquad \text{for momentum conservation} \qquad (2.2\ (b))$$

$$h_o + U_o^2/2 = h_e + U_e^2/2 \qquad \text{for energy conservation} \qquad (2.2\ (c))$$

In these equations, the subscripts o denote initial conditions in the test gas, and e conditions where all degrees of freedom are excited; i.e. thermal equilibrium. U_o is the shock wave velocity, ρ is the density and h is the energy of the gas.

Two additional equations are used,

$$R = P_o W_o/(\rho_o T_o) = P_e W_o/(\rho_e T_e) \qquad (2.3)$$

the ideal gas law and

$$h = (1-X_o)(5/2)RT + X_o((7/2)RT + E) \qquad (2.4)$$

for linear molecules, where E is the vibrational energy and X_o is the mole fraction of the vibrating molecule, $(1-X_o)$ is the mole fraction of the inert diluting gas (Ar in our case).

From eq. 2.2 (a) and 2.2 (c), U_o can be obtained;

$$U_o = \sqrt{\frac{2(h_e-h_o)}{(1-\rho_o^2/\rho_e^2)}} \qquad (2.5)$$

From eq. 2.2 and 2.4 ρ_o/ρ_e can be obtained;

$$\rho_o/\rho_e = [1/(2T_o)][-2(F-T_e+T_o)+(2F-T_e+T_o)^2+4T_oT_e] \qquad (2.6)$$

where $F = (W_o/R)(h_e-h_o)$

For a given T_e, we have ρ_e and U_o. P_e is easily determined from (2.3). We now draw graphs of T_e vs U_o and P_e vs U_o. By interpolation from these graphs we can deduce the pressure and temperature from a measured shock velocity.

2.7 Laser Schlieren system

In the laser Schlieren system the time dependence of the laser beam deflection (which is proportional to the density gradient caused by the energy transfer) is measured and hence the rate of vibrational relaxation is determined.

The principle of the laser schlieren system has been

discussed in detail by Teitelbaum (13) and by Kiefer et al (109). A brief résumé of the mathematical equations involved in calculation of the vibrational relaxation time is given below.

Under conditions where (a) the refractive index $\eta = 1$, (b) deflections are small and (c) the laser beam is perpendicular to the axial flow, the deflection of the laser beam by a refractive index gradient $d\eta/dy$ is given (107, 110) by:

$$\theta = l\, d\eta/dy \qquad (2.7)$$

where l is the internal dimension of the test section and y is the coordinate of the laser beam in the shock tube (See fig 2.5).

The relation between the refractive index, η, and the gas density, ρ, is given by the Gladstone-Dale law (111):

$$\eta = 1 + \beta\rho \qquad (2.8)$$

where β is the specific refractivity of the gas. θ is then given by:

$$\theta = \beta\, l\, d\rho/dy \qquad (2.9)$$

The second term of eq. 2.8, $\beta\rho$, is negligible compared to 1 for gases, and therefore, condition (a) is satisfied. Condition (b) is also satisfied under our experimental conditions (the largest deflection was 10^{-4} radians). Condition (c) is easily satisfied (see section 2.9).

In a mixture of several gases, the specific refractivity β is related to the individual specific refractivities of each component, β_i, by (110):

$$\beta = \Sigma \beta_i X_i W_i \,/ \Sigma X_i W_i \qquad (2.10)$$

where X_i and W_i are respectively the mole fraction and the molecular weight of component i.

Figure 2.5 Laser beam deflection on photodiode.

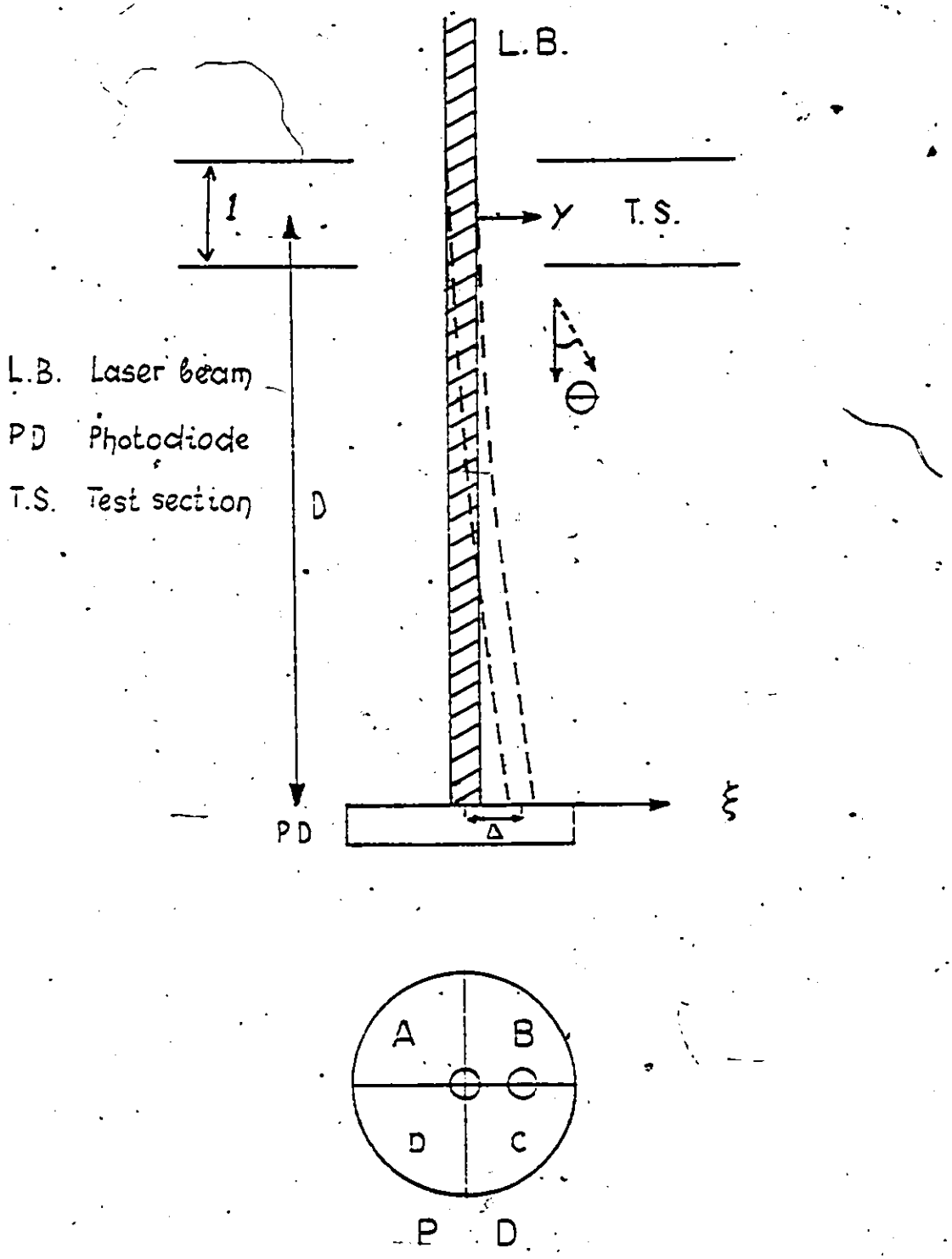

For small deflections, θ, the displacement of the laser beam on the photodiode is given by $\Delta = D\theta$ where D is the distance from the centre of the shock tube to the photodetector (fig. 2.5). Hence, the deflection at the photodiode is:

$$\Delta = \beta D 1 d\rho/dy. \qquad (2.11)$$

Kiefer (109) has shown that in the limit of large D (as in this case), geometric optics can be applied except for the beam-shock front interaction. Then, if y is the coordinate of the laser beam in the shock tube, the coordinate, ξ, at the photodetector is:

$$\xi(Y) = ya/a_o + \Delta = ya/a_o + \beta 1 D d\rho/dy \qquad (2.12)$$

which is a sum of the deflection due to the density gradient Δ, and the divergence inherent in the laser beam, a/a_o, where a_o and a are the laser beam radii at the shock tube centre and at the photodiode respectively.

It has been shown (13) that the voltage generated by the shock wave deflection is given by:

$$V = V_o G \sqrt{\frac{8}{\pi}} \frac{\beta 1 D}{a} \frac{\Delta \rho}{\tau^* U} \exp\left(-\frac{t_1}{\tau^*}\right)\left(1 - \frac{a_o K}{aU\tau^*}\right)^{-1} \qquad (2.13)$$

where G is the gain of the amplifier, V_o is the maximum signal, t_1 and τ^* are respectively the time and the relaxation time in laboratory coordinates and $K = \beta 1 D \Delta\rho/(U_o \tau^*) \exp(-t_1/\tau^*)$. A plot of log V vs t_1 should give approximately a straight line with slope:

$$S = -1/(2.303\,\tau^*)$$

and intercepts:

$$\log V_o G \sqrt{\frac{8}{\pi}} \frac{\Delta \rho}{\tau^* U} \frac{\beta 1 D}{a} \left(1 - \frac{a_o K}{aU\tau^*}\right)^{-1} \qquad (2.14)$$

The observation section for the laser Schlieren system is schematically represented in fig. 2.4. The laser beam crosses the shock tube at right angles through optically flat windows and falls perpendicularly onto a four-quadrant photodiode. The deflection of the laser beam caused by the vibrational energy transfer is detected by the photodiode, amplified with an amplifier developed in our laboratory (see section 2.8 for details), and then stored in a digital wave form analyser of 10 nsec horizontal resolution and 0.1/256 volt vertical resolution (Gould Biomation 8100). Some time after the experiment is completed the digital signal is extracted and displayed on a digital oscilloscope (a second channel of the same one used for the shock wave velocity determinations). The laser-Schlieren method is known for its high spatial and temporal resolution (rise time of 0.02 μsec. and spatial resolution of $\sim$0.05 mm for shock wave velocity between 1.5 and 2.1 mm/μsec. (13)). The minimum density gradient which could be measured is determined by the statistical noise. It is equal to 10^{-9} g/cm^4, and the maximum density gradient was found to be 10^{-3} g/cm^4 (13).

The beam splitter, and mirrors are mounted on standard optical benches. The laser and optical benches rest on the same large piece of concrete (~1000kg) supported by several thick rubber stoppers. In this way vibrational frequencies greater than 12 Hz can be damped out. However, since both the source and detector are oscillating in phase, the only noise measured is the inherent electronic noise and that due to laser instability. The heavy shock tube itself is clamped to the concrete floor of the

laboratory, thus avoiding recoil of the shock tube itself. The shock tube was not in physical contact with the optics.

2.8 Photodiode and amplifier

A four-quadrant photodiode (United Detector technology PIN-SPOT/8) of 1 cm^2 active area, 0.5 mA/mW sensitivity, 0.25 mA dark current, 25 pf capacity and a noise power of $2x10^{-8}$ watts has been used to detect the laser deflection beam. It provides a fast (one nsec. response time) and efficient response to visible light (signal to noise ratio better than 20,000:1) (13). Each quadrant is connected to an external lead. The current generated by each quadrant is given by:

$$V_i = r_i s_i p_i \qquad (2.15)$$

Where p_i is the light power falling on it, s_i is the sensitivity of the quadrant and r_i is the load resistor (100Ω) (fig. 2.6)

The leads A and C are connected to a differential video amplifier (Fairchild μA733C) of 10 nsec rise-time and low noise in order to maintain a good response quality. The leads B and D are also connected to a second differential amplifier (fig.2.6). The two differential signals can be subtracted and added at the input of the digital waveform analyzer and then displayed on the Nicolet oscilloscope. Then:

$$V_1 - V_2 = rsG\,(p_B + p_C - p_D - p_A) \qquad (2.16\ (a))$$

and

$$V_1 + V_2 = rsG\,(p_B + p_A - p_D - p_C) \qquad (2.16\ (b))$$

where G is the gain of the amplifier.

$V_2 - V_2$ is the difference between the laser light falling on the right half and the left half of the photodiode. Hence V_1 -

Figure 2.6 Photodiode and amplifier operation.

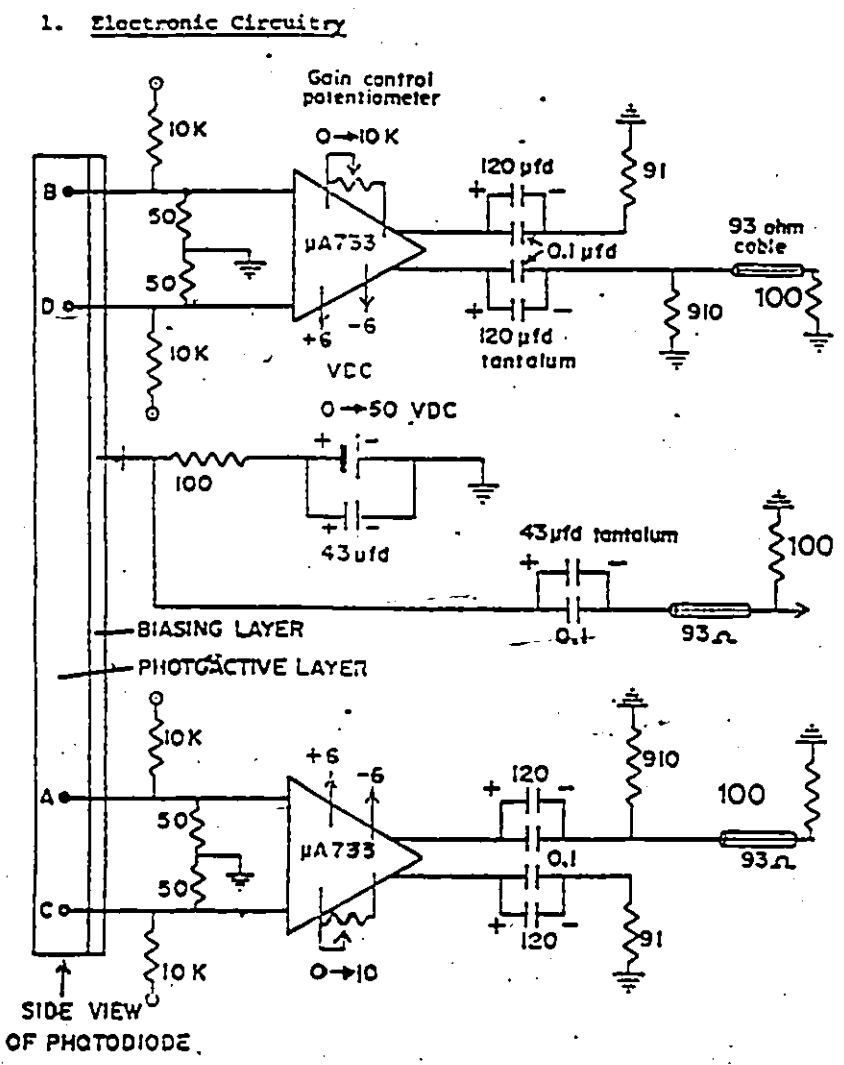

adapted from ref. 13

V_2 measures the deflection in the horizontal direction which is caused by the density gradient of the shock wave. Similarly, $V_1 + V_2$ would be a measure of the laser beam deflection in the vertical direction.

A third signal generated by all four elements of the photodiode summed together is also obtained and can be fed into a third oscilloscope. The source of this signal is the bias potential of the photodiode (fig. 2.6). If the deflection of the laser beam is large or if stray scattered light enters the photodiode, the amplitude of this signal will change. In preliminary experiments we found no unusual signs of stray light, or of large deflections beyond the beam-shock front interaction. Therefore we did not monitor the signal on a regular basis.

The unamplified signal from each quadrant can also be followed by measuring the potential drop across a 10 K resistor connected in series with each of the four elements (fig. 2.6). These were continuously monitored in 2 sets of differential pairs to ensure that the beam was centered on the photodiode.

The photodiode and the electronic circuit of the amplifier including storage capacitors are protected from pickup or interference by housing the ensemble in a single solid metal box. The box can be displaced and rotated in all directions by mounting it on the optical bench. Short terminated cables ensured a time response of better than 0.1 μsec. This was checked by imposing a pulsed signal from a wave form generator. The rise time was found to be better than 0.1 μsec.

2.9 Calibration and alignment of the schlieren optical system

Calibration and alignment of the schlieren optical system was performed periodically. Before any measurement could be done we had to ensure that the unamplified signals measured at each quadrant were the same. This was accomplished by measuring the voltage generated by using an oscilloscope (Telequipment Oscilloscope Type 01011) when the laser beam falls entirely on each of the four quadrants. It was found that all four signals were identical within less than 0.1%.

The gain of each differential amplifier could be adjusted by measuring the amplified signal from any two adjacent quadrants and then changing the potentiometer until the two amplified signals equalized. The gain can be measured by comparing the amplitude of the amplified and the unamplified signals.

The laser beam can be centered on the photodiode by measuring the differential signal simultaneously from two horizontally adjacent and two vertically adjacent quadrants. The photodiode is displaced vertically and horizontally until null output is obtained from both differences. This calibration is necessary before each experiment.

The following one-time alignment was performed before any measurement could be done. First, the horizontal boundary of the photodiode was made parallel to the shock tube axis in order to ensure that the measured voltage generated by the shock wave corresponds to the axial density gradient. A straight line was drawn on the outer shock tube wall parallel to the shock tube axis. Then the mirror which reflects the laser beam onto the

photodiode was rotated around its vertical axis and the trajectory of the reflected laser beam on the shock tube wall was compared to the line drawn on the shock tube wall. If the trajectory of the reflected beam was parallel to the line drawn, the vertical axis of the mirror was therefore normal to the shock tube axis. If this were not the case, the position of the mirror was adjusted until the two axes were perpendicular. The reflected laser beam was then allowed to fall onto the photodiode. The mirror was again pivoted around its vertical axis and the laser beam swept across the photodiode face. The generated voltage was observed on the oscilloscope. If the "horizontal" photodiode boundary was parallel to the shock tube axis, the generated voltage $(V_1 + V_2)$ would be constant and remain unchanged throughout the entire displacement of the laser beam. If this was not the case, the photodiode was rotated in its socket around the axis perpendicular to its face until the desired constant signal was obtained.

The laser beam crossing the shock tube and falling onto the photodiode should be normal to the shock tube axis and to the horizontal boundary of the photodiode respectively. This condition could be met by superimposing the incident laser beam with the reflected one from the observation windows of the shock tube and the photodiode surface respectively at a distance of several meters. The laser beam was kept normal to the shock tube axis and to the photodiode in the horizontal plane. However, in the vertical plane along which we expected no schlieren deflections a slight deviation from normality was deliberately

made in order that the photodiode not reflect radiation back into the laser source.

2.10 Experimental procedure and observation

Before any experiment, the shock tube was evacuated down to $\sim 10^{-2}$ torr using a rotary pump then down to a pressure of $\sim 10^{-5}$ torr using diffusion pumps (same pumps used to evacuate the storage tanks). The test gas was introduced into the test section. Before introducing the driver gas (He) and bursting the diaphragm, the laser beam was centered at the photodiode to make sure that all four quadrants generated the same voltage. The Biomation and the Nicolet oscilloscopes were reset. Then the driver gas was introduced at a pressure high enough to burst the aluminum diaphragm. The strength of the shock wave depended on the driver pressure, and this could be controlled by varying the thickness and the strength of the aluminum diaphragm. When the shock wave crossed the laser beam used for the velocity measurement, three spikes were successively registered on the Nicolet oscilloscope allowing the shock wave velocity to be measured (see sections 2.5 and 2.6). When the shock wave crossed the laser beam destined for the quantitative laser schlieren system, the waveform analyzer (Biomation) was triggered by the signal generated by the shock front itself, and the signal thus registered in the Biomation unit, was later transferred to the Nicolet oscilloscope and stored on a magnetic disc. Since the Biomation unit was equipped with a pretriggering function it was easy to observe the signal even before shock arrival and thus have an unequivocal zero base line.

Fig. 2.7 shows a typical example of a laser schlieren signal obtained from a mixture of 5% C_2H_2 in Ar. This signal like all other signals is characterized by a small negative and large positive spikes caused by interaction of the laser beam with the curved shock front itself, and a nearly exponential decay which is due to the density gradient during relaxation of the test gas. Only one part of the relaxation zone is observed in the laser schlieren signal, the other part is covered by the shock front itself. A plot of the logarithm of the voltage vs time might give a straight line if the decay is truly exponential, or a mild curve if this is not the case. For some experiments we obtained a straight line within the experimental error. For some other experiments, a mild curve gave a better representation of the decay. However, from one single experiment it is impossible to draw any conclusion about the shape of the log-plot of the voltage vs time curves, for three important reasons a) We are measuring only a small portion of the relaxation zone. Over one or two natural lifetimes, it is difficult to distinguish a sum of 2 exponentials one of which decays at say twice the rate of the other from a pure exponential decay by graphical means. b) In the unhidden signal, the signal to noise ratio near equilibrium is relatively small for molecules that decay as fast as N_2O or C_2H_2, so that we could not measure subtleties in a single experiment despite the well known capabilities of laser schlieren for high precision sensitive measurements. c) In any experiment, there is a finite temperature change, which in principle affects the value of $P\tau'$ (the vibrational relaxation time in gas particle

Figure 2.7 Laser schlieren signal for C_2H_2-Ar mixture.

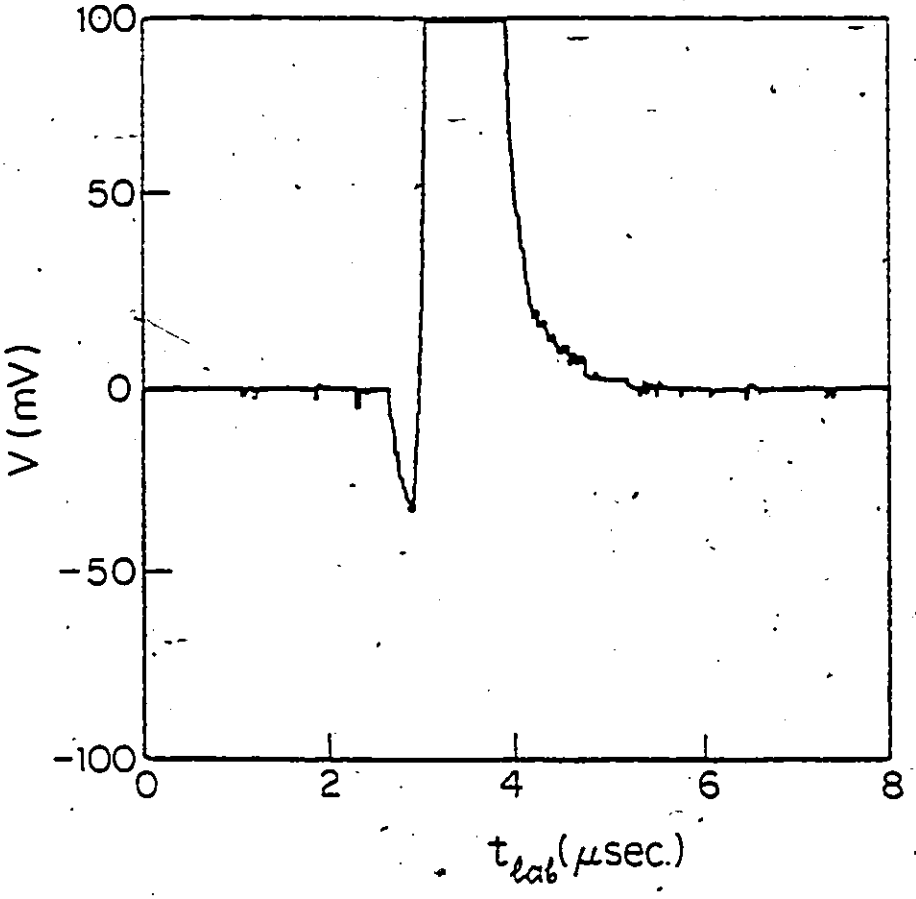

5.0% C_2H_2 Ar mixture, P_o = 2.75 torr,
P_D = 314 torr, U_o = 1.396 mm/μsec.,
Te = 1841 K, Pτ = 0.137 μsec. atm.

coordinates). Thus a time dependent $P\tau'$ does not necessarily imply anything about the intrinsic constancy of $P\tau'$. In fact we needed to extend the time regime in order to decide about the shape of the log-plot curves. This could be achieved by varying the initial pressure of the test gas. Increasing the pressure of the test gas has two important effects on the laser schlieren signal: a) it increases the signal size and therefore increases the signal-to-noise ratio, b) it extends the time regime. In fact $P\tau'$ is the constant in question. At higher P, τ' decreases. At a fixed measuring time, t (~1 μsec), the measurement corresponds to a larger t/τ'.

A large number of experiments were performed at different test gas pressures and different driver gas pressures. A wide range of temperatures and time regimes were accessible for pure gases and for mixtures. This sytematic variation of our experimental conditions allowed us to study the effect of the time regime on the vibrational relaxation time at fixed temperature and the effect of temperature on the vibrational relaxation time at fixed time as well as the effect of temperature and of time on the validity of the linear mixture rule. All of these results are discussed in detail in the next chapter.

2.11 Data reduction

Three methods were used to calculated vibrational relaxation times of pure gases and of mixtures. The Blackman method (112), Kiefer's method (109) and a point-by-point analysis developed by Teitelbaum (83).

The first method is based on the validity of the Bethe-Teller law. The vibrational relaxation time is assumed to be constant, the measured voltage is an exponential decay and a plot of the logarithm of the voltage vs time is nearly linear. The slope, S, of the log-plot of the voltage is directly related to the vibrational relaxation time. The reciprocal of the slope 1/(2.303S) is indeed the apparent vibrational relaxation time in laboratory coordinates (laboratory time), τ^*. The laboratory time t_l, is related to the gas particle time t_g during which the gas molecules have actually been heated. From considerations of the gas compression, it can be shown (106) that the time for which the gas particles have been in the shock wave is given by $\int_0^t \rho/\rho_0 dt$ which is approximately $t_l \rho/\rho_0$. Therefore the relaxation time in gas-particle coordinates is obtained by multiplying 1/(2.303S) by the equilibrium density ratio.

The specific heat C_p can be written in the form:

$$C_p = C_p' + C_{vib} \qquad (2.17)$$

where C_p' is the specific heat due to the external degrees of freedom and C_{vib} is the contribution to the specific heat due to vibration. It turns out that the vibrational relaxation time as determined from the slope of a log plot should be multiplied by the specific heat ratio $C_p/(C_p-C_{vib})$ in order to correct the results for the variation of the translational temperature. At low temperatures, the fractional population of the vibrationally excited molecules is very small and the ratio $C_p/(C_p-C_{vib})$ is very close to 1. At high temperature, the population of vibrationally excited molecules is high. C_{vib} then becomes

important and the ratio $C_p/(C_p - C_{vib})$ can approach 2 in extreme cases. Finally, by multiplying the relaxation time by the equilibrium pressure in atm, one normalizes the results to one atmosphere. The final expression for the vibrational relaxation time in gas particle coordinates is then:

$$P\tau' = -\frac{\rho_e}{\rho_o}\ \frac{C_p}{C_p - C_{vib}}\ \frac{p_e}{p_o}\ \frac{p_o}{760}\ \frac{1}{2.303S} \qquad (2.18)$$

This procedure, due to Blackman (112), assumes no coupling between the rate equation and the hydrodynamic equations. It was used in this work to obtain a good approximation of $P\tau'$ and its temperature dependence.

In a more rigorous procedure due to Kiefer (109), the rate of change of the density is measured at each point of time, Thus, one can obtain an estimate of the vibrational relaxation time at each point of time, according to the following phenomenology:

$$P\tau' = \frac{-P(1-dE_\infty/dE)}{d/dt\ \ln(\tau dE/dt)} \qquad (2.19)$$

dE/dt can be written as:

$$dE/dt = (dE/d\rho)(d\rho/dy)(dy/dt_1)(dt_1/dt_g)$$
$$= (dE/d\rho)(d\rho/dy)(U_o)(\rho_o/\rho) \qquad (2.20)$$

Also

$$dE_\infty/dE = (dE_\infty/dT)(dT/d\rho)(d\rho/dE)$$
$$= C_{vib}(dT/d\rho)(d\rho/dE) \qquad (2.21)$$

In the point-by-point analysis, an analytical expression based on a solution of the Hugoniot equations and their derivatives is obtained. The vibrational relaxation time is

given by:

$$P\tau'' = \frac{-(E-E_\infty)\rho}{(dE/d\rho)(d\rho/dy)U_o\rho_o}\left[(P_o + P_oU_o^2(1-\rho_o/\rho)\right] \quad (2.22)$$

In this equation τ'' is a phenomenological relaxation time defined by:

$$\tau'' = \frac{-(E-E_\infty)}{dE/dt}$$

The first step in the point-by-point method as well as in Kiefer's method is to convert the voltage profile to a density profile. If we assume that the density gradient in the hidden region is exponential and the time origin is at the shock front, the density of the first point can be calculated by integrating from $t_1=0$ to t_1. Since we do not know whether the density profile is of an exponential form or not, and we were not sure that the time zero corresponds to the arrival of the shock front to the laser beam, we decided to start the integration from the end near equilibrium. One major problem arises from this integration. This problem is due to the fact that near equilibrium the signal is too small to characterize $(E-E_\infty)$ and hence τ' precisely. Furthermore, since τ' at all times depends to varying degrees on ρ, i.e. on the integration, residual error is found at all times.

Table 2.1 shows an example of a calculation of the vibrational relaxation time of pure N_2O by the three methods discussed above. In the point-by-point method the vibrational relaxation times are very small near equilibrium and increase gradually as time decreases to reach a constant value. It is

quite likely that this behavior is due to the buildup of error resulting from backwards integration. On the other hand, the constant values of the vibrational relaxation time calculated by the point-by-point method were 30 to 50% less than those calculated by the Blackman method. We believe that this smaller value of $P\tau''$ calculated by the point-by-point method (a different phenomenology than the Blackman or Kiefer method) is already an indication of non-constancy of relaxation times.

If we compare the $P\tau'$ values calculated by Blackman's method to those calculated by Kiefer's method we find that the difference is less important; in fact $P\tau'$ calculated by Blackman's method is only 5-10% larger than that calculated by Keifer's method. Since our aim was to determine the variation of $P\tau'$ with time and temperature, any method will help us to achieve this. For this purpose we used the relatively simple Blackman method.

The accuracy of the vibrational relaxation times measured by the Blackman method depends mainly on the slopes of lnV vs t_1 plots. Other factors such as the ratio of the densities, temperatures and pressures behind the shock wave, the ratio of the heat capacities and the initial pressures were more than 99 % accurate. Thus, precise measurement of the slope of the ln V vs t_1 plots is the most important parameter determining the precision of our measurements. This depends on the type of molecules, i.e., for N_2O, the measured τ^* (lab-scale) is relatively high (τ^*=0.224-1.42 μsec.) and the precision on the vibrational relaxation time was always better than 5%. On the

Table 2.1 Vibrational relaxation times of pure N_2O deduced by 3 different methods. (Initial conditions: P_o=2.28 torr, P_D=140 torr, T_o=295 K, U_o=0.933 mm/μsec.)

Thermodynamic Variables	t_1 sec	V mVolt	$P\tau'$ (1) μsec.atm.	$P\tau''$ (2) μsec.atm.	$P\tau'$ (3) μsec.atm.
$\frac{T_e}{T_o}$ = 2.38	3.07	92.8	0.416	0.230	0.400
	3.22	80.0	"	0.228	0.400
	3.38	67.2	"	0.231	0.400
$\frac{P_e}{P_o}$ = 13.9	3.58	56.0	"	0.228	0.399
	3.78	46.4	"	0.224	0.399
	4.13	30.4	"	0.235	0.398
$\frac{\rho_e}{\rho_o}$ = 5.83	4.41	24.6	"	0.218	0.398
	4.67	17.6	"	0.227	0.397
	4.93	13.9	"	0.216	0.396
	5.23	11.3	"	0.212	0.394
	5.53	7.50	"	0.198	0.392
	5.93	4.96	"	0.178	0.390
	6.33	3.28	"	0.146	0.384
	6.73	2.17	"	0.098	0.387

(1) Blackman's method

(2) Point-by-Point method

(3) Kiefer's method

N.B. τ^* = 0.967 μsec.

other hand, measurement for C_2H_2 and C_2H_2-Ar mixtures is more difficult because of the speed of the relaxation ($\tau^* = 0.095$-0.86 μ sec) and the errors in the measured vibrational relaxation times were better than 15 %.

CHAPTER 3: EXPERIMENTAL RESULTS

3.1 Vibrational relaxation of pure N_2O

A total of 70 experiments were performed with pure N_2O. Results are summarized in table A.1, appendix A, and represented graphically in fig. 3.1 to 3.9. By solving the Rankine-Hugoniot equations (see section 2.6), the thermodynamic variables ρ_e/ρ_o, P_e/P_o and T_e/T_o can be calculated and represented graphically (Fig. B.1 - B.3, appendix B),. From the velocity measurements, all thermodynamic variables can be determined with better than 1% accuracy.

The ratio $C_p/(C_p-C_{vib}) = C_p/(7/2R)$ is calculated from the C_p values at different temperatures given in the JANAF thermochemical tables (108). A plot of $C_p/(C_p-C_{vib})$ vs. temperature is shown in fig. B.4, appendix B. From the equilibrium temperature T_e, the ratio $C_p/(C_p-C_{vib})$ can be determined for each individual experiment.

In Table A.1, the most important parameters in the relaxation process are summarized. The initial pressure of the test gas P_o varied from 0.16 to 25.8 torr, and the pressure in the driver section , P_D, required to burst the aluminum diaphragm varied from 119 torr to 703 torr. The slowest shock wave (U_o=0.569 mm/μsec.) corresponds to the lowest temperature (T_e=451K), and the fastest shock wave (U_o=1.987 mm/μsec.) corresponds to the highest temperature (T_e=1893K). Since a large portion of the relaxation zone is dominated by shock front interference at the beginning of the relaxation, and since the signal-to-noise ratio near equilibrium is low in the majority of

our experiments, measurements started after a minimum of 0.97 μsec. and ended after a maximum of 7.89 μsec. as measured from the time the shock front arrived at the laser beam. Thus in the majority of our experiments, measurement started after 4-6 relaxation times (t_{min}/τ^*) and ended after 5-7 relaxation times (t_{max}/τ^*). The measured portion of the relaxation zone extended over 1.5-2.5 relaxation times for most of our experiments. In this narrow region a plot of log V vs. t_1 was nearly linear for most of our experiments and we obtained an average relaxation time for each experiment in this way. However, some experiments exhibited an apparent non-linearity. In these cases, the curve was divided into 2 or 3 portions and each portion was treated separately and the corresponding average relaxation times were found, so that for some experiments more than one relaxation time was determined. The reciprocal of the slope of the log plot curves, $1/(2.303S)$, was the relaxation time in laboratory coordinates τ^*. It varied from 0.224 to 1.42 μsec. The vibrational relaxation time for each experiment was calculated using the Blackman method (112) (eq. 2.18, section 2.11). It variedfrom 0.096 to 1.30 μ sec.atm. A dimensionless time-scale can be defined by multiplying the total gas kinetic collision frequency Z_{total} by the laboratory time or by the gas particle time. In this latter case the collision number is obtained. Since, qualitatively, it does not make any qualitative difference whether a laboratory time or gas particle time is used, the former was used. The resulting number Zt is related to the collision number by the relation:

Collision number = $Z_{total}\ t_1\ \rho_e/\rho_o = Zt\rho_e/\rho_o$

where $Z_{total} = X_M Z_{MM} + (1-X_M) Z_{ArM}$, X_M is the mole fraction of the polyatomic molecule, Z_{MM} is the collision frequency for pure polyatomic molecule M, and Z_{ArM} is the collision frequency for polyatomic molecule M infinitely dilute in argon. Each collision frequency can be calculated using the equation:

$$Z = r^2 \pi \sqrt{\frac{8kT}{\pi \nu}} \frac{N}{v} \qquad (3.1)$$

where N is the total number of molecules and v is the volume

$$Z_{total} = r_M^2 \pi \sqrt{\frac{8kT_e}{\pi \mu_{M-M}}} \frac{P_e}{kT_e} X_M + \pi \left(\frac{r_M + r_{Ar}}{2}\right) 2 \sqrt{\frac{8kT_e}{\pi \mu_{M-Ar}}} \frac{P_e}{kT_e} X_{Ar} \qquad (3.2)$$

where μ is the reduced mass, r_M and r_{Ar}, the collision radii of M and Ar are found from ref. 113. For pure N_2O as well as for pure C_2H_2, the second term of equation 3.2 drops out. Values of Zt for pure N_2O lie between 49 and 3707. These results are summarized in table A.1.

3.1.1 The effect of Zt on the vibrational relaxation time of pure N_2O.

The most important factors affecting the vibrational relaxation time $P\tau'$ are the equilibrium temperature T_e and the extent from equilbrium, Zt. The variation of $P\tau'$ with Zt at different temperatures is shown in fig. 3.1 to fig. 3.7. In these figures, experiments having similar temperatures have been collected. Closed symbols correspond to our experimental results and the open symbols correspond to the experimental results of Dove et al. (94). In the low temperature region (450-584 K, fig. 3.1), $P\tau'$ increases with increasing Zt in the range

1650 to 2200 collision, and reaches an equilibrium value of 0.77 sec.atm. at high Zt (Zt>2200). At higher temperatures (fig. 3.2) low Zt (700-1300) were probed under our experimental conditions. In this region, $P\tau'$ increases more rapidly with the Zt and aproaches an equilibrium value at high Zt. However we were not able to measure a vibrational relaxation time at Zt higher than 1300, and therefore the equilibrium value of $P\tau'$ was not reached under our experimental conditions for T_e>788 K. At even higher temperatures (fig. 3.3 and 3.4), the vibrational relaxation time increases even more rapidly and the vibrational relaxation seems to proceed far from equilibrium. At extremely high temperatures, (1610-1755 K, fig. 3.6 and 3.7), relatively small Zt were probed (less than 300) and the Zt effect on the vibrational relaxation time is reversed. In this case the vibrational relaxation time decreases with increasing Zt. It was very difficult to find the temperature regime for which the vibrational relaxation time was apparently unaffected by Zt since it is a weak dependence over a broad temperature regime. However, by examining curves in fig. 3.4 and 3.6 we can deduce that this region of temperature lies between 1106 and 1610 K. We did not obtain enough experimental results in this temperature regime to enable us to locate the transition temperature precisely. A few experiments were made between 1230 and 1330 K (fig. 3.5). The scatter in the results in this temperature regime was so high that it was impossible to decide whether the curve of fig. 3.5 increased or decreased with Zt. For this reason we assumed that the vibrational relaxation time remains unaffected by Zt in this temperature regime.

Figure 3.1 Variation of the vibrational relaxation time of pure N_2O with Zt at T=450-584 K.

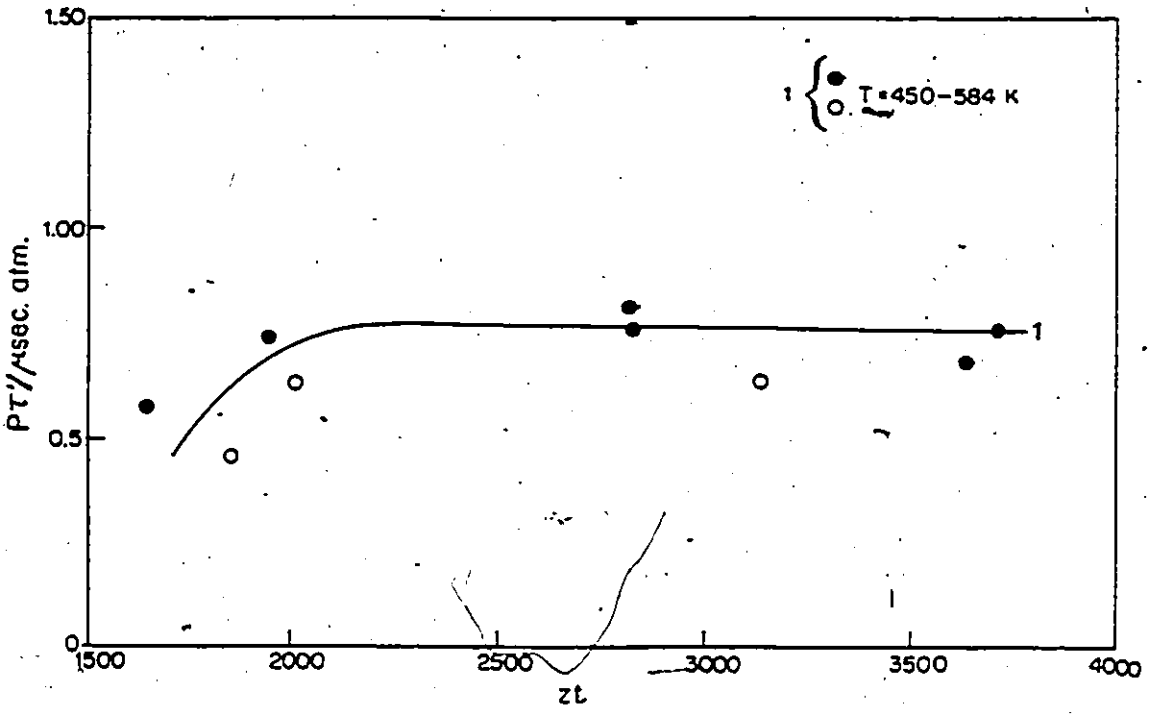

Figure 3.2 Variation of the vibrational relaxation time of pure N_2O with Zt at T=649-711 K and 746-788 K.

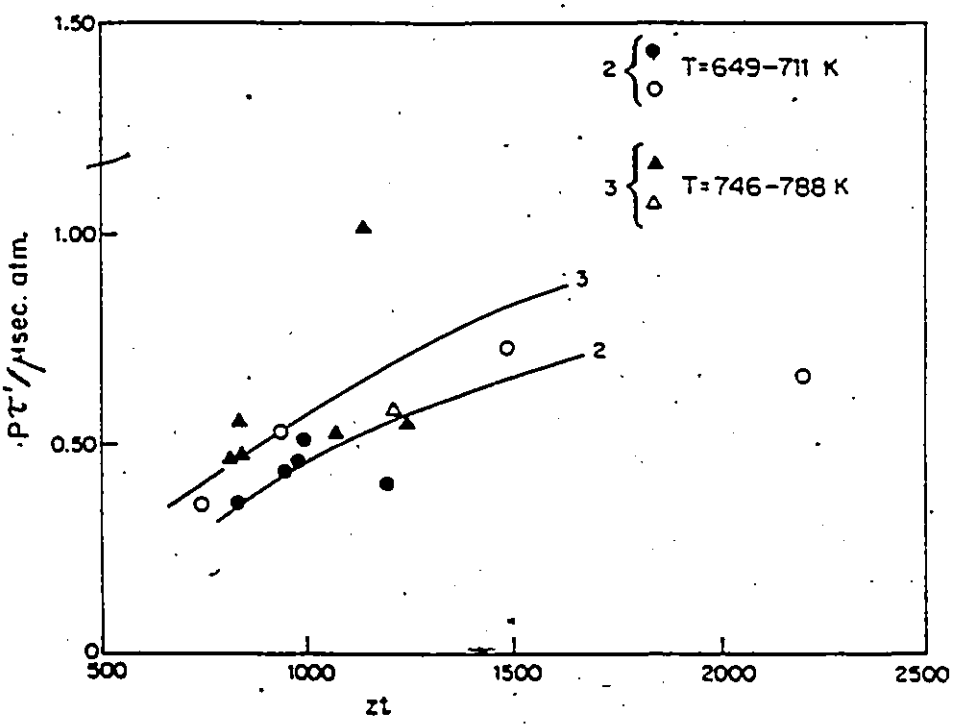

Figure 3.3 Variation of the vibrational relaxation time of pure N_2O with Zt at T=809-879 K and 906-991 K.

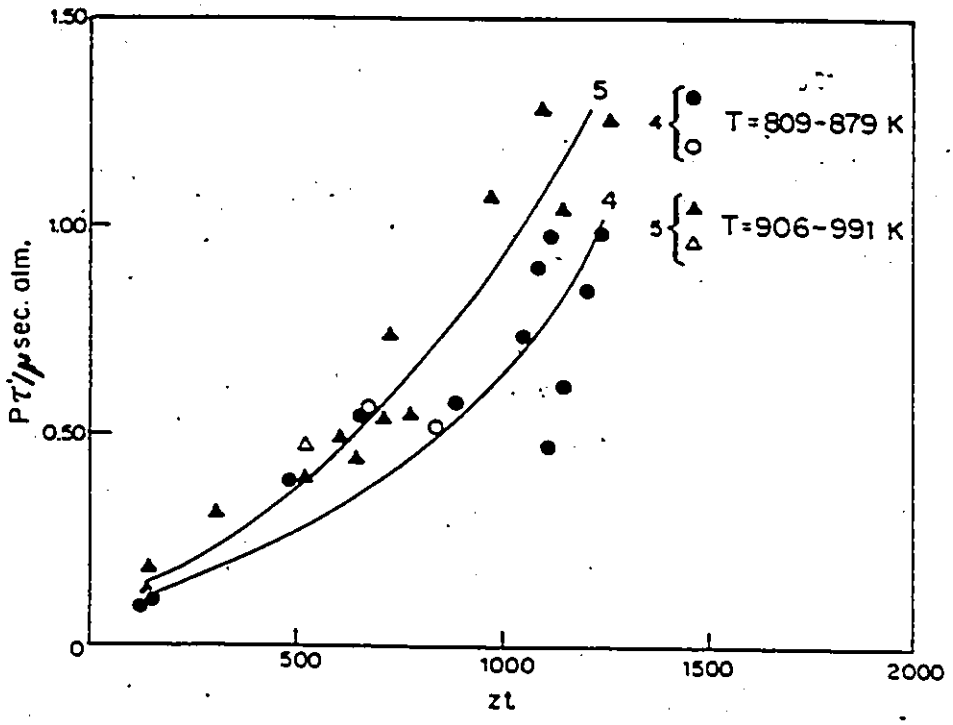

Figure 3.4

Figure 3.5

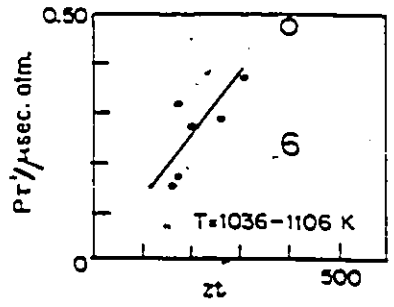

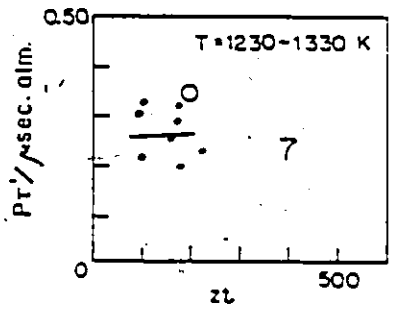

Figure 3.6

Figure 3.7

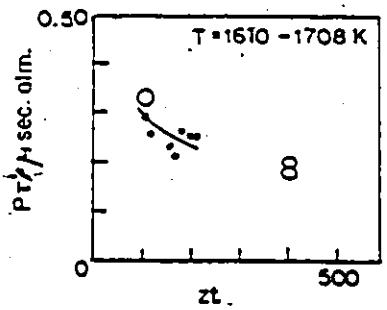

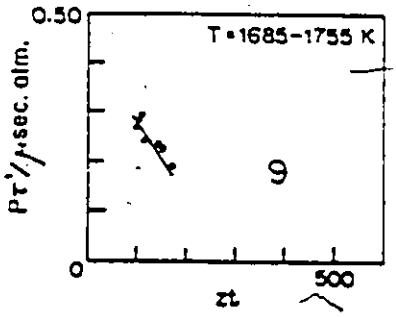

Since the temperature from experiment to experiment could not be maintained constant to better than ±50 K and sometimes ±100 K. The scatter observed in figs. 3.1-3.7, e.g. therefore reflect this uncertainty as well as the precision of measuring τ^* (~5%) and the intrinsic uncertainty in Zt (i.e. t~1±0.5 μs.) arising from the choice of a single point in time as representative of an average τ^* for each experiment.

All curves in fig. 3.1 to 3.7 are summarized in fig. 3.8, at low temperature, $P\tau'$ increases with temperature and with Zt. At high temperature $P\tau'$ decreases with increasing temperature and Zt. This intriguing pattern of deceleration and acceleration of rates, as well as the basic question of the non-constancy of the relaxation rate coefficient impelled us to examine the details of the relaxation mechanism more closely (see Chapt. 5).

3.1.2 The effect of temperature on the vibrational relaxation time of pure N_2O.

The effect of temperature on the vibrational relaxation time at different Zt can be deduced from fig. 3.8. From the curves of this figure vibrational relaxation times were extrapolated and/or interpolated at Zt = 100, 150, 200, 300, 600, 800, 1000, 1200 and 1400 respectively. Results are summarized in table 3.1 and represented graphically in fig.3.9. At the beginning of the relaxation (Zt = 100, 150, 200), the vibrational relaxation time increases with temperature in the low temperature region and decreases with temperature in the high temperature region (curves 1-3). As Zt increases, the vibrational relaxation time becomes more sensitive to the temperature and increases more rapidly with

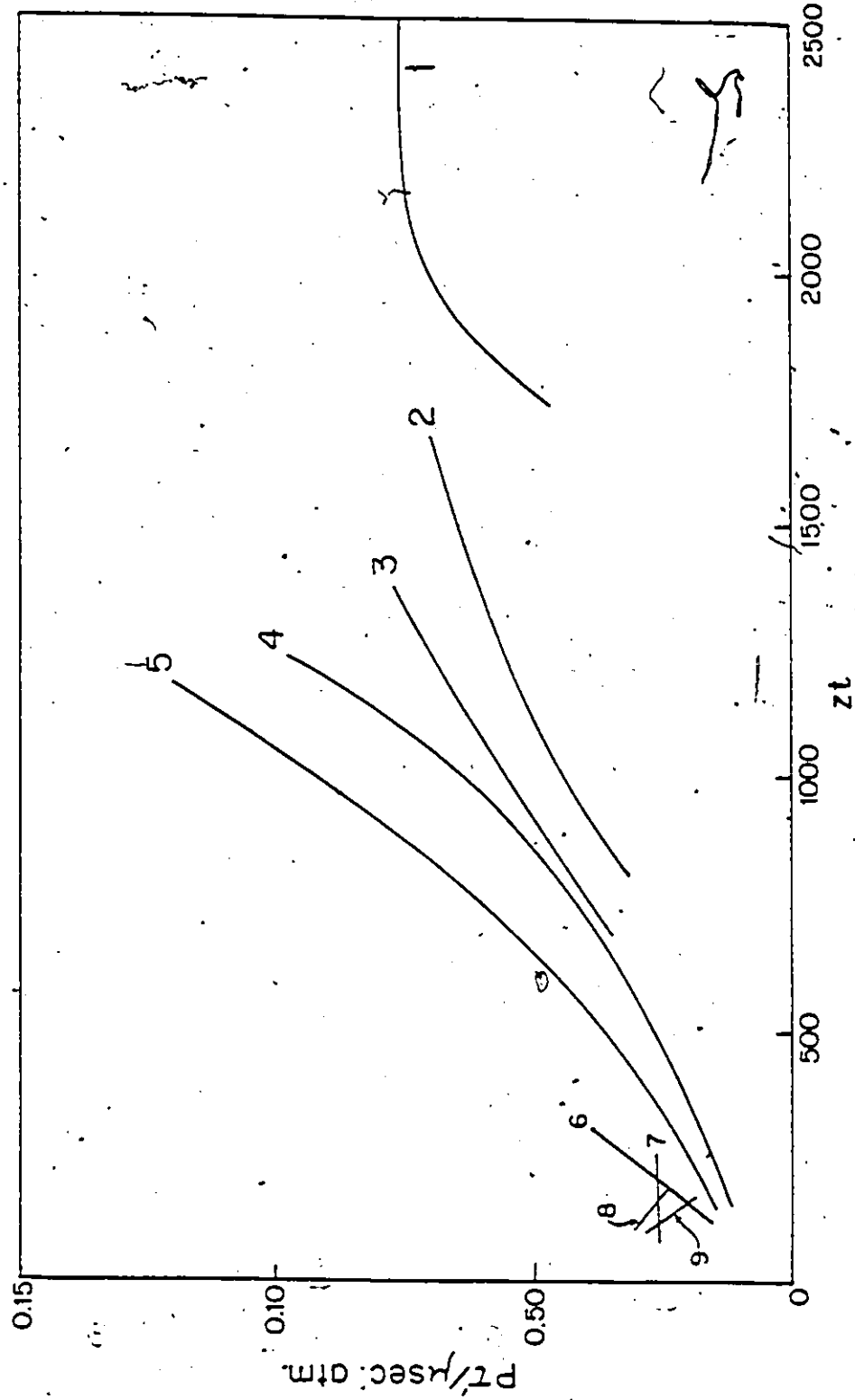

Figure 3.8 Variation of the vibrational relaxation time of pure N_2O with Zt (curves of figs. 3.1-7).

Figure 3.9 Variation of the vibrational relaxation time of pure N_2O with temperature at different Zt.

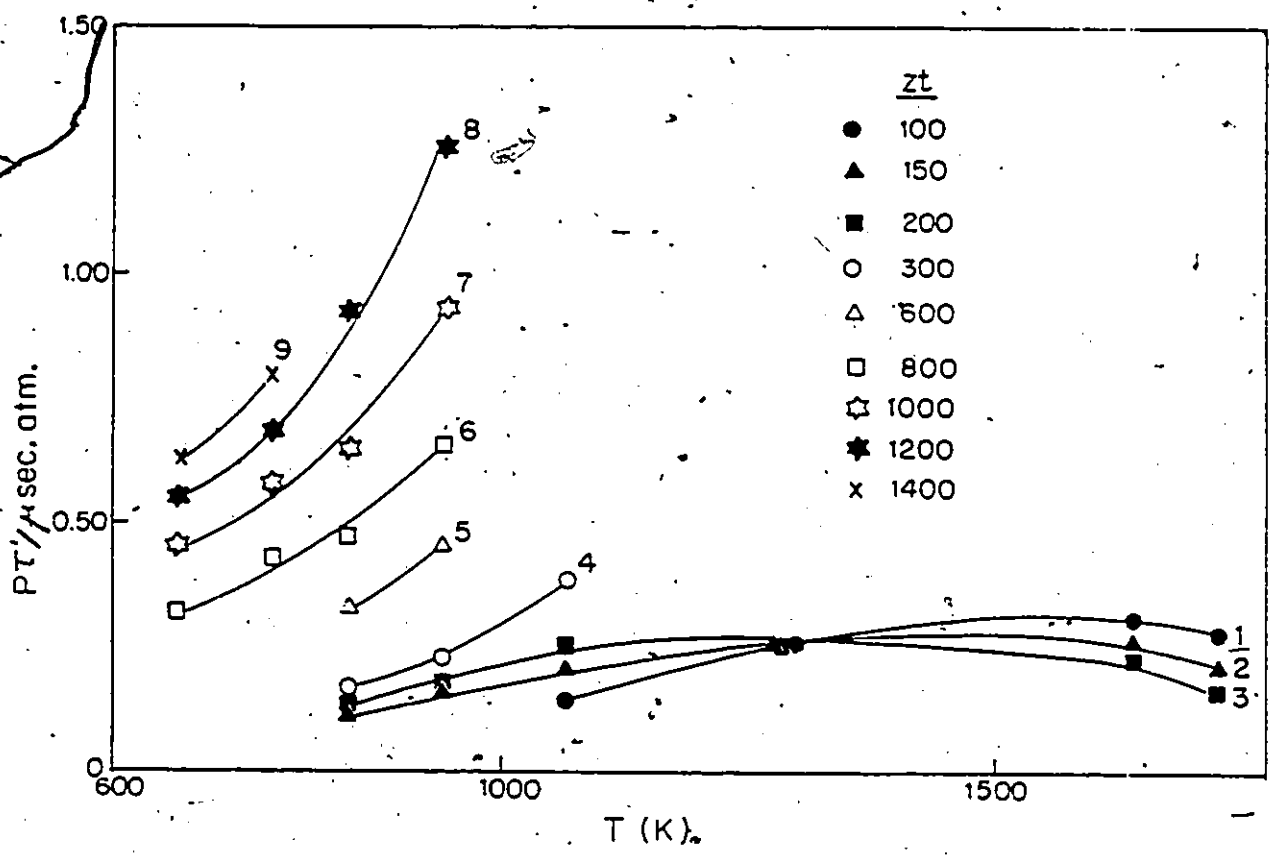

temperature (curves 4-9). Since the effect of Zt on the vibrational relaxation time at high temperature is opposite to that at low temperature (see previous section), curves representing the variation of the vibrational relaxation time with temperature cross at a transition temperature (curves 1, 2 and 3).

Table 3.1 Vibrational relaxation times (μsec.atm.) of pure N_2O as a function of temperature and Zt.

Zt \ T (K)	672 ± 26	765 ± 16	843 ± 25	939 ± 29	1063 ± 26	1283 ± 34	1645 ± 38	1729 ± 31
100					0.14	0.26	0.31	0.28
150			0.11	0.15	0.20	0.26	0.26	0.21
200			0.13	0.17	0.25	0.26	0.23	0.16
300			0.17	0.23	0.39			
600			0.33	0.46				
800	0.32	0.43	0.47	0.67				
1000	0.45	0.57	0.65	0.94				
1200	0.55	0.69	0.93	1.26				
1400	0.63	0.80						

3.2 Vibrational relaxation of pure C_2H_2

A total of 82 individual experiments were performed with pure C_2H_2. Results are summarized in table A.2, appendix A, and represented graphically in fig. 3.10 to 3.15.

Most of the details about the presentation of our experimental results as well as the calculation of some parameters have been discussed in the previous section (section 3.1) and will not be repeated here.

The thermodynamic variables are represented graphically in fig. B.5 to B.7, appendix B, as a function of the shock wave velocity. From the shock wave velocity measurement, all thermodynamic variables can be determined using these figures. In fig. B.8, appendix B, a plot of $C_p/(C_p-C_{vib})$ is shown and from the equilibrium temperature, the ratio $C_p/(C_p-C_{vib})$ can be determined as we did in the case of N_2O.

In table A.2 the most important experimental conditions in the relaxation process are summarized. The initial pressures of the test gas P_o vary from 0.204 torr to 1.18 torr. The low pressures (compared to those of N_2O) were necessary because of the rapidity of the relaxation. We were not able to measure the vibrational relaxation time for experiments performed at pressures higher than 1.18 torr. The relaxation zone was no longer well defined there. The pressure in the driver section, P_D, required to burst the aluminum diaphragm varied from 87 to 415 torr. However not many experiments were performed with high P_D pressure. Under such conditions the laser schlieren signal was very sharp and the residual relaxation signal was too small to allow an accurate measurement of the relaxation time. Since we were limited by a very small range of test gas pressures and driver gas pressures, the shock wave velocities U_o varied between 1.146 and 2.042 mm/μsec. only and The corresponding equilibrium temperatures varied from 613 to 1184 K. Measurements of the relaxation time from the laser schlieren signal were made after a minimum of 0.82 μsec. and ended after a maximum of 2.59 μsec. as measured from the shock front arrival at the laser beam. Thus,

in the majority of our experiments, measurements began after 4-6 relaxation times (t_{min}/τ^*) and ended after 5-7 relaxation times (t_{max}/τ^*), and the measured portion of the relaxation zone corresponded to 1.5-2.5 relaxation times for most of our experiments. Vibrational relaxation times in laboratory coordinates (τ^*) appear in table A.2. They vary from -0.35 μsec. for the low temperature experiments to -0.16 μsec. for the high temperature experiments. The corresponding vibrational relaxation times in gas particle coordinates seem to fluctuate around 0.07 μsec.atm. Finally the values of Zt were below 275 (for all experiments) in contrast to N_2O where Zt reached values of several thousand.

3.2.1 The effect of Zt on the vibrational relaxation time of pure C_2H_2.

The variation of the vibrational relaxation time with Zt at different temperatures is represented in figs 3.10 to 3.13. In these figures, experiments having the same or similar temperatures were collected. In a first attempt, we tried to collect experiments within a narrow temperature range. i.e., in fig. 3.11, we tried to make 4 groups of experiments having temperature ranges 749 to 764, 770 to 773, 793 to 802 and 826 to 838 K, repectively. However, temperature ranges were too small for the limited number of experiments in each range so that it was impossible to draw separate curves for each of the temperature ranges selected. For this reason, temperature ranges were increased to include more experiments and are indicated for each curve of fig. 3.10 to 3.13. In all cases we observed that the relaxation time increased with increasing Zt. No sign of

Figure 3.10 Variation of the vibrational relaxation time of pure C_2H_2 with Zt at T=613-713 K and 726-740 K.

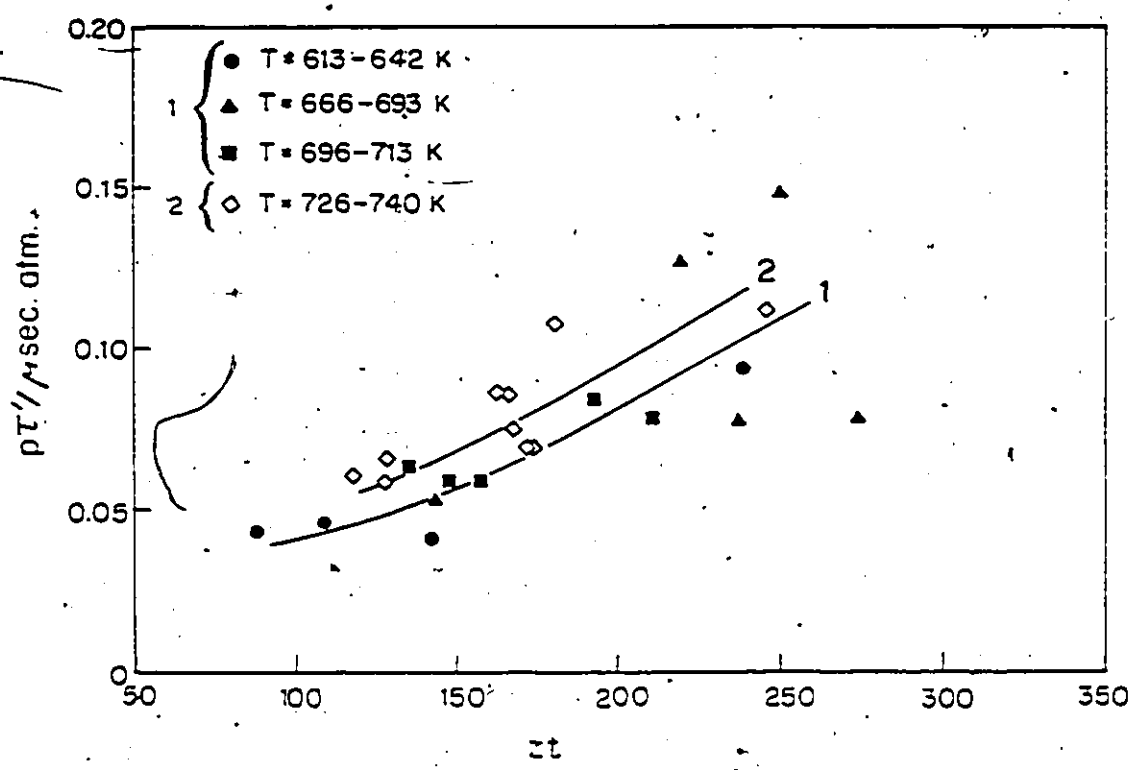

Figure 3.11 Variation of the vibrational relaxation time of pure C_2H_2 with Zt at T=749-802 K and 826-838 K.

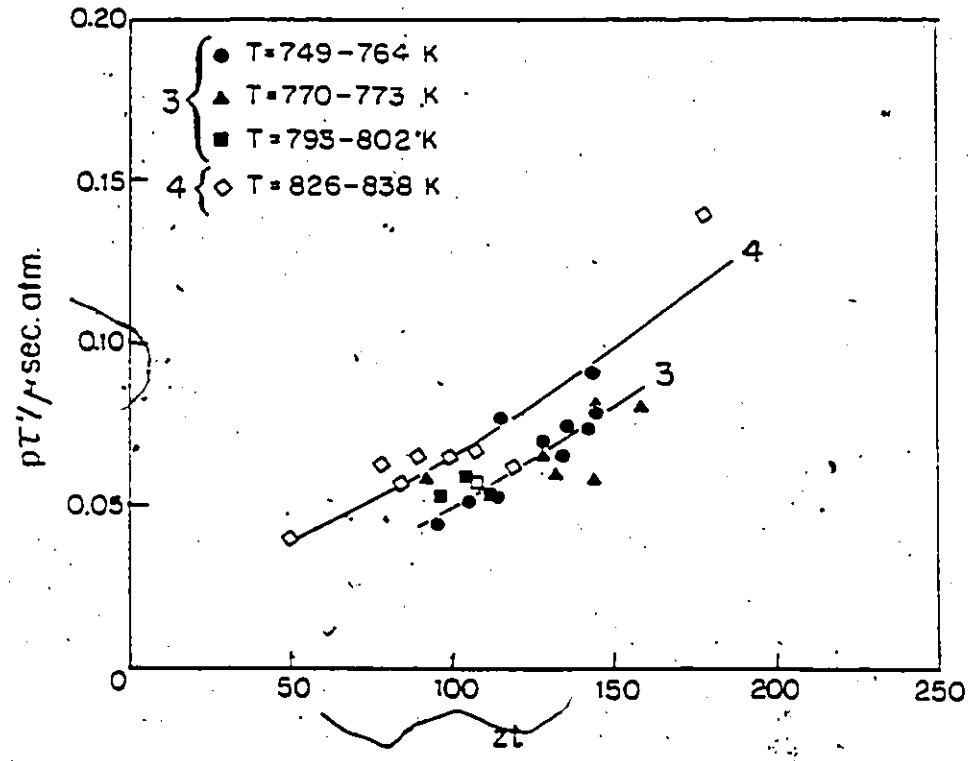

Figure 3.12 Variation of the vibrational relaxation time of pure C_2H_2 with Zt at T=844-1003K.

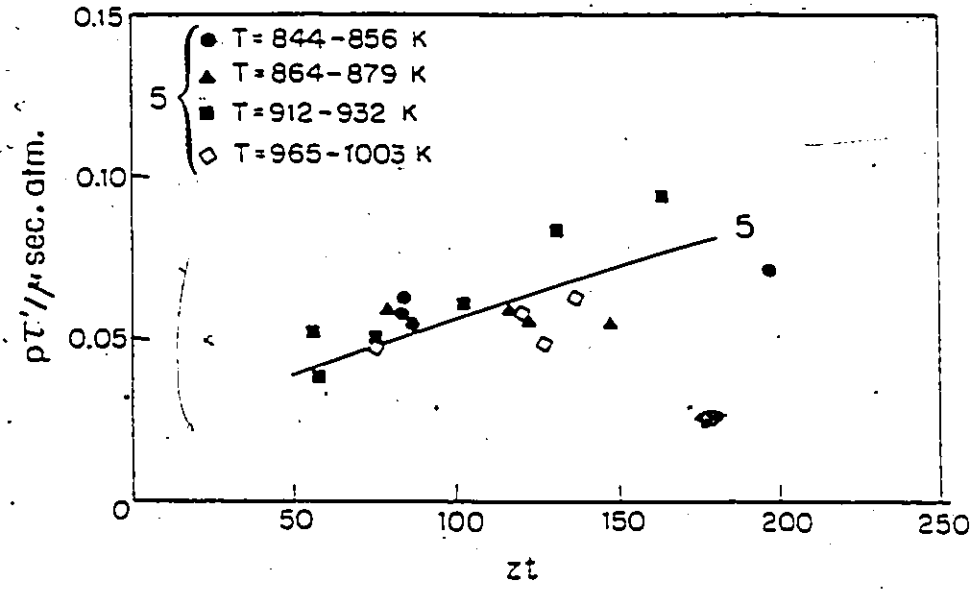

Figure 3.13 Variation of the vibrational relaxation time of pure C_2H_2 with Zt at T=1032-1184 K.

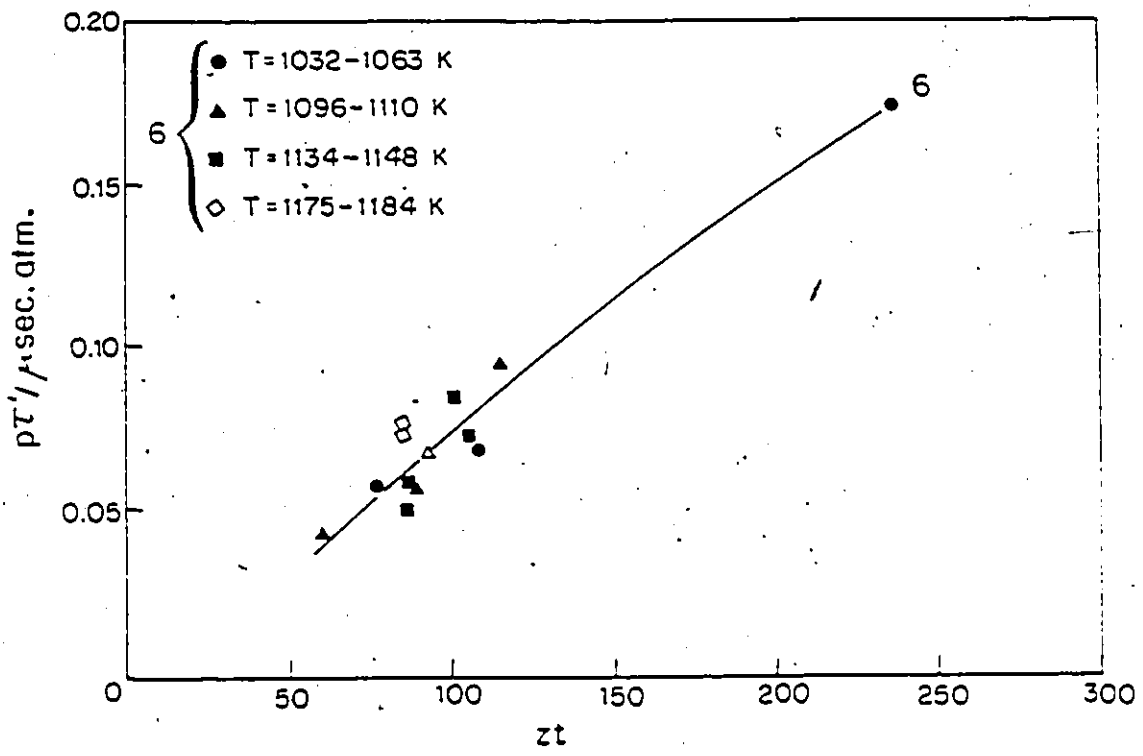

equilibrium or near-equilibrium relaxation was observed. All curves of fig. 3.10 to 3.13 appear on the same graph in fig. 3.14 for comparison. Most curves increase with Zt with nearly the same slope. The only exception comes from the curve corresponding to the temperature range 844-1003 K (curve 5). This curve increases more slowly with Zt and crosses all other curves. The reason behind this curious behaviour is not known. This cannot be explained by the experimental error. It may be due to a change of mechanism of the relaxation of C_2H_2 in the temperature range 844-1003 K.

3.2.2 The effect of temperature on the vibrational relaxation times of pure C_2H_2

The effect of temperature on the vibrational relaxation time at different Zt can be deduced from curves of fig. 3.14. From these curves, vibrational relaxation times were determined at Zt = 100, 150, 200, and 250. Results are summarized in table 3.2 and represented graphically in fig. 3.15. Two curves of $P\tau'$ vs T have been drawn for each collision number. In one curve (dashed), $P\tau'$ increases monotonically with the temperature. In the second curve (solid), a maximum and a minimum appear respectively at 830 and 909 K. This is due to the unusual behavior of the curve corresponding to T_e=844-1003 K of fig. 3.14 (curve 5). However we can conclude that generally relaxation time increases with temperature.

Figure 3.14 Variation of the vibrational relaxation time of pure C_2H_2 with Zt (curves of figs. 3.10-13).

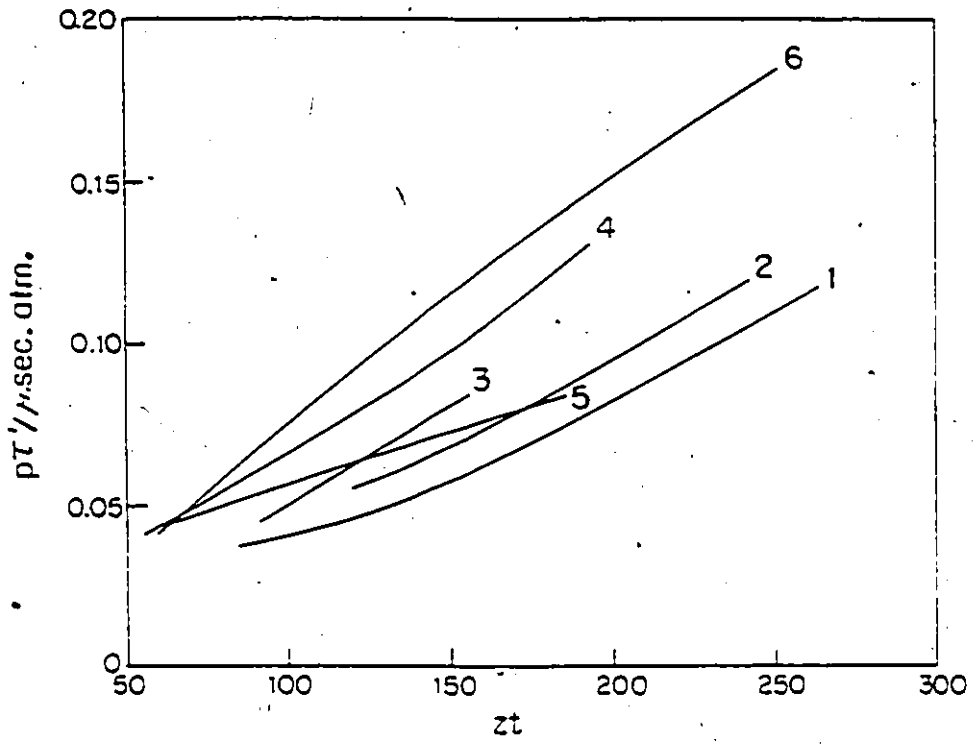

Figure 3.15 Variation of the vibrational relaxation time of pure C_2H_2 with temperature at different Zt.

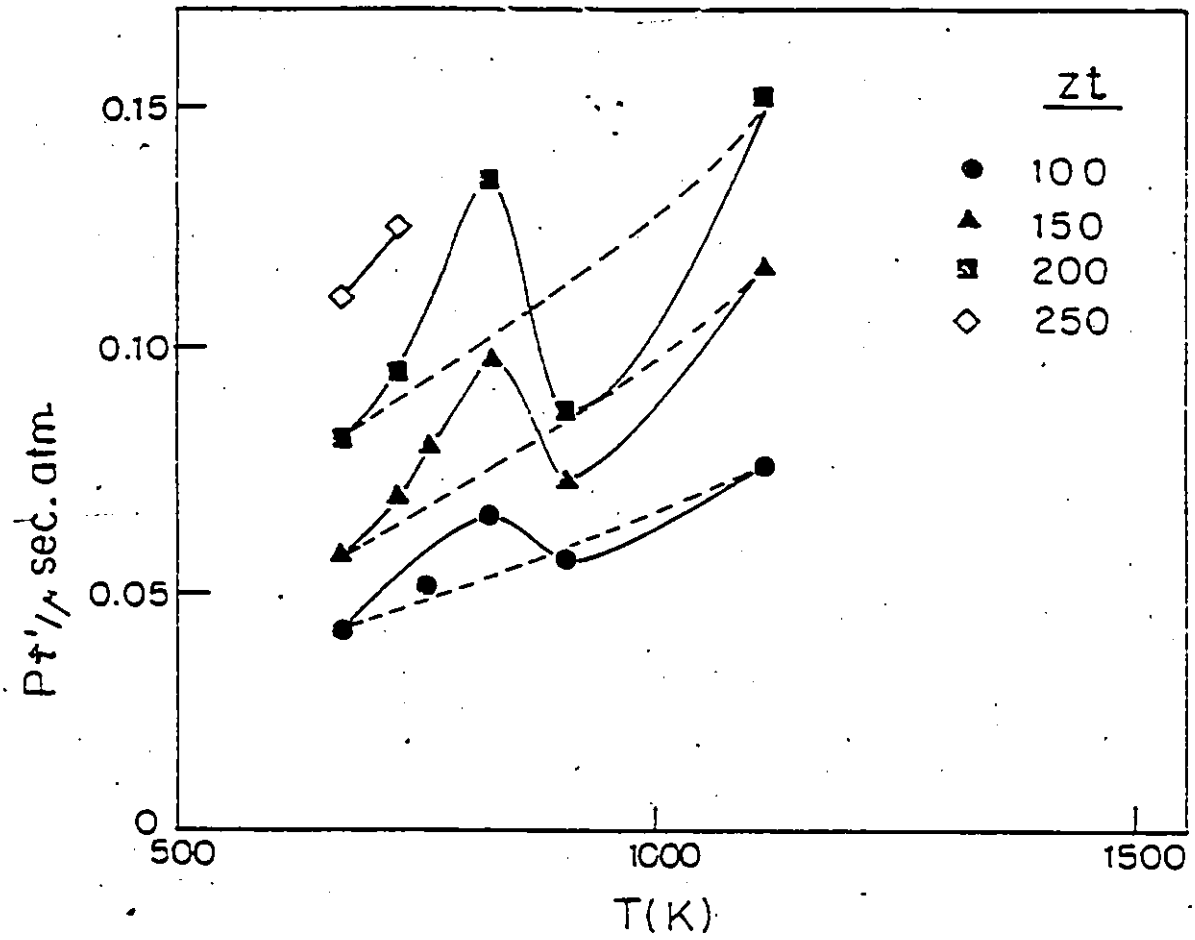

Table 3.2 Vibrational relaxation times (μsec.atm.) of pure C_2H_2 as a function of temperature and Zt.

Zt \ T (K)	675± 32	733± 5	769± 16	830 ± 5	909 ± 53	1114 ± 45
100	0.041	--	0.050	0.065	0.056	0.075
150	0.057	0.069	0.081	0.098	0.072	0.116
200	0.081	0.095		0.135	0.087	0.151
250	0.110	0.125				

3.3 Vibrational relaxation times of C_2H_2-Ar mixtures.

Vibrational relaxation times of mixtures of 50.5, 23.6, 12.1, 5.0, 2.5, and 1.0 mole percent of C_2H_2 in Ar have been measured. A total of 53, 46, 74, 58, 32 and 34, experiments respectively were performed for each mixture. The results are summarized in tables A.3 to A.8, appendix A, and represented graphically in figs. 3.16 to 3.47.

Curves representing the variation of the thermodynamic variables with the shock wave velocity as well as curves representing the variation of the ratio $C_p/(C_p-C_{vib})$ with the equilibrium temperature will not be presented for the mixtures since these curves are similar to the corresponding C_2H_2 and N_2O curves which have already been presented.

For mixtures of 2.5% and 1.0% mole fraction of C_2H_2, the signal-to-noise ratio was rather low. More than half of the experiments performed in these mixtures were rejected for the lack of precision. For this reason, not many experiments appear in table A.7 and A.8.

In tables A.3 to A.8 the parameters affecting the relaxation

process are presented and the range of experimental conditions and results extracted from these tables as well as the range of experimental conditions and results for pure C_2H_2 are represented in table 3.3. At large C_2H_2 mole fraction only experiments performed with low pressure test gas are measureable, i.e., 0.202-1.18 torr for pure C_2H_2 and 0.33-1.73 torr for 50.5 % C_2H_2-Ar mixture. At low C_2H_2 concentration, the range of test gas pressures could be increased i.e., 1.10-9.42 torr for the 5.0% C_2H_2-Ar mixture. The range of shock wave velocities was nearly the same for all mixtures. However the range of equilibrium temperatures is displaced towards high temperature as the concentration of C_2H_2 was decreased. The probed time range (t_{min} and t_{max}), the laboratory relaxation time and the vibrational relaxation time seem to be unaffectd by the concentration of C_2H_2 in the mixtures. However the Zt range increased with decreasing C_2H_2 concentration.

3.3.1 The effect of Zt on the vibrational relaxation time of C_2H_2-Ar mixtures.

The variation of the vibrational relaxation time $P\tau'$ with Zt for different temperature ranges and mole fractions is represented graphically in figs. 3.16 to 3.35. As in the case of pure C_2H_2, we tried to collect experiments in small ranges of temperature. However, the rapidity of the vibrational relaxation made measurement very difficult, and therefore the experimental error was very high, so that it was impossible to draw a separate curve for each of the narrow temperature ranges selected. For this reason, the temperature ranges were increased for most of

Table 3.3 Range of experimental conditions and results for vibrational relaxation of C_2H_2-Ar mixtures.

Variable / % C_2H_2	P_o torr	P_D torr	U_o mm/μsec.	T_e K	t_{min} & t_{max} μsec.		τ^* μsec.	$P\tau'$ μsec.atm.	Zt
100.0	0.204-1.18	87-415	1.146-2.042	613-1184	0.82	2.59	0.137-0.454	0.0394-0.176	50-274
50.5	0.330-1.73	-	0,929-1.864	659-1596	0.58	3.08	0.129-0.572	0.0156-0.159	75-300
23.6	0.416-2.43	-	1.044-1.863	926-2201	0.86	2.29	0.192-0.680	0.0450-0.167	60-363
12.1	0.630-4.98	-	0.919-1.866	888-2657	0.91	2.71	0.221-0.778	0.0410-0.178	99-666
5.0	1.10-9.42	-	0.789-1.664	771-2488	0.67	2.97	0.187-0.860	0.0270-0.214	96-991
2.5	1.08-3.61	-	1.121-1.668	1341-2621	1.06	2.29	0.197-0.543	0.0236-0.223	121-491
1.0	1.26-3.42	-	1.132-1.651	1386-2645	1.00	2.16	0.0905-0.644	0.0180-0.226	160-433

Figure 3.16 Variation of the vibrational relaxation time of the 50.5 % C_2H_2-Ar mixture with Zt at T=659-872 K, 934-984 K and 1019-1099 K.

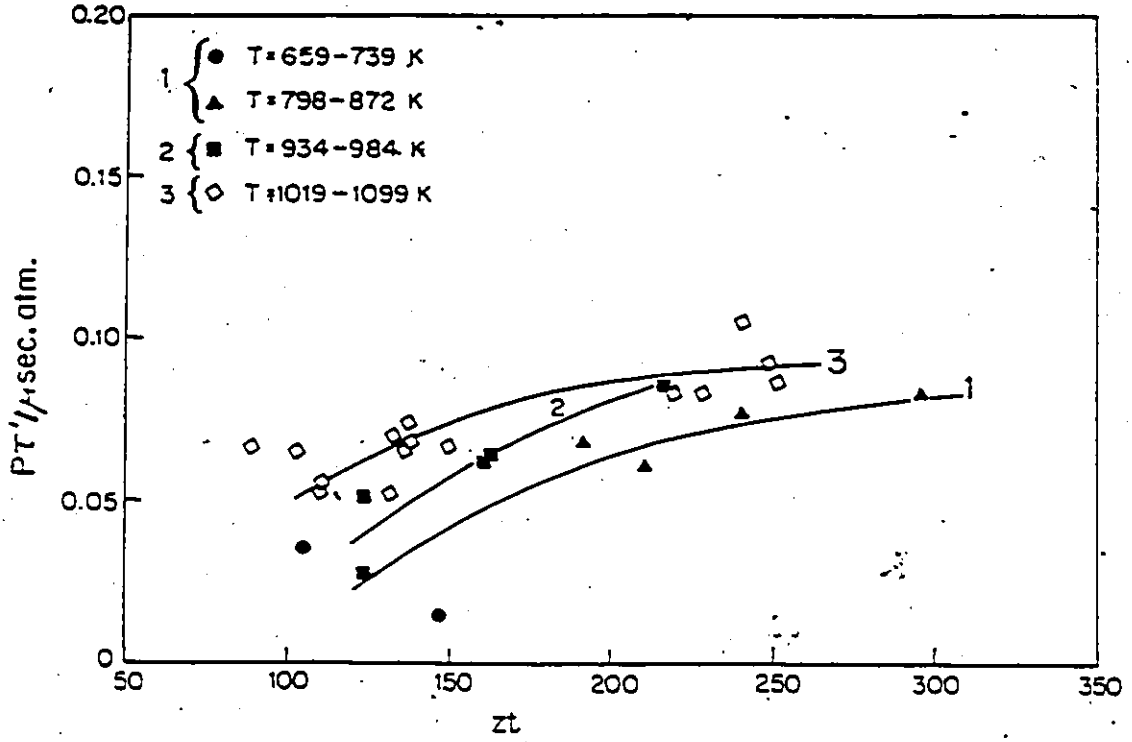

Figure 3.17 Variation of the vibrational relaxation time of the 50.5 % C_2H_2-Ar mixture with Zt at T=1241-1596 K.

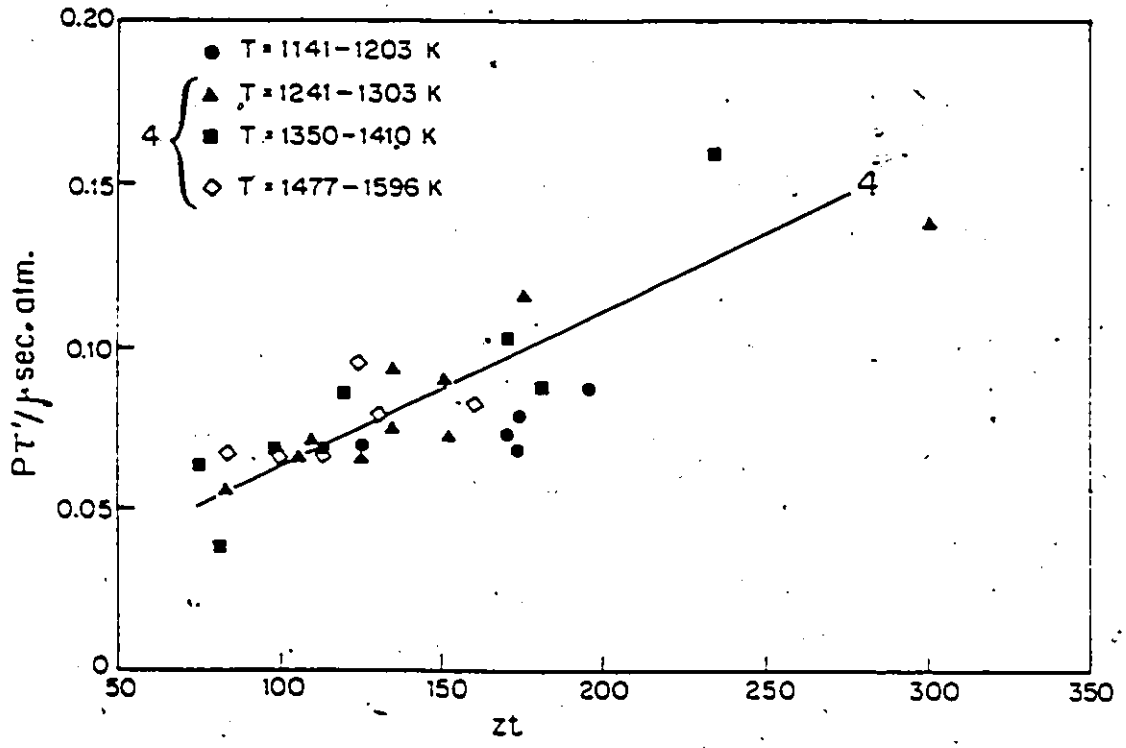

Figure 3.18 Variation of the vibrational relaxation time of the 50.5 % C_2H_2-Ar mixture with Zt (curves of figs. 3.16-17).

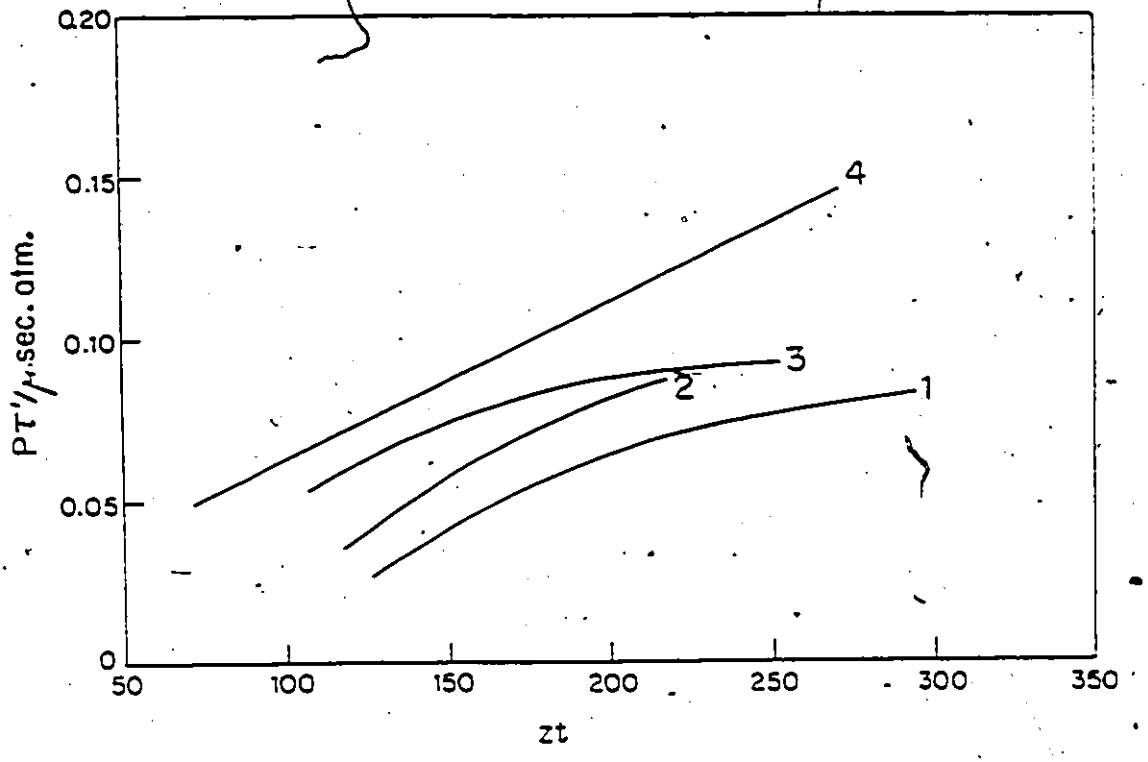

Figure 3.19 Variation of the vibrational relaxation time of the 23.6 % C_2H_2-Ar mixture with Zt at T=926-1035 K, 1124-1239 K and 1283-1348 K.

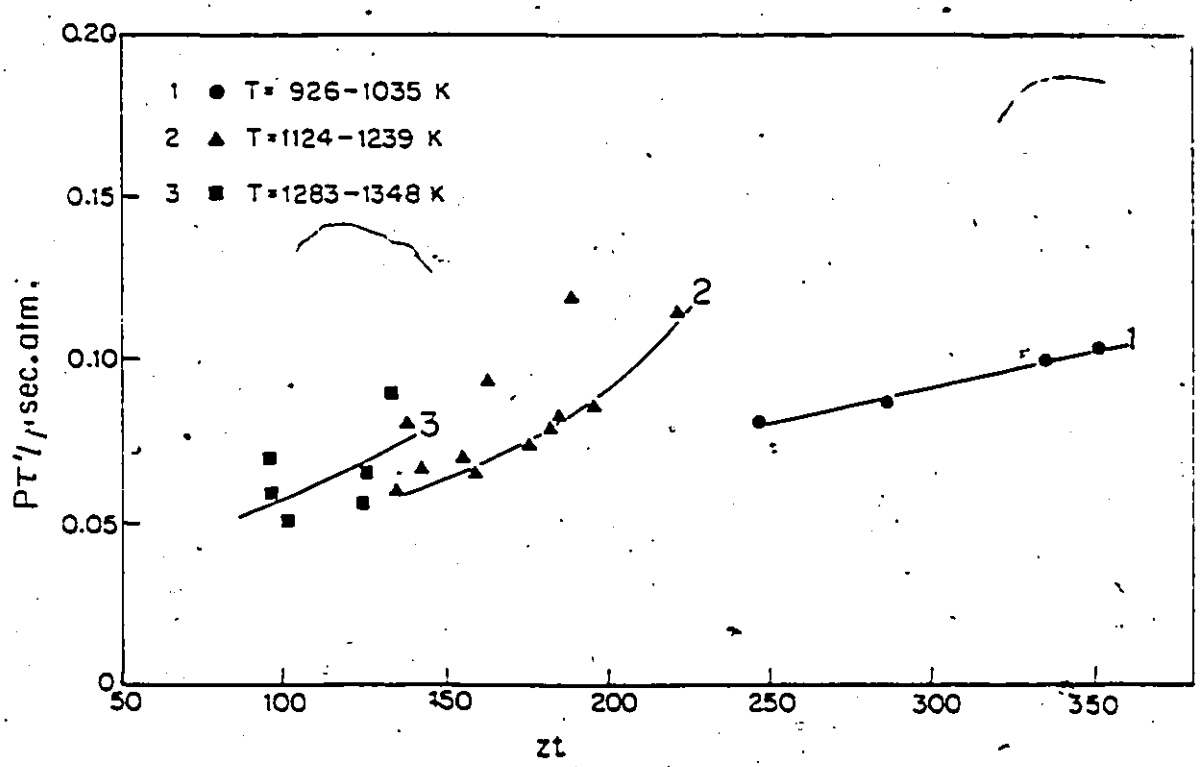

Figure 3.20 Variation of the vibrational relaxation time of the 23.6 % C_2H_2-Ar mixture with Zt at T=1407-1596 K and 1652-1747 K.

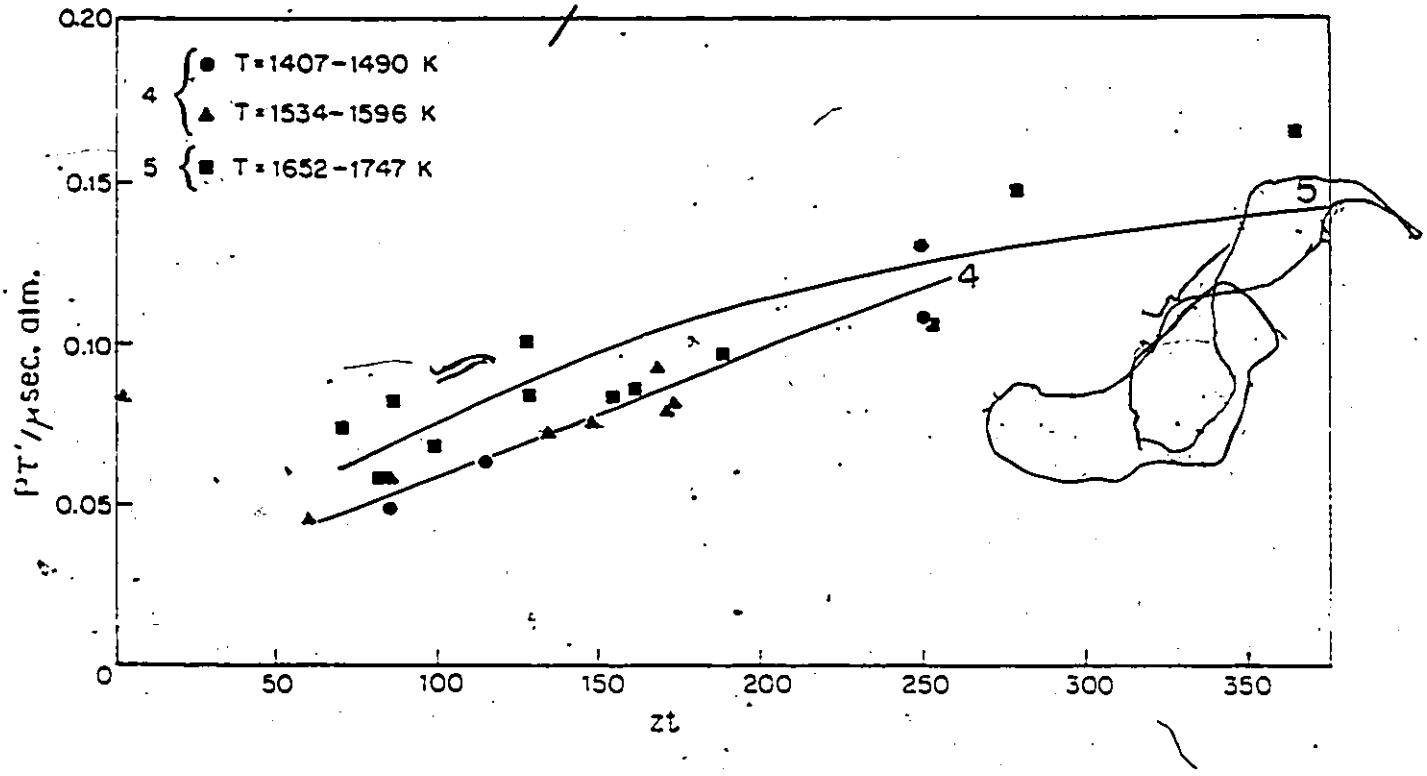

Figure 3.21 Variation of the vibrational relaxation time of the 23.6 % C_2H_2-Ar mixture with Zt at T=1796-1880 K and 1932-2295 K.

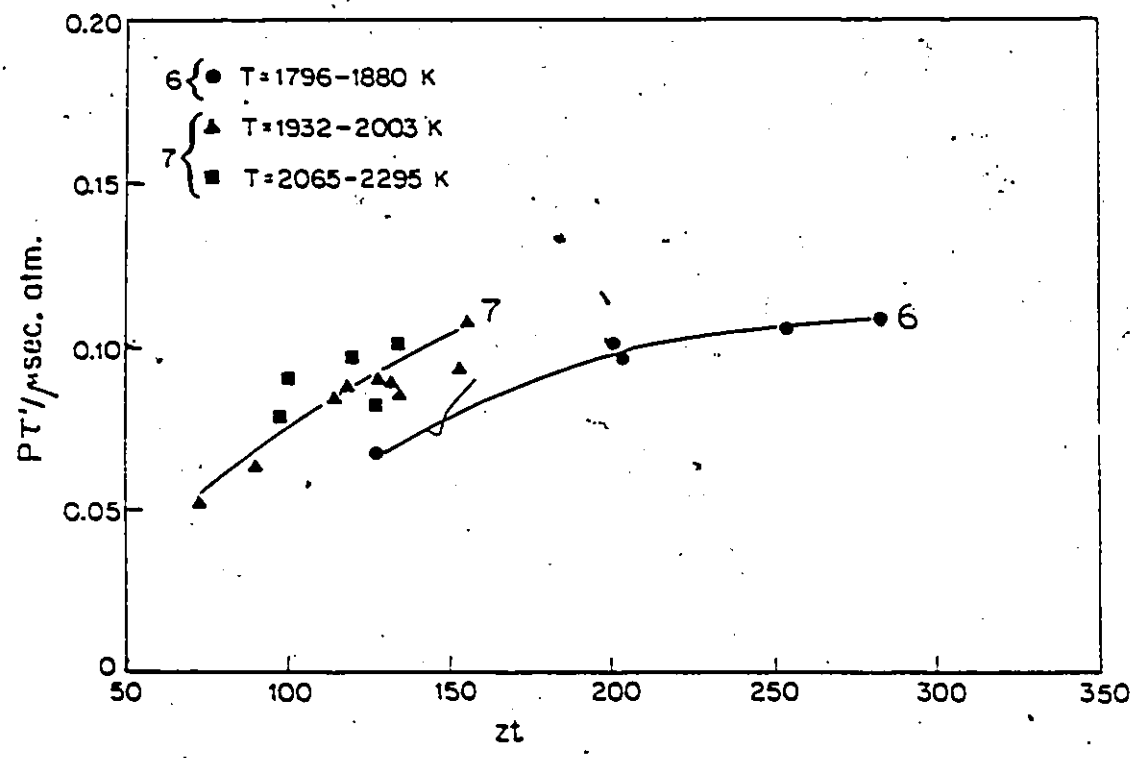

Figure 3.22 Variation of the vibrational relaxation time of the 23.6 % C_2H_2-Ar mixture with Zt (Curves of figs. 3.19-21).

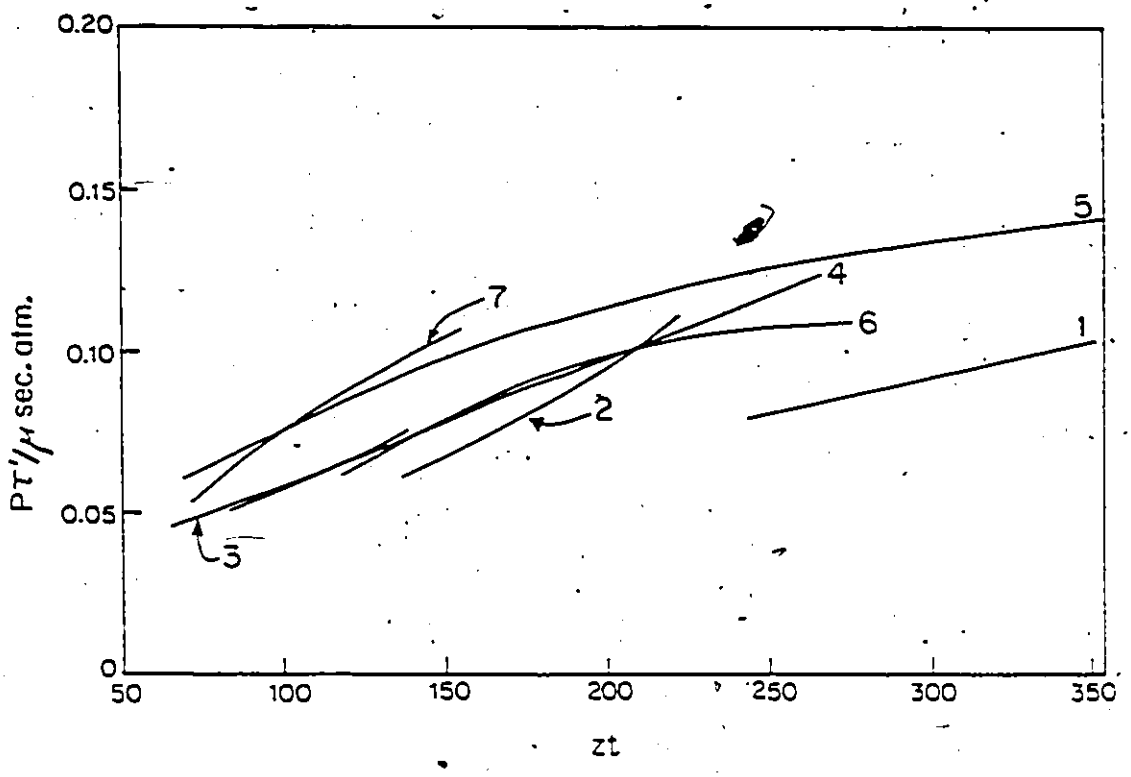

Figure 3.23 Variation of the vibrational relaxation time of the 12.1 % C_2H_2-Ar mixture with Zt at T=999-1054 K, 1222-1293 K and 1322-1477 K.

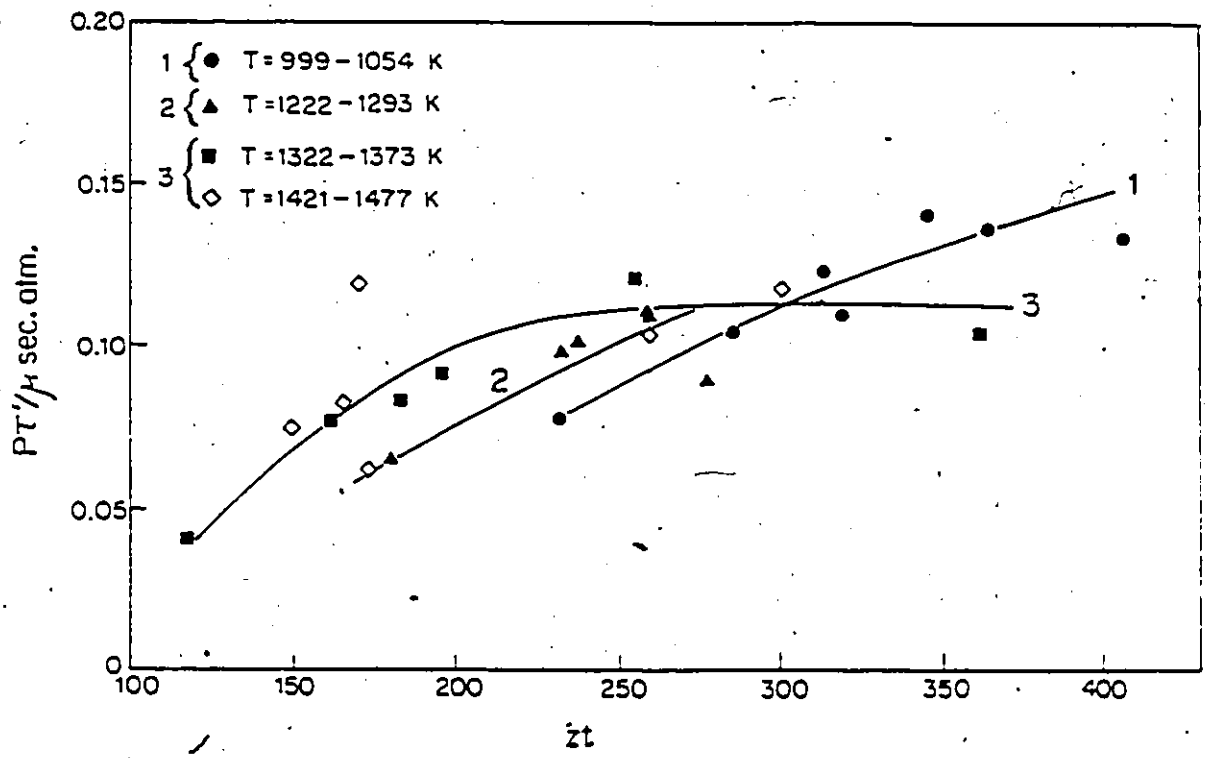

Figure 3.24 Variation of the vibrational relaxation time of the 12.1 % C_2H_2-Ar mixture with Zt at T=1498-1826 K.

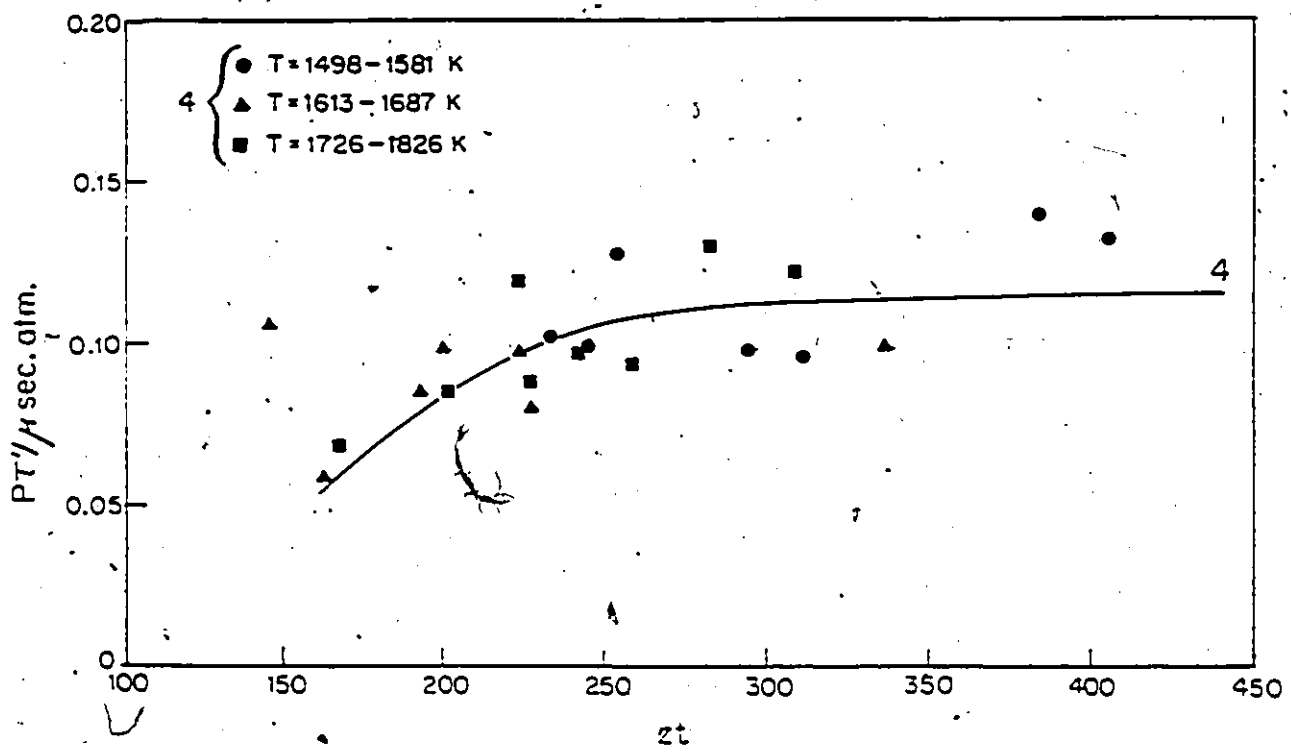

Figure 3.25 Variation of the vibrational relaxation time of the 12.1 % C_2H_2-Ar mixture with Zt at T=1874-2060 K and 2090-2657 K.

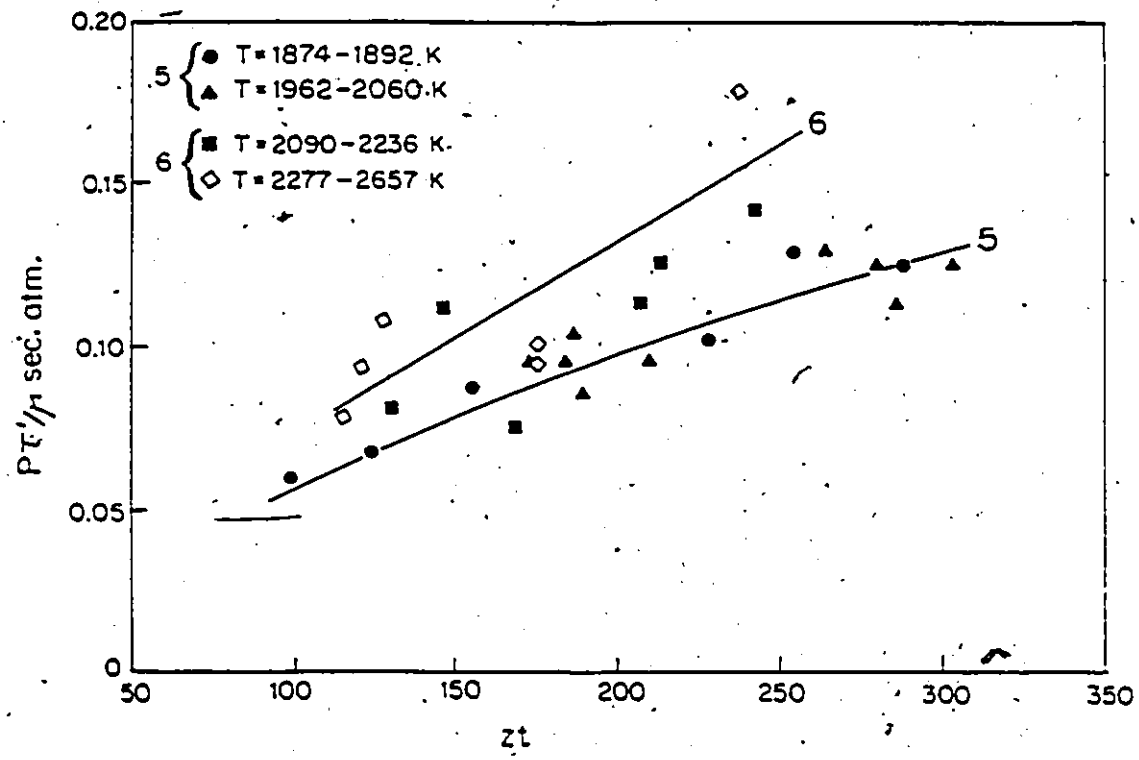

Figure 3.26 Variation of the vibrational relaxation time of the 12.1 % C_2H_2-Ar mixture with Zt (Curves of figs. 3.23-25).

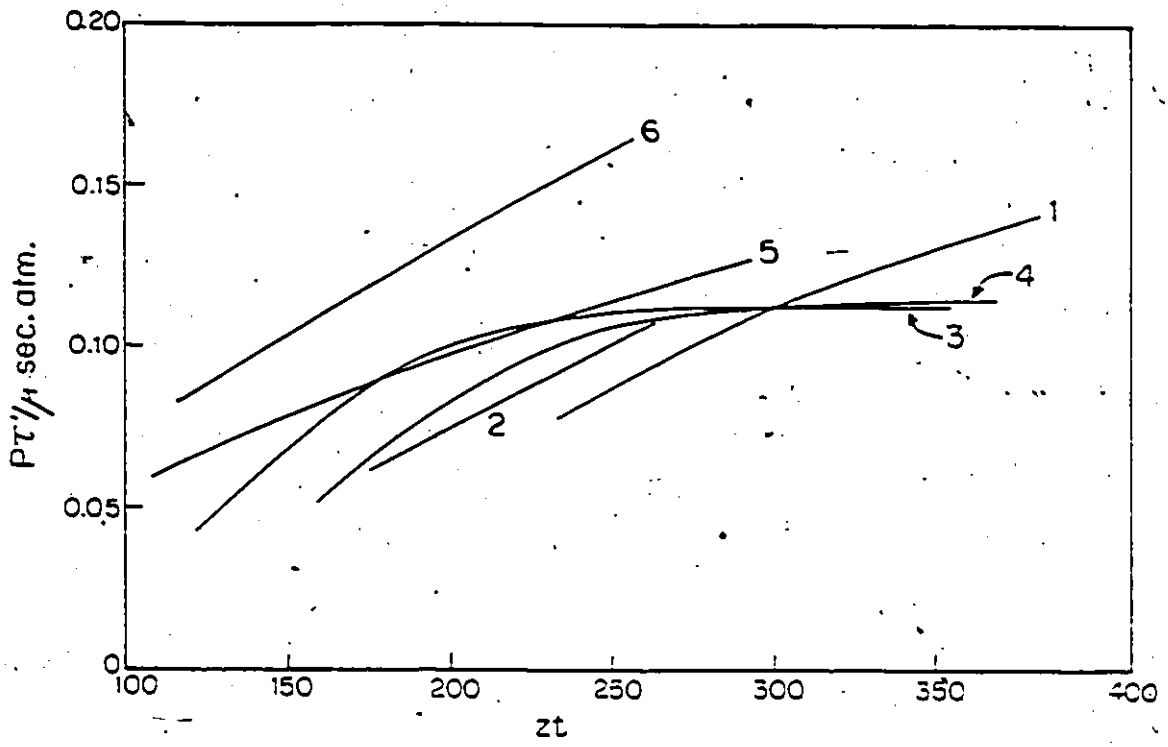

Figure 3.27 Variation of the vibrational relaxation time of the 5.0 % C_2H_2-Ar mixture with Zt at T=984-1108 K, 1285-1448 K and 1495-1604 K.

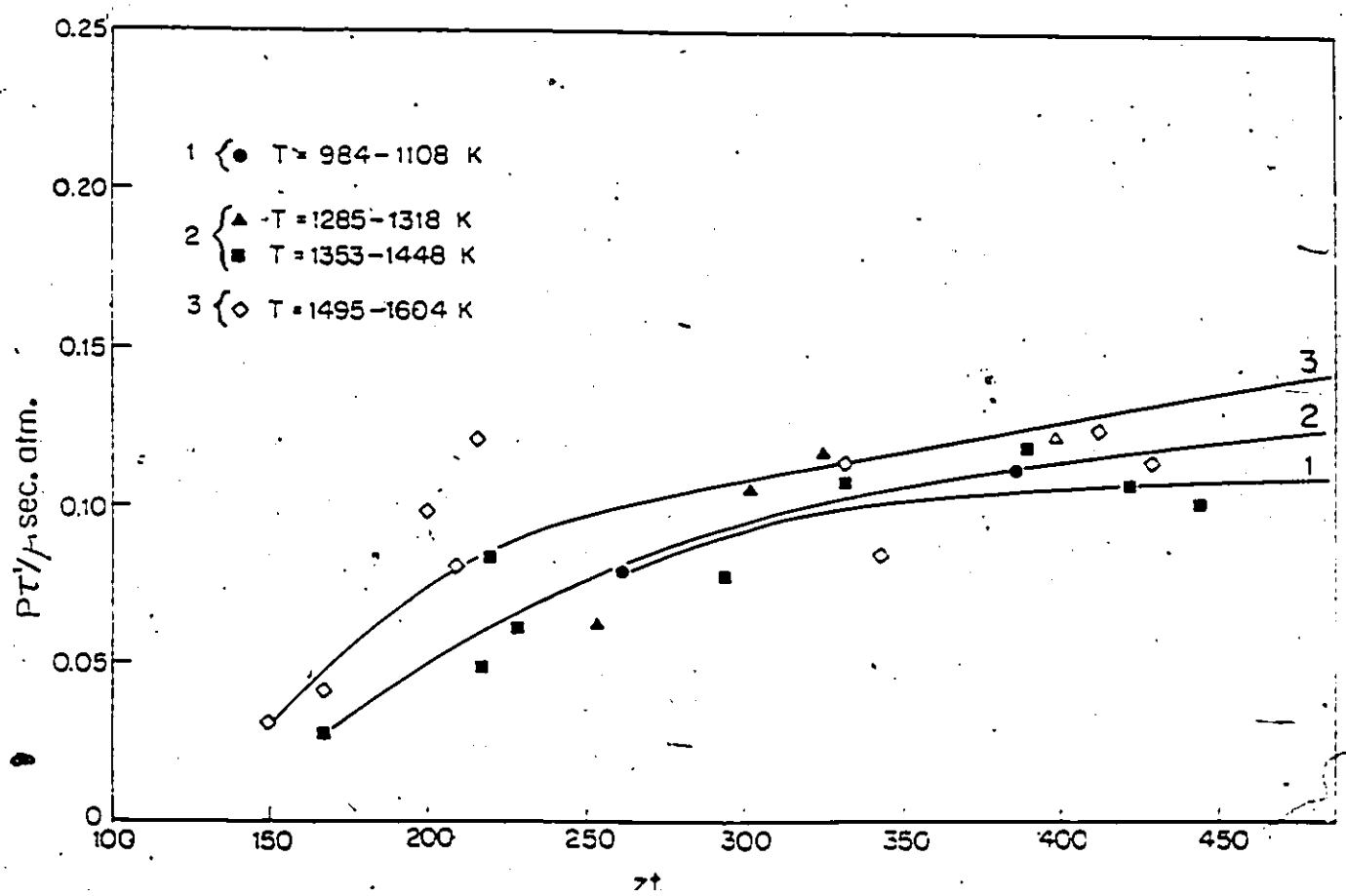

Figure 3.28 Variation of the vibrational relaxation time of the 5.0 % C_2H_2-Ar mixture with Zt at T=1640-2488 K.

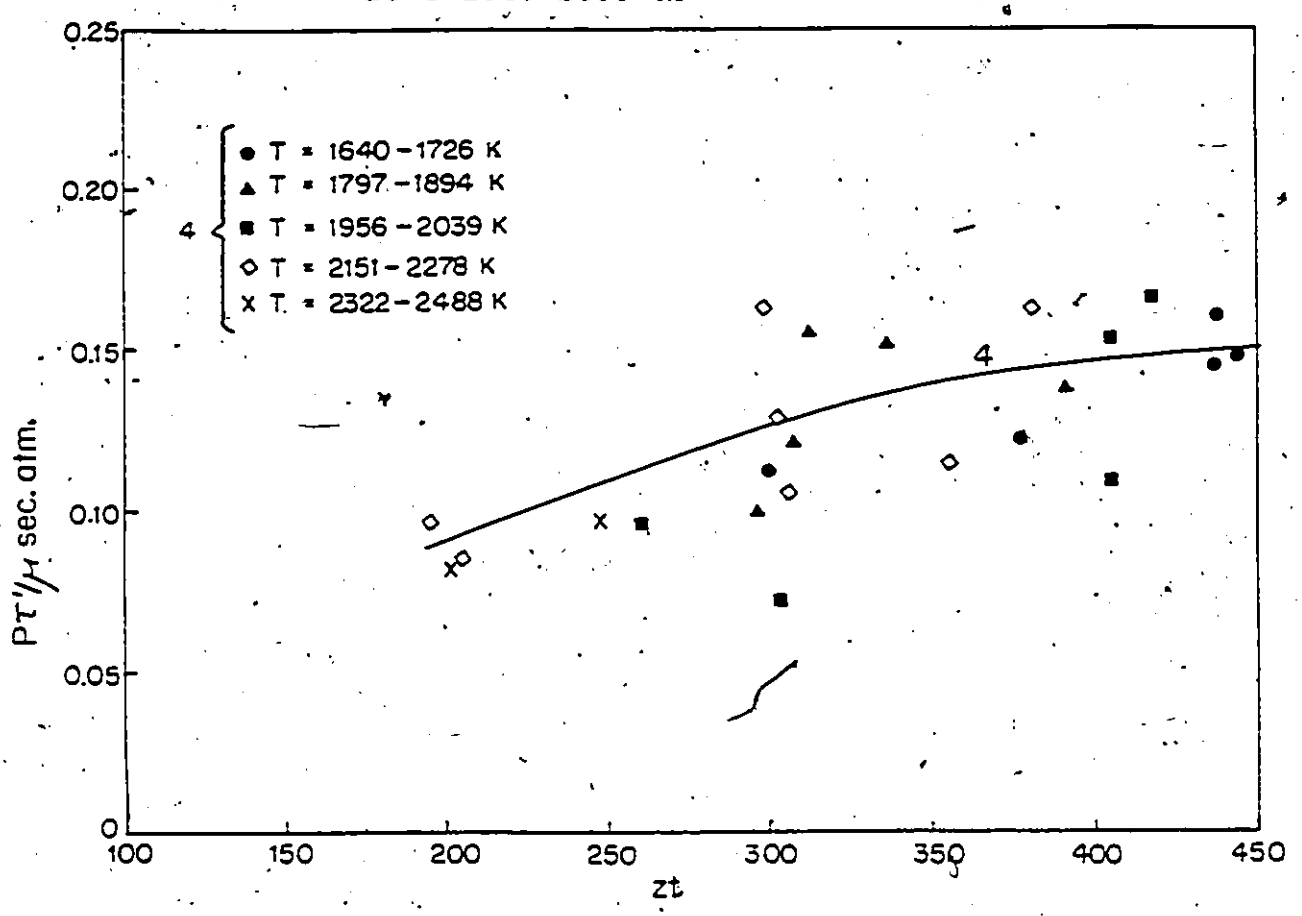

Figure 3.29 Variation of the vibrational relaxation time of the 5.0 % C_2H_2-Ar mixture with Zt (Curves of figs. 3.27-28).

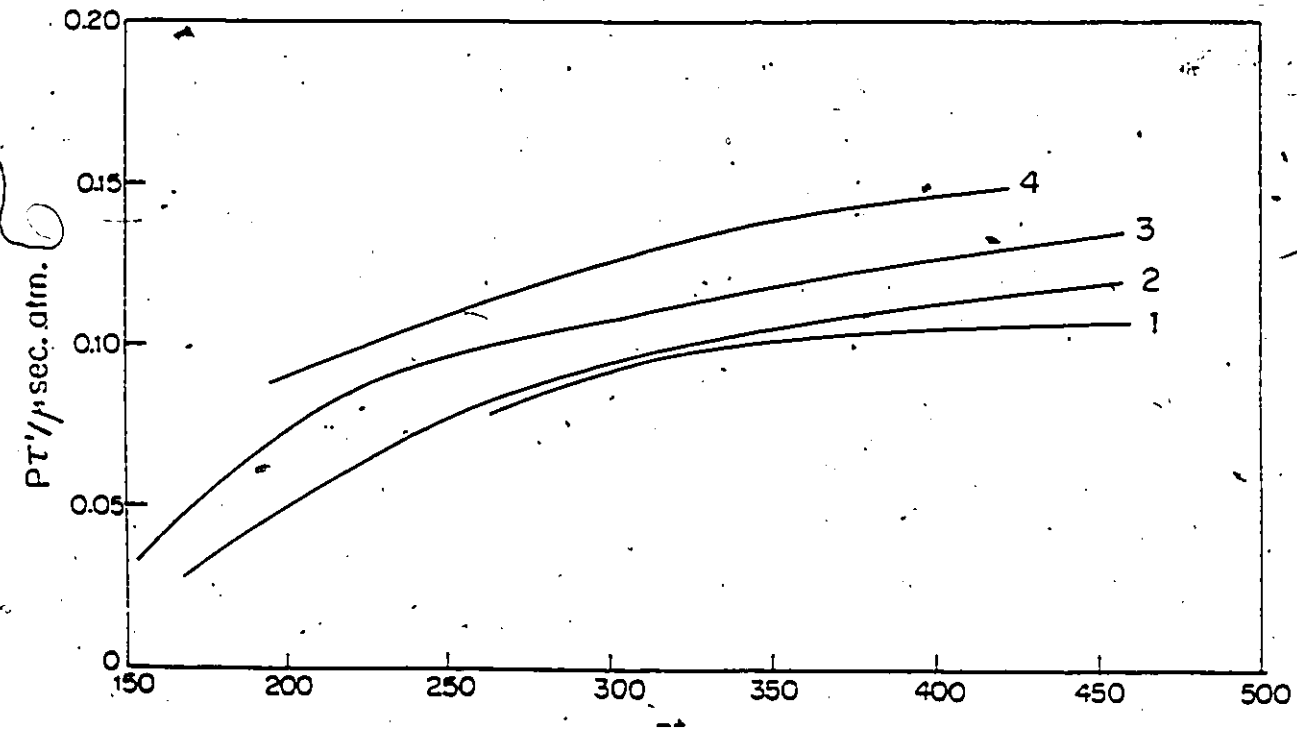

Figure 3.30 Variation of the vibrational relaxation time of the 2.5 % C_2H_2-Ar mixture with Zt at T=1341-1791 K.

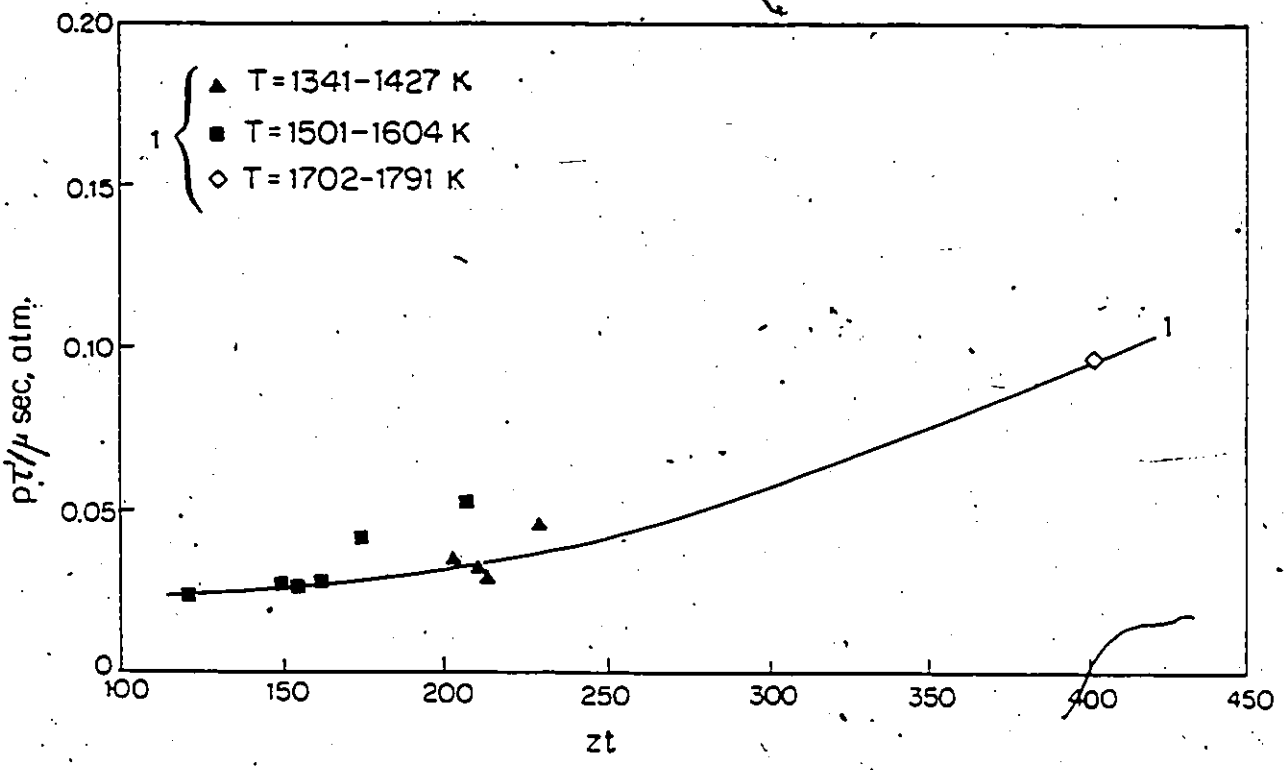

Figure 3.31 Variation of the vibrational relaxation time of the 2.5 % C_2H_2-Ar mixture with Zt at T=1920-2024 K, 2094-2201 K and 2239-2621 K.

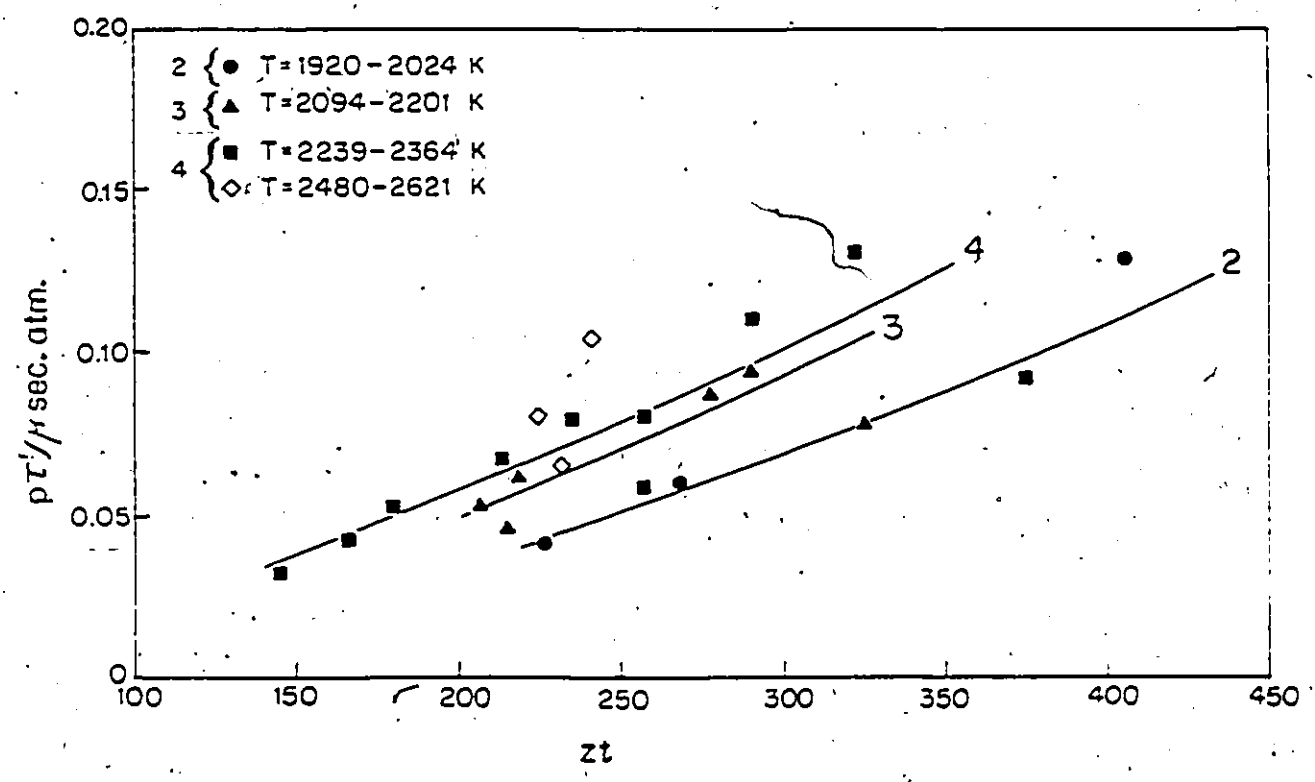

Figure 3.32 Variation of the vibrational relaxation time of the 2.5 % C_2H_2-Ar mixture with Zt (Curves of figs. 3.30-31).

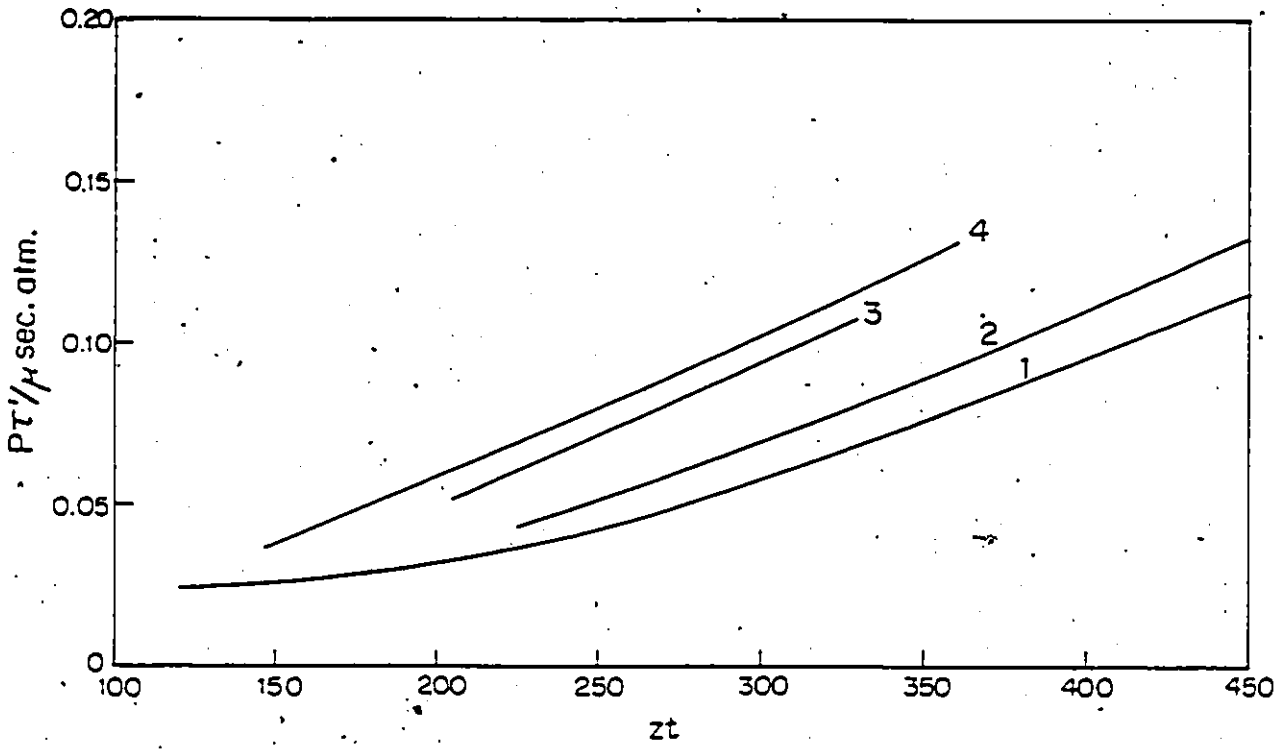

Figure 3.33 Variation of the vibrational relaxation time of the 1.0 % C_2H_2-Ar mixture with Zt at T=1386-2039 K.

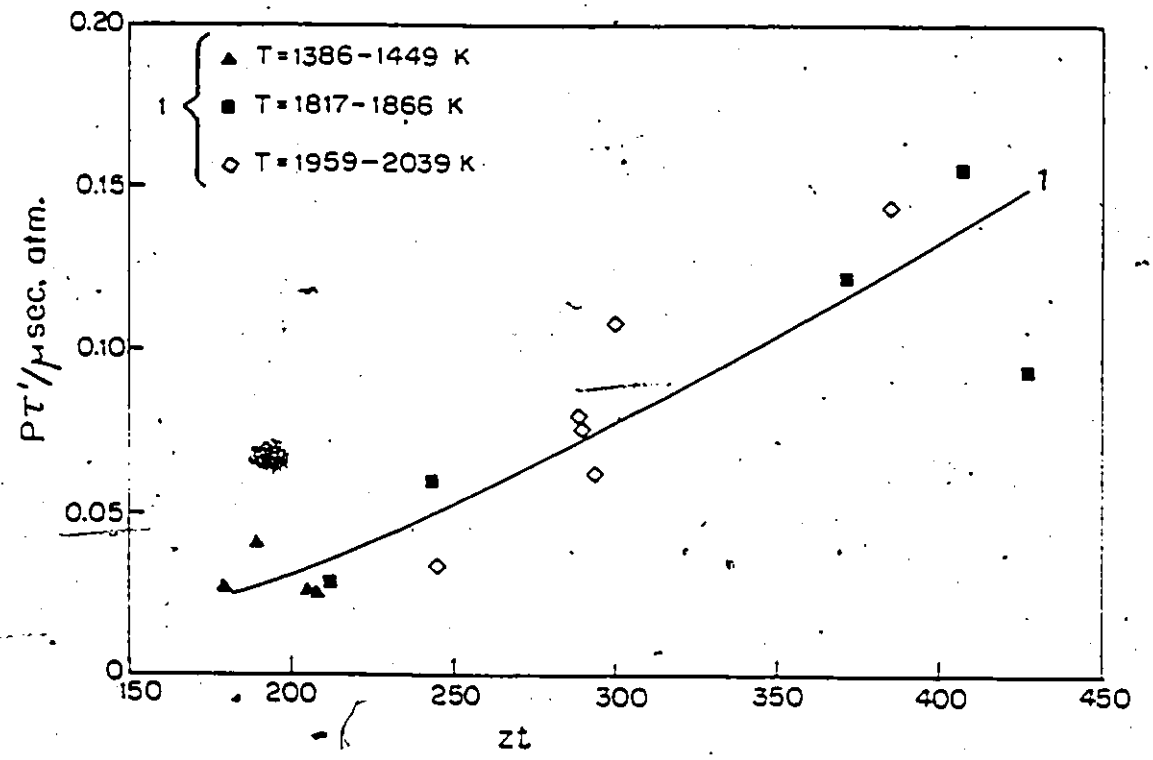

Figure 3.34 Variation of the vibrational relaxation time of the 1.0 % C_2H_2-Ar mixture with Zt at T=2064-2645 K.

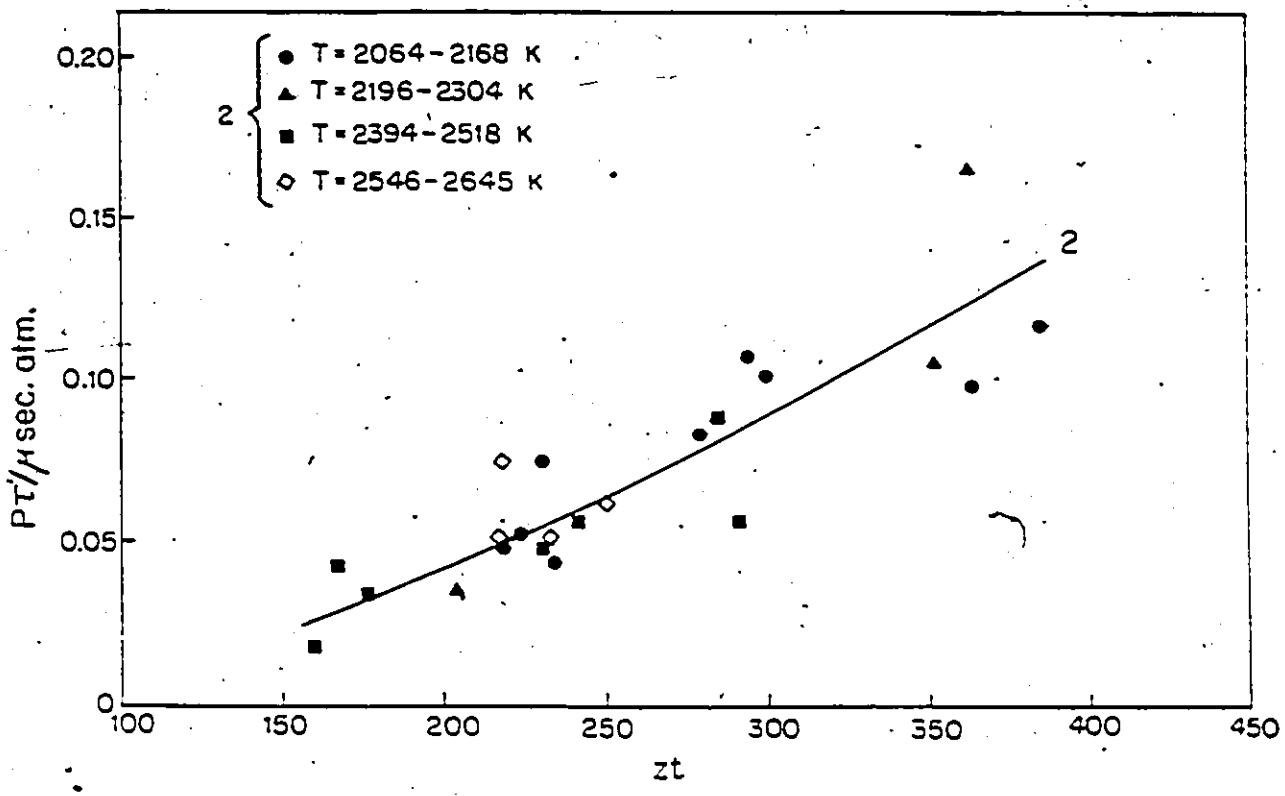

Figure 3.35 Variation of the vibrational relaxation time of the 1.0 % C_2H_2-Ar mixture with Zt (Curves of figs. 3.33-34).

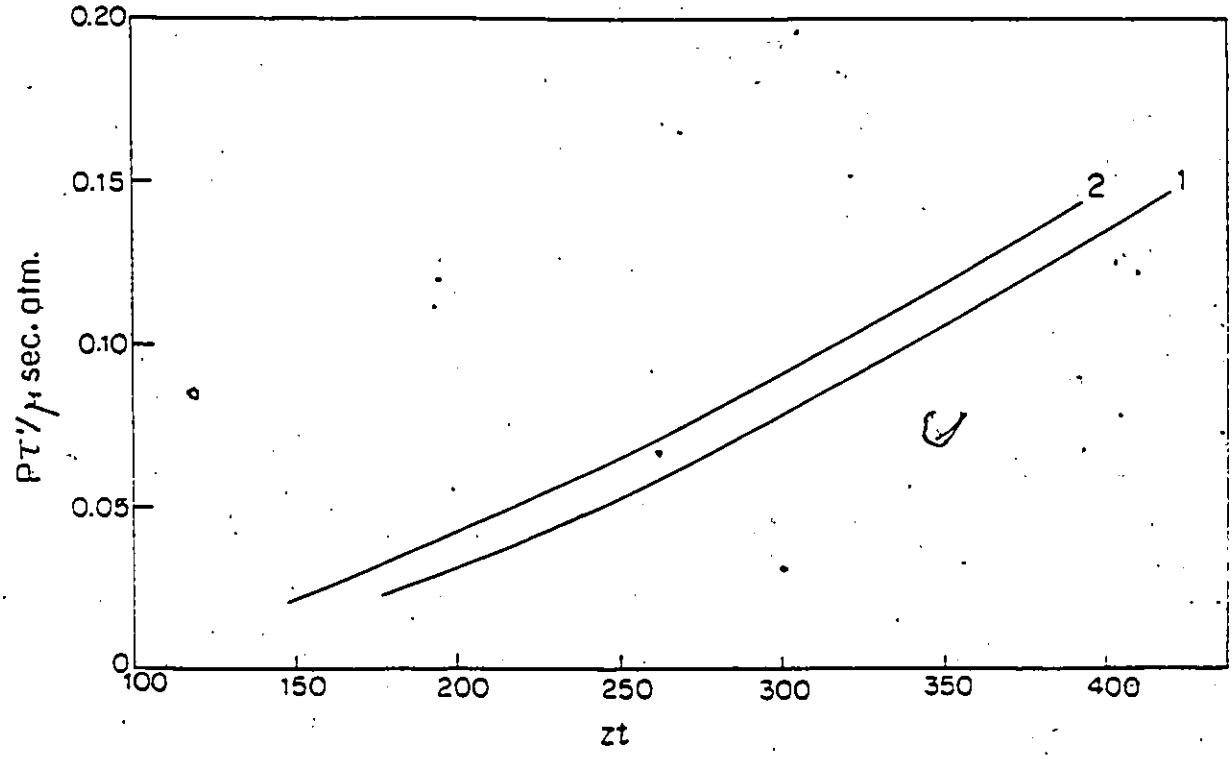

the mixtures especially at low mole fraction where the temperature range was as high as 600 K. In order to facilitate comparison of curves of the same mole fraction, they were drawn on the same graph (fig. 3.18, 3.22, 3.26, 3.29, 3.32 and 3.35, for mixtures of 50.5, 23.6, 12.1, 5.0, 2.5 and 1.0% C_2H_2 in Ar respectively). In all curves of these figures the relaxation time increased with increasing Zt. This is the same as for pure C_2H_2 and pure N_2O. However, the shape of the curves changed from one mixture to another. For example, while for pure C_2H_2 no sign of equilibrium or near equilibrium could be detected (fig. 3.14), in some mixtures, especially in the mixture containing 5.0% C_2H_2 (fig. 3.29) and in certain curves of the mixture containing 50.5% (curve 3 fig. 3.18), 23.6% (curve 6 fig. 3.22) and 12.1% (curves 3 and 4 of fig. 3.26) C_2H_2 in Ar, an equilibrium or near-equilibrium value of the vibrational relaxation time was observed. In the mixtures of low mole fraction of C_2H_2 (2.5 and 1.0% C_2H_2) (fig. 3.32 and 3.35,) it seems that the equilibrium or near-equilibrium relaxation time is far from being reached. However, the imprecision, the large temperature range as well as the small number of experiments performed for these mixtures make these curves less reliable than curves corresponding to higher mole fraction.

3.3.2 The effect of temperature on the vibrational relaxation time of C_2H_2-Ar mixtures.

The temperature dependance of the relaxation time of C_2H_2-Ar mixtures can be deduced from curves of fig. 3.18 to 3.22, 3.26, 3.29, 3.32 and 3.35. From these curves, vibrational relaxation times were determined at different Zt and different temperature

and the results are summarized in tables A.9 to A.16, appendix A. In each of these tables, the inverse of the vibrational relaxation time, $1/P\tau'$, and the temperature range for every mixture are indicated at different Zt. These tables will be used for testing the linear mixture rule in the next section.

The temperature dependence of the relaxation time at different Zt is represented for every mixture in separate figures (fig. 3.36 to 3.41). As was found in the case of pure C_2H_2, some curves exhibit a minimum as well as a maximum (see for example fig. 3.38 (12.1% C_2H_2)) and this is due to the fact that certain curves cross others for some mixtures. However we can readily see that the relaxation time generally increases with increasing temperature (at constant Zt) for all mixtures under investigation. This is in agreement with the results of pure C_2H_2 and pure N_2O.

3.4 Linear Mixture Rule

In order to test the validity of the linear mixture rule, the reciprocal of the vibrational relaxation time or the phenomenological rate coefficient $(P\tau)^{-1}$ was plotted vs C_2H_2 mole fraction at different Zt and different temperature regions. Figs. 3.42 to 3.45 show the Zt dependence of the mixture rule for different temperature regions and figs. 3.46 to 3.47 show the temperature dependance of the mixture rule for different Zt. The data were taken from tables A.9 to A.16. In all of these figures, the effective relaxation rate coefficient increases slowly with decreasing C_2H_2 mole fraction, then suddenly increases sharply at low mole fraction to reach a maximum near

Figure 3.36 Variation of the vibrational relaxation time of the 50.5 % C_2H_2-Ar mixture with temperature at different Zt.

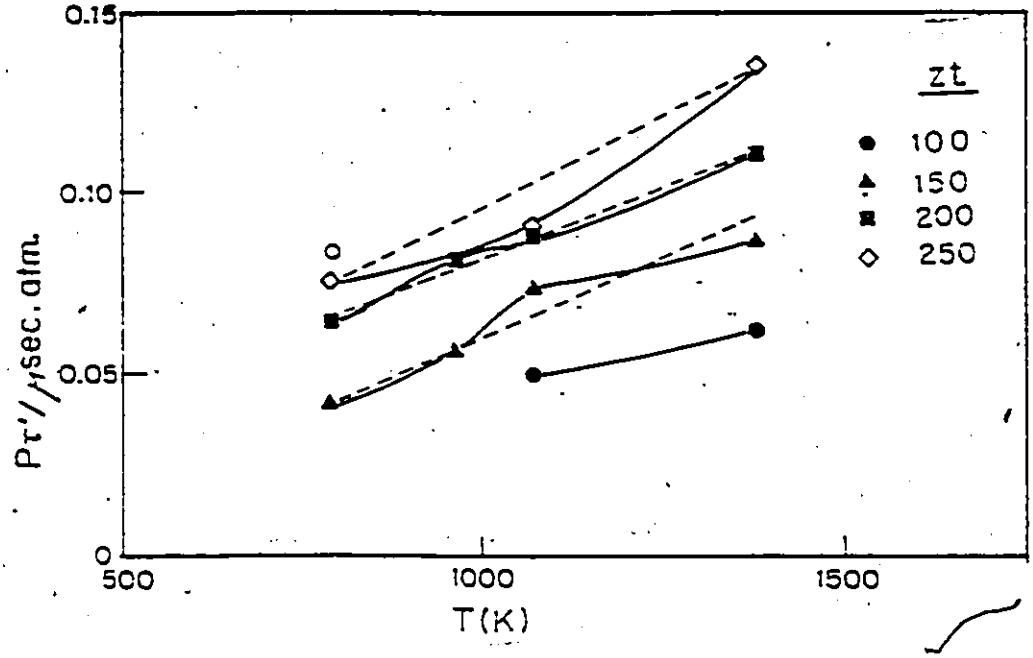

Figure 3.37 Variation of the vibrational relaxation time of the 23.6 % C_2H_2-Ar mixture with temperature at different Zt.

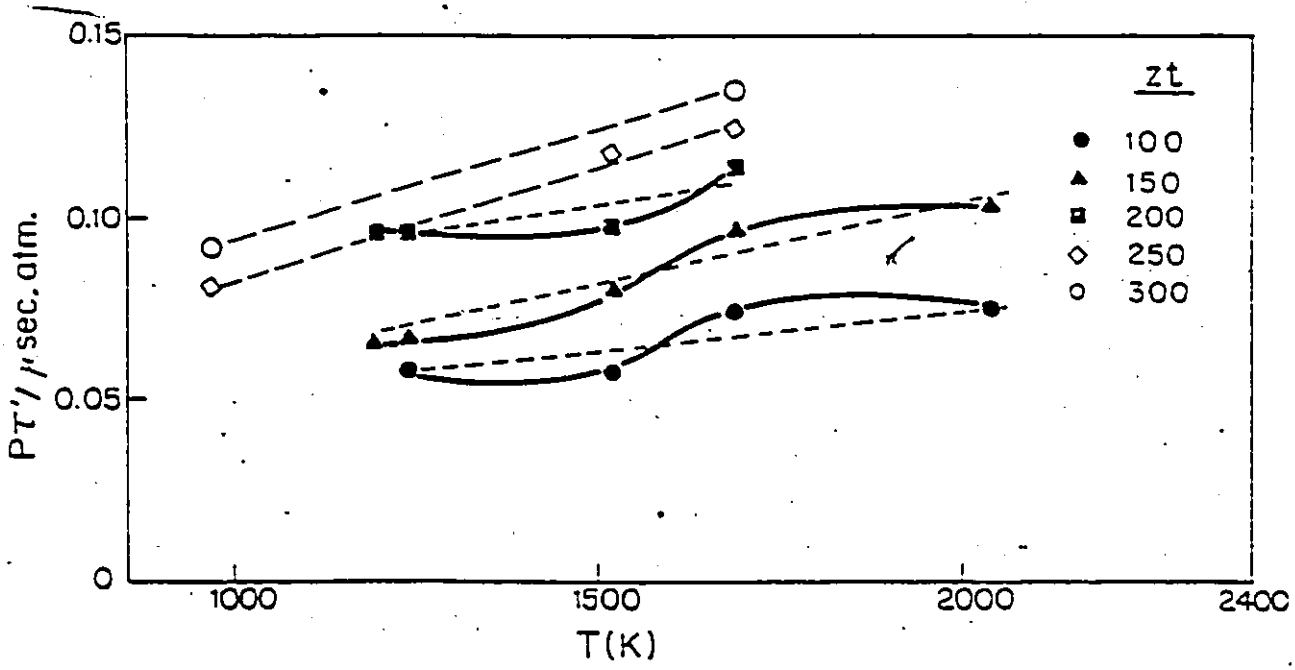

Figure 3.38 Variation of the vibrational relaxation time of the 12.1 % C_2H_2-Ar mixture with temperature at different Zt.

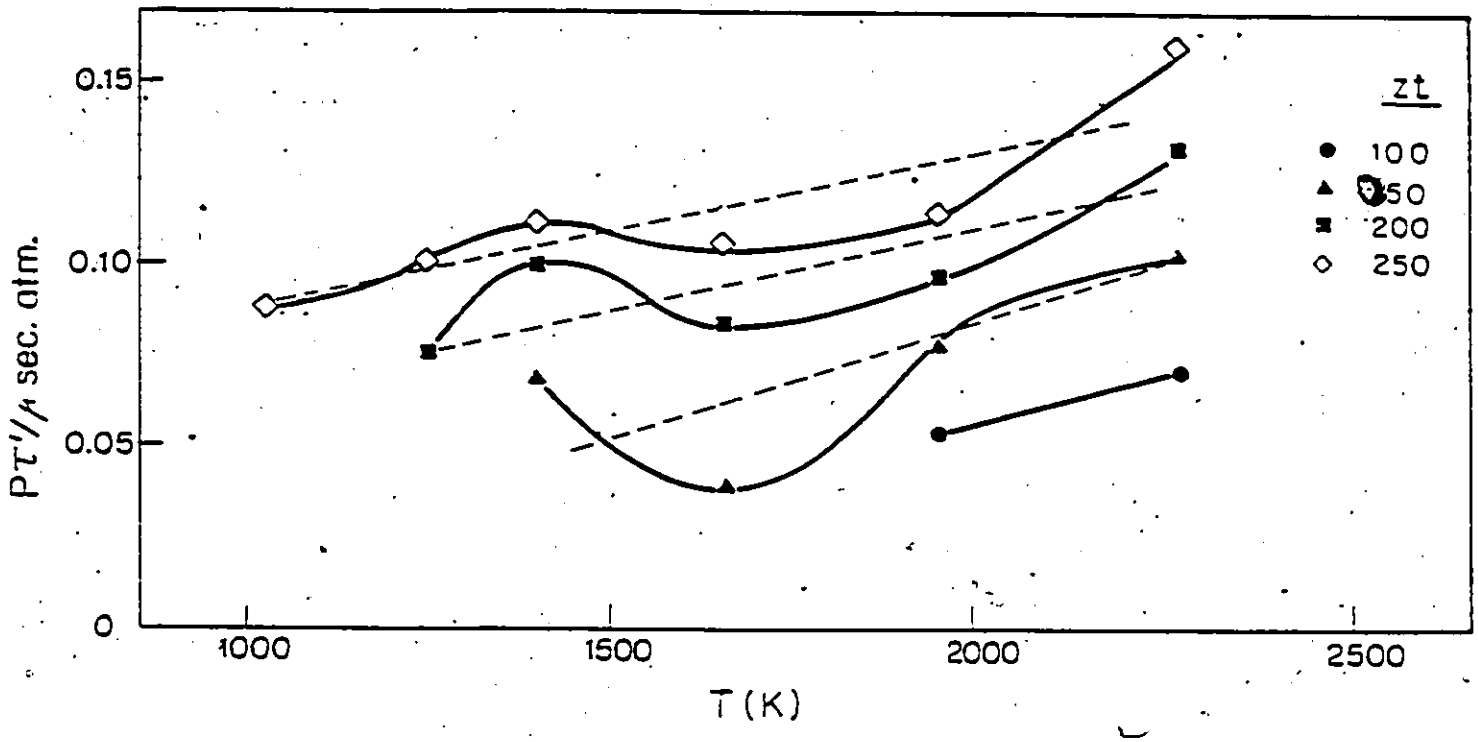

Figure 3.39 Variation of the vibrational relaxation time of the 5.0 % C_2H_2-Ar mixture with temperature at different Zt.

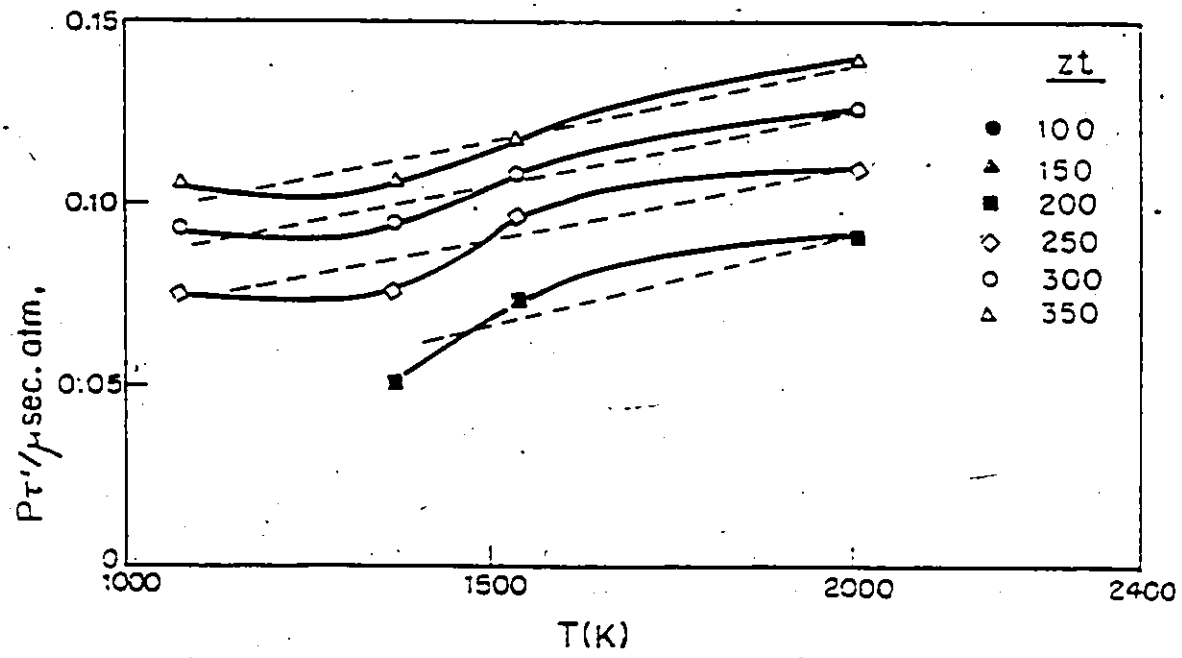

Figure 3.40 Variation of the vibrational relaxation time of the 2.5 % C_2H_2-Ar mixture with temperature at different Zt.

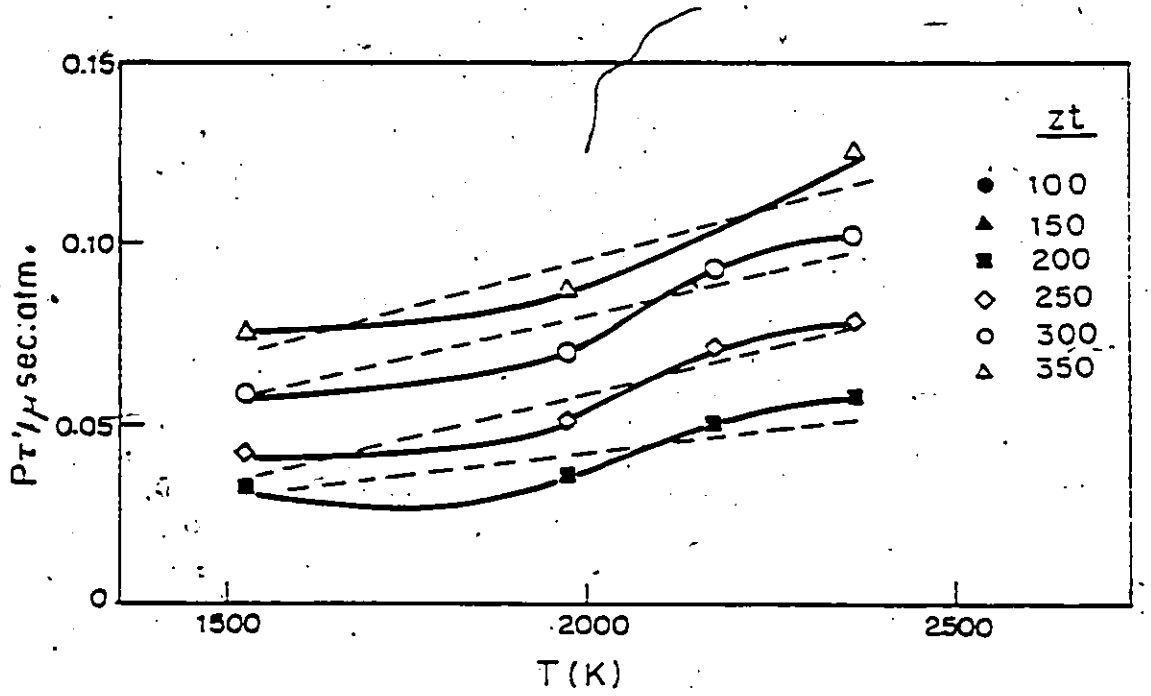

Figure 3.41 Variation of the vibrational relaxation time of the 1.0 % C_2H_2-Ar mixture with temperature at different Zt.

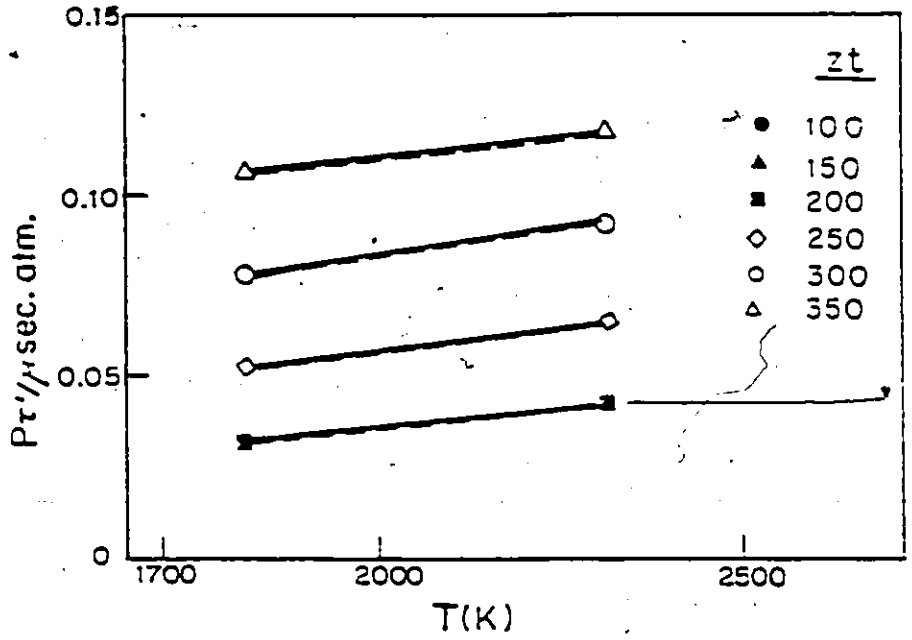

Figure 3.42 Variation of the reciprocal of the vibrational relaxation time of C_2H_2-Ar mixtures with mole fraction and Zt at T=1300-1500 K.

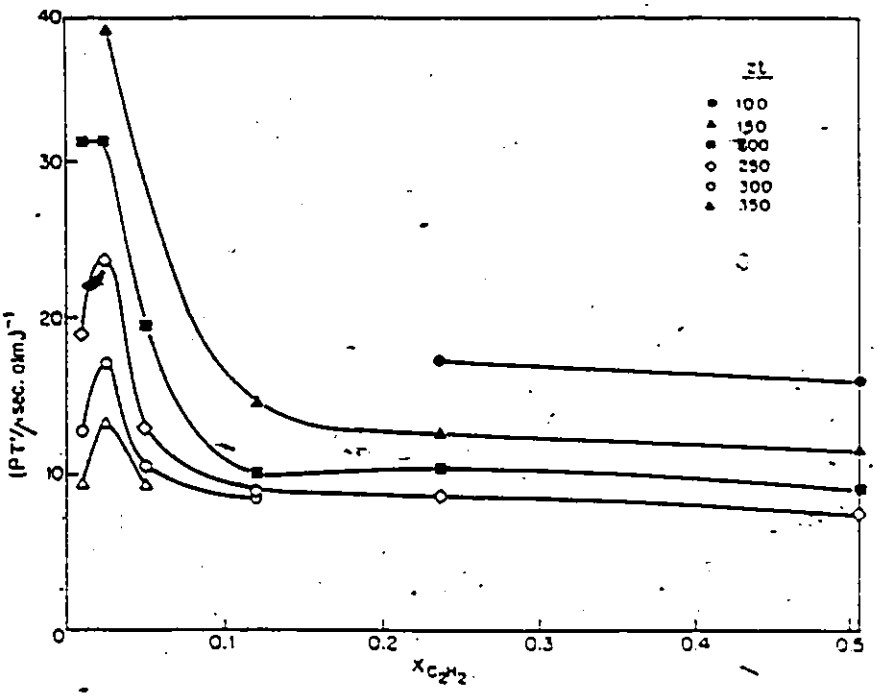

Figure 3.43 Variation of the reciprocal of the vibrational relaxation time of C_2H_2-Ar mixtures with mole fraction and Zt at T=1400-1600 K.

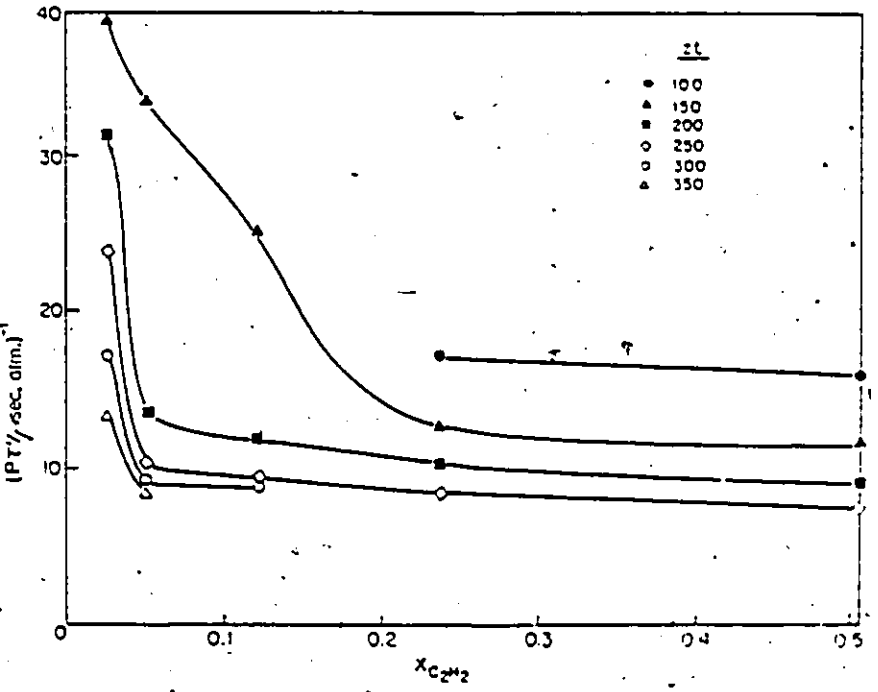

Figure 3.44 Variation of the reciprocal of the vibrational relaxation time of C_2H_2-Ar mixtures with mole fraction and Zt at T=1600-1800 K.

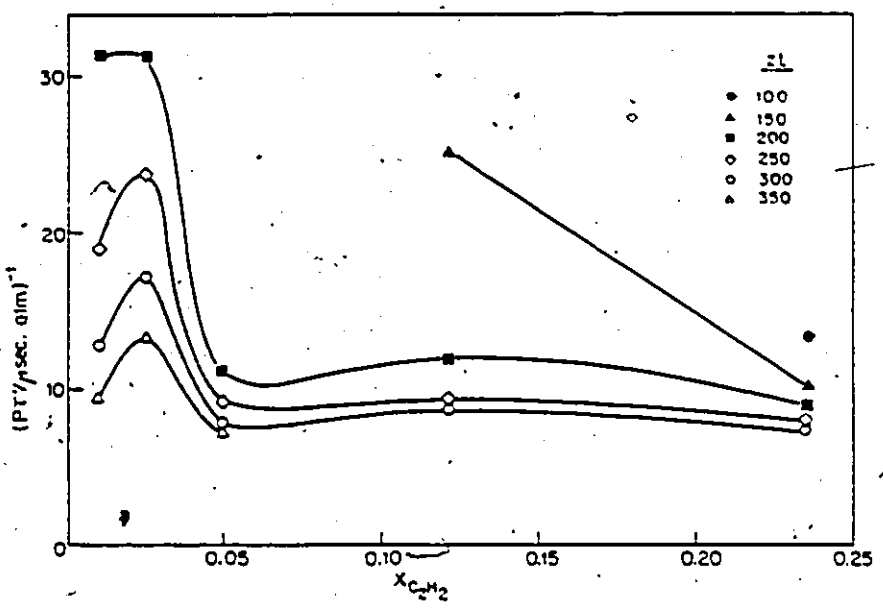

Figure 3.45 Variation of the reciprocal of the vibrational relaxation time of C_2H_2-Ar mixtures with mole fraction and Zt at T=1800-2000 K.

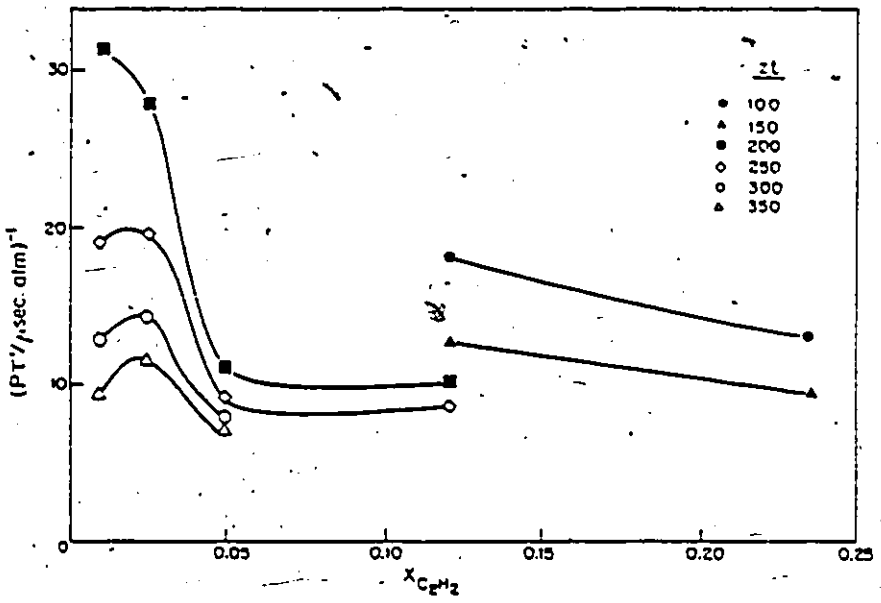

Figure 3.46 Variation of the reciprocal of the vibrational relaxation time of C_2H_2-Ar mixtures with mole fraction and temperature at Zt=200.

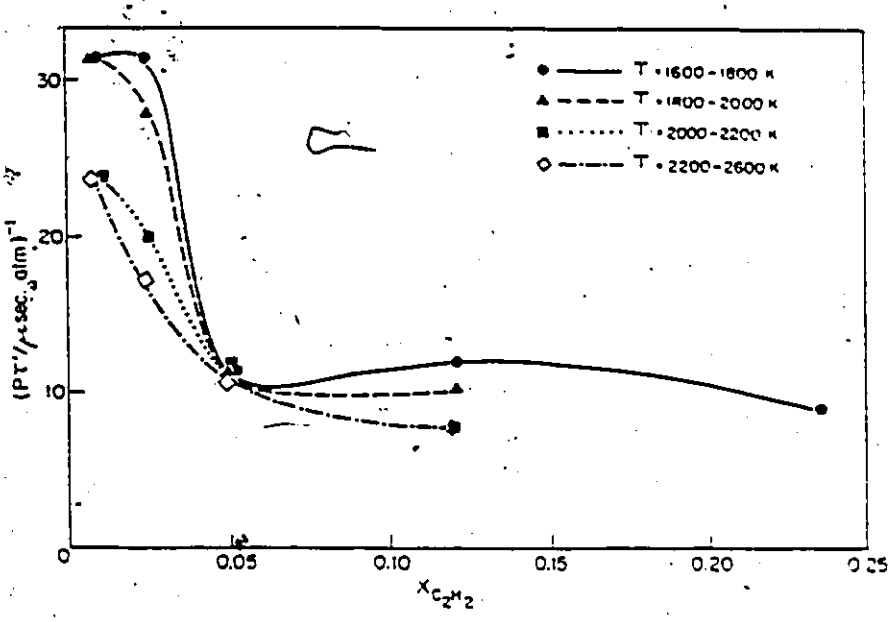

Figure 3.47 Variation of the reciprocal of the vibrational relaxation time of C_2H_2-Ar mixtures with mole fraction and temperature at Zt=250.

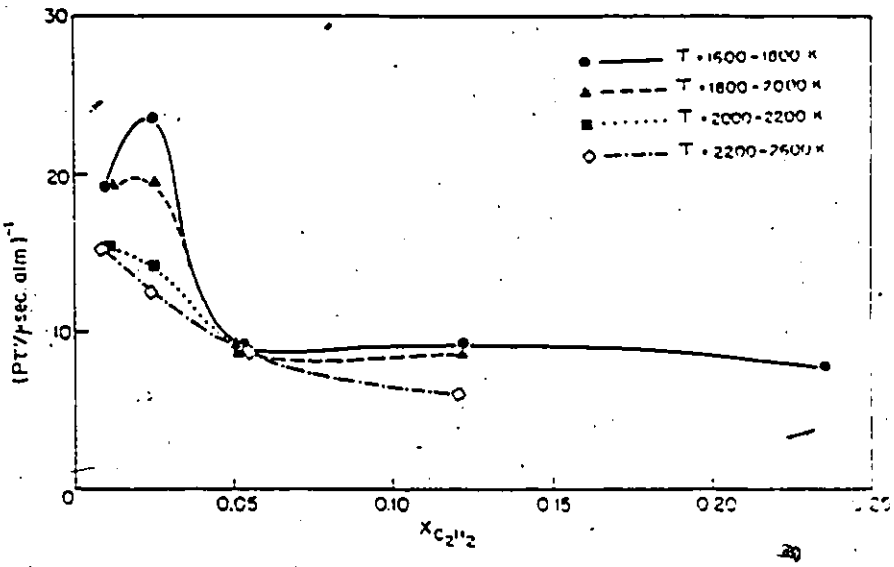

2.5% C_2H_2. Then it decreases rapidly. The maximum becomes smaller and tends to disappear at high Zt. We can conclude that the mixture rule approaches linearity under these conditions. Although many examples in the literature show deviation from linearity in the mixture rule plots, no deviation from linearity similar to this one has yet been observed. However Teitelbaum (29, 78) did predict similar curves by solving the master equation for vibrational relaxation of diatomic molecules. The details of this analysis as well as the curves obtained were presented in the first chapter (section 1.5). It was concluded that the linear mixture rule is valid only at equilibrium (high Zt). This is in agreement with what we found in our experiments. Additionally, it is expected that deviation from linearity will be more pronounced at higher temperatures. Our results are inconclusive on this point. Figures 3.46 and 3.47 show that maxima are displaced to lower mole fractions as the temperature increases. We were unable to measure at sufficiently low mole fractions to observe maxima in $P\tau$ for T>2000 K. We therefore do not know how large the deviations are there.

Interestingly, deviations from linearity for N_2O-Ar mixtures and CH_4-Ar mixtures (fig. 1.15) are different qualitatively from the present observations for C_2H_2-Ar mixtures. If the former two are characteristic of polyatomic systems, the present one appears to behave more like predicted for diatomic molecules.

CHAPTER 4: COMPUTER SIMULATION OF VIBRATIONAL RELAXATION

Vibrational relaxation times of N_2O, C_2H_2 and mixtures of N_2O and C_2H_2 with Ar can be calculated by solving the master equation for the vibrational relaxation processes. We saw earlier that a diatomic molecule treated as a harmonic oscillator subjected to Landau-Teller selection rules leads to the Bethe-Teller law (eq. 1.8, section 1.1.3). Equation 1.8 is applicable only to harmonic oscillators for which the V-V processes do not contribute to the energy transfer. By introducing the anharmonicity for both T-V and V-V processes, with the limitation that $\Delta v = \pm 1$, the master equations for a pure diatomic molecule can be reduced to a simple analytical rate law (29, 78) (eq. 1.28, section 1.5).

N_2O and C_2H_2 are polyatomic molecules. Several vibrational modes and combinations of modes are available so that neither equation 1.8 nor equation 1.28 can be used to represent the vibrational relaxation of polyatomic molecules. An analytical expression for the rate of change of vibrational energy for polyatomic molecules is not yet available. Several energy transfer pathways can be involved in polyatomic molecules such as T-V, intermolecular intermode V-V, intermolecular intramode V-V, intramolecular intermode V-V and intramolecular intramode V-V. It seems to be very difficult to obtain an analytical expression for the rate of change of vibrational enery for polyatomic molecules. The rate of energy transfer is given by:

$$dE/dt = dE/dt(T\text{-}V) + dE/dt(V\text{-}V \text{ intermolecular intermode}) + dE/dt(V\text{-}V \text{ intermolecular intramode}) + dE/dt(V\text{-}V \text{ intramolecular intermode}) + dE/dt(V\text{-}V \text{ intramolecular intramode}) \quad (4.1)$$

We did not attempt to obtain an analytical expression for the rate of energy change for polyatomic molecules. Instead, we calculated the vibrational relaxation time for N_2O, C_2H_2, N_2O-Ar and C_2H_2-Ar mixtures by <u>numerical</u> integration of the master equations. Results will be presented in this chapter.

4.1 Vibrational energy levels

4.1.1 N_2O

The vibrational energy levels of N_2O are given by:

$$E(cm^{-1}) = 1299.3(v_1 + 0.5) + 596.5(v_2 + 1.0) + 2276.5(v_3 + 0.5) - x_{11}(v_1 + 0.5)^2 - x_{22}(v_2 + 1.0)^2 - x_{33}(v_3 + 0.5)^2 + x_{12}(v_1 + 0.5)(v_2 + 1.0) + x_{13}(v_1 + 0.5)(v_3 + 0.5) + x_{23}(v_2 + 1.0)(v_3 + 0.5) + g_{22}L^2 - E(0,0,0) \quad (4.2)$$

where v_1, v_2 and v_3 are the vibrational quantum numbers of ν_1, ν_2, and ν_3 respectively. x_{ij} and g_{22} are the spectroscopic constants used for calculating corrections to the rigid rotator-harmonic oscillator approximation (cm^{-1}) (113).

$x_{11} = -3.25$ $\quad x_{12} = 4.75$ $\quad g_{22} = 3.03$

$x_{22} = -2.28$ $\quad x_{23} = -12.45$

$x_{33} = -13.75$ $\quad x_{13} = -26.15$

L takes the values $\pm v_2$, $\pm v_2\text{-}2 \ldots 0$ or 1

Vibrational energy levels up to 6000 cm^{-1} were calculated using the above equation. Results are summarized in table 4.1

Table 4.1 Energy levels of N_2O

Level	Before Regrouping				After Regrouping			
	Total Degeneracy	Average Energy cm^{-1}	Relative Population 295 K	750 K	Total Degeneracy	Average Energy cm^{-1}	Relative Population 295 K	750 K
(0,0,0)	1	0	0.8879	0.4136	1	0	0.8879	0.2643
(0,1,0)	2	588	0.1009	0.2677	2	589	0.1002	0.2263
(0,2,0) (1,0,0)	3 1	1175 1285	0.0086 0.0017	0.1302 0.0351	4	1203	0.0103	0.1870
(0,3,0) (1,1,0)	4 2	1759 1878	0.0007 0.0002	0.0566 0.0225	6	1799	0.0009	0.1189
(0,0,1) (0,4,0)	1 5	2224 2340	0.0000 0.0000	0.0058 0.0232	6	2321	0.0000	0.0560
(1,2,0) (2,0,0)	3 1	2469 2564	0.0000 0.0000	0.0109 0.0030	4	2493	0.0000	0.0292
(0,1,1) (0,5,0)	2 6	2800 2918	0.0000 0.0000	0.0038 0.0092	8	2889	0.0000	0.0330
(1,3,0) (2,1,0)	4 2	3058 3162	0.0000 0.0000	0.0047 0.0019	6	3093	0.0000	0.0184
(0,2,1) (1,0,1) + (0,6,0)	3 8	3374 3493	0.0000 0.0000	0.0019 0.0041	11	3461	0.0000	0.0199
(1,4,0)	5	3644	0.0000	0.0019	5	3644	0.0000	0.0069
(2,2,0) (3,0,0)	3 1	3757 3834	0.0000 0.0000	0.0009 0.0003	4	3777	0.0000	0.0046
(0,3,1) (1,1,1) + (0,7,0)	4 10	3945 4067	0.0000 0.0000	0.0008 0.0017	14	4032	0.0000	0.0111

Table 4.1 Cont'd.

(1,5,0)	6	4227			6	4227	0.0000	0.0036
(2,3,0)	4	4351						
(0,0,2)	1	4419			7	4386	0.000	0.0034
(3,1,0)	2	4438						
(0,4,1)	5	4514			5	4514	0.0000	0.0020
(0,8,0)	9	4639			12	4640	0.0000	0.0040
(1,2,1)	3	4642						
(2,0,1)	1	4735			8	4799	0.0000	0.0021
(1,6,0)	7	4808						
(2,4,0)	5	4941			7	4953	0.0000	0.0015
(0,1,2)	2	4983						
(3,2,0)	3	5039						
(0,5,1)	6	5080			10	5070	0.0000	0.0018
(4,0,0)	1	5101						
(0,9,0)	10	5208			14	5211	0.0000	0.0020
(1,3,1)	4	5218						
(2,1,1)	2	5320			10	5373	0.0000	0.0011
(1,7,0)	8	5386						
(2,5,0)	6	5530			9	5535	0.0000	0.0008
(0,2,2)	3	5545						
(3,3,0)	4	5636						
(0,6,1)	7	5643			14	5651	0.0000	0.0011
(1,0,2)	1	5652						
(4,1,0)	2	5709						
(1,4,1)	5	5791			5	5791	0.0000	0.0003
(2,2,1)	3	5904						
(1,8,0)	7	5930			11	5927	0.0000	0.0006
(3,0,1)	1	5980						

including the degeneracy and the relative population at 295 and 750 K for each vibrational level. They are also represented graphically in fig. 1.3 (section 1.3). All energy levels were also condensed into one column in fig.1.3. Since the number of energy levels less than 6000 cm^{-1} is very high (51 levels) for a numerical integration, all energy levels within 100 cm^{-1} of each other were condensed and replaced with an average energy level of an appropriately increased degeneracy. They are summarized in table 4.1 and represented graphically in fig. 1.3. Both regroupings represented in table 4.1 and fig. 1.3 were used in the calculation.

In our calculation we first determined the effect of this arbitrary regrouping, as well as of the arbitrary cutoff at 6000 cm^{-1}. We were satisfied that these simplifications did not affect the generality of our results and certainly not the qualitative conclusions. Physically, the regrouping meant that those energy levels within a single group were kinetically indistinguishable; i.e. once one of these levels became (de)populated the remainder in that group became instantaneously equilibrated with it.

4.1.2 C_2H_2

The vibrational energy levels of C_2H_2 are given by:

$$E(cm^{-1}) = 3373.1(v_1 + 0.5) + 1973.8(v_2 + 0.5) +$$
$$3281.9(v_3 + 0.5) + 611.6(v_4 + 1.0) + 729.3(v_5 + 1.0) +$$
$$x_{11}(v_1 + 0.5)^2 + x_{22}(v_2 + 0.5)^2 + x_{33}(v_3 + 0.5)^2 +$$
$$x_{44}(v_4 + 1.0)^2 + x_{55}(v_5 + 1.0)^2 + x_{12}(v_1 + 0.5)(v_2 + 0.5) +$$
$$x_{13}(v_1 + 0.5)(v_3 + 0.5) + x_{14}(v_1 + 0.5)(v_4 + 1.0) +$$

$$x_{15}(v_1 + 0.5)(v_5 + 1.0) + x_{23}(v_2 + 0.5)(v_3 + 0.5) +$$
$$x_{24}(v_2+0.5)(v_4 + 1.0) + x_{25}(v_2 + 0.5)(v_5 + 1.0) +$$
$$x_{34}(v_3 + 0.5)(v_4+1.0) + x_{35}(v_3 + 0.5)(v_5 + 1.0) +$$
$$x_{45}(v_4 +1.0)(v_5+ 1.0) + g_{44}L_4^2 + g_{55}L_5^2 - E(0,0,0,0,0) \quad (4.3)$$

where x_{ij}, g_{44} and g_{55} are the spectroscopic constants used in calculating anharmonic corrections to the rigid rotator-harmonic oscillator approximation (108):

X_{11}=-24.08	X_{22}=-7.92	X_{34}=-9.06	
X_{12}=-16.94	X_{23}=-1.38	X_{35}=-5.73	g_{44}= 1.1
X_{13}=-99.01	X_{24}=-6.15	X_{44}=-5.38	g_{55}= 2.49
X_{14}=-16.46	X_{25}=-0.85	X_{45}=-12.65	
X_{15}=-11.75	X_{33}=-25.69	X_{55}=-2.27	

$L_4 = \pm v_4, v_4-2, \ldots\ldots 1 \text{ or } 0$

$L_5 = \pm v_5, v_5-2, \ldots\ldots 1 \text{ or } 0$

Vibrational energy levels up to 5500 cm^{-1} were calculated by using the above equation. Results are summarized in table 4.2 including the degeneracy corresponding to each vibrational level, and are also represented graphically in fig. 1.9 (section 1.4) along with the vibrational mode and degeneracy corresponding to each vibrational level. All energy levels are collected in the same column of fig. 1.9. Since the number of energy levels < 5500 cm^{-1} is very high, (93 levels), all energy levels within 100 cm^{-1} of each other were condensed into one level and an average energy and appropriate degeneracy were assigned. This procedure was repeated for the new series of energy levels and another series of energy levels was obtained. These two successive regroupings are summarized in table 4.2 and represented graphically in fig.

Table 4.2 Energy Levels Of C_2H_2.

	No Regrouping		1st Regrouping*				2nd Regrouping	
Level	Total Degeneracy	Average Energy cm^{-1}	Total Degeneracy	Average Energy cm^{-1}	Relative Population 295 K	750 K	Total Degeneracy	Average Energy cm^{-1}
(0,0,0,0,0)	1	0	1	0	0.8389	0.2499	1	0
(0,0,0,1,0)	2	600.3	2	600.3	0.0897	0.1580	4	652.0
(0,0,0,0,1)	2	703.0	2	703.0	0.0544	0.1297		
(0,0,0,2,0)	3	1212	7	1257	0.0128	0.1568	7	1257
(0,0,0,1,1)	4	1291						
(0,0,0,0,2)	3	1403	3	1403	0.0027	0.0508	3	1403
(0,0,0,3,0)	4	1835	10	1868	0.0009	0.0694	17	1911
(0,0,0,2,1)	6	1890						
(0,1,0,0,0)	1	1942	7	1973	0.0004	0.0397		
(0,0,0,1,2)	6	1978						
(0,0,0,0,3)	4	2101	4	2101	0.0001	0.0177	4	2101
(0,0,0,4,0)	5	2470	24	2521	0.0001	0.0476	24	2521
(0,0,0,3,1)	8	2501						
(0,1,0,1,0)	2	2536						
(0,0,0,2,2)	9	2565						
(0,1,0,0,1)	2	2644	10	2659	0.0000	0.0152	10	2659
(0,0,0,1,3)	8	2663						

Table 4.2 Cont'd

(0,0,0,0,4)	5	2795	5	2795	0.0000	0.0059	5	2795
(0,0,0,5,0)	6	3117						
(0,0,0,4,1)	10	3123						
(0,1,0,2,0)	3	3142	32	3140	0.0000	0.0193		
(0,0,0,3,2)	12	3163					49	3173
(0,0,1,0,0)	1	3165						
(0,1,0,1,1)	4	3226						
(0,0,0,2,3)	12	3237	17	3235	0.0000	0.0086		
(1,0,0,0,0)	1	3239						
(0,1,0,0,2)	3	3344	13	3345	0.0000	0.0053		
(0,0,0,1,4)	10	3345					19	3390
(0,0,0,0,5)	6	3487	6	3487	0.0000	0.0019		
(0,0,0,5,1)	12	3757						
(0,0,1,1,0)	2	3757						
(0,1,0,3,0)	4	3759						
(0,0,0,4,2)	15	3772	64	3787	0.0000	0.0112		
(0,0,0,6,0)	7	3774						
(0,1,0,2,1)	6	3819						
(0,0,0,3,3)	16	3823						
(1,0,0,1,0)	2	3823					90	3821
(0,0,1,0,1)	2	3863						
(0,2,0,0,0)	1	3863						
(0,0,0,2,4)	15	3906	26	3904	0.0000	0.0036		
(0,1,0,1,2)	6	3912						
(1,0,0,0,1)	2	3930						

Table 4.2 Cont'd

(0,0,0,1,5)	12	4024	16	4028	0.0000	0.0018	23	4073
(0,1,0,0,3)	4	4040						
(0,0,0,0,6)	7	4176	7	4176	0.0000	0.0006		
(0,0,1,2,0)	3	4360						
(0,1,0,4,0)	5	4388						
(0,0,0,5,2)	18	4394						
(0,0,0,6,1)	14	4402						
(1,0,0,2,0)	3	4418	85	4412	0.0000	0.0045		
(0,0,0,4,3)	20	4419						
(0,1,0,3,1)	8	4423						
(0,0,1,1,1)	4	4442					141	4455
(0,0,0,7,0)	8	4444						
(0,2,0,1,0)	2	4456						
(0,0,0,3,4)	20	4479						
(0,1,0,2,2)	9	4493						
(1,0,0,1,1)	4	4501						
(0,0,1,0,2)	3	4557	56	4520	0.0000	0.0024		
(0,2,0,0,1)	2	4569						
(0,0,0,2,5)	18	4573						
(0,1,0,1,3)	8	4596	11	4602	0.0000	0.0004		
(1,0,0,0,2)	3	4619						
(0,0,0,1,6)	14	4700	19	4709	0.0000	0.0006	30	4670
(0,1,0,0,4)	5	4734						
(0,0,0,0,7)	8	4862	8	4862	0.0000	0.0002	8	4862

Table 4.2 Cont'd

(0,0,1,3,0)	4	4974					
(1,0,0,3,0)	4	5025					
(0,0,0,6,2)	21	5026					
(0,0,0,5,3)	24	5027					
(0,1,0,5,0)	6	5028					
(0,0,1,2,1)	6	5032	120	5039	0.0000	0.0019	
(0,1,0,4,1)	10	5039					
(0,2,0,2,0)	3	5055					
(0,0,0,7,1)	16	5058					
(0,0,0,4,4)	25	5063					
							201 5075
(1,0,0,2,1)	6	5084					
(0,1,0,3,2)	12	5085					
(0,1,1,0,0)	1	5106					
(0,0,1,1,2)	6	5123					
(0,0,0,8,0)	9	5125	81	5129	0.0000	0.0011	
(0,0,0,3,5)	24	5133					
(0,2,0,1,1)	4	5145					
(0,1,0,2,3)	12	5164					
(1,1,0,0,0)	1	5164					
(1,0,0,1,2)	6	5178					
(0,0,0,2,6)	21	5236					
(0,0,1,0,3)	4	5249					
(0,2,0,0,2)	3	5267	42	5256	0.0000	0.0004	
(0,1,0,1,4)	10	5277					
(1,0,0,0,3)	4	5304					
							64 5301
(0,0,0,1,7)	16	5373	22	5387	0.0000	0.0002	
(0,1,0,0,5)	6	5424					

* Since we used this regrouping in our calculation except on one occasion where we tested the effect of regrouping on τ'/τ vs Y curves, only the relative population of these vibrational levels is indicated.

1.9. Only the two latter regroupings were used in our calculation. Results will be discussed below.

4.2 Master equation for vibrational relaxation

The rate of change of fractional population of the individual levels, N_i, can be expressed by a master equation composed of contributions from T-V and V-V processes. In this analysis, energy levels of N_2O and C_2H_2 are represented in a column of increasing energy (see tables 4.1 and 4.2). The distinction between vibrational modes is ignored, so that intramolecular intermode energy transfer is not considered as a V-V process. For simplicity only intermolecular processes involving changes in vibrational quantum numbers in both collision partners are denoted as V-V energy transfer. For example reactions such as:

$$C_2H_2(\mathcal{V}_1,0,0,0,0) + M \longrightarrow C_2H_2(0,0,0,0,\mathcal{V}_4) + M$$

where M is any collision partner whose vibrational quantum number does not change upon collision is treated as a T-V process and the above equation can be described by:

$$C_2H_2(i) + M \longrightarrow C_2H_2(j) + M$$

where i and j simply indicate the level of energy of C_2H_2.

The master equation for T-V processes is:

$$(dN_i/dt)_{TV} = [\sum_{i\neq j} k^M_{ji} N_j - \sum_{j\neq i} k^M_{ij} N_i] \; N \qquad (4.4)$$

where N_i, N_j are the populations of the molecules having vibrational quantum number i and j respectively, N is the total number of molecules, k_{ij} is the rate coefficient for the transition from level i to level j, and k_{ji} is that for the reverse process. At equilibrium, microscopic reversibility

gives:

$$k^M_{ij} N_{ieq} = k^M_{ji} N_{jeq}$$

and equation 4.4 becomes:

$$(dN_i/dt)_{TV} = \sum_{j\neq i} k^M_{ji}[N_j - (N_j/N_i)_{eq} N_i] N \qquad (4.5)$$

In a mixture of C_2H_2 with Ar for example energy exchange occurs by means of collisions of C_2H_2 with C_2H_2 and with Ar. If $X_{C_2H_2}$ is the mole fraction of C_2H_2, $1-X_{C_2H_2}$ is the mole fraction of Ar. The master equation includes contributions from C_2H_2-C_2H_2 collision as well as from C_2H_2-Ar collisions:

$$(dN_i/dt)_{TV} = [X_{C_2H_2} \sum_{j\neq i} k^{C_2H_2}_{ji} (N_j - (N_j/N_i)_{eq} N_i) + (1-X_{C_2H_2}) \sum_{j\neq i} k^{Ar}_{ji} (N_j - (N_j/N_i)_{eq} N_i)]N \qquad (4.6)$$

The Master equation for V-V process such as:

$C_2H_2(i) + C_2H_2(k) \rightleftharpoons C_2H_2(j) + C_2H_2(l)$ is:

$$(dN_i/dt)_{VV} = X_{C_2H_2}[\sum_k \sum_{l\neq k} \sum_{j\neq i} k^{ji}_{lk} N_j N_l - \sum_k \sum_{l\neq k} \sum_{j\neq i} k^{ij}_{kl} N_i N_k] N \qquad (4.7)$$

At equilibrium, microscopic reversibility gives:

$$k^{ji}_{lk} N_{jeq} N_{leq} = k^{ij}_{kl} N_{ieq} N_{keq}$$

Eq. 4.7 becomes:

$$(dN_i/dt)_{VV} = X_{C_2H_2} \sum_k \sum_{l\neq k} \sum_{j\neq i} k^{ji}_{lk} [N_j N_l - N_i N_k (N_j N_l)_{eq}/(N_i N_k)_{eq}] N \qquad (4.8)$$

In order to reduce the number of parameters from thousands to a more manageable number, we used a physically reasonable scaling law for T-V

$$k^{C_2H_2}_{ji} = k^{C_2H_2}_{10} (E'/600.3) [\exp(-\lambda_{C_2H_2}|\Delta E_{ji}|)]/[\exp(-\lambda_{C_2H_2}|\Delta E_{01}|)] \qquad (4.9)$$

and

$$k^{Ar}_{ji} = \phi\, k^{C_2H_2}_{10} (E'/600.3) [\exp(-\lambda_{Ar}|\Delta E_{ji}|)]/[\exp(-\lambda_{Ar}|\Delta E_{01}|)] \qquad (4.10)$$

where $\phi = (k_{10}^{Ar}/k_{10}^{C_2H_2})$ E' is the energy of level i or j, whichever is higher and 600.3 cm^{-1} = E $(0,0,0,v_4,0)$

In the above two equations $\lambda_{C_2H_2}$ and λ_{Ar} are constants depending possibly only on temperature. ϕ represents the relative Ar to C_2H_2 efficiencies for V-T energy transfer.

For the V-V process:

$$k_{1k}^{ji} = \gamma\, k_{10}^{C_2H_2}(E''/600.3)(E'/600.3)\exp(-\lambda_{VV}|\Delta E|) \qquad (4.11)$$

where $\gamma = k_{01}^{10}/k_{10}^{C_2H_2}$ represents the relative efficiency of V-V processes compared to T-V processes, $\Delta E = E_l + E_j - E_i - E_k$ and E" is the energy of level k or l, whichever is higher.

In equation 4.9, 4.10 and 4.11, the preexponential factor is the analogue of the usual spectroscopic transition probability. The overlap factor for each collision partner whose quantum number changes, is proportional to the quantum number of the upper state (42) which we interpreted as being proportional to the energy content of that state (referred to $(0,0,0,v_4,0)$). The exponential factor is commonly used to model energy transfer in the dissociation of polyatomic molecules. It has an empirical basis (see Lambert-Salter law, section 1.1.8) as well as a theoretical basis (see SSH-Theory, section 1.1.6). From the Lambert-Salter law, we found that λ=0.0083 for H-containing molecules and 0.017 for other molecules. Theoretically the exponential dependance of the rate coefficient on ΔE is very complicated (eq. 1.15, section 1.1.6). By calculating the transition probability, P, using SSH-Tanczos theory (eq. 1.15) and by plotting lnP vs ΔE, a mild curvature is observed over the ΔE range, 300 to 2400 cm^{-1} (fig. 4.1). However, the curves are

Figure 4.1 Variation of the transition probability for pure N_2O with temperature (SSH-Tanczos theory).

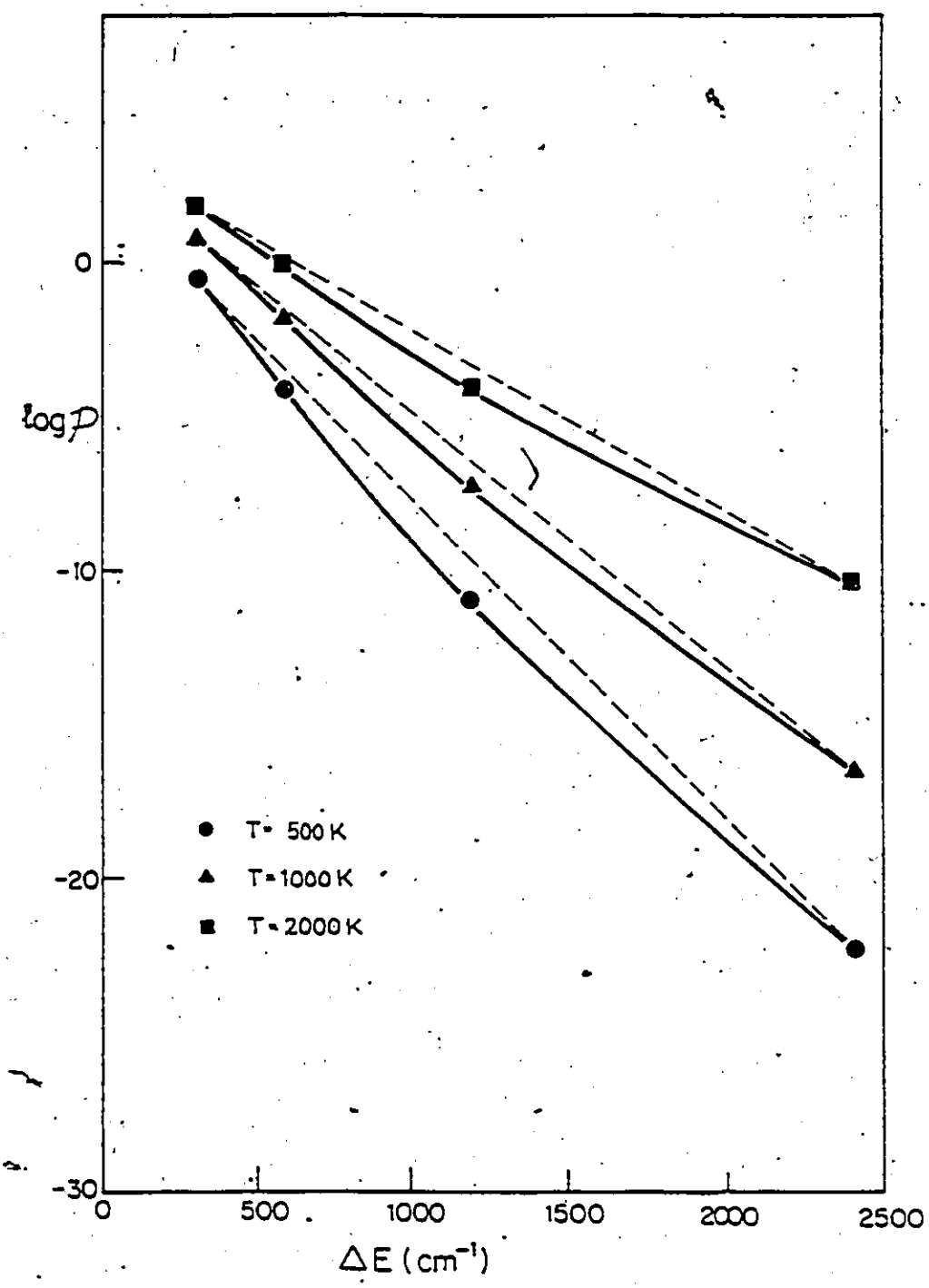

almost linear for small intervals of ΔE. This justifies use of the exponential dependance of our rate constant. λ is calculated from the slope of fig. 4.1. It lies between 0.0064 at 2000 K and 0.014 at 500 K which are of the same order of magnitude as the empirical value of Lambert and Salter. We did not use the SSH-Tanczos theory to do a complete study of the vibrational relaxation of N_2O or C_2H_2 because this theory assumes a very special interaction potential. Without committing ourselves to any particular potential we can at least use the SSH prediction concerning the exponential dependence on ΔE in order to minimize the number of parameters in our calculations. The dependance on intermolecular potential is implied in γ, ϕ, (i.e. K_{10}) and λ.

If $Y=Nk_{10}^{C_2H_2}t$ and if we replace all rate coefficients by equations 4.9 to 4.11 then equations 4.6 and 4.8 respectively become:

$$[1/(Nk_{10}^{C_2H_2})](dN_i/dt)_{TV} = (dN_i/dy)_{TV} =$$
$$X_{C_2H_2}\sum_{j\neq i}(E'/600.3)[\exp(-\lambda_{C_2H_2}|\Delta E_{ji}|)]/[\exp(-\lambda_{C_2H_2}|\Delta E_{01}|)]$$
$$x\,(N_j - (N_j/N_i)_{eq}N_i)$$
$$+(1-X_{C_2H_2})\sum_{j\neq i}\phi\,(E'/600.3)[\exp(-\lambda_{Ar}|\Delta E_{ji}|)]/[\exp(-\lambda_{Ar}|\Delta E_{01})]$$
$$x(N_j - (N_j/N_i)_{eq}N_i) \qquad (4.12)$$

and $(dN_i/dy)_{VV} =$

$$X_{C_2H_2}\sum_{k}\sum_{l\neq k}\sum_{j\neq i}\gamma(E'/600.3)(E''/600.3)\exp(-\lambda_{VV}|\Delta E|)x$$
$$[N_jN_l - N_iN_k(N_jN_l)_{eq}/(N_iN_k)_{eq}] \qquad (4.13)$$

The total rate of change of vibrational energy is the sum of equations 4.12 and 4.13.

According to the Beth-Teller law, the vibrational relaxation time for a diatomic molecule,

$$\tau = 1/[N(k_{10} + k_{01})]$$

is constant. This is true under very limited conditions especially when no V-V processes are involved. The above equation can be rearranged in the following manner:

$$\begin{aligned}\tau &= 1/[N(k_{10} - k_{10}\exp(-h\nu/kT)] \\ &= 1/[Nk_{10}(1-\delta)] \quad \text{where} \quad \delta = \exp(-h\nu/kT) \\ &= t/[y(1-\delta)] \end{aligned} \tag{4.14}$$

so that $t/\tau = y(1-\delta)$

In this work we use the theoretical harmonic oscillator VT relaxation time τ, merely to scale the times and phenomenological relaxation times τ'. Calculation of the absolute value of k_{10} is thus not necessary. Teitelbaum (29), has solved the detailed master equation for the vibrational relaxation of Morse diatomic molecules using a similar model to ours. He concluded that the Bethe-Teller law is exactly valid only in the limit of zero anharmonicity or approximately valid for infinitely slow V-V processes or when the initial population is not Boltzmann. It is not known whether the same applies for polyatomic molecules. In any case, under conditions where V-V processes are not negligible, the vibrational relaxation time can not be a constant. A phehomenological relaxation time is defined as:

$$\tau' = -(E-E_\infty)/(dE/dt) \tag{4.15}$$

Analagously to the experimental procedure τ' varies with time in general. A rearrangement of eq. 4.15 leads to:

$$\tau'/\tau = -[(E-E_\infty)/dE/dy)](1-\delta) \tag{4.16}$$

A computer program using an extension of Gear's Algorithm (114) was used to solve the series of differential equations

(the sum of eqs. 4.12 and 4.13). N_i and dN_i/dY were obtained at different values of Y, and consequently E and dE/dY were calculated:

$$E = \sum E(i)\ N_i \qquad (4.17)$$

$$dE/dy = \sum E(i)\ dN_i/dY \qquad (4.18)$$

Knowing E, and dE/dY at each value of Y as well as E_∞ the value of the energy at equilibrium, τ'/τ can be calculated at each value of Y (eq. 4.16) and the variation of τ'/τ with Y determined. This is the equivalent of $P\tau'$ vs Zt which was used in the analysis of our experimental results.

Some simplifications had to be introduced to our computer program in order to make the calculation tractable. The first limitation concerned the amount of energy exchanged upon collision. Ideally of course we would like to allow all transitions from vibrational level i and k to vibrational levels j and l. However, then the number of transitions would be extremely high, and the execution time of our computer program would be so long that one calculation of the vibrational relaxation time would take hundreds of hours on the AMDAHL V7A computer. In order to limit the number of transitions allowed we restricted the amount of energy exchanged for a transition. We allowed only those transitions for which $|E(j)-E(i)|$, $|E(l)-E(k)|$ for V-T and $|E(j)+E(l)-E(i)-E(k)|$ for V-V are less than a maximum value of E_a. By examining Table 4.1 and fig. 1.3 for N_2O and Table 4.2 and fig. 1.9 for C_2H_2, we find that for N_2O $E(1)-E(0)=588\ cm^{-1}$ so that E_a for N_2O should be at least $588\ cm^{-1}$ while for C_2H_2 it is $703\ cm^{-1}$. By choosing $E_a = 703\ cm^{-1}$ we thus

allowed all direct processes connecting the lowest bending mode to ground. Direct transitions of e.g. the higher energy stretching modes to ground, were so improbable according to our model that they could well be omitted without significantly altering our results. Instead, those modes were constrained to relax via intramolecular or intermolecular intermode exchange processes.

The number of vibrational energy levels and the regrouping (or condensation) of vibrational energy levels are important parameters in the calculation. The number of vibrational energy levels calculated are very high (51 for N_2O up to 6000 cm^{-1} and 93 for C_2H_2 up to 5500 cm^{-1}). Unfortunately we cannot include all of them in our calculation. The execution time of our computer program varies according to the fourth power of the number of levels. Reducing the number of levels by a factor of 2 or 3 reduced the computation time by a factor of 16 or 81 respectively. This could be accomplished either by regrouping vibrational energy levels or by eliminating some high energy vibrational levels altogether. Both methods were tried and the results are discussed in section 4.4.

4.3 Linear mixture rule for a diatomic molecule

In order to test the validity of our theoretical treatment, we simulated the relaxation of a diatomic molecule for which an analytical solution of the master equation exists (29,78), at least for certain values of parameters.

The vibrational relaxation parameters used are:

$\lambda_{Ar} = \lambda_{Dia} = \lambda_{VV} = hc/2kT = 0.00093$ cm at 750 K, $\phi = 0.1$ and

γ = 100. The vibrational energy levels are: 0.0, 495, 985, 1470, 1950, 2425, 2895, 3360, 3820, 4275, 4725 cm^{-1}, each with unit degeneracy. The maximum energy transfer which we allowed for in the simulation was chosen to be the largest separation between any two successive levels (i.e. 495 cm^{-1}) in order that V-T energy transfer occur only between two adjacent levels ($\Delta v = \pm 1$). Under these conditions and shock perturbation (initial Boltzmann distribution) we expect the linear mixture rule to be obeyed and a plot of τ/τ' vs mole fraction should start with $\tau/\tau' \sim 1.0$ for the pure diatomic molecule and end at $\tau/\tau' \sim 0.1$ when ϕ = 0.1 within the approximation of the model.

Values of τ'/τ were calculated at mole fractions: 0.00, 0.005, 0.01, 0.02, 0.05, 0.1, 0.3, 0.5, 0.7, and 1.0. The resulting τ'/τ vs Y curves are illustrated in fig. 4.2. τ/τ' at equilibrium was extracted from the curves of fig. 4.2 and plotted against the mole fraction in fig. 4.3. This curve is linear except at low mole fractions where the curve decreases slightly with decreasing mole fraction of diatomic molecule. τ/τ' varies between 0.983 at X=1 and 0.0987 at X=0.0. These results are in agreement with what is expected for a diatomic molecule within the approximations made in the analytical solution (29,78). We believe that our program functions as it should and can be used to make predictions for polyatomic molecules.

4.4 Results of the Computer Simulation

The rate of change of the vibrational energy level populations, dN_i/dt, and of the reduced vibrational relaxation

Figure 4.2 Effect of mole fraction on the variation of τ'/τ with Y for a diatomic molecule.

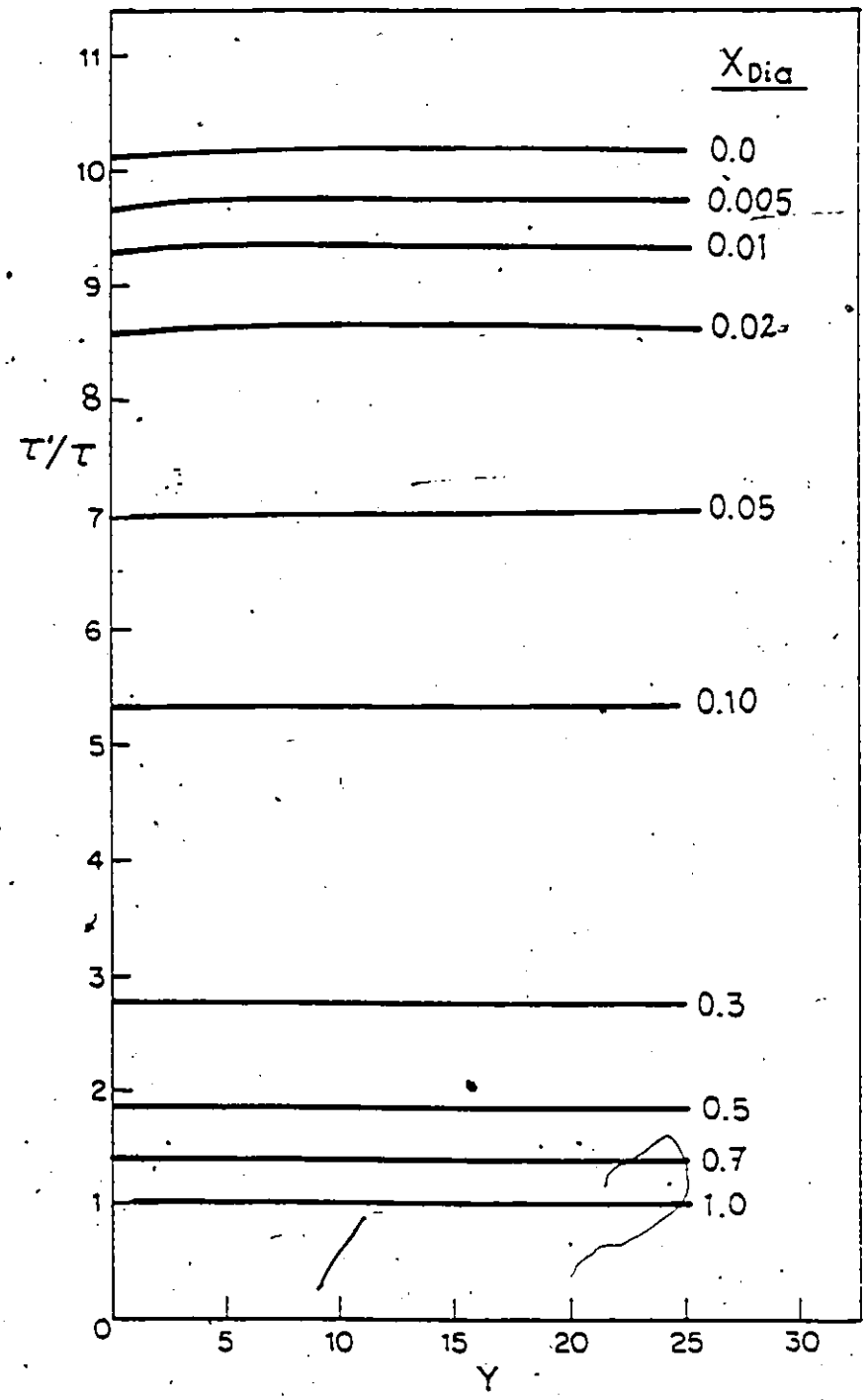

Figure 4.3 Variation of τ/τ' with mole fraction for a diatomic molecule.

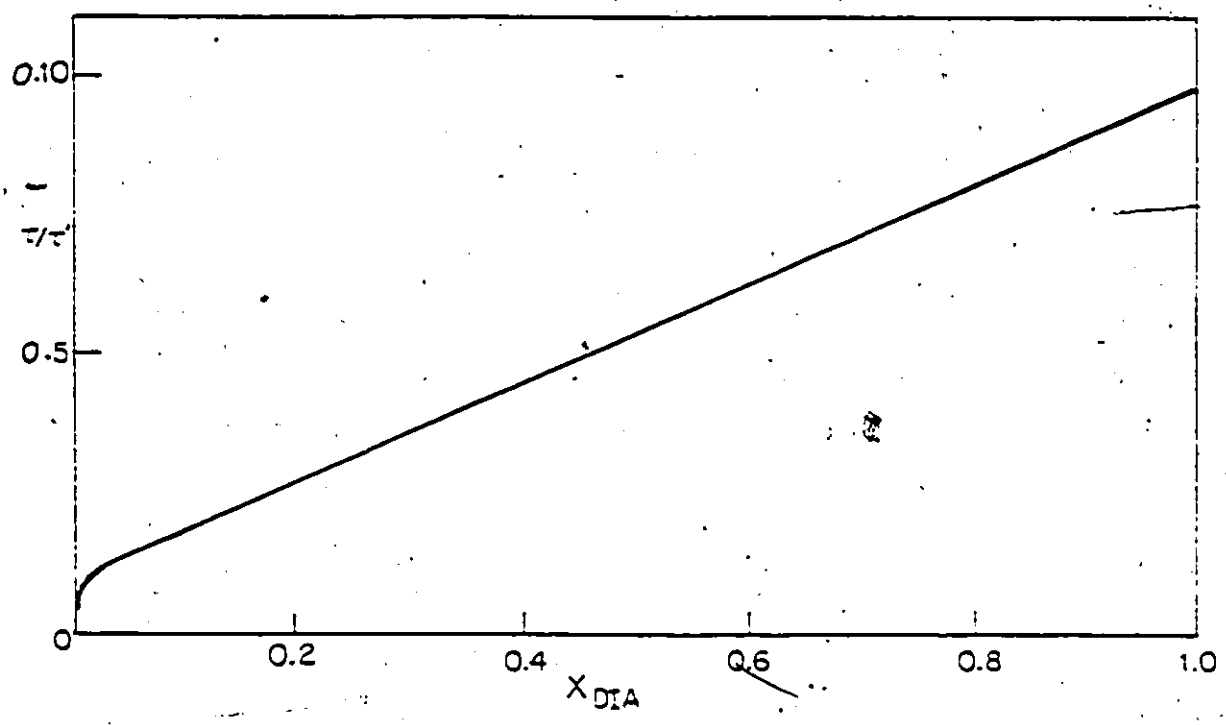

time τ'/τ depend on seven parameters. Two of them are known: the temperature, T, and the mole fraction. The five other parameters are theoretically and experimentally unknown. These are:

$\lambda_{C_2H_2}$ or λ_{N_2O}, λ_{Ar}, λ_{VV}, ϕ and γ.

Without an additional parameter k_{10}, we can only study the dependence of the shape of the curves representing τ'/τ vs Y on each of these parameters. To perform such a study, standard values for the parameters were chosen and the corresponding curve was called the standard curve. Then each parameter was varied individually and the corresponding sensitivity curve was plotted and compared with the standard one. Standard and modified parameters are shown in Table 4.3.

Table 4.3: Vibrational relaxation parameters used in the computer simulation

	mole fraction	T(K)	$\lambda_{C_2H_2}$ and λ_{N_2O}	λ_{Ar}	λ_{VV}	ϕ	γ
standard parameters	0.50	750	0.01	0.01	0.01	0.1	100
modified parameters	0.0 to 1.0	320 500	0.001 0.02	0.001 0.02	0.05 0.1	0.01 1.0	0.0 10 1000

Values of λ are empirically smaller than unity, we arbitrarily chose a value of 0.01 cm for the three λ's (see section 4.2 for justification). ϕ ($k_{10}^{Ar}/k_{10}^{N_2O}$ or $k_{10}^{Ar}/k_{10}^{C_2H_2}$) was also chosen to be smaller than unity since the rate of energy transfer of polyatomic molecules by collision with an atom is experimentally found to be less than the rate of energy transfer by collision with another polyatomic molecule. γ ($k_{10}^{01}/k_{10}^{C_2H_2}$ or

$k_{10}^{01}/k_{10}^{N_2O}$) is usually higher than unity since V-V processes are known to be very efficient compared to V-T processes (6). Unfortunately we do not know the magnitude of these parameters in reality and we arbitrarily chose the values in table 4.3 in order to get a qualitative picture of the relaxation.

Before modifying these parameters, we have to know how many vibrational levels to include in the calculation, and what the effect of regrouping of the vibrational energy levels on the shape of the τ'/τ vs Y curves is. We shall consider first the N_2O molecule, then the C_2H_2 molecule.

4.4.1 N_2O

In a first attempt we used the first 21 vibrational levels of N_2O (Up to 4067 cm^{-1} maximum energy), (see table 4.1 and fig.1.3). Then we added 5 more vibrational levels (26 levels with 4514 cm^{-1} max energy). In both cases, curves of τ'/τ vs Y are very similar (see fig. 4.4). This is because at 750 K (which is the standard temperature) the relative population of high vibrational levels is very small and does not affect the behavior of τ'/τ significantly. However at much higher temperature, the population of vibrational levels having high energy becomes important and we expect the shape of the two curves to be different then. As long as the population of the high energy levels is relatively small, we can exclude these vibrational levels from our calculation. Since at 750 K the two curves are very similar we decided to use the first 21 levels in our computer simulation as a standard number. In a second attempt we used the regrouped vibrational energy levels of N_2O (12 levels of

4032 cm^{-1} maximum energy) in our calculation. The resulting curve is illustrated in the same figure (fig. 4.4). It seems that the regrouping of vibrational energy levels affects the shape of our curves markedly in contrast to the effect of the maximum energy considered. Therefore regrouping was avoided in the case of N_2O by eliminating the vibrational levels of high energy and thus reducing the total number of vibrational levels from 51 to 21. Once the number of vibrational levels was decided upon, we could study the dependence of τ'/τ on other parameters.

For the standard set of parameters τ'/τ decreases with increasing Y. By changing each of the parameters except for the temperature, the shape of the curves does not change significantly. They are simply displaced towards higher or lower equilibrium values of τ'/τ depending on the individual parameter.

Fig. 4.5 shows the effect of temperature (keeping the other parameters fixed) on the variation of τ'/τ with Y. At standard temperature (750 K), τ'/τ decreases rapidly as the relaxation approaches equilibrium. However, at low temperature (320 K), the curve increases from a lower value of τ'/τ, crosses the standard curve near the beginning of the relaxation then decreases very slowly as the relaxation approaches equilibrium. The variation of τ'/τ with Y is very small at low temperatures (near room temperature). This is because at low temperatures, only the ground and first excited state are significantly populated (a two-level system can be described by a time-independent rate constant). The temperature dependence of τ'/τ will be discussed

Figure 4.4 Effect of the number of energy levels on the variation of τ'/τ with Y for N_2O.

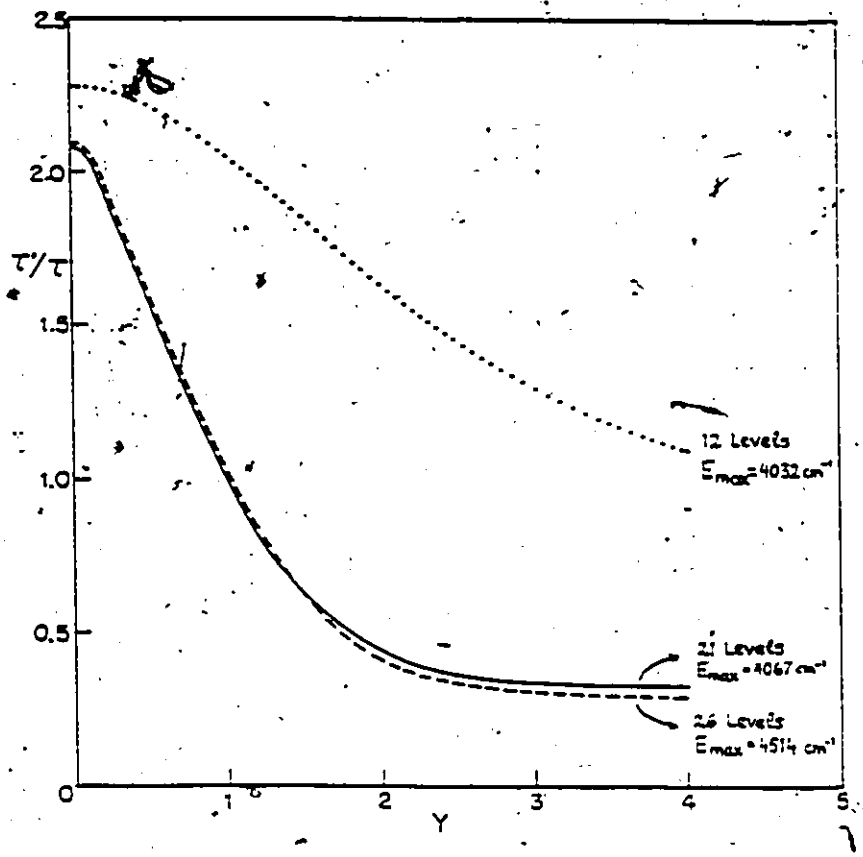

Figure 4.5 Effect of the temperature on the variation of τ'/τ with Y for N_2O.

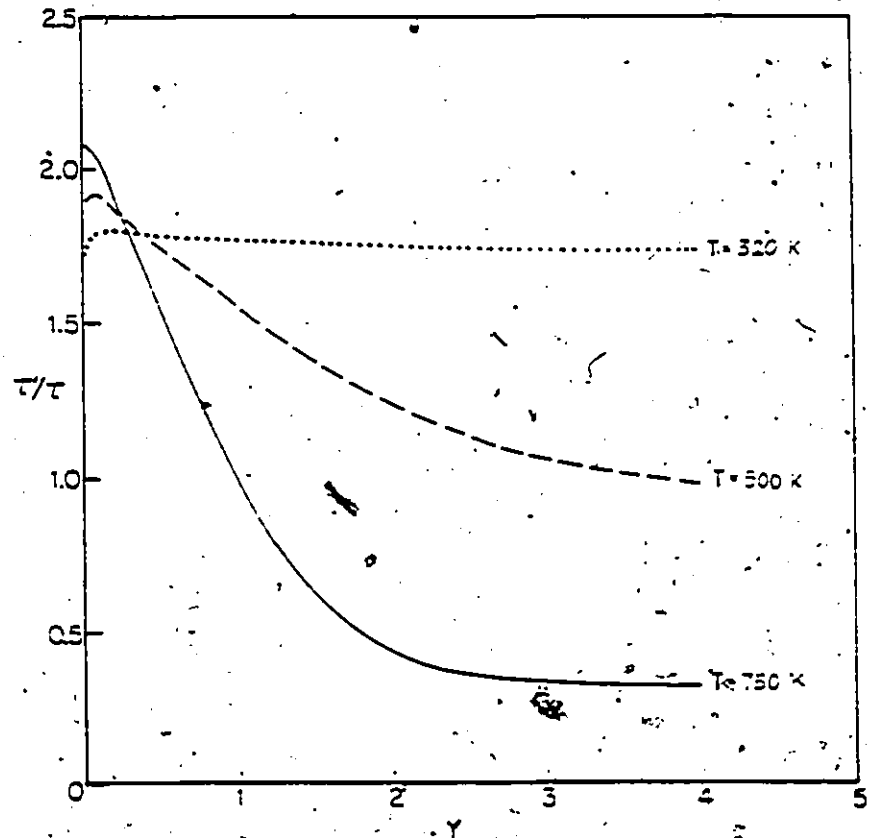

in more detail below in the discussion section.

The dependence of τ'/τ on λ_{Ar} does not seem to be significant, (fig. 4.6). By decreasing λ_{Ar}, τ'/τ only slightly increases. The small dependence of τ'/τ on λ_{Ar} is expected since Ar here is an inefficient collider (ϕ = 0.11.

The dependence of τ'/τ on λ_{N_2O} is much more important than on λ_{Ar}. By decreasing λ_{N_2O} by the same factor as λ_{Ar}, the curve is displaced significantly towards a higher value of τ'/τ (Fig. 4.7).

The dependence of τ'/τ on λ_{VV} is reversed (fig. 4.8). In this case, an increase of λ_{VV} leads to an increase in τ'/τ. Increasing λ_{N_2O} or λ_{Ar} actually suppresses V-T processes. Decreasing λ_{VV} accentuates the V-V processes in the relaxation mechanism. For both operations the relaxation speeds up. This indicates that V-V processes are more important than V-T processes. However, at the beginning of the relaxation (at small value of Y), the difference between the standard curve and other curves is very small. This difference increases as Y increases and becomes very significant near equilibrium. This indicates that the V-V processes become more important as time goes on.

The dependance of τ'/τ on γ ($k_{10}^{01}/k_{10}^{N_2O}$) confirms our interpretation that V-V processes are determining the rate (fig. 4.9). For γ=0 all V-V processes are eliminated; the corresponding τ'/τ is nearly constant, to within 12%, so the relaxation can be closely related to the process (0,1,0) $\rightleftharpoons$ (0,0,0). However, as soon as a small V-V contribution is introduced the relaxation accelerates particularly for larger

Figure 4.6 Effect of λ_{Ar} on the variation of τ'/τ with Y for N_2O.

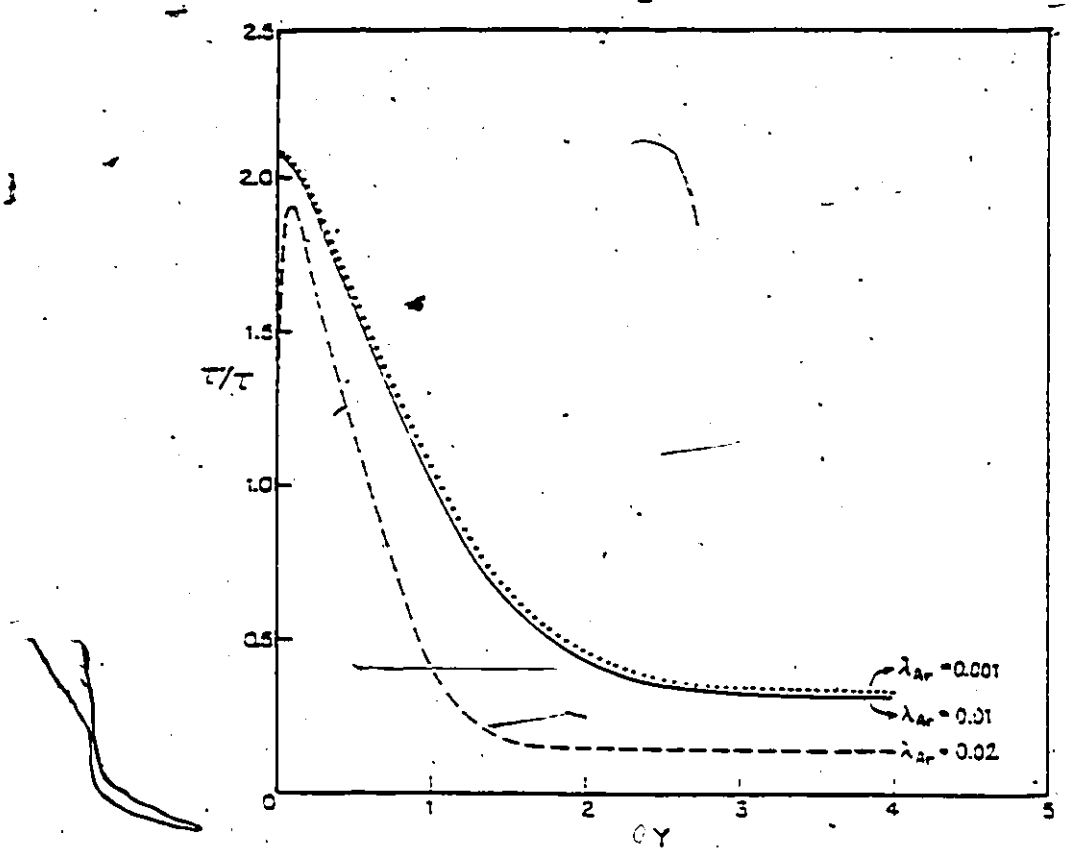

Figure 4.7 Effect of λ_{N_2O} on the variation of τ'/τ with Y for N_2O.

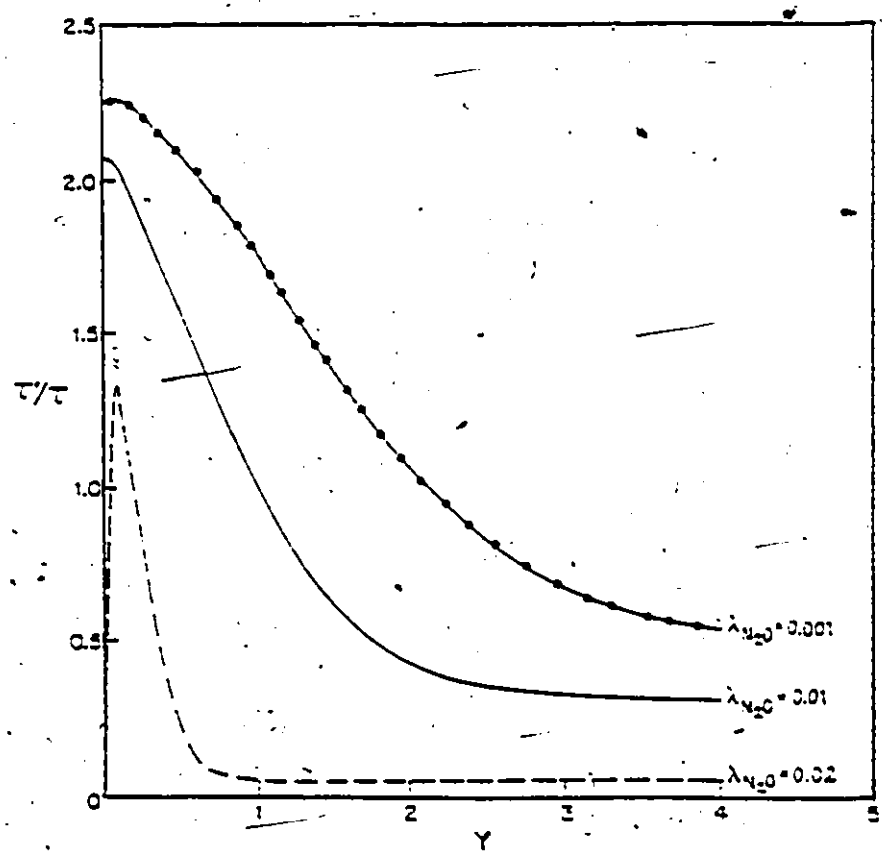

Figure 4.8 Effect of λ_{VV} on the variation of τ'/τ with Y for N_2O.

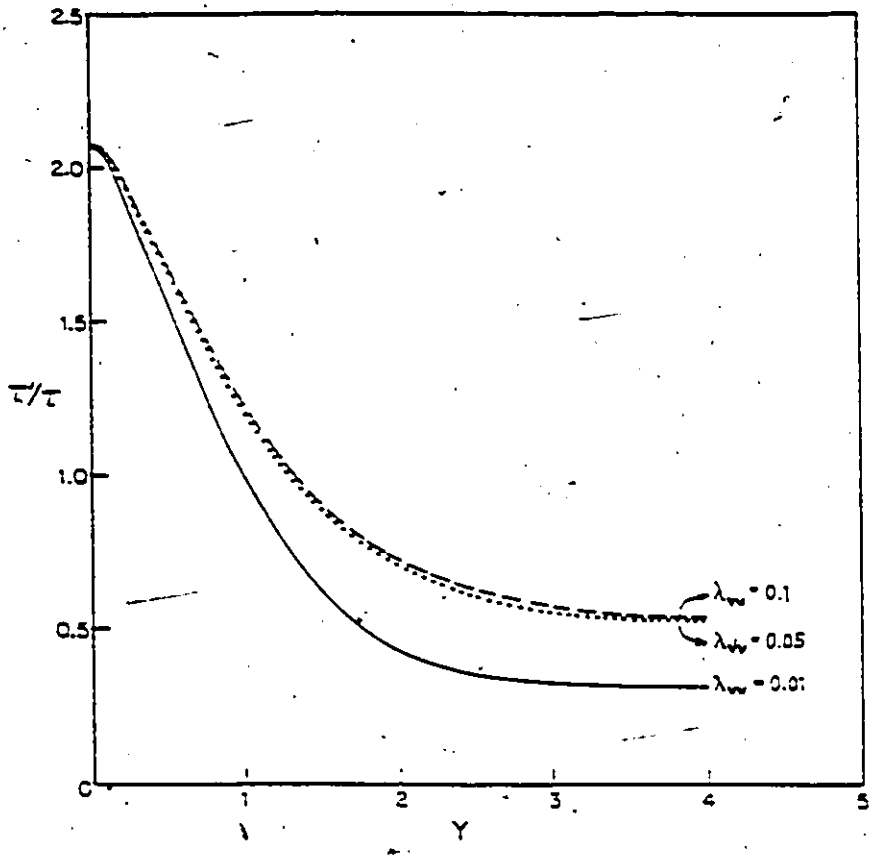

Figure 4.9 Effect of γ on the variation of τ'/τ with Y for N_2O.

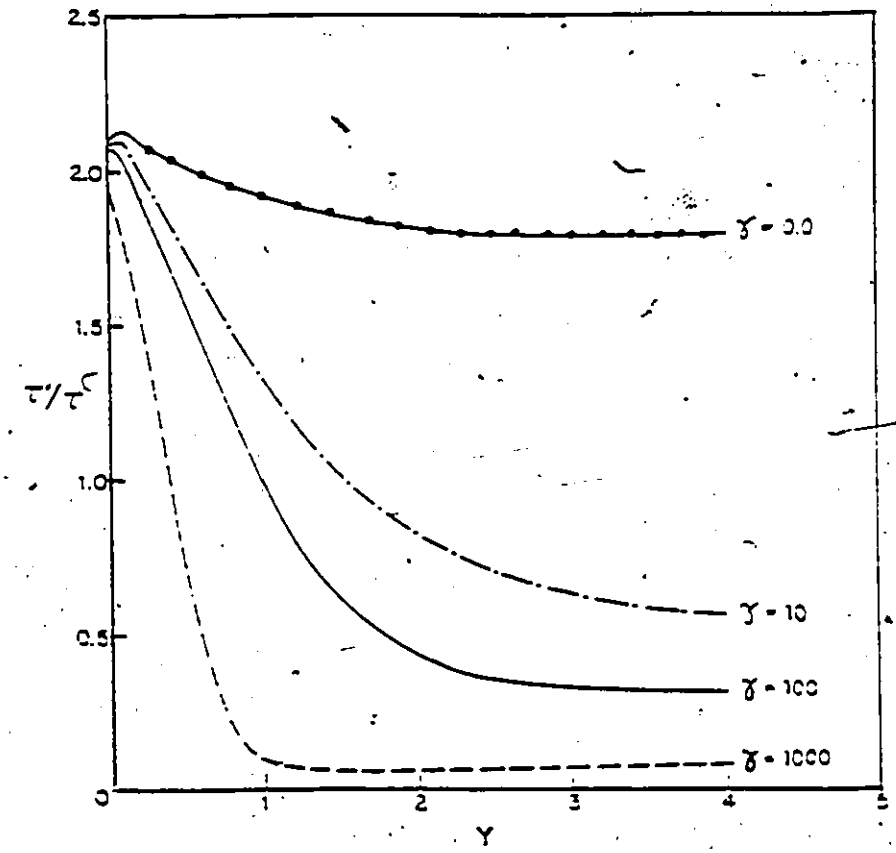

values of γ. This indicates again that V-V processes are important and become more so at longer time.

Finally, a decrease of ϕ leads to displacement of the curve to higher values of τ'/τ (fig. 4.10). However, in this case the difference between this and the standard curve is more important at the begining of relaxation and decreases as the relaxation approaches equilibrium. This means that near equilibrium where V-V processes are the important ones, it doesn't matter whether the V-T processes involve Ar or N_2O as collision partners.

The mole fraction dependence will be discussed along with the linear mixture rule in section 4.5.

4.4.2 C_2H_2

The dependance of the τ'/τ vs Y curves of C_2H_2 on each of the vibrational relaxation parameters does not differ markedly from the case of N_2O. In this section, only the differences between the N_2O and C_2H_2 curves will be discussed. These differences arise from the difference betwen the vibrational energy levels of the two molecules.

Most of the curves of τ'/τ vs Y exhibit a maximum at the beginning of the relaxation. They appear only in some curves of N_2O. Only the behavior near the maximum will be discussed in this section. Beyond this maximum, these curves are similar to the N_2O curves and need not be discussed in detail.

Fig. 4.11 shows the dependance of the τ'/τ vs Y curves on the regrouping of vibrational levels. We saw earlier, in section 4.4.1 that a regrouping of the vibrational levels affects

Figure 4.10 Effect of ø on the variation of τ'/τ with Y for N_2O.

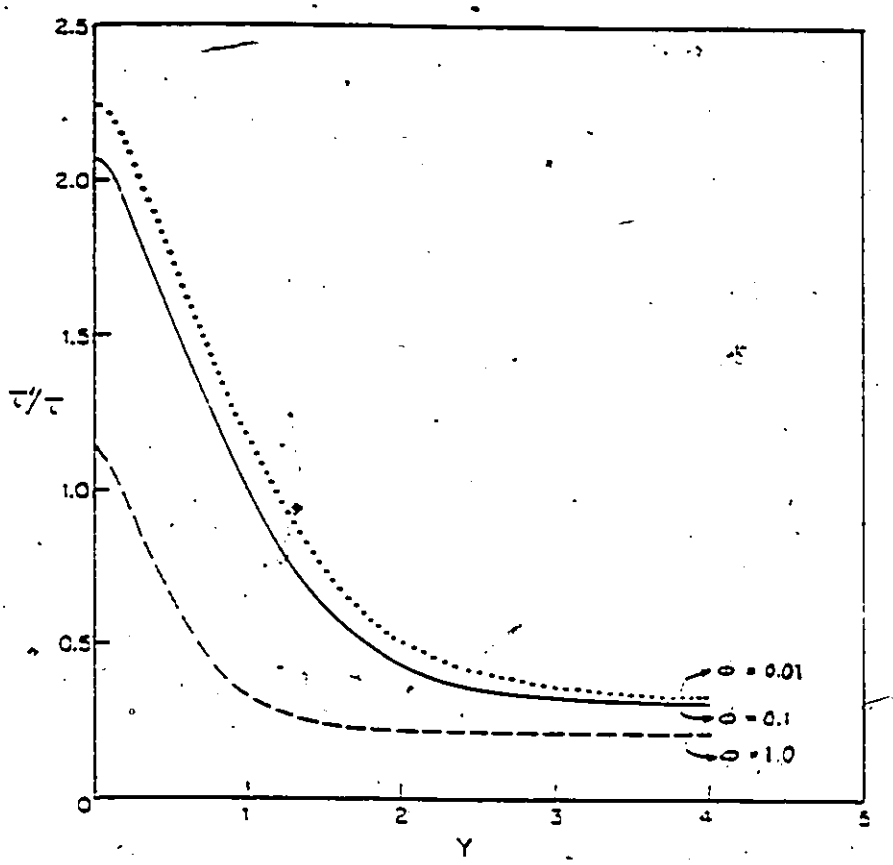

the shape of the curves of τ'/τ vs Y significantly. In a first attempt we used a single regrouping of the 93 vibrational levels of C_2H_2 to 28 vibrational levels (up to 5387 cm^{-1} maximum energy). Then the highest 7 vibrational levels were eliminated and only 21 vibrational levels (up to 4520 cm^{-1}) were used. In both cases, curves representing τ'/τ vs Y are very close (fig. 4.11. This is because at 750 K the relative populations of high energy vibrational levels is very small and does not affect the behavior of τ'/τ vs Y curves. In a second regrouping of the vibrational energy levels down to 15 (up to 4670 cm^{-1} maximum energy). the corresponding curve is completely different from the two other curves (fig. 4.11) so that we finally decided to use the first 21 vibrational levels of the first regrouping. Because of the costliness of calculations using all 93 energy levels regrouping can not be avoided. For this reason the curves of τ'/τ vs Y in the case of C_2H_2 are approximations. However we believe that the 21-level system is a good approximation to the real system.

The behavior of τ'/τ vs Y curves near the maximum depends on each parameter. For example the curve corresponding to T=320 K starts at a higher value of τ'/τ than the standard curve does (fig. 4.12). It does not show a maximum at early time, and it does not cross the standard curve as in the case of N_2O. The effect of other parameters near the maximum is very complicated. In some cases, curves cross each other at 2 points, one before and one after the maximum. (eg. fig. 4.14) In some other cases, they cross each other at one point (i.e. fig. 4.15

Figure 4.11 Effect of the number of energy levels on the variation of τ'/τ with Y for C_2H_2.

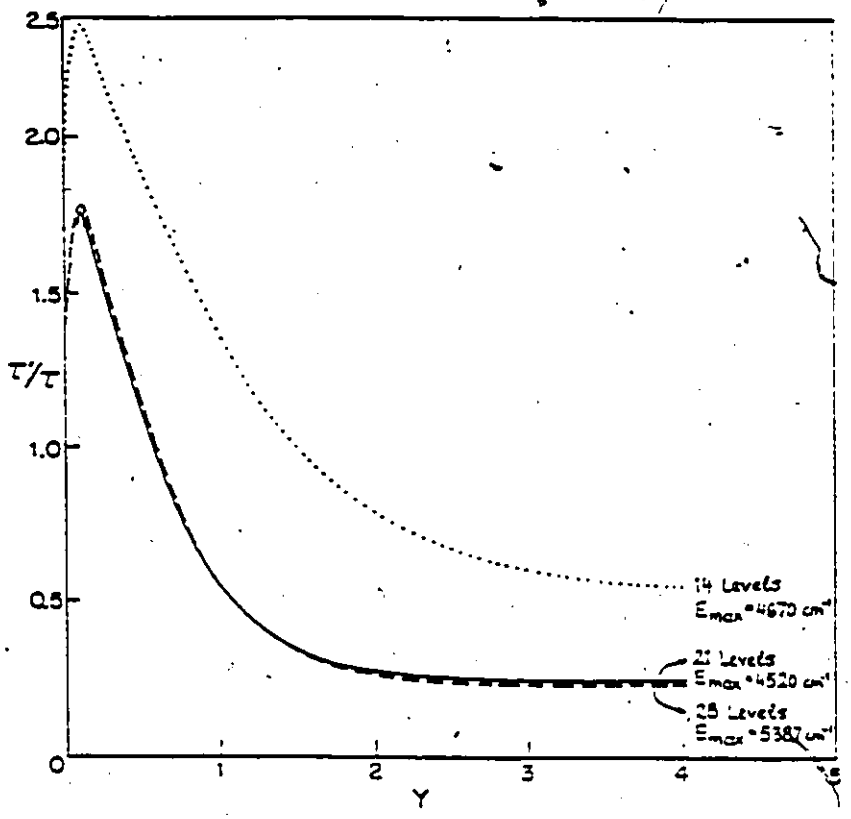

Figure 4.12 Effect of temperature on the variation of τ'/τ with Y for C_2H_2.

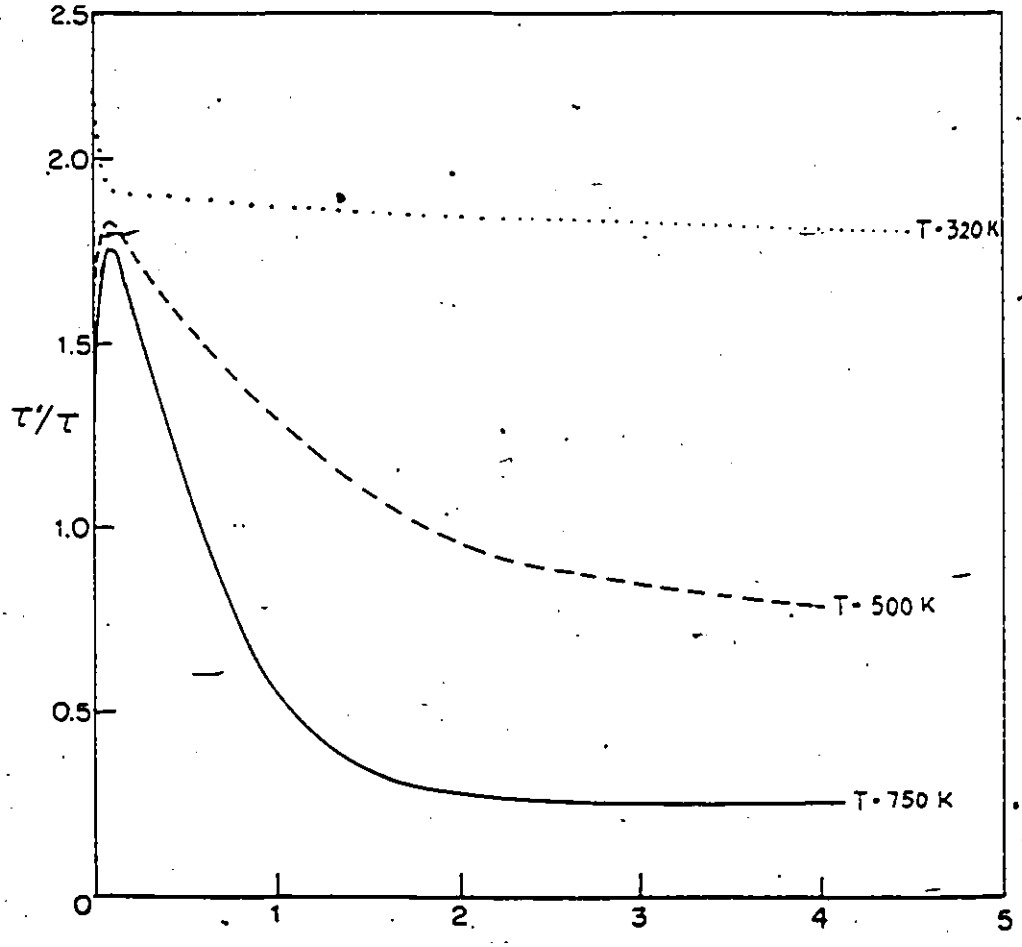

Figure 4.13 Effect of λ_{Ar} on the variation of τ'/τ with Y for C_2H_2.

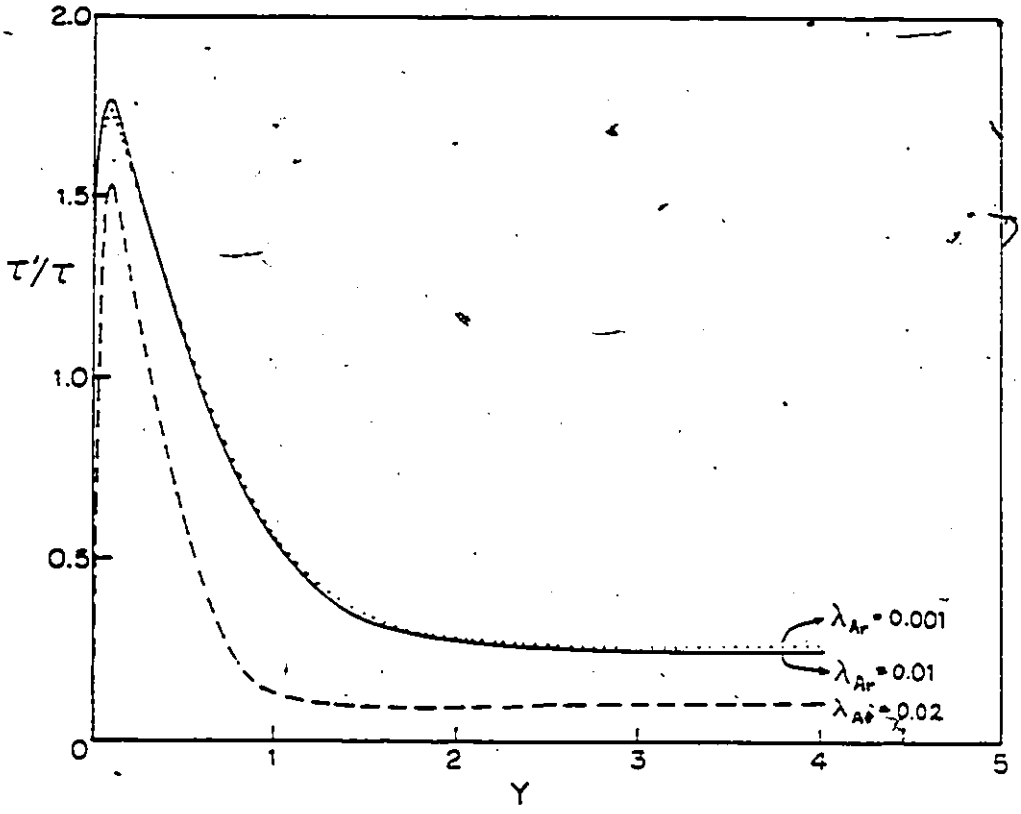

Figure 4.14 Effect of $\lambda_{C_2H_2}$ on the variation of τ'/τ with Y for C_2H_2.

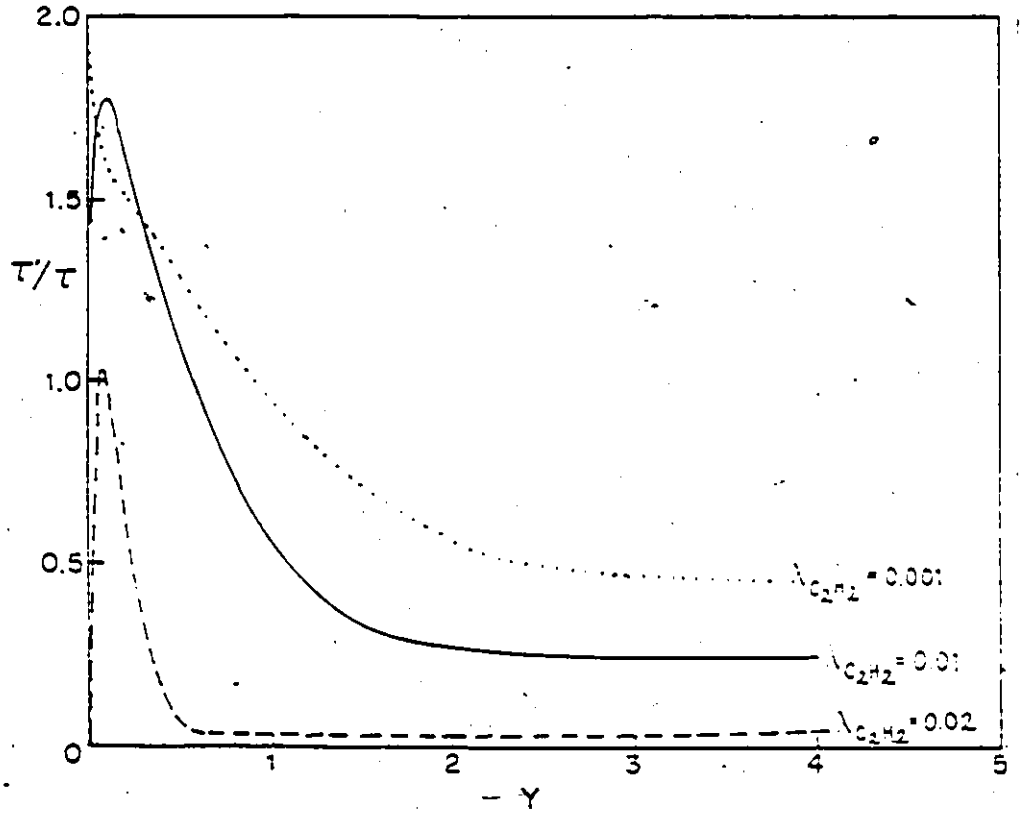

Figure 4.15 Effect of λ_{VV} on the variation of τ'/τ with Y for C_2H_2.

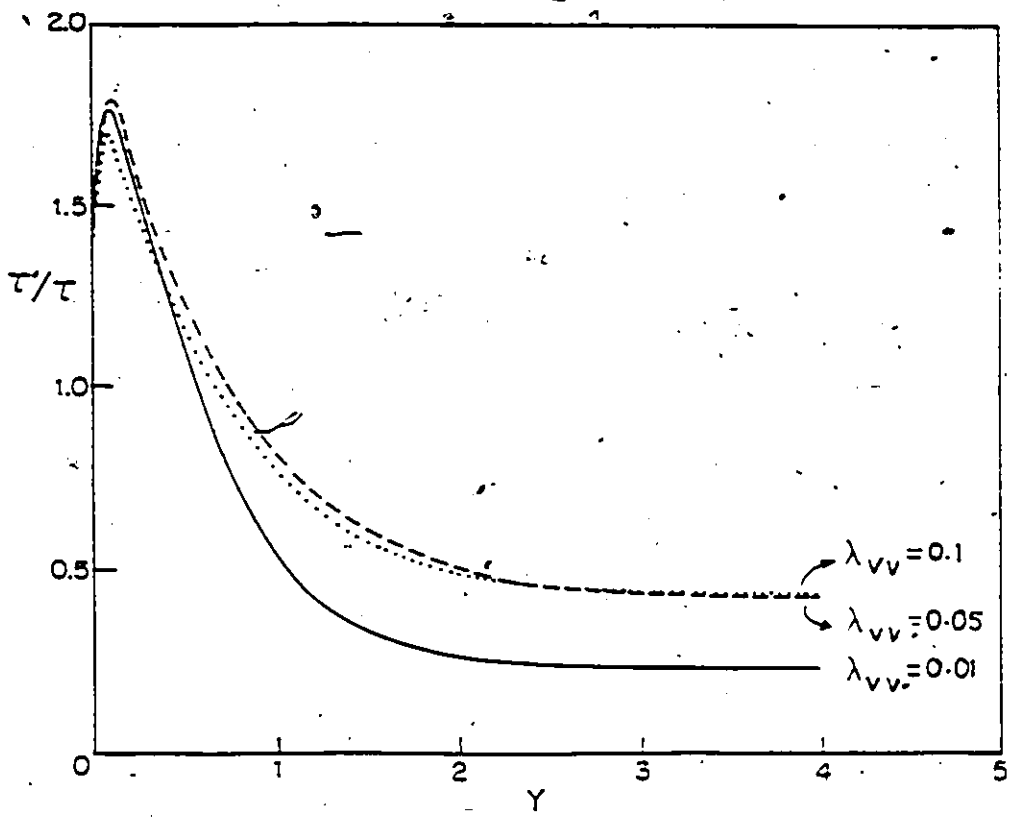

Figure 4.16 Effect of γ on the variation of τ'/τ with Y for C_2H_2.

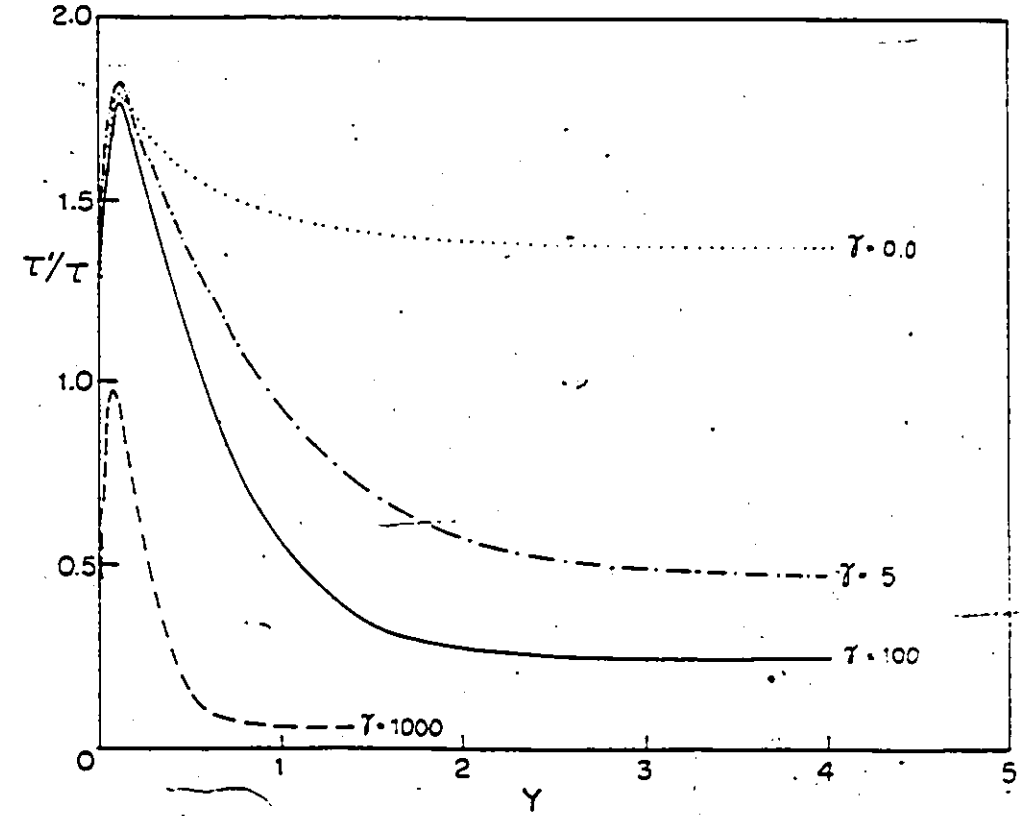

Figure 4.17 Effect of ø on the variation of τ'/τ with Y for C_2H_2.

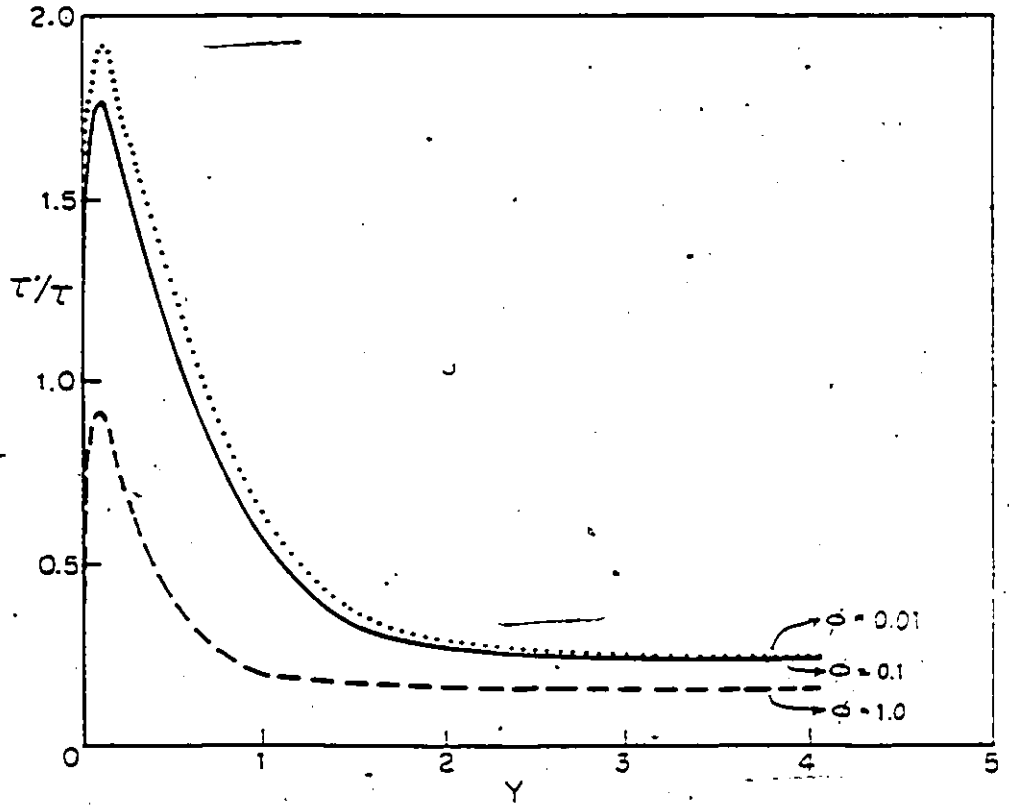

and 4.16). Finally, many curves do not cross each other at all (i.e. fig. 4.12 and 4.17).

We are unable to explain these differences in behavior near the maximum. However, we conclude that the maximum itself is due to a change in the mechanism of the relaxation process. Two mechanisms are apparently involved. One, before the maximum, corresponds to relaxation of the vibrational levels of low energy and the second, beyond the maximum corresponds to the relaxation of vibrational levels of high energy.

The mole fraction dependence will be discussed along with the linear mixture rule in section 4.5.

4.5 Molar fraction effect and linear mixture rule

The dependence of τ/τ' (the equivalent of $1/P\tau'$) vs Y curves on the mole fraction of relaxer for both N_2O and C_2H_2 molecules was studied in order to test the validity of the linear mixture rule.

Calculations for N_2O and C_2H_2 were performed at mole fraction = 0.0, 0.005, 0.01, 0.02, 0.05, 0.1, 0.3, 0.5, 0.7 and 1.0 using the standard vibrational relaxation parameters. The results are illustrated in Fig.4.18 for N_2O and fig. 4.19 for C_2H_2. In these figures, τ'/τ decreases with increasing mole fraction and the curves become steeper and approach equilibrium at an earlier time as the mole fraction increases. This is to be expected because, aside from the additional V-V routes which N_2O or C_2H_2 collision partners allow, the relative V-T efficiency was 10:1 in favour of N_2O or C_2H_2 (i.e. ϕ=0.1). Values of τ'/τ were read off fig. 4.18 and 4.19 at Y = 1.0, 2.0, 5.0, and

Figure 4.18 Effect of mole fraction on the variation of τ'/τ with Y for N_2O.

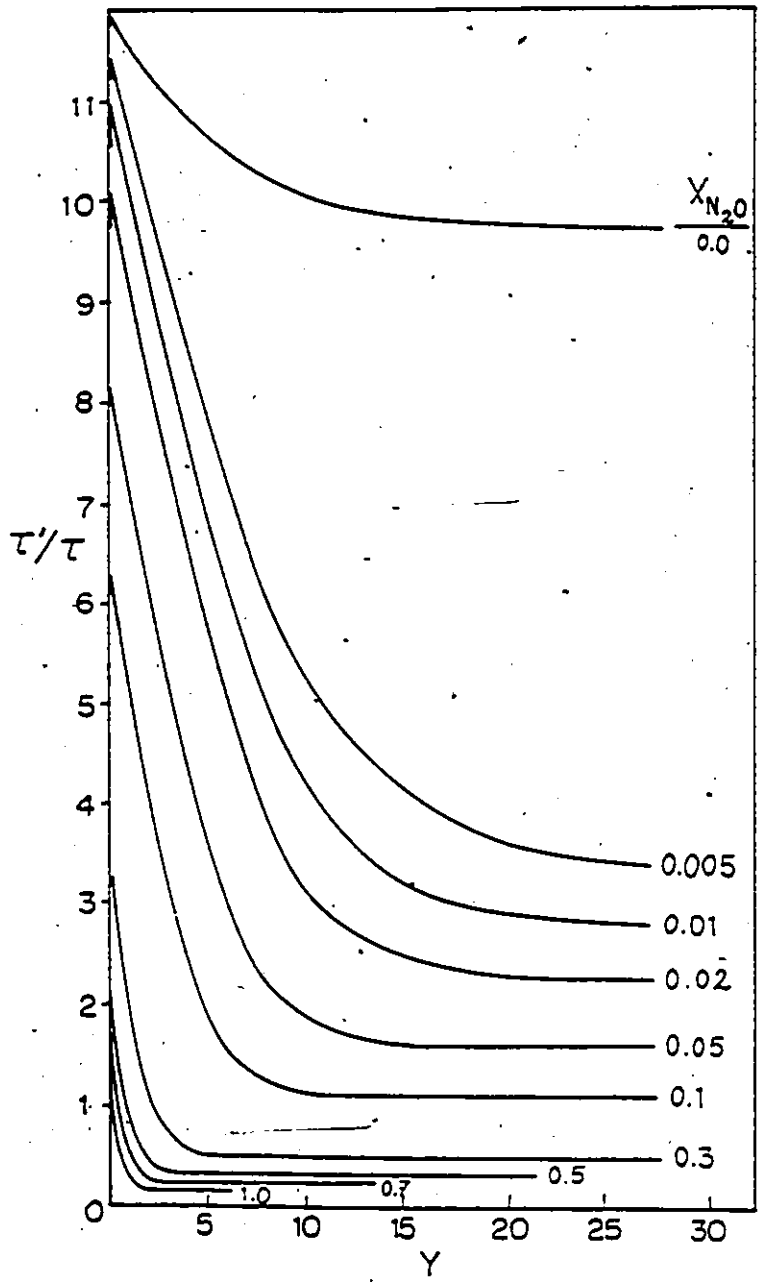

Figure 4.19 Effect of mole fraction on the variation of τ'/τ with Y for C_2H_2.

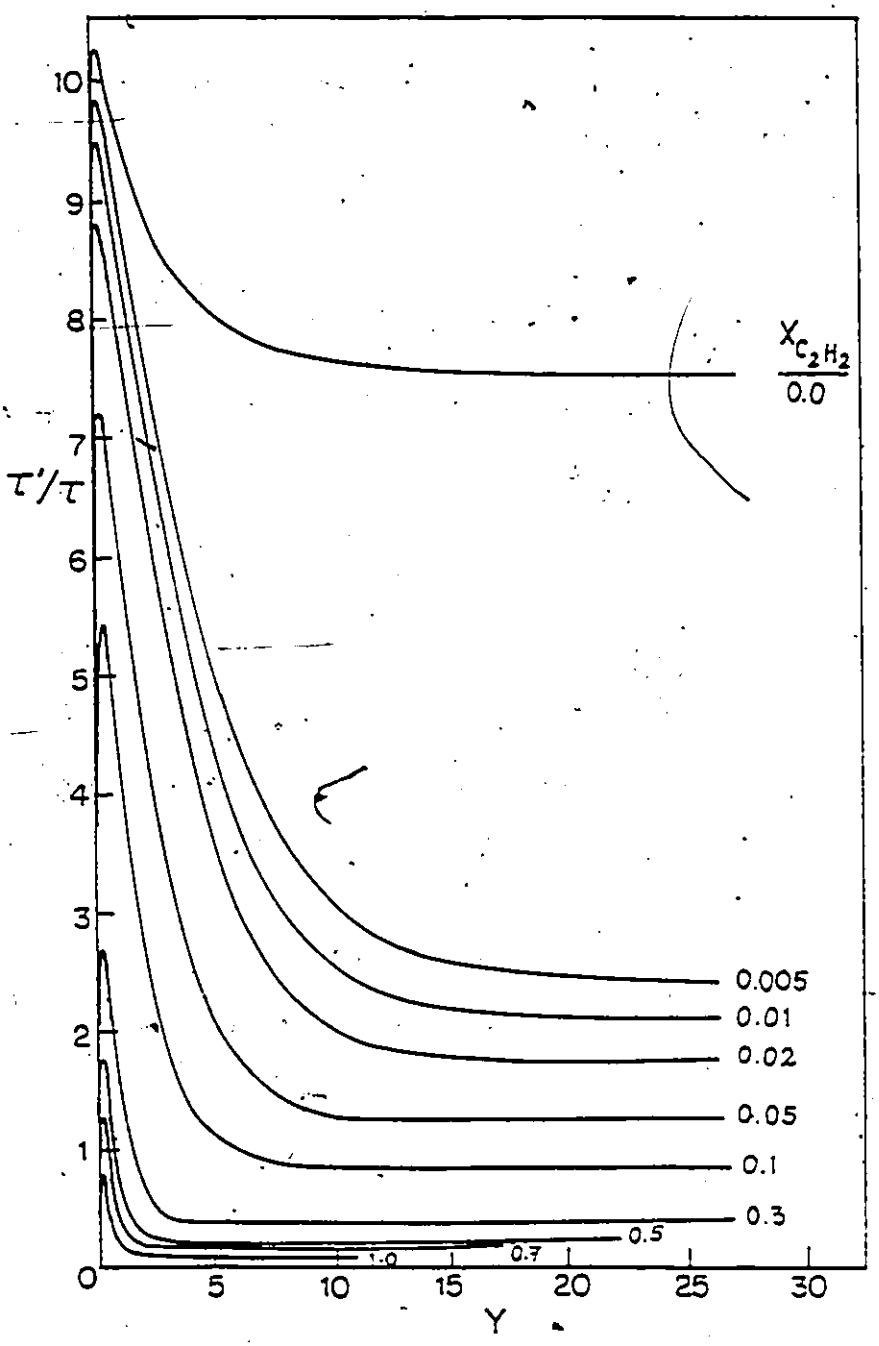

at equilibrium. The corresponding plots of τ/τ' (the equivalent of $1/P\tau'$) vs mole fraction, X, are illustrated in fig. 4.20 for N_2O and in fig. 4.21 for C_2H_2 respectively. It is clear that the linear mixture rule is not obeyed. According to the linear mixture rule, a plot of τ/τ' vs X should be linear and should start at $\tau/\tau' = 1.0$ at X = 1.0 and end at $\tau/\tau' = 0.1$ at X = 0.0 if $\phi = 0.1$ and if V-V processes are unimportant. All curves obtained in fig. 4.20 and 4.21 started at τ/τ' much higher than 1.0 (indicating the contribution of V-V processes) and end at $\tau/\tau' = 0.1$. The deviation from linearity is more obvious at the beginning of the relaxation (e.g.Y=1.0). These curves approach linearity as the relaxation approaches equilibrium. However, near equilibrium the curve drops off sharply at low mole fraction of X.

Curves of fig. 4.20 and fig. 4.21 do not resemble any of our experimental mixture rule plots where a maximum was observed at low mole fractions, similar to what is expected for diatomic molecules. Possibly for other choices of vibrational relaxation parameters the theoretical curves would exhibit a maximum at low mole fraction also. We did not try to find the values of the parameters which lead to perfect agreement between experiment and theory. These are very time consuming and expensive calculations, and our aim (as mentioned above) was to merely show that a time-invariant relaxation time does not exist and that its consequence is a non-linear mixture rule. We believe we have shown this.

The linear mixture rule has also been tested at low

Figure 4.20 Variation of τ/τ' with mole fraction of N_2O at different Y.

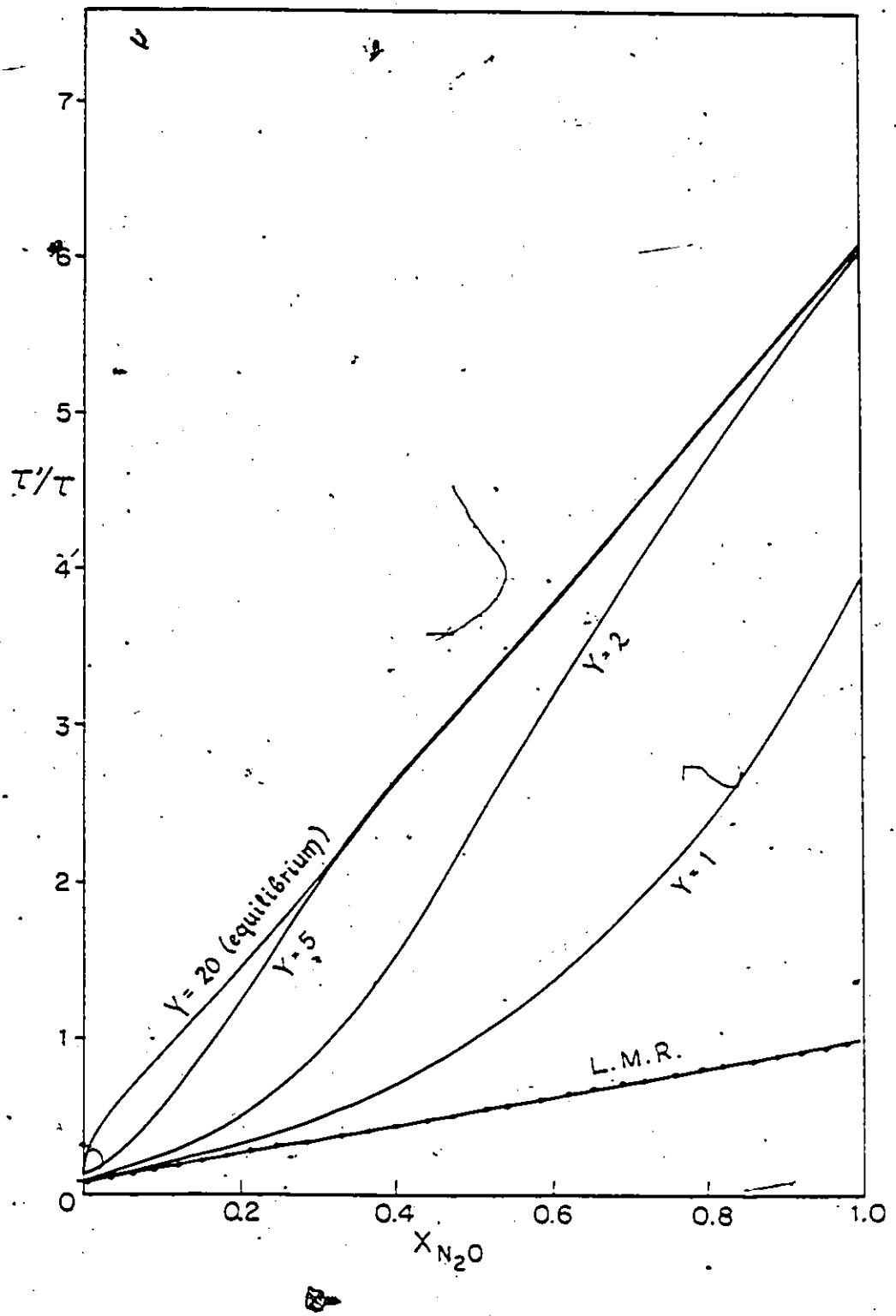

Figure 4.21 Variation of τ/τ' with mole fraction of C_2H_2 at different Y.

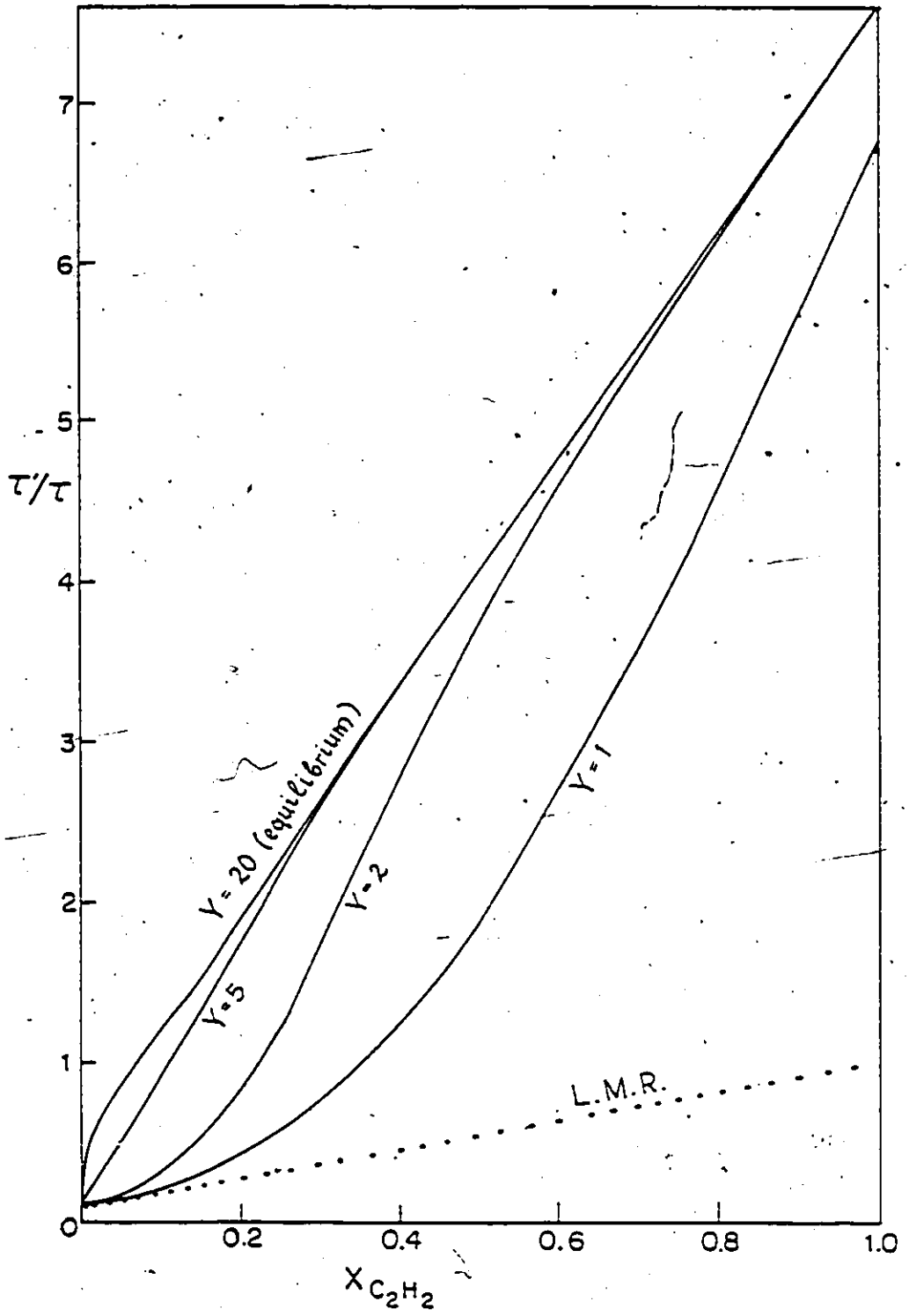

temperature for both N_2O and C_2H_2. Vibrational relaxation parameters have been selected in such a way that curves representing τ'/τ vs Y increased with Y before they reach equilibrium: T = 320 K, $\lambda_{Ar} = \lambda_{N_2O} = 0.001$, $\lambda_{VV} = 0.05$, ϕ = 0.01 and $\gamma = 5$ for N_2O and T = 320 K, $\lambda_{Ar} = {}_{C_2H_2} = 0.001$, λ_{VV}, ϕ and γ are standard for C_2H_2 (see section 5.2 for details). Results of the linear mixture rule are shown in figs. 4.22 and 4.23. In both cases, curves representing τ/τ' vs mole fraction are nearly linear and do not change significantly with the extent from equilibrium. These results are expected since it has been found theoretically and experimentally that the mixture rule approaches linearity at low temperature.

4.6 Simulation of laser experiments for N_2O

In laser-induced fluorescence experiments, the initial population is at equilibrium at temperature T. After the laser shot, a certain fraction, δ, of the ground state levels $\nu_o=(0,0,0)$ are excited to $\nu_1 = (1,0,0)$, say. In this way the population of the ground state level is reduced by an amount $\delta N_{\nu_o,eq}(T)$ and it becomes:

$$N_{\nu_o}(T) = N_{\nu_o,eq}(T) - \delta N_{\nu_o,eq}(T)$$

and the population of the excited vibrational level (ν_1) is increased by the same amount:

$$N_{\nu_1,eq}(T) = N_{\nu_1,eq}(T) + \delta N_{\nu_o,eq}(T)$$

τ', as defined in eq.4.15, describes the relaxation of the total energy. We can also decompose the energy into its 3 components (one for each mode) and thus define three corresponding τ's using expressions analogous to (eq. 4.15).

Figure 4.22 Variation of τ/τ' with mole fraction of N_2O at low temperature.

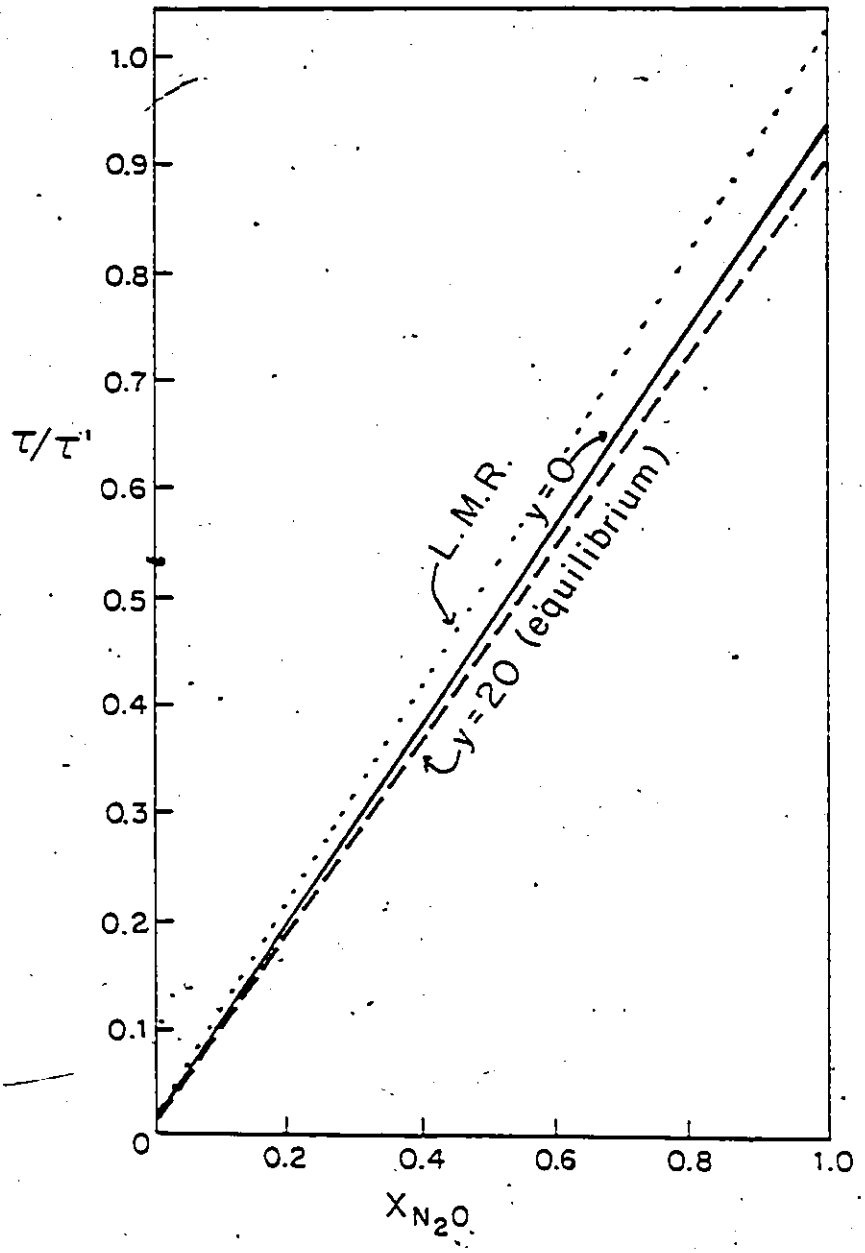

Figure 4.23 Variation of τ/τ' with mole fraction of C_2H_2 at low temperature.

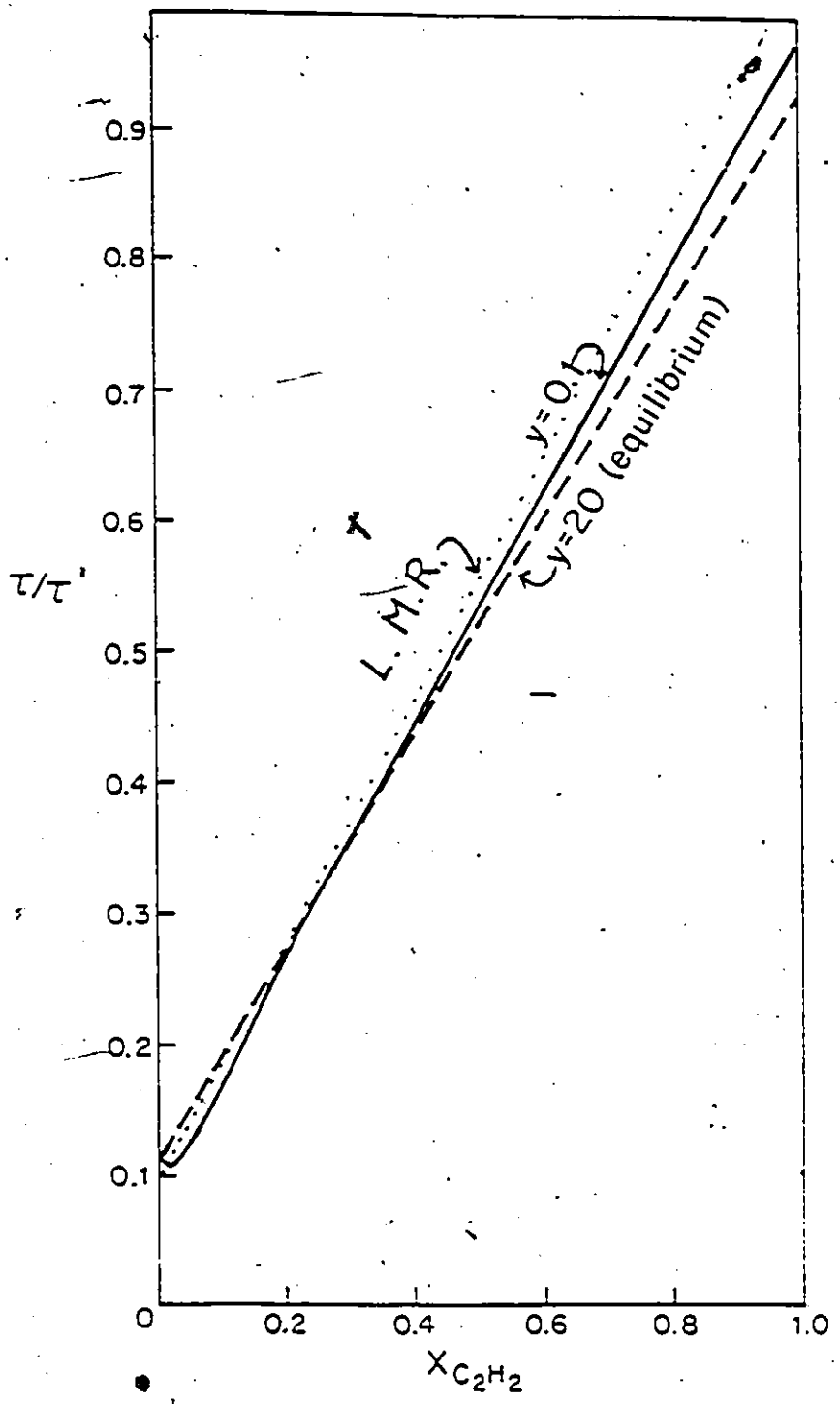

This is useful for comparing the equilibrations subsequent to laser-excitation of specific vibrational modes.

Vibrational relaxation times have been calculated for several values of ζ: 0.001, 0.01, 0.1, 0.5, for all three vibrational modes, ν_1=(1,0,0), ν_2=(0,1,0), ν_3=(0,0,1) with the same standard parameters used in the shock wave simulation (Table 4.3). Only the main features of this calculation will be presented in this section.

The fundamental frequencies of N_2O are such that near-resonance between modes occurs relatively low on the energy scale. e.g. (0,2,0) and (1,0,0); (0,0,1) and (0,4,0) are ~100 cm^{-1} apart. We expect that after an initial transient the 3 modes would relax similarly. Figs. 4.24 - 4.26 show that the transient is extremely short indeed.

Fig. 4.24 shows the variation of τ'/τ with Y of each vibrational mode, (1,0,0), (0,1,0) and (0,0,1) and of the total vibrational energy after excitation of the (0,1,0) mode by a fraction ζ = 0.5. Despite the initial selectivity all three modes relax with the same time "constant" after ~0.05 time units. We note that (0,1,0) loses energy initially after the excitation with τ'/τ = 0.005 and finally with τ'/τ= 0.25 near equilibrium. Simultaneously, (1,0,0) gains energy and attains a steady rate after Y~0.05 thus indicating that the process (0,1,0) ——> (1,0,0) is operative. Then (1,0,0) and (0,1,0) transfer their energy to (0,0,1) and the latter reaches a maximum at Y~0.03. The three vibrational modes reach a constant value of τ'/τ=0.25 after an extremely short transient period (Y~0.05). The final

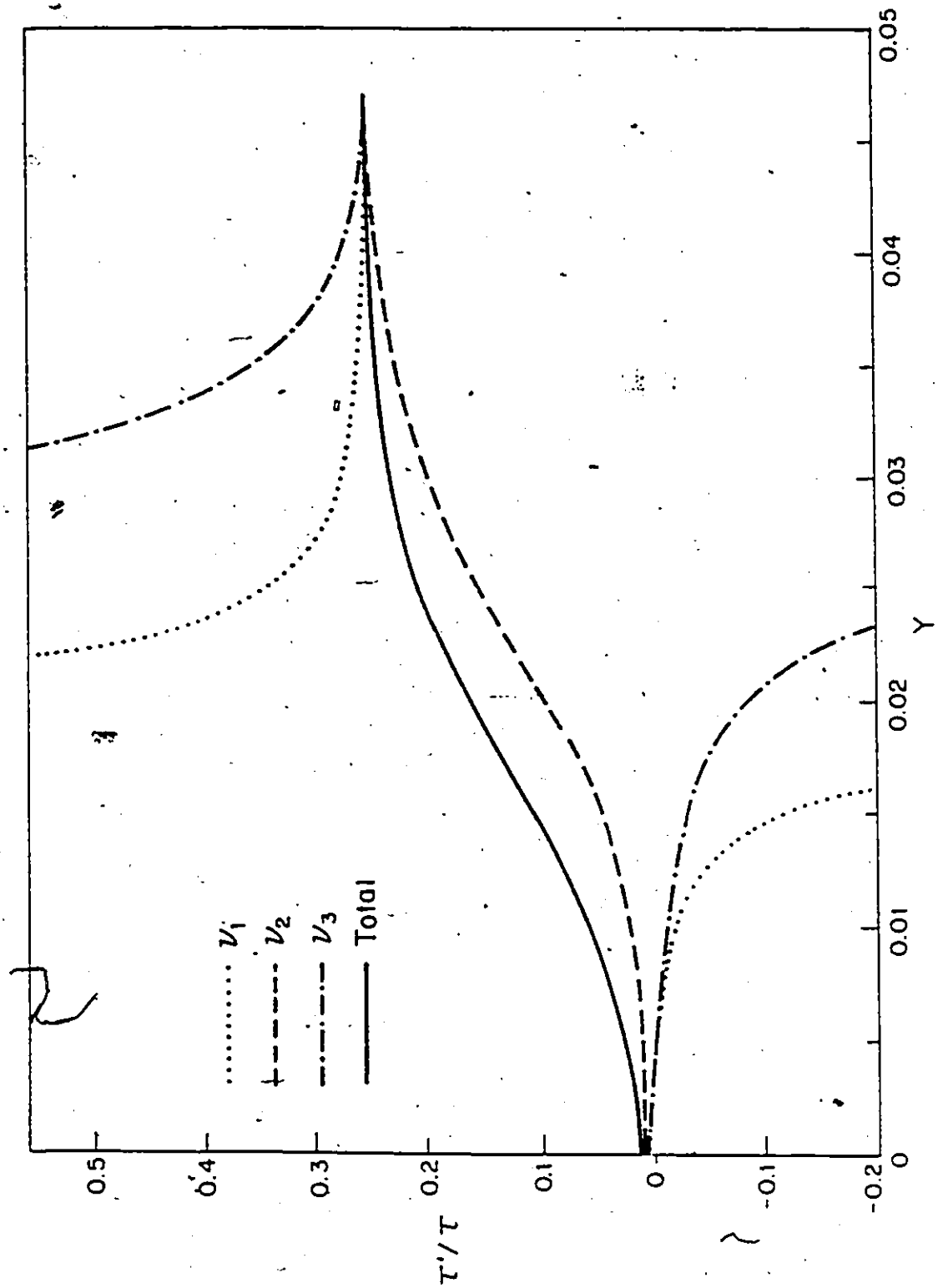

Figure 4.24 Simulation of a laser experiments for N_2O, (ν_2 excited, ζ=0.5, standard parameters).

coupled relaxation of all three modes (with $\tau'/\tau \approx 0.25$) probably involves a complicated set of V-V processes, which will be discussed later.

Fig. 4.25, shows that exciting different modes affects the transient period only. The higher the energy of the excited mode is, the shorter is the transient period. This is expected since the rates of deactivation are proportional to $\exp(-\Delta E)$.

Fig. 2.26 shows the effect of the degree of perturbation of the ν_2, mode on the observed relaxation of the ν_2 mode. Note the different time scale with the shock wave simulation. Clearly, a shock perturbation is followed by a relatively long incubation time, in contradistinction to the short transient of a laser-excitation experiment. At first sight this result is quite surprising. Afterall, itwas shown (29, 76) that for diatomic molecules, the time-dependence of τ' was extended when the molecules are laser-excited, but non-existent when shock-excited. However, on second thought it is quite reasonable. A new factor (variable state density) has entered the picture. Time-dependence of τ' due to V-V processes has been reinforced for laser-excitation of polyatomics. Whereas laser-excitation results in the direct population of those levels which are instrumental in mode coupling, shock excitation must proceed via the lowest rungs on the vibrational ladder. It is only after a significant incubation time related to the rate constant for level (0,0,0) $\longrightarrow$ (0,1,0) that the important densely packed levels are reached, or at least that level ν_1 is sufficiently populated for intra- or inter-molecular V-V processes to become

Figure 4.25 Simulation of a laser experiment for N_2O, effect of exciting different modes, (ζ=0.5, standard parameters).

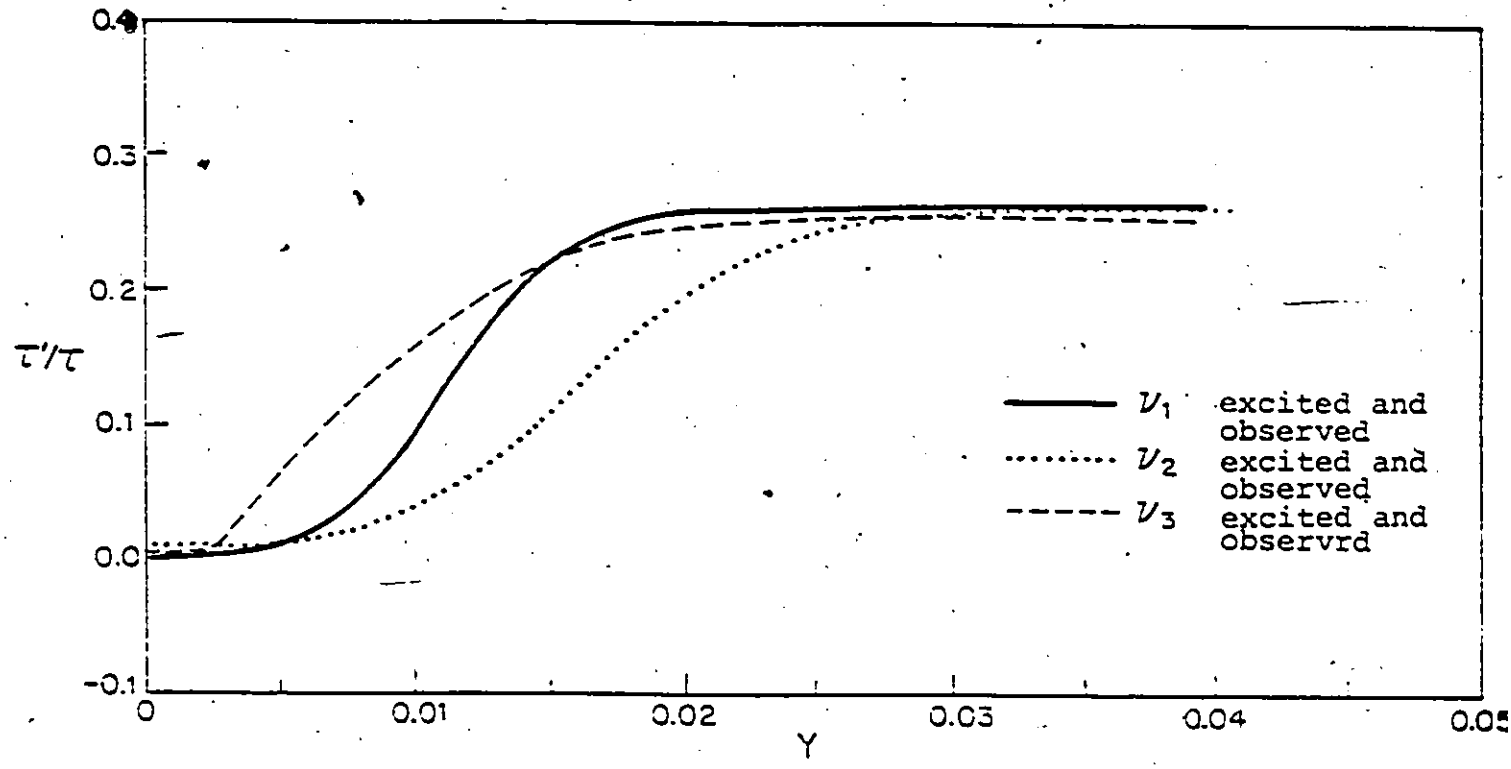

Figure 4.26 Simulation of a laser experiment for N_2O; effect of degree of excitation δ, ν_2 excited and observed, (standard parameters)

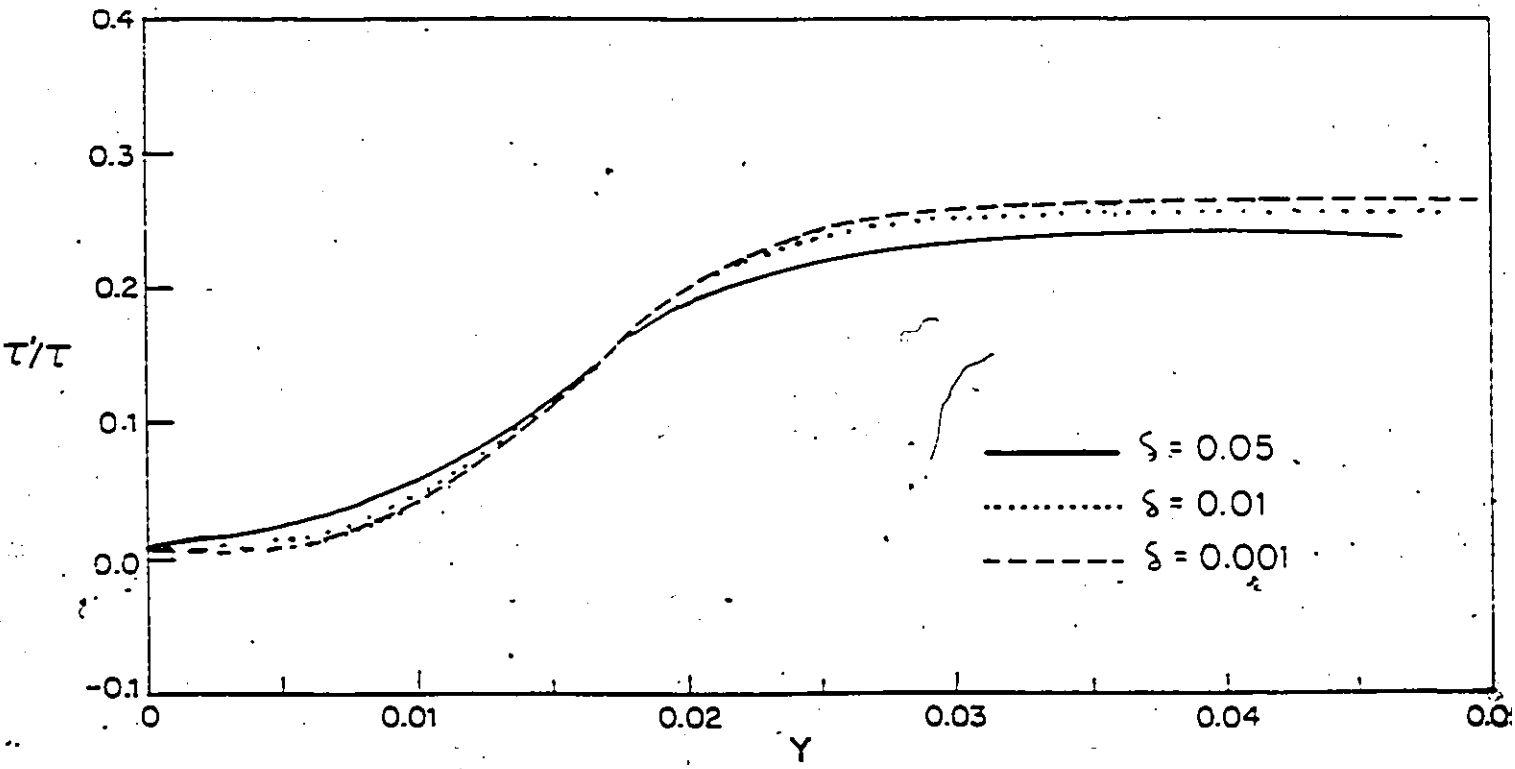

operative. At low temperatures the relaxation is essentially complete by then, at high temperatures it accelerates thereafter. The difference in behavior from laser-excitation will prove to be of some importance for interpretting the confusing data of fig. 1.4. However, it is important to note that as long as one is measuring close to equilibrium, both laser experiments and shock wave experiments should yield the same value of τ'_0/τ.

CHAPTER 5: DISCUSSION

Both our experimental results and theoretical predictions show the same phenomenon - namely the failure of the Bethe-Teller law. In other words, a single relaxation time cannot be said to exist for the vibrational relaxation of N_2O nor for C_2H_2. The question of whether this is a general phenomenon is an important one because of the widespread use of rate constants and because of the widespread interpretation in terms of one or two microscopic energy transfer rate constants. The picture painted by Cottrell (6) appears to be greatly oversimplified: once intermolecular energy transfer processes begin to play a role, the relaxation cannot be described in terms of decay via the lowest mode.

Our calculations indicate that at certain temperatures (i.e. ~600K for N_2O (see fig. 5.14 section 5.2.1)) the mechanism switches from one where the relaxation slows down to one where it is accelerating, as more and more densely packed vibrational levels become accessible. We observed the same effect in our N_2O experimental results albeit at ~1300K (fig. 3.8 section 3.1.1). Presumably a better choice of parameters could result in better agreement between experiment and theory. However, our aim was not to achieve quantitative agreement, rather to show that our results are physically reasonable. For acetylene we were unable to observe the switchover in mechanism experimentally, because it is technically difficult to achieve high enough temperatures for such a low molecular weight gas in a shock tube.

The constancy of $P\tau$ has been discussed in detail in Section

1.5. It is known (29, 78) that for diatomic molecules, the vibrational relaxation time is generally not constant. It depends on several factors, i.e. the anharmonicity, the initial distribution of vibrational levels, whether it is Bolzmann or not, the importance of V-V energy transfer and the time-regime of relaxation t/τ. τ' is constant only under conditions where the initial distribution is Boltzmann such as in shock tube experiments. This result for diatomics seems to contradict our present experimental and theoretical results where shock waves were used and the measured or calculated vibrational relaxation times were not independent of t/τ. The basic difference between diatomics and polyatomics is that the density of states for the latter is not constant. This indicates that the constancy of the state-degeneracy determines the constancy of $\tau'(t)$.

The most important conclusion is that the Beth-Teller law cannot be applied to polyatomic molecules. Nevertheless general rules which could be helpful in determining the vibrational relaxation mechanism of polyatomic molecules exist (31). These rules have been discussed in detail in section 1.2, and were used as guidelines for developing our model.

In this project, we did not try to obtain quantitative agreement between our experiments and calculations. Instead we tried to find an appropriate mechanism for the vibrational relaxation of polyatomic molecules which could explain qualitatively the type of behavior obtained in our experimental results for N_2O and C_2H_2. Before we try to find a suitable mechanism for the vibrational relaxation of N_2O and C_2H_2 we shall

compare our results with the computer simulation results as well as with the literature results.

5.1 Comparison with literature results

5.1.1 N_2O

All known results on the vibrational relaxation of N_2O have been discussed and represented graphically in the first chapter (section 1.3). In all those cases a Landau-Teller plot of log $P\tau$ vs $T^{-1/3}$ was drawn to show the temperature dependence of the vibrational relaxation time (fig. 1.4). In order to compare our results with the literature results we have to plot log $P\tau$ vs $T^{-1/3}$ at different Zt. Such a plot is represented in fig. 5.1. By comparing the shape of our curves to those in the literature we conclude that our results are in apparent disagreement with other worker's results. In most cases log $P\tau$ increases almost linearly with $T^{-1/3}$. In our results, log $P\tau$ decreases with increasing $T^{-1/3}$ except at high temperature where our results seem to be in agreement with what has been published up to now.

If we plot our results on the same graph as those in the literature (fig 5.2) we can see that despite the disagreement in the shape of our curves our vibrational relaxation times are of the same order of magnitude as the literature values and a large portion of our curves overlap with them, especially with other shock tube data. Moreover, if we neglect the effect of Zt and we consider the overall experimental results, we can see that log $P\tau$ increases with $T^{-1/3}$ on the average. Can we conclude that our results are in agreement with the literature results? Can we conclude that published results only fortuitously obey the

Figure 5.1 Landau-Teller plot for pure N_2O at different Zt. (Extracted from fig. 3.9).

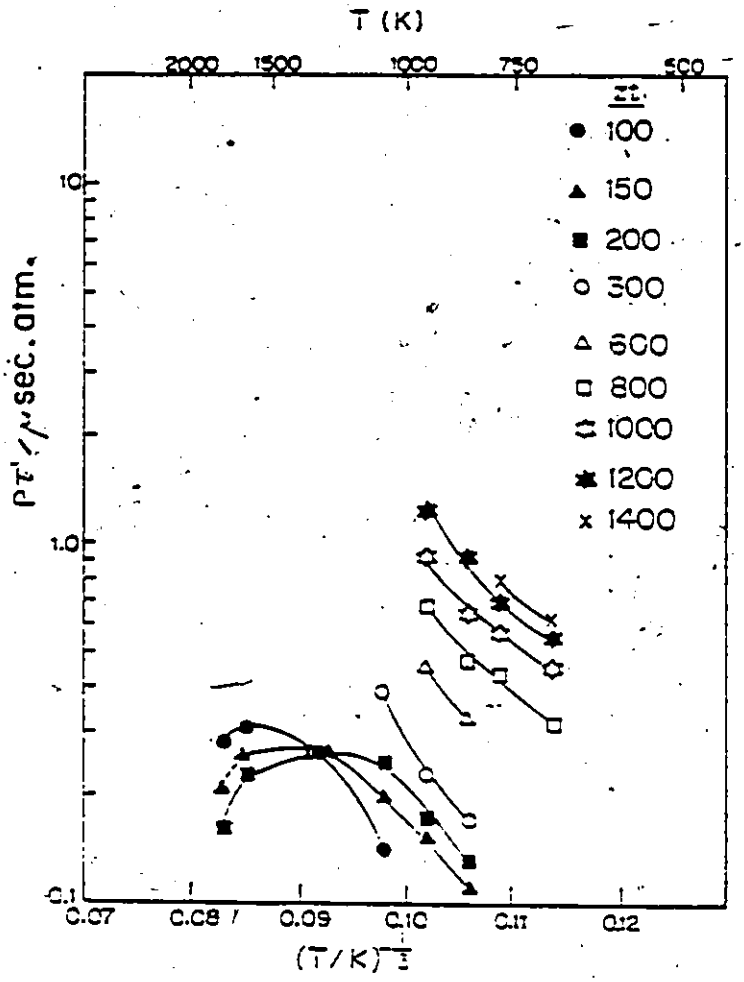

Figure 5.2 Comparison between present experimental results and the literature results for pure N_2O.

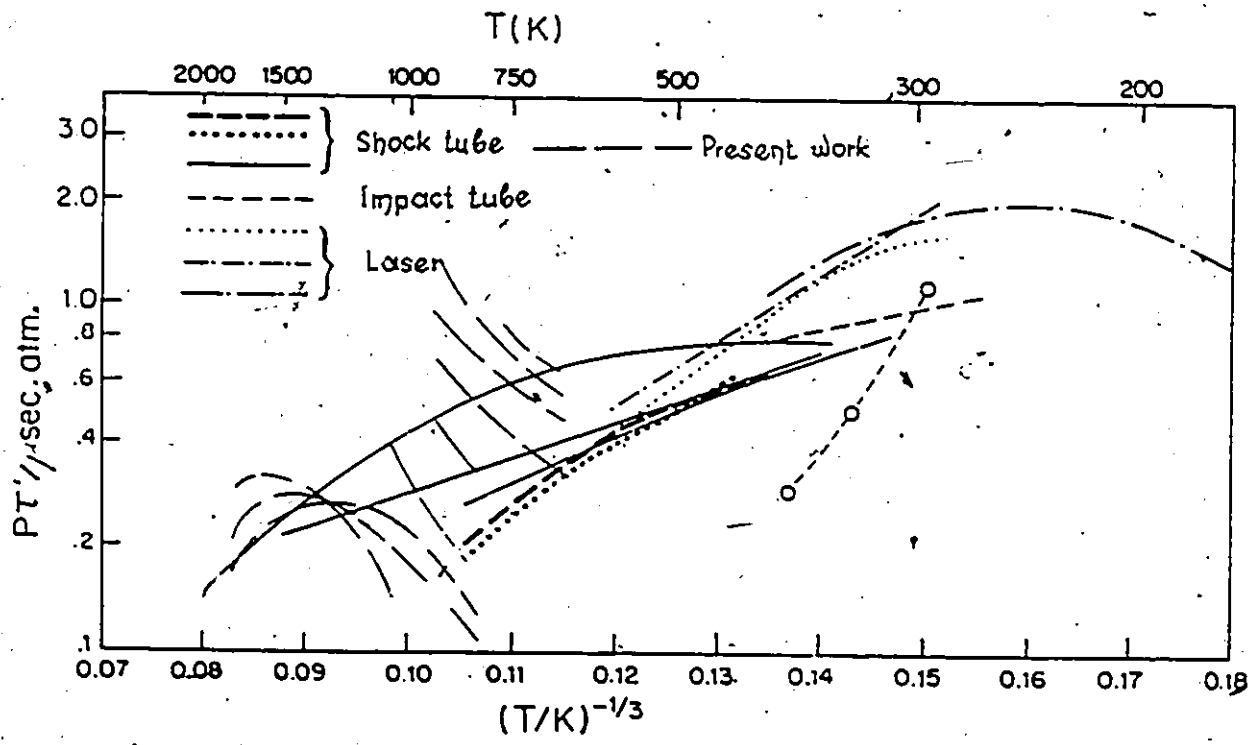

Landau-Teller law? Actually, in all other literature data, the extent from equilibrium (i.e. Zt) was ignored, and yet we now know that this factor is extremely important. Moreover, not all the experimental conditions were mentioned in the literature. It is possible to perform two different experiments with the same shock wave velocity (same temperature) with two different diaphragms; in this case, the pressure of the driver gas and the pressure of the test gas are different, thus 2 different Zt's are probed; hence two different vibrational relaxation times are obtained (see table A.1- A.8 for some examples). We believe that the discrepancy in the literature results is mainly due to the use of different but unknown initial conditions and therefore to different and unknown values of Zt.

Is it possible to obtain Landau-Teller plots similar to those in fig. 1.4 from our experimental data? If we assume, that the discrepancy in the literature results is due to the probing of different Zt's, we should be able to reproduce the literature results by plotting log $P\tau'$ vs $T^{-1/3}$ using the appropriate conditions. To do this, we classify our experimental data according to the driver gas pressure and we plot log $P\tau'$ vs $T^{-1/3}$ for each regime of driver gas pressure (which represents different values of Zt). Results are presented in figs. 5.3 to 5.6. In all cases we observed that log $P\tau'$ increased with $T^{-1/3}$ exactly as in the literature. In fig. 5.7, all curves of figs. 5.3 to 5.6 appear on the same graph. Now we can see the effect of driver gas pressure on relaxation time. It is evident from the curves of fig. 5.7 that the pressure of the driver gas (keeping

Figure 5.3 Landau-Teller plot for pure N_2O at P_D=450-550 torr.

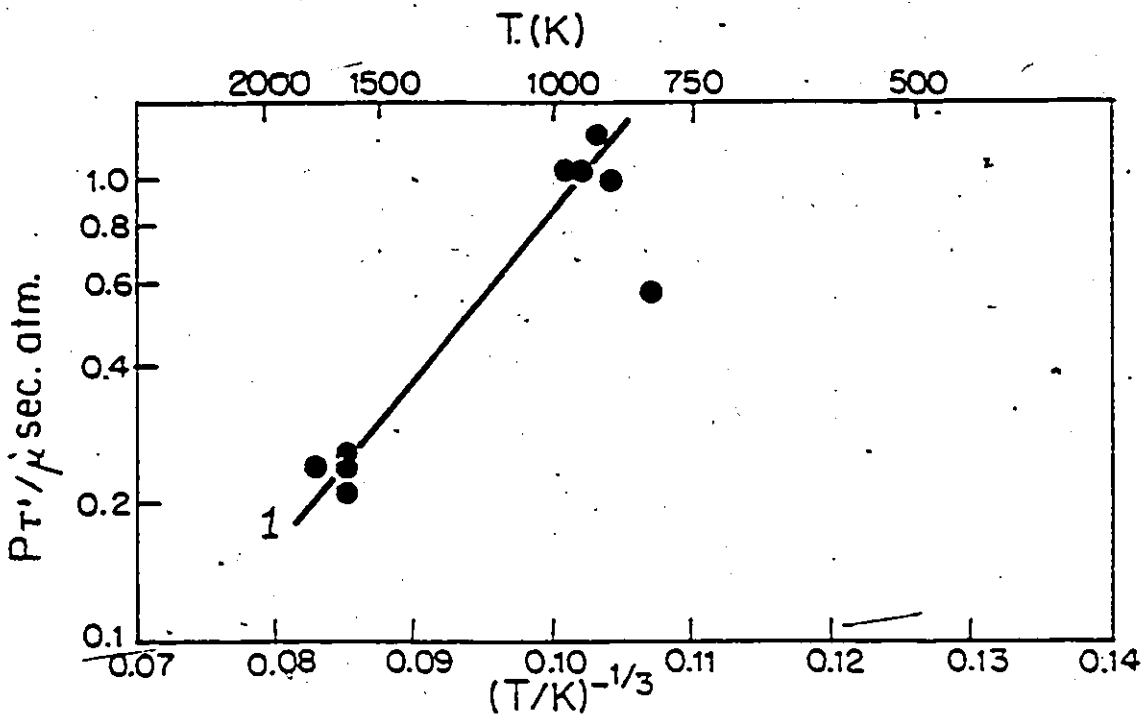

Figure 5.4 Landau-Teller plot for pure N_2O at P_D=280-350 torr.

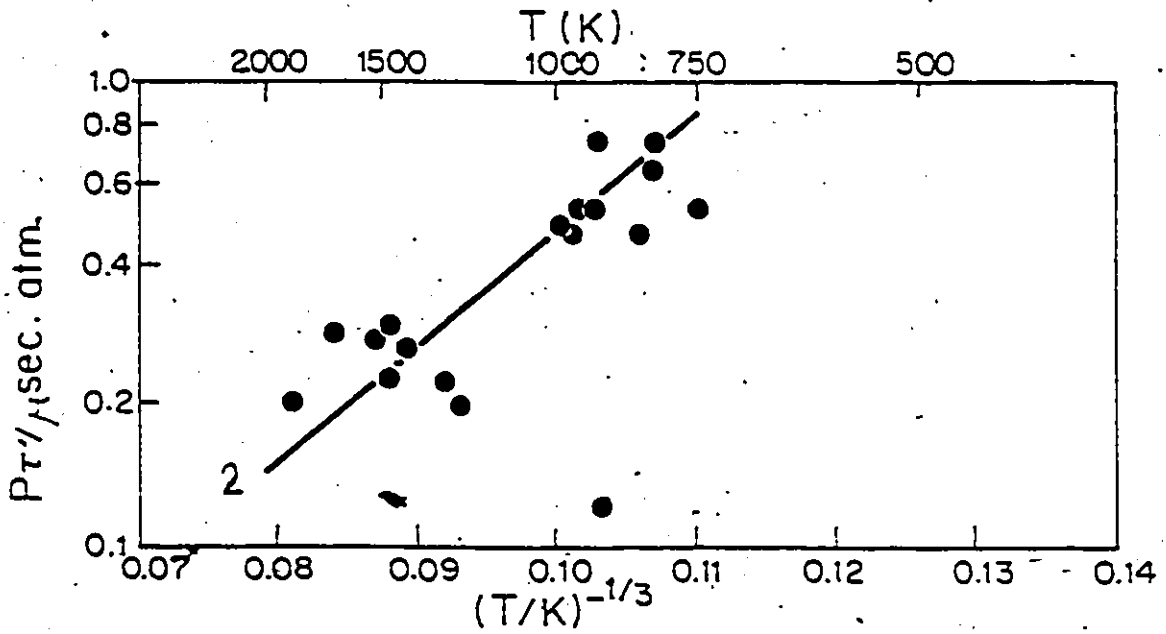

Figure 5.5 Landau-Teller plot for pure N_2O at P_D=180-220 torr.

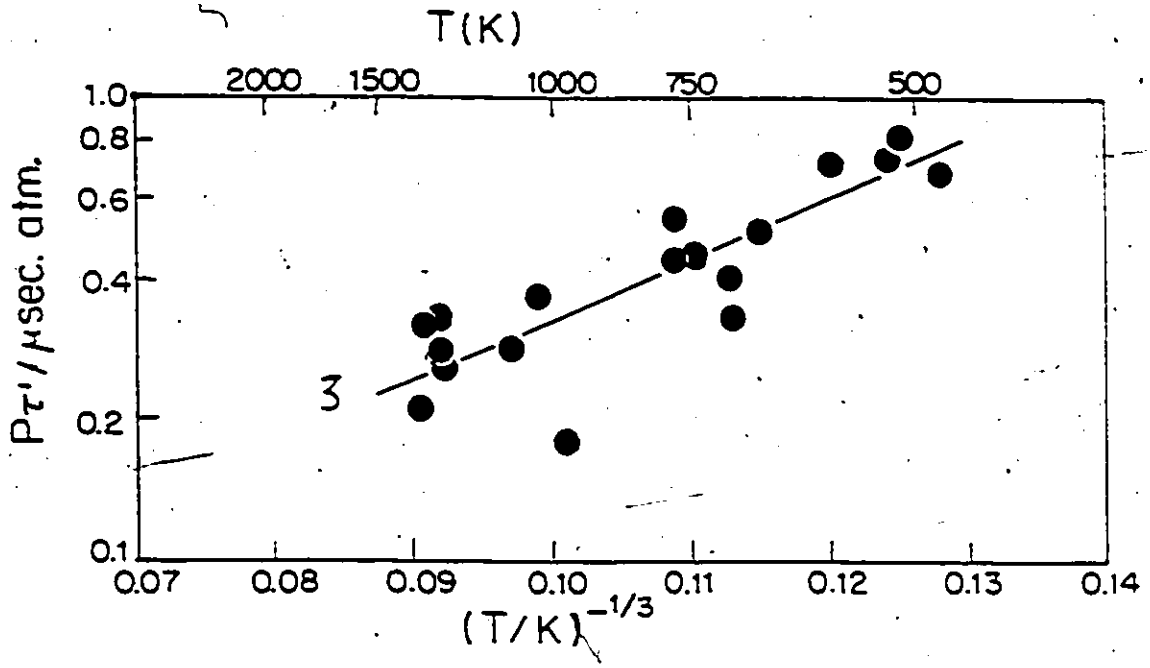

Figure 5.6 Landau-Teller plot for pure N_2O at P_D=120-150 torr.

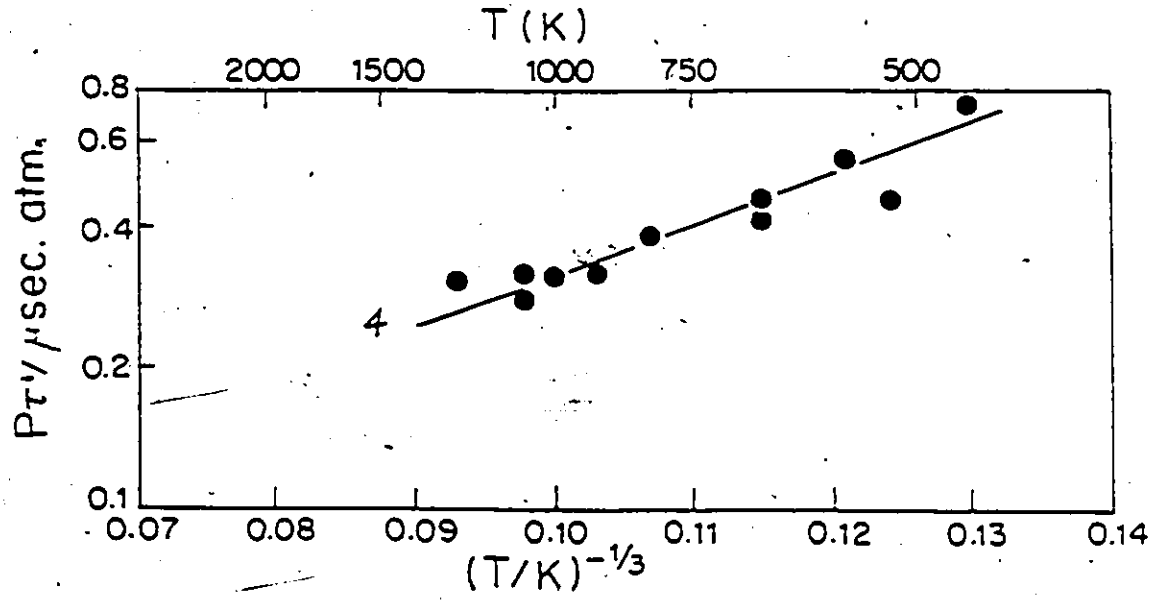

Figure 5.7 Landau-Teller plot for pure N_2O at different P_D.

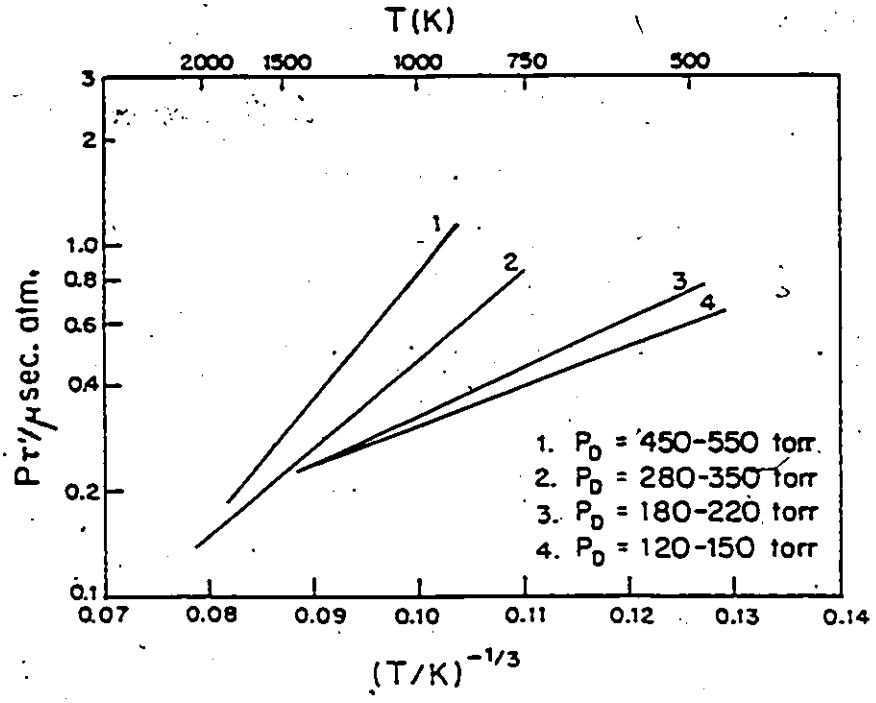

Figure 5.8 Comparison between present experimental results and the literature results for pure N_2O.

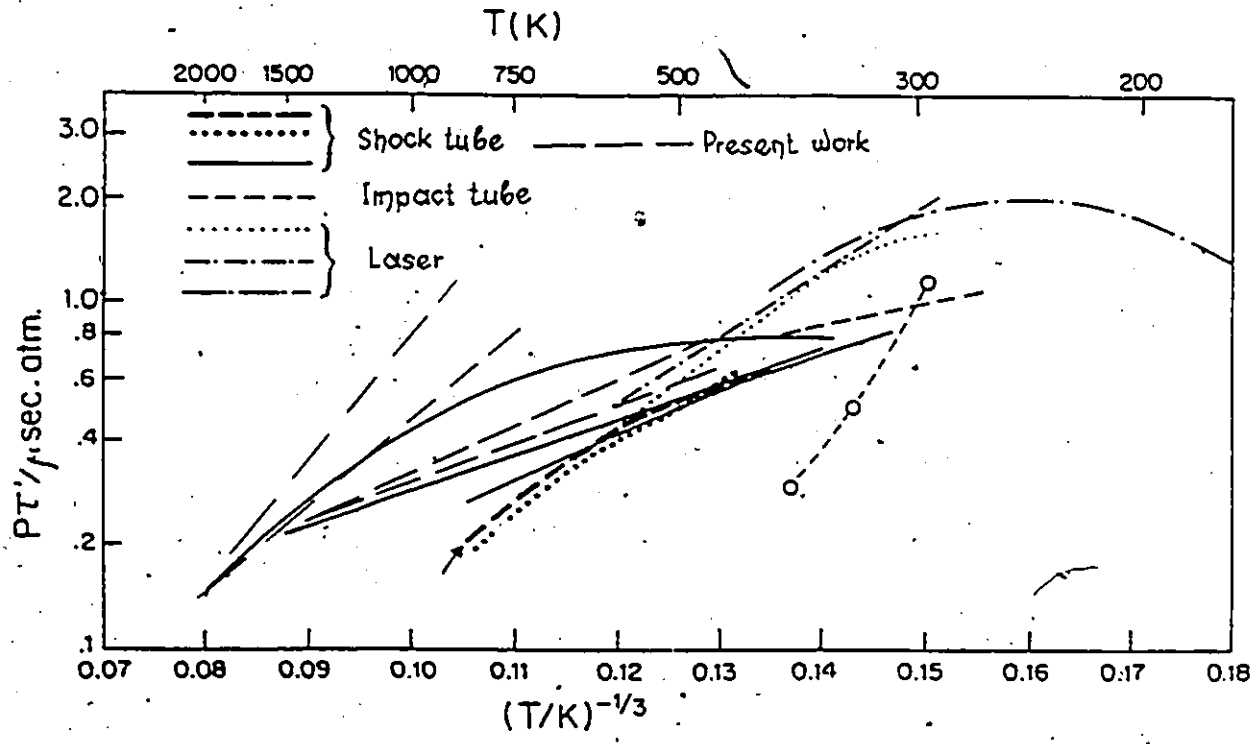

the temperature constant) or equivalently varying Zt affects the relaxation time markedly.

Now we can compare our results to the literature results. In fig. 5.8, curves of fig. 5.7 and fig. 1.4 appear on the same graph. It seems now that our results are in very good agreement with other shock tube results. In fact three of our curves are located between the curve of Dove et al (37) and the curves of Simpson et al (34-36).

We believe now that the discrepency in the literature results is mainly due to the systematic probing of different Zt (or different extents from equilibrium). Until the present study there was no theoretical treatment predicting this effect.

5.1.2 C_2H_2

In order to compare our results with the literature results a plot of log $P\tau'$ vs $T^{-1/3}$ at different Zt is needed as in the case of N_2O. Such a plot is represented in fig. 5.9. We can easily see that log $P\tau'$ decreases with increasing $T^{-1/3}$. This behaviour is in disagreement with the behaviour previously reported (74) which shows that the relaxation becomes faster as the temperature increases. However, by plotting log $P\tau'$ vs $T^{-1/3}$ for each regime of driver gas pressure as we did in the case of N_2O, we can obtain results which are in good agreement with the literature results (fig. 5.10, and 5.11). Unfortunately, not many results have been published on the vibrational relaxation of C_2H_2, and the comparison of our results with others is very limited.

Figure. 5.9 Landau-Teller plot for pure C_2H_2 at different Zt.

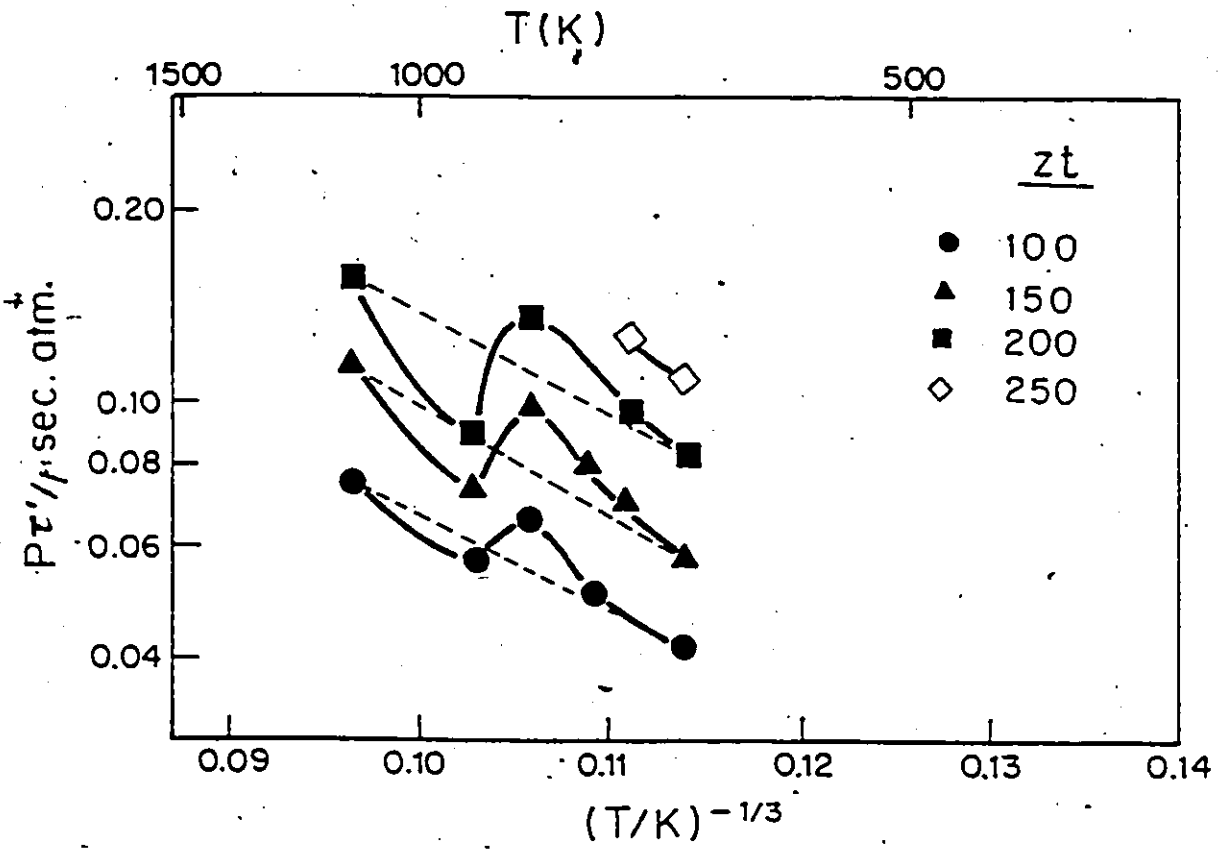

Figure 5.10 Landau-Teller plot for pure C_2H_2 at different P_D.

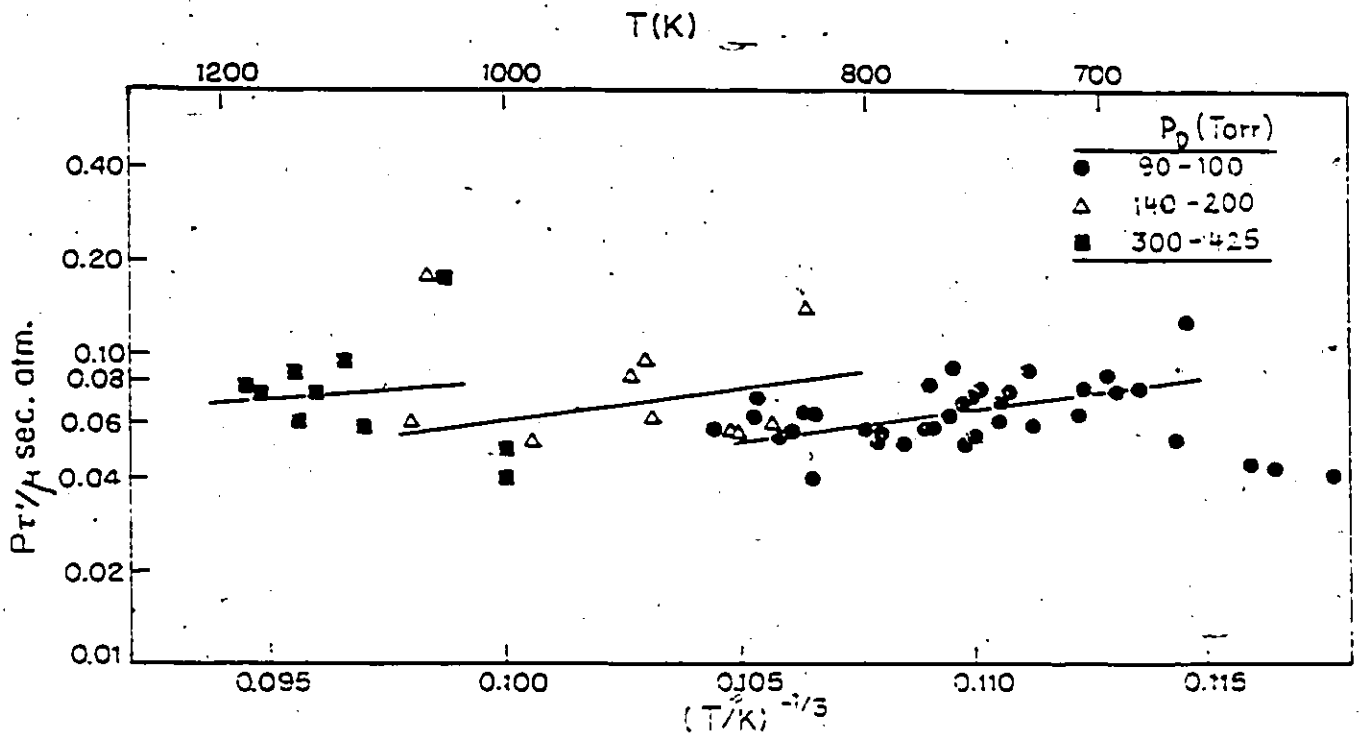

Figure 5.11 Comparison between present experimental results and the literature results for pure C_2H_2.

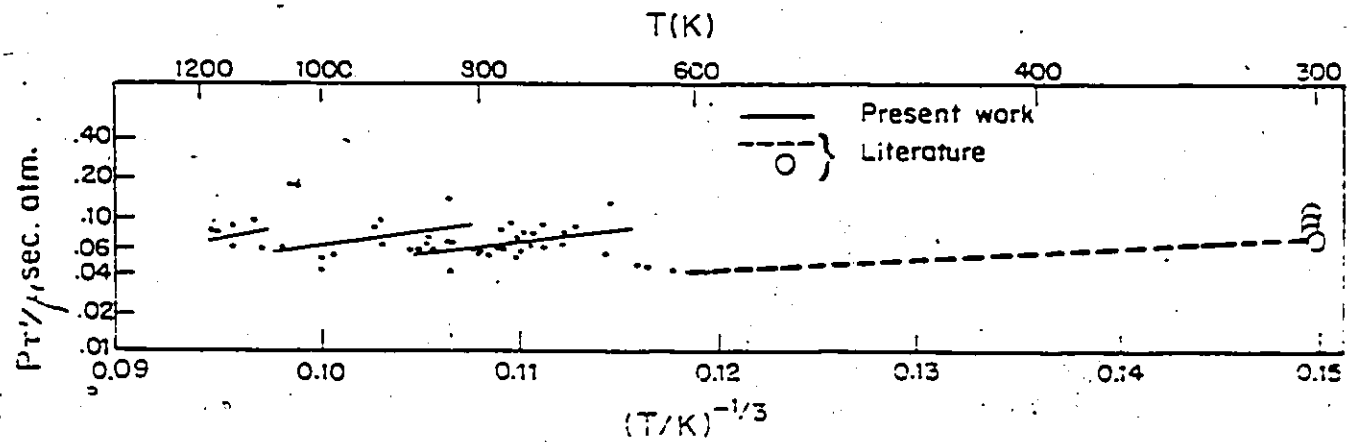

5.1.3 Linear mixture rule

It is interesting to compare the deviations from the LMR as observed for N_2O, CH_4 and C_2H_2 (present work). Both N_2O and CH_4 show similar non-linear mixture rules (105) (fig. 1.15 section 1.5). C_2H_2 shows a prominent maximum in its plot of rate coefficient vs mole fraction (figs.3.42-3.47 section 3.4). The magnitude of the maximum in C_2H_2 results is more important than in the N_2O and CH_4 results, and it is more important in CH_4 than in N_2O. We saw in sections 1.5, 3.4 and 4.5 that the mixture rule plot approaches linearity (the maximum decreases as the relaxation approaches equilibrium); thus is possible toattribute the difference in the amplitude of the maximum to the extent from equilibrium. i.e. we can say that N_2O-Ar measurements are closer to equilibrium than CH_4-Ar measurements, and the results for C_2H_2 are far away from equilibrium.

5.2 Comparison between the computer simulation results and the experimental results.

All simulated curves of τ'/τ vs Y decrease with increasing Y and reach a final value at high Y. In our experimental results most of the curves representing $P\tau'$ vs Zt, which is the equivalent of τ'/τ vs Y, increase with increasing Zt. Some of them reach their limiting value during the observation period and some of them do not. However, in the case of N_2O, $P\tau'$ decreases with increasing Zt at sufficiently high temperature. At first sight it seems that our experimental results agree with the theoretical calculations at high temperature and disagree with them at low temperatures. However, we have to remember that the values of all parameters chosen in the theoretical calculation

were arbitrary. The real values of these parameters may be quite different and depend on temperature and might give curves which are completely different in shape from the curves already obtained.

Is it possible to obtain curves of τ'/τ vs Y which are at least in qualitative agreement with the experimental low temperature ones by modifying the values of the model's parameters?

In section 4.4, we showed that modification of the parameters affected the shape and the amplitude of curves representing τ'/τ vs Y. Thus it is possible to modify some or all of the parameters in the direction which causes τ'/τ to increase with Y. We started by modifying 2 parameters only, then we modified the third parameter and so on, until all parameters were adjusted.

5.2.1 N_2O

Fig. 4.5, section 4.4.1, shows that decreasing the temperature from 750 K to 320 K leads to a large increase in the value of τ'/τ. Thus we decided to use T=320 K as a starting point. The resulting curve was plotted in fig. 5.12 (curve 1). In this curve τ'/τ essentially decreases with increasing Y. By changing λ_{Ar} from 0.01 to 0.001 we increased the influence of V-T processes involving Ar, but since Ar's efficiency is relatively small (ϕ=0.1) τ'/τ still decreases with increasing Y(curve 2). However the magnitude of τ'/τ is increased in this case, as expected. By changing λ_{N_2O} from 0.01 to 0.001 (curve 3), τ'/τ again increases as expected. This time we succeeded in

Figure 5.12 Variation of τ'/τ with Y for N_2O with different sets of vibrational relaxation parameters.

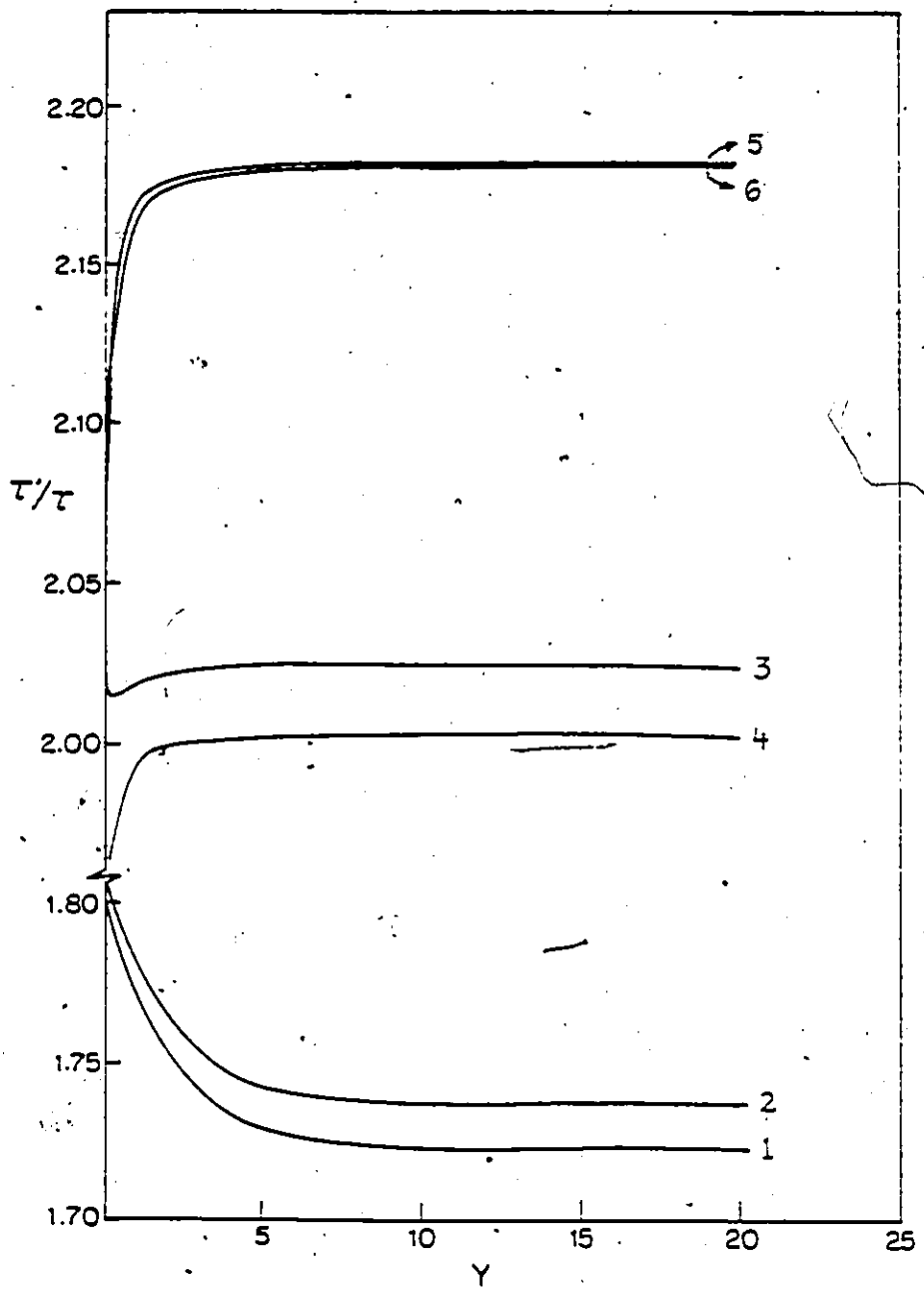

1 : X_{N_2O} = 0.5, T = 320 K, λ_{Ar}, λ_{N_2O}, λ_{VV}, ϕ and γ are standard

2 : " , " , λ_{Ar} = 0.001, λ_{N_2O}, λ_{VV}, ϕ and γ are standard

3 : " , " , " , λ_{N_2O} = 0.001, λ_{VV}, ϕ and γ are standard

4 : " , " , " , " , λ_{VV} = 0.05, ϕ and γ are standard

5 : " , " , " , " , " , ϕ = 0.01 γ is standard

6 : " , " , " , " , " , " γ = 5

increasing the influence of V-T processes, and as a result the shape of the curve is completely altered. τ'/τ now essentially increased with increasing Y until it reaches its final value. However a small spike appearing at the beginning of relaxation indicates residual V-V character. Changing λ_{VV} from 0.01 to 0.05 suppresses V-V processes and leads to a decrease in the magnitude of τ'/τ (curve 4). However, the spike disappears, as is expected when V-V processes are suppressed. Changing ϕ from 0.1 to 0.001 leads to large increases in the value of τ'/τ (curve 5). Finally, changing γ from 100 to 5 (curve 6) does not seem to affect significantly the shape of curve 5, because we have by now suppressed the V-V processes to such an extent that they no longer influence the relaxation.

We conclude that the vibrational relaxation parameters can be modified in a direction which leads to qualitative agreement with the experimental curves. In fig. 5.12 curves 3,4,5 and 6 all resemble the low temperature experimental ones. However, we still have to show that even if τ'/τ increases with increasing Y in the low temperature regime, τ'/τ nevertheless still decreases with Y at high temperatures for the same choice of parameters.

We found that increasing the temperature leads to a decrease of τ'/τ so that if we take any curve of fig.5.12 where τ'/τ increases with Y, and if we increase the temperature, we find that τ'/τ decreases with increasing Y. The effect of increasing temperature is illustrated in fig. 5.13 where the calculation was performed for 500, 750 and 1000K under conditions where $X_{N_2O}=1.0$, $\lambda_{Ar}=0.001$, $\lambda_{N_2O}=0.001$, $\lambda_{VV}=0.05$, $\phi=0.01$ and $\gamma=5$.

Figure 5.13 Temperature effect on the variation of τ'/τ with Y for pure N_2O ($\lambda_{Ar}=\lambda_{N_2O}=0.001$, $\lambda_{VV}=0.05$, $\phi=0.01$ and $\gamma = 5$).

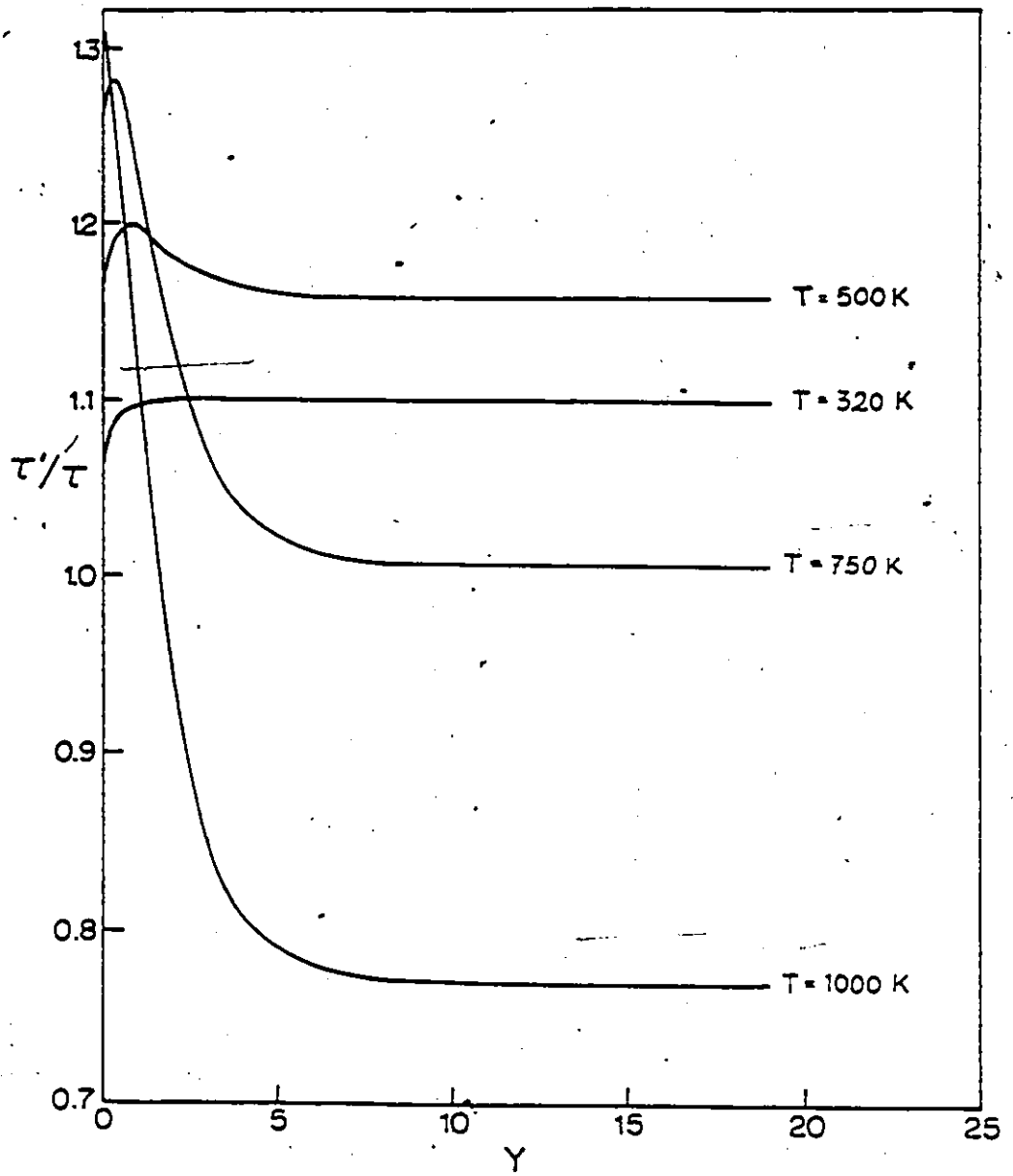

We used X_{N_2O}=1.0 because all of our experimental observations were for pure N_2O. The results of the calculation are in very good semi-quantitative agreement with our experimental results: whereas at low temperatures τ'/τ increases with increasing Y and reaches a constant value, at high temperatures τ'/τ decreases with increasing Y for the same set of parameters and reaches a constant value at equilibrium. This behavior could be explained by the fact that at low temperature (below ~600K), only low energy levels are populated; it is sufficient to consider the first four levels (0,0,0), (0,1,0), (0,2,0), (1,0,0). At the early stage of the relaxation, the fastest processes are occuring first so that small $P\tau'$ are measured; as the relaxation approaches equilibrium, slower processes will be measured and of course $P\tau'$ increases. At equilibrium, the slowest process which is in this case (0,0,0) $\rightleftharpoons$ (0,1,0) will be measured and determines the rate of reaction. Above 600 K, vibrational levels of higher energy are populated; in this case combinations of vibrational modes such as (1,1,0), (0,1,1), (1,0,1) ....etc. are populated and the energy level separation becomes smaller so that relaxation processes become faster giving smaller values of $P\tau'$. As the temperature and/or Zt increases (above 500 K), vibrational levels of higher energy as well as more combinations of vibrational modes will be populated. This causes the energy level separation to decrease further and relaxation processes to continue to accelerate. This behavior at higher temperature could also be explained by a mechanism involving a competition between 2 processes, one faster than the other. As the

temperature increases the faster process dominates the relaxation. This mechanism will be discussed in some detail in a separate section.

The temperature effect can be studied alternatively by plotting τ'/τ vs T at different values of Y as we did for our experimental results. Results of such plots are illustrated in fig. 5.14. Values of τ'/τ were determined from curves of fig. 5.13 at Y= 0.1, 0.2, 0.5, and 3. The results are in agreement with what was found experimentally (fig. 3.9, section 3.1.2). For both experimental and calculated results, the relaxation time first increases then decreases with increasing temperature. The curves cross each other at certain temperatures.

Unfortunately we were not able to reproduce all of the experimental results. The turn-around temperature for time dependence of τ'/τ was found to be 1280 K experimentally whereas our simulations indicate that it is somewhere between 400 and 700 K. Certainly a different choice of parameters would bring this also into agreement. We must emphasize that our aim was not to obtain perfect agreement, but rather to show that our experimental results are physically reasonable.

5.2.2 C_2H_2

The computer calculations performed for N_2O (previous section) were repeated for C_2H_2. The results are illustrated in fig. 5.15. These results are different from the results of N_2O (compare fig. 5.15 to fig. 5.12) and even in contradiction with what was expected at high temperature according to figs. 4.11 to fig. 4.17 (section 4.4.2). For example, we expect the curve of

Figure 5.14 Variation of τ'/τ with temperature for pure N_2O at different Y ($\lambda_{Ar}=\lambda_{N_2O}=0.001$, $\lambda_{VV}=0.05$, $\phi=0.01$ and $\gamma=5$).

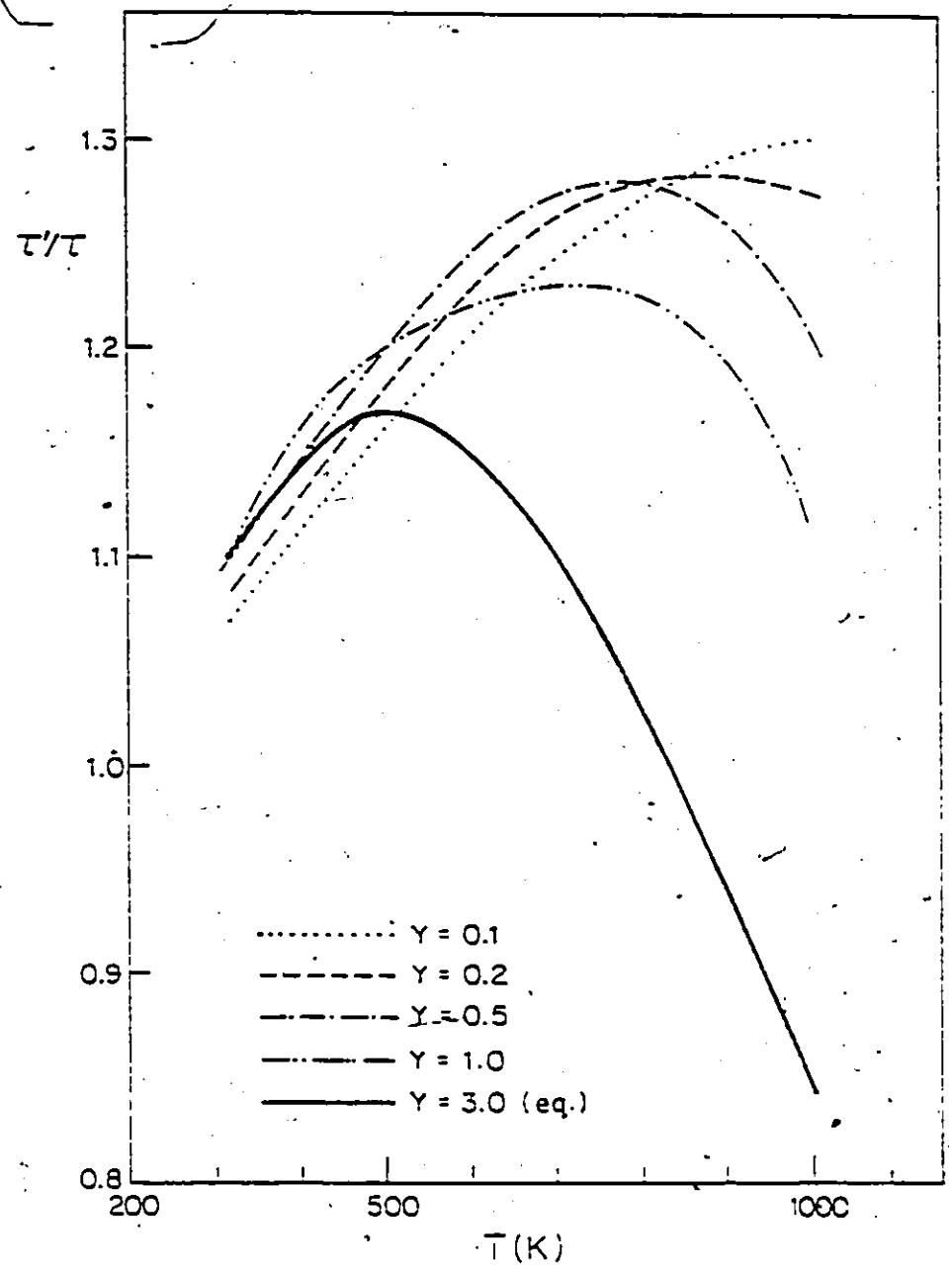

Figure 5.15 Variation of τ'/τ with Y for C_2H_2 with different sets of vibrational relaxation parameters.

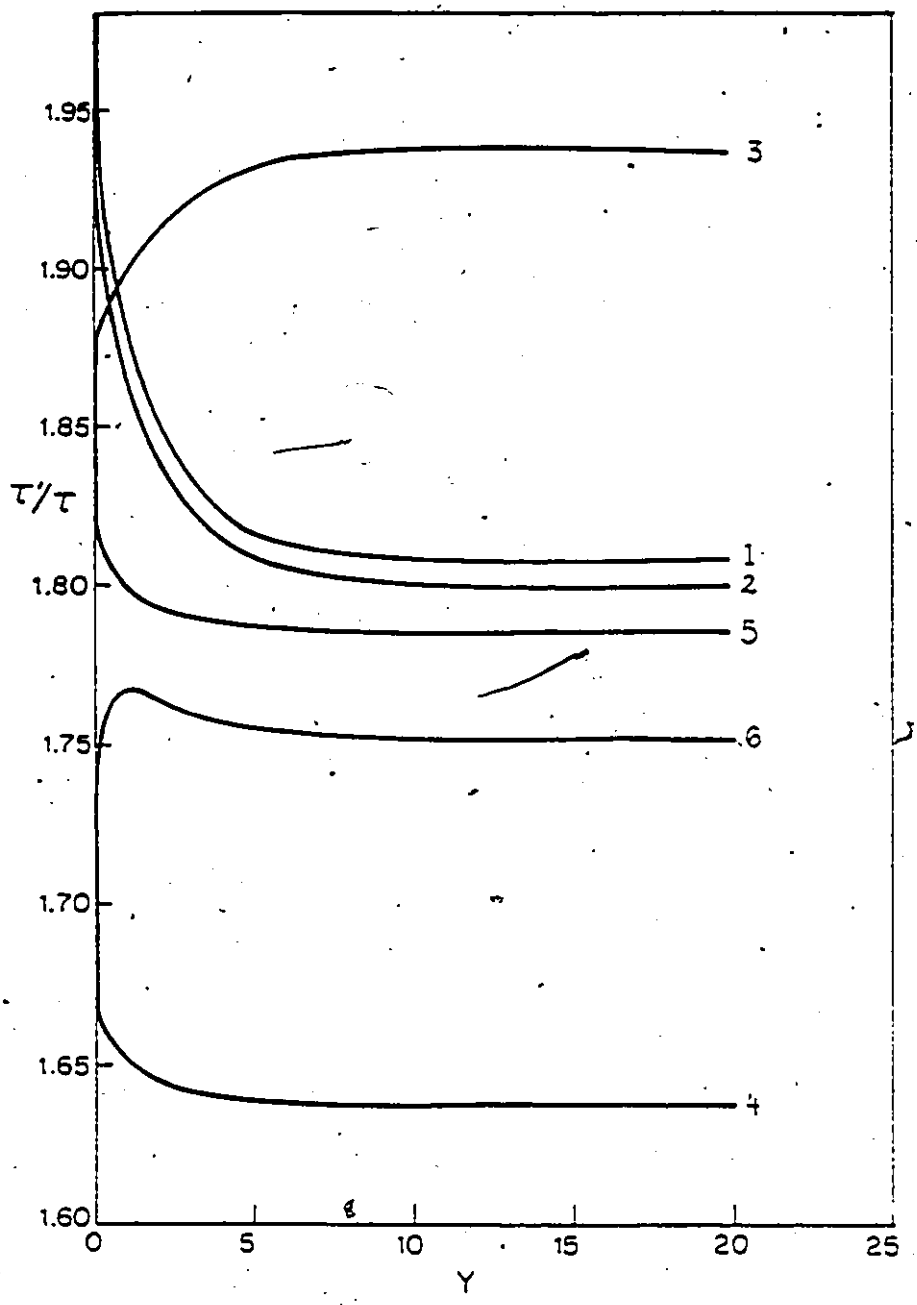

1 : $X_{C_2H_2} = 0.5$, T = 320 K, λ_{Ar}, $\lambda_{C_2H_2}$, λ_{VV}, ϕ and γ are standard

2 : " , " , $\lambda_{Ar} = 0.001$, $\lambda_{C_2H_2}$, λ_{VV}, ϕ and γ are standard

3 : " , " , " , $\lambda_{C_2H_2} = 0.001$, λ_{VV}, ϕ and γ are standard

4 : " , " , " , " , $\lambda_{VV} = 0.05$, ϕ and γ are standard

5 : " , " , " , " , " , $\phi = 0.01$ γ is standard

τ'/τ to increase when changing λ_{Ar} from 0.01 to 0.001 (see fig. 4.13). In fig. 5.15 (curve 2) we see the opposite effect at 320 K. The same happens when modifying λ_{VV} from 0.01 to 0.05 (curve 4) etc. The differences between the low temperature (320 K) and the high temperature (750 K) results may be due to the behavior of τ'/τ vs Y curves near the maximum. As was mentioned in section 4.4.2, the behaviour of these curves are very complicated near the maximum and probably unknown. We saw that some curves cross the standard one at 2 points, some other curves at one point and some curves do not cross the standard one at all while changing the vibrational relaxation parameters. Thus the difference between the high temperature and the low temperature behavior should be expected. The difference between N_2O and C_2H_2 results is due to the difference in the vibrational energy level diagram betwen these two molecules and therefore apparently to different relaxation mechanisms.

The only vibrational relaxation parameters where τ'/τ increases with Y corresponds to T=320 K, λ_{Ar}=0.001, $\lambda_{C_2H_2}$=0.001, λ_{VV}, ϕ and γ are standard (curve 3). The change in the shape of the curve occurs after modifying $\lambda_{C_2H_2}$ from 0.01 to 0.001. Therefore we believe that this V-T parameter is a very important parameter in determining the shape of the relaxation profile of C_2H_2 at least.

The effect of temperature on the shape of the curve 3 is illustrated in fig. 5.16. At low temperatures (320 K), τ'/τ increases with Y and approaches a constant value near equlibrium. As the temperature increases, the shape of the curve changes and

Figure 5.16 Temperature effect of the variation of τ'/τ with Y for pure C_2H_2 ($\lambda_{Ar}=\lambda_{C_2H_2}=0.001$, $\lambda_{VV}=0.01$, $\phi=0.1$ and $\gamma=100$).

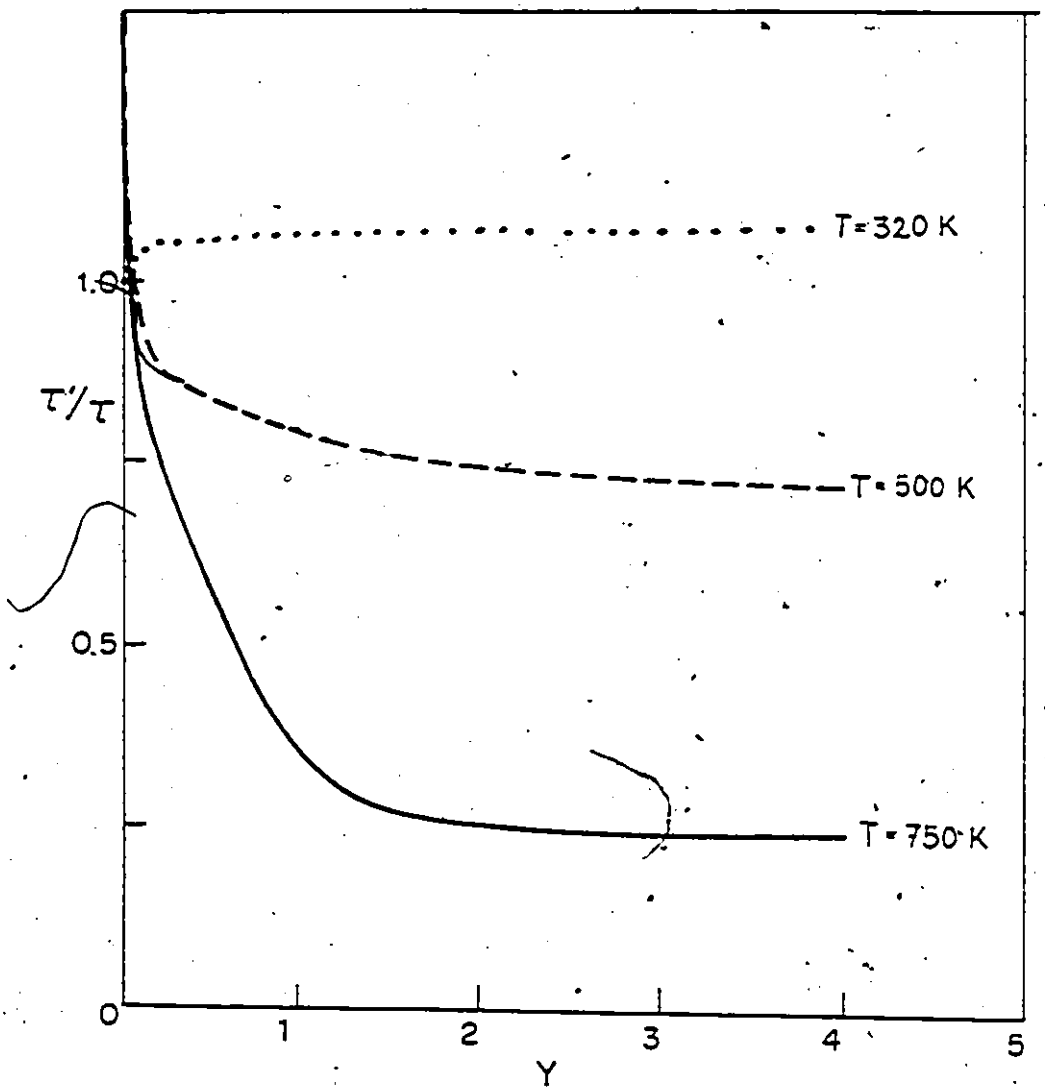

τ'/τ decreases with Y and approaches a constant value near equilibrium. We did not try to make a more detailed analysis of the temperature dependance of the vibrational relaxation of C_2H_2 as we did for N_2O. However, we believe that under certain vibrational relaxation parameters, it is possible to obtain curves similar to those in fig. 5.14.

We have thus been able to show that for certain values of vibrational relaxation parameters, ($\lambda_{Ar}=\lambda_{C_2H_2}=0.001$, remaining parameters being standard) it is possible to obtain theoretical results which are in qualitative agreement with the experimental results where the relaxation time increases as the relaxation approaches equlibrium. However, none of our experimental curves shows an acceleration where $P\tau'$ decreases with Zt, therefore the turn-around temperature was not reached; we believe that this temperature is higher that 1184 K which is the highest temperature measured under our experimental conditions, and probably at T>1200 K relaxation times which decrease with Zt would be measured.

5.2.3 Linear mixture rule

One result of this study is the observation of a marked deviation from the linear mixture rule, particularly at about 2.5% C_2H_2. The deviation is more pronounced at early stages of the relaxation. Our calculations show similarly that deviations are stronger at early stages of the relaxation. Although the exact form of the deviations is not reproduced, we must emphasize that our aim was merely to show that deviations are to be expected, and that the distribution of population among the

vibrational levels is the controlling factor. A judicious choice of parameters would presumably improve the agreement. For example allowing for slower V-T transitions (with energy gap $|\Delta E| > 704$ cm^{-1}) together with very poor intermode coupling would result in more dramatic low temperature decelerations. The same effect might be achieved by allowing the microscopic rate constant to depend explicitly on the identity of the initial and final modes.

So far we have solved the master equation for a temperature of at most 750 K where the experimentally observed deviations are still quite small (105), and it would be desirable to continue these solutions to higher temperatures. For systems with linear master equations, the computed deviations tend to increase with temperature as the multilevel character of the process becomes more pronounced (82). We know that systems with nonlinear master equations show a similar effect (76). Unfortunately the cost of the computations increases very rapidly with temperature because of the necessity to include many more levels and to allow transitions with larger gaps.

We conclude that the master equation computations support the experimental observations. They also support the warning that inverse relaxation times linearly extrapolated to infinite dilution must be regarded with caution. At present the potential parameters of this system are not well enough known to allow detailed quantitative computation of the magnitude of this effect, and further experimental investigations of relaxation rates at low mole fractions of polyatomic gases are highly

desirable.

5.3 Mechanism of the relaxation

5.3.1 N_2O

The variation of the vibrational relaxation times of N_2O with temperature are shown in fig. 5.2 (section 5.1.1). This figure contains the results of our present study superimposed on the results shown in fig. 1.4. It is a contour map of $P\tau'$ at fixed Zt. Clearly, almost anything can be explained on the basis of systematic differences in the portion of the relaxation zone probed. Bhangu (33) reported an explicit time dependence for $P\tau'$. His results and those of Griffith et al (32) quite clearly correspond to the early portion of the relaxation zone. The shock tube results of Simpson (34-36) were obtained from a conscious effort to measure far from equilibrium (115). Those of Dove et al (37) from an attempt to probe close to equlibrium (although this was technically impossible to achieve at low temperatures). The results of all of these studies are consistent with our present observations that at $T \leq 1300$ K, $P\tau'(t) < P\tau'(\infty)$. Furthermore the overall temperature dependence of $P\tau'$ is different for different systematics of measurement. Our individual curves in fig. 5.2 correspond to fixed Zt. A different temperature dependance is expected for each fixed Zt. The individual data in fig. 1.4 or 5.2 can be classified according to closeness to $P\tau'(\infty)$, i.e. essentially how much bimolecular V-V character they have. As mentioned above, results of Dove et al are close to $P\tau'(\infty)$. However, at low temperatures it becomes technically more difficult to measure at large enough

values of t/τ, i.e. one is far from equilibium. Therefore, the results of Dove and Simpson approach each other as T->300 K, and they both simultaneously deviate from $P\tau'(\infty)$. They all merge with the ultrasonic dispersion data at T$\leq$ 450 K (43-47), which are also far from equilibrium, in that the ν_3 mode is energetically inaccessible on the time scale of the experiment and cannot be observed because of its negligible contribution to the heat capacity. This agreement at room temperature is due to the fact that at room temperature, only the bending mode ν_2 is excited in the gas compression technique and the corresponding vibrational relaxation time is measured. The only measurement of the vibrational relaxation time of the ν_1 mode resulted in value of 1.3 μsec.atm. which is very close to the vibrational relaxation time of ν_2. This could be due to the fact that a rapid equilibrium is established via V-V processes between ν_1 and ν_2, as our calculations show (fig. 4.24 section 4.6):

$N_2O(1,0,0)+N_2O(0,0,0) \longrightarrow N_2O(0,2,0)+N_2O(0,0,0)$ $\quad \Delta E = 110\ cm^{-1}$

Vibrational relaxation time of the above rapid process was measured by Kung (69,70). He found a value of 0.062 μsec.atm. We concluded that whether ν_1 or ν_2 are excited at room temperature, only the vibrational relaxation time of ν_2 will be measured. Therefore the low temperature gas compression techniques including the impact tube data and the $P\tau'$ (t~0) - shock tube data lead to a steady-state $P\tau'$ which is related to processes in the ν_1, and ν_2 modes, in agreement with those laser experiments directly probing those modes (48, 51, 52, 89, 70). The $P\tau'(\infty)$-shock tube data lead, on the other hand, to an

equilibrium $P\tau'(\infty)$ involving all 3 modes.

The laser-induced relaxation experiments with ν_3 are, in principle, complicated by the fact that no estimate is given for the degree of perturbation. It is difficult to judge whether a given experiment is near equilibrium or not. However in practice, it is probably not a serious matter for laser experiments. Figures 4.24-4.26 (section 4.6) show that regardless of which mode is monitored or which mode is excited or even to what degree it is excited, after a very short time (related to the V-V and V-T coupling processes) $P\tau'$ is essentially a constant, and indeed has the same value (as $t \longrightarrow \infty$) that it does in the shock wave simulation ($\tau'/\tau = 0.25$). Therefore, it seems not to matter to $P\tau'(\infty)$ here whether the energy is provided thermally or photochemically. The high energy ν_3 level is populated directly by a photon or indirectly but quickly via available collisional coupling processes, so that laser data shows the same behaviour as high temperature shock tube data but at lower temperatures and earlier times.

Data on the vibrational relaxation of ν_3 are illustrated in table 1.1 for room temperature and in fig.1.4 or 5.2 for other temperatures. Relaxation times measured by laser techniques where ν_3 is excited, are larger than those measured by gas compression techniques by a factor ranging up to 2.5 (fig. 1.4), therefore ν_3 equilbration is more difficult than the equilibration of just the ν_1, ν_2 modes. At higher temperatures this process (ν_3 equilibration) speeds up because the critically excited molecules become more concentrated. At T>1300 K the

process ceases to become rate determining. Instead, the excited molecules are instrumental in creating a new relaxation route which competes even with the route responsible for ν_1, ν_2 relaxation. This conclusion is consistent with our present observations that at T>1300 K the relaxation accelerates with time.

One should note that the unusual temperature dependence of the laser-induced ν_3 fluorescence experiments at low temperatures less than 300 K does not seem to account for the large evolution of heat and the probably large distortion it causes to the energy relaxation, even though this is recognized to be a problem (116). For modest effects the correction takes the form of the factor $C_p/(C_p-C_{vib})$. For pure N_2O it varies from 1.33 at 300 K to 1.84 at 900 K. For more severe heating the rate constants themselves are affected.

In the following we denote $P\tau'_{\nu_1\nu_2}$ as the vibrational relaxation time when ν_1 and/or ν_2 are excited and $P\tau'_{\nu_1\nu_2\nu_3}$ when all vibration modes are excited. Is it possible to identify the rate-determining steps responsible for $P\tau_{\nu_1\nu_2}$ and $P\tau'_{\nu_1\nu_2\nu_3}$? Standard theories which assume perfect coupling between modes (6) predict that the multimode system relaxes with a time constant, $P\tau'(\infty)$ given by

$$P\tau'(\infty) = (C_i/\textstyle\sum_j C_j)^{-1}\, P\tau_i \qquad (5.1)$$

where $P\tau_i$ is the time constant associated with the rate determining step (usually the relaxation of the lowest-energy mode) and C_i is the vibrational heat capacity of mode i, given by

$$C_i = R\theta_i^2 \exp(\theta_i/T)/(\exp[\theta_i/T]-1)^2$$

where

$$\theta_i = h\nu_i/K$$

Equation 5.1 is strictly applicable only to perfect intermode coupling and small perturbations (which might not be applicable here).

First, we test the validity of equation 5.1 for a case where intermode coupling is not perfect. In fig. 5.13 we have simulated a low temperature shock wave experiment. After the transient period, τ'/τ reaches the values 1.11, and 1.20 at 320, and 500 K respectively. These are very close to the predictions of 1.08 and 1.23 of equation 5.1 as applied to the V-T relaxation of ν_2 as being rate-determining. At high temperatures, our calculations using eq. 5.1 indicate that τ'/τ is influenced somewhat by imperfect coupling. Nevertheless, we feel reassured by the large rate constant for the (0,2,0) $\longrightarrow$ (1,0,0) process reported by Kung (66,67). Therefore, in agreement with other authors, we relate $P\tau'_{\nu_1\nu_2}$ to the process (0,1,0) $\rightleftharpoons$ (0,0,0). Using equation 5.1 and our definitions for $P\tau'$ in Section 1.1.3:

$$1/P\tau = Nk_{10}(1-\exp[-h\nu_2/KT] = (1/P\tau'_{\nu_1\nu_2})(1 + C_1/C_2) \qquad (5.2)$$

Secondly, having identified $P\tau'_{\nu_1\nu_2}$ with $P\tau$, we note from fig. 1.4 that, at $T \leq 1300$ K, $P\tau'_{\nu_1\nu_2\nu_3}/P\tau$ varies from 2.5 to 1 in the temperature range 300-1300 K; whereas $(C_1+C_2+C_3)/C_2$ varies from 1.08 to 1.72, $(C_1+C_2+C_3)/C_3$ from 300 to 5.85, while $\tau'(\infty)/\tau$ from our simulations of fig. 5.13 never get larger than 1.3. This means not only that the V-T relaxation of ν_3 —> (0,0,0) cannot be rate-determining, but that also equation 5.1 cannot be used when intermode coupling is not perfect. Because of this

imperfect coupling, the values of $P\tau$ as obtained from equations 5.1 and 5.2 are underestimated, and therefore $P\tau'_{\nu_1\nu_2\nu_3}/P\tau$ is closer to 1. This means that we cannot rule out the possibility that even when ν_3 is excited ν_2 —> (0,0,0) is rate-determining, at least for T<1300 K. Most other authors suppose that (0,0,1) —> ν_2 is rate-determining but opinion is divided as to which final state is involved: (0,4,0), (1,1,0) or (0,3,0). However none of these processes has ever been observed directly.

The following abbreviated mechanism appears to describe the known result for N_2O vibrational relaxation at low temperatures.

$$(0,0,0) \rightleftharpoons (0,1,0) \qquad (1)$$

$$(0,1,0) + (0,1,0) \rightleftharpoons (0,2,0) + (0,0,0) \qquad (2)$$

$$(0,2,0) + (0,1,0) \rightleftharpoons (0,3,0) + (0,0,0) \qquad (3)$$

$$(0,3,0) + (0,1,0) \rightleftharpoons (0,4,0) + (0,0,0) \qquad (4)$$

$$(0,2,0) \rightleftharpoons (1,0,0) \qquad (5)$$

$$(0,4,0) \rightleftharpoons (0,0,1) \qquad (6)$$

where step (5) is representative of $\nu_1\nu_2$ coupling, and step (6) is representative of $\nu_3\nu_2$ coupling. The intramode relaxation in ν_2 (steps 2,3,4) is practically instantaneous. Furthermore $\nu_2 \rightleftharpoons \nu_1$ is practically instantaneous, so that at those low temperatures where ν_3 is inaccessible to thermal experiments, it is sufficient to consider simply steps (1), (2), (5), with the $(0,0,0) \rightleftharpoons \nu_2$ process being rate-determining.

For experiments where ν_3 is accessible there are 2 possible interpretations:

1) Step (6) i.e. $\nu_2 \rightleftharpoons \nu_3$ is rate-determining at low temperatures. In order to account for the high temperature

acceleration, a new route to (0,0,1) must be postulated, which becomes more important at high temperatures. Furthermore, constrained by the experimental observation that at T>1300 K $P\tau_{\nu_1\nu_2\nu_3} < P\tau$, this new route must completely avoid the route $(0,0,0) \rightleftharpoons (0,1,0)$ at least beyond a critical incubation time otherwise the relatively slow $(0,0,0) \rightleftharpoons (0,1,0)$ process would be rate determining. The fast V-V process

$$(1,0,0)+(0,0,0) \longrightarrow (0,2,0)+(0,1,0) \quad \Delta E = 479 \text{ cm}^{-1} \qquad (7)$$

followed by the fast step (5) has the same effect as step (1). However the V-V process is faster overall (in our model it is about twice as fast at 750 K). The higher the temperature, the greater the concentrations of states such as (1,0,0) at equilibrium. Therefore in shock tube experiments when concentrations increase with time, we expect an autocatalytic production of (0,1,0), and therefore of (0,2,0). Finally, the V-V step

$$(0,2,0) + (0,1,0) \longrightarrow (0,0,1) + (0,0,0) \qquad (8)$$

completes the mechanism. Step (7) followed by Step (8) is equivalent to the effective route $(1,0,0) \longrightarrow (0,0,1)$ which would normally not be considered as important because of the high endothermicity. However, the new V-V processes break up this high-energy route into two relatively low energy routes which can compete with step (6), and also overcome a potential bottleneck at step (1). As long as step (7) is faster than step (1), it will also be faster than step (6), according to this interpretation.

2/ Alternatively, $\nu_2 \rightleftharpoons \nu_3$ is very fast. All steps (2)-(6) are

at pre-equilibrium, and the rate is determined by step (1) i.e. $(0,0,0) \rightleftharpoons \nu_2$. In order to account for the high-temperature acceleration, the same V-V process, step (7) can be postulated as in the first interpretation. Since the bottleneck step (1) is avoided in this way, the autocatalysis proceeds at a rate determined by step (7) and (8).

In our present study we used the numerical simulations only to learn about the properties of the relaxation system in general. We varied the parameters over a wide range. In fig. 5.13 the choice of parameters was such that the autocatalytic effect appeared at ~600 K compared with ~280 K experimentally. We are gratified that our model reproduces the experimental results qualitatively without having to make the unpalatable proposal that steps such as step (6) could be rate-determining. However, it would be useful to have additional experimental checks on our parameters in order to enable us to use our model for predictive purposes, not only for N_2O but possibly also for other systems.

Summarizing, we have been able to categorize all results into two groups, according to whether $P\tau'\nu_1\nu_2$ or $P\tau'\nu_1\nu_2\nu_3$ was measured. We have identified $P\tau'\nu_1\nu_2$ with k_{10}, and $P\tau'\nu_1\nu_2\nu_3$ with a competition between steps (1) and (7). This interpretation is consistent with our numerical simulation of the relaxation mechanism, which additionally predicts correctly that at "low" temperatures $P\tau'$ increases with time, while at "high" temperatures it decreases with time. In general, we have therefore shown both experimentally and theoretically that the

phenomenological relaxation time is not a constant and that its value, even close to equilibrium, is not simply related to a V-T rate coefficient but also contains significant V-V character. Our calculations show and our experiments are consistent with the interpretation that the high energy levels involved (directly excited by laser or indirectly by thermal means after an incubation time) allow for the circumvention of the bottleneck step (1).

5.3.2 C_2H_2

There are few experimental results with which we can compare our own. Overall, our $P\tau'$ agree in magnitude and temperature dependence with acoustic measurements (71-73,74). Only single dispersions were noted by Lambert and Salter (72); however, Edmonds and Lamb did note an unusual pressure dependence at low frequencies (71) in their absorption measurements. Hager et al (75,76) measured the relaxation of the ν_2 and ν_3 mode. They found that the ν_2 mode relaxes in 650 collisions; whereas $\nu_5 \longrightarrow$ ground takes 1100 collisions (table 1.2, section 1.4). In view of the fact that (according to their interpretation, $\nu_2 \longrightarrow \nu_5$) a 1239 cm^{-1} energy gap is involved for ν_2 relaxation, whereas only 703 cm^{-1} is involved for ν_5 relaxation, plus the fact that ν_2 relaxation involves a transformation of stretching to combinations and harmonics of bending vibrations, then this is indeed an unexpected result, as they rightly stated. It seems more reasonable that the similarity of ν_2 and ν_5 relaxation times is an indication that ν_2 merely tracks ν_5; i.e. if $\nu_2 \rightleftharpoons \nu_5$ equilibration were instantaneous, bottlenecking at $\nu_5 \rightleftharpoons 0$ would

make both ν_2 and ν_5 relax at similar rates near equilibrium. We have noted in our simulation of laser experiments that regardless of the complex nature of the ensemble of a vast number of transition probabilities, the various modes of e.g. N_2O eventually relax at similar rates, with the only modifying factor possibly being the degree of perturbation. In view of our present observations that PT can increase by factors of 2 or 3 over a large time regime and Hager's observations that the ν_2 mode was more perturbed (1%) than the ν_5 mode (0.05%), the laser experiments are in perfect accord with our interpretation. It is unfortunate that the observed cooling in the laser experiments (which is not present in our own experiments) tend to mask the intrinsic deceleration which our calculations predict should also occur. Since our experiments were performed at higher temperatures further comparison is unwarranted. Therefore, it would be interesting if the laser experiments could be extended to cover a large dynamic range of time and to higher temperatures. Since the C_2H_2 laser operates on the $\nu_2 \longrightarrow \nu_5$ transition (75,76) additional experiments would be desirable for its optimization.

5.3.3 Linear mixture rule

The validity of the mixture rule was discussed in detail in section 1.5. Briefly, it is known that the linear mixture rule is obeyed under very restricted conditions. We believe that non linearity is the rule and cases where the linear mixture rule is obeyed are rather exceptional cases. If in the majority of the reported data, the linear mixture rule seems to be obeyed within

experimental error, probably with more accurate measurements, a deviation from linearity would be detected. Moreover, measurements are generally not carried out at low enough mole fraction or high enough temperature where the deviation from linearity is very important so that even if curves representing $1/P\tau'$ vs X seem to be linear, this does not mean that the linear mixture rule is obeyed. All theoretical treatments confirm this conclusion (see section 1.5). It has been shown that whether the vibrational relaxation time is calculated by the SSH-Tanczos theory (84-86) or by solving the detailed master equation (29,78), the linear mixture rule breaks down. Moreover some early experimental data show an apparent non-linear mixture rule (50,83,102-105). Our experimental results strongly support this conclusion. Our results are expected for two reasons: first of all, most of our measurements were carried out during the early stages of relaxation, long before equilibrium was reached. As was pointed out by Schlag and Valance (79), at this stage of relaxation the linear mixture rule breaks down. As we approach equilibrium, the maximum which appears in our curves decreases and the mixture rule approaches a linear one. In ref (78) it was shown for diatomics that when intermolecular intramode V-V process are important mixture rule curves exhibit a maximum at low mole fraction. Those theoretical curves (fig. 1.12, section 1.5) are similar to ours. This suggests to us that the maximum which appears in our experimental curves is genuine and is due to the intermolecular intramode V-V processes which are important at the beginning of the relaxation (small Zt) and which become less

important as the relaxation approaches equilibrium (i.e. at high Zt). Under conditions of low mole fraction of relaxer, intermolecular intramode V-V processes become less important and $1/P\tau'$ approaches a value determined by the relatively slower V-T processes, in agreement with our observation of a rapid decrease in plots of $(P\tau')^{-1}$ vs X. The second mechanistic reason for the failure of the linear mixture rule in our study is that we are dealing with polyatomic molecules where several vibrational modes share the energy and therefore several vibrational relaxation routes are possible. This means that the rate law for the vibrational relaxation of polyatomic molecules is very complicated. Intermolecular intermode V-V processes cannot be avoided any more than the intramode ones except at the lowest mole fractions. However, unlike intramode processes, intermode V-V processes actually become more important closer to equilibrium, so that even though mixture rule plots become more linear, they also go futher away from the straight line expected for pure V-T processes (see fig. 4.20, or 4.21 section 4.5).

Conclusion

Several conclusions can be deduced from our experimental and numerical data as well as from the literature data:

1: Vibrational relaxation times are usually not constant. They depend on the regime of relaxation (i.e. on t/τ, or Zt (the collision number). In order to compare the relaxation times of a given molecule measured by several authors using different techniques or even the same technique, the regime of relaxation under which the relaxation time was measured must be specified otherwise the results would be irreconcilable. This information has always tended to be ignored because it has always been thought that the rate of vibrational relaxation of diatomic molecules and even of polyatomic molecules follows the Bethe-Teller law. This is true for diatomic molecules under very limited conditions, but not at all for polyatomic molecules. Therfore, we strongly suggest that for any measurement of the vibrational relaxation time, the regime of the relaxation should be specified along with the temperature and initial degree of excitation.

2: We mentioned in the introduction several examples where the linear mixture rule was used in order to extract limiting rate constants at mole fraction = 0 and 1. Since it has been found theoretically and experimentally that the linear mixture rule is generaly not valid and the deviation is always positive, we believe that data extracted by linear extrapolation to the limits of the mole fraction range are probably incorrect and that this kind of extrapolation should be avoided.

3. Since this is the first time a systematic study of the time dependence and the mole faction dependence of the vibrational relaxation times of polyatomic molecules was carried out, we believe that much more work (experimental and theoretical) is needed in order to understand the relaxation properties of polyatomic molecules as well as the linear mixture rule, i.e. more polyatomic molecules should be studied in order to check for generality. Molecules with large vibrational relaxation times are preferred especially at high temperatures. They allow for more accurate determination of the dependance on the regime of relaxation and on temperature. The regime of relaxation should be extended in order to reach equilibrium. This could be achieved by using higher test gas pressures in a newly designed shock tube (e.g. longer test section and stronger diaphragm). By doing so a complete picture of the relaxation can be obtained (starting from the beginning of the relaxation and ending at equilibrium). The same study should be repeated with diatomic molecules (i.e. measuring the vibrational relaxation time at the beginning of the relaxation) in order to compare its behaviour with that of polyatomic molecules. Finally, the computer simulation should be continued by varying the vibrational relaxation parameters in order to obtain better agreement between the experimental and calculated relaxation times. This will lead to better determination of the vibrational relaxation parameters. The values of λ, γ, ϕ etc. are practically unknown at present.

Claims to original research

1) A shock-tube - laser-Schlieren system was constructed allowing for fast sensitive measurements of density gradients in high temperature gases.

2) Two new features of vibrational relaxation of polyatomic molecules were reported for the first time.

a) Vibrational relaxation time of some polyatomic molecules are not constant and therefore cannot be described in terms of decay via the lowest vibrational mode. The vibrational relaxation time of N_2O and of C_2H_2 increases with the number of collisions suffered in the low temperature regime and for N_2O decreases with the number of collisions suffered in the high temperature regime.

b) The linear mixture rule is not obeyed: a plot of the reciprocal of the standard vibrational relaxation time vs mole fraction exhibits a maximum at low mole fraction. The amplitude of the maximum decreases as the relaxation approaches equilibrium.

3) An extensive mechanism (comprising about 20 000 separate energy transfer processes) was modeled to describe the relaxation. The associated differential equations were solved numerically for the first time. The solution gave important information concerning the observable energy relaxation rate.

4) It was shown conclusively and for the first time that intermolecular energy transfer processes are responsible for

a) the non-constancy of the vibrational relaxation time and

b) the breakdown of the linear mixture rule.

5) The literature results are classified according to closeness to equilibrium. This classification explains for the first time, the many descrepancies evident in the literature.

Appendix A: Tables

Table A.1 Experimental results for the vibrational relaxation of pure N_2O.

P_o	P_D	U_o	T_e	t_{min} & t_{max}		τ^*	$P\tau$	Zt
torr	torr	mm/μsec.	K	μsec.		μsec.	μsec.atm.	
16.7	119	0.569	451	5.48	7.89	1.42	0.760	3703
25.8	216	0.616	478	3.07	4.37	0.601	0.690	3632
18.3	207	0.669	512	2.76	4.30	0.735	0.82	2818
19.4	211	0.681	519	2.80	3.75	0.588	0.746	2836
10.9	138	0.689	525	2.97	4.48	0.614	0.452	1856
7.69	139	0.730	555	3.25	5.34	0.889	0.570	1651
10.9	189	0.772	584	2.51	4.07	0.663	0.720	1954
4.47	131	0.858	649	2.57	4.22	0.719	0.460	975
4.63	144	0.859	649	2.62	3.74	0.644	0.424	949
4.00	237	0.882	664	2.67	3.53	0.560	0.361	832
4.47	187	0.880	664	2.62	4.00	0.741	0.515	990
6.28	211	0.918	696	2.27	3.06	0.359	0.404	1195
3.81	200	0.940	711	2.14	3.18	0.460	0.336	748
4.24	194	0.977	746	2.12	2.96	0.491	0.457	841
7.50	265	0.978	749	1.85	2.37	0.320	0.526	1239
6.59	355	1.000	761	1.76	2.22	0.340	0.511	1067
3.92	200	1.000	764	1.92	3.14	0.481	0.448	810
4.15	213	1.018	779	1.78	3.09	0.533	0.554	842
6.05	388	1.030	788	1.74	2.71	0.635	1.00	1137
5.42	282	1.055	809	1.88	2.91	0.415	0.628	1142
4.95	541	1.060	814	1.58	2.44	0.420	0.580	881
2.00	146	1.066	820	2.04	3.45	0.663	0.385	487
5.65	313	1.077	826	1.67	2.40	0.436	0.740	1045
5.57	300	1.074	829	1.99	2.47	0.283	0.469	1115
0.68	379	1.085	835	2.20	2.84	0.512	0.105	155
2.90	235	1.081	835	1.93	3.10	0.630	0.552	659
6.50	381	1.110	858	1.63	2.41	0.491	1.05	1239
5.42	367	1.115	867	1.63	2.50	0.512	0.915	1084
5.89	385	1.122	867	1.72	2.50	0.440	0.855	1197
0.680	283	1.118	876	1.82	2.33	0.415	0.096	134
5.73	510	1.133	879	1.56	2.42	0.506	1.00	1112
5.57	435	1.157	906	1.46	3.06	0.614	1.25	1262
0.680	335	1.160	909	1.65	2.68	0.478	0.122	147
1.10	146	1.172	911	1.86	3.69	0.753	0.315	310
3.77	304	1.167	915	1.52	2.30	0.900	0.747	726
"	"	"	"	2.50	3.20	0.518	1.299	1089
3.81	324	1.171	915	1.43	2.22	0.357	0.523	708
3.89	330	1.195	941	1.58	2.27	0.344	0.550	783
2.16	240	1.213	948	1.89	2.67	0.427	0.394	529
5.10	486	1.208	950	1.47	3.11	0.512	1.08	972
0.510	179	1.216	962	1.96	3.52	0.823	0.181	147
4.77	453	1.220	965	1.42	3.06	0.512	1.04	1150
2.98	305	1.234	976	1.68	3.39	0.320	0.432	650
3.06	350	1.248	991	1.30	2.26	0.333	0.478	609
0.646	251	1.288	1036	1.76	2.63	0.409	0.147	164

Table A.1 Continued

P_o	P_D	U_o	T_e	t_{min} & t_{max}		τ^*	$P\tau'$	z_t
torr	torr	mm/μsec.	K	μsec.		μsec.	μsec.atm.	
1.18	191	1.301	1041	1.65	2.84	0.600	0.367	311
0.612	120	1.310	1053	1.78	3.76	0.790	0.274	199
0.612	119	1.320	1066	1.38	3.29	0.968	0.322	168
0.646	414	1.327	1077	1.95	2.65	0.451	0.164	179
1.02	212	1.362	1106	1.56	2.52	0.476	0.289	261
0.353	124	1.471	1230	1.08	2.82	1.13	0.305	93
0.646	342	1.482	1246	1.72	2.31	0.385	0.195	183
0.628	202	1.506	1266	1.31	2.44	0.542	0.286	167
0.544	194	1.518	1286	1.58	2.42	0.549	0.255	159
0.942	346	1.524	1292	1.19	2.04	0.279	0.225	223
0.416	216	1.527	1296	1.15	2.32	0.937	0.333	102
0.550	198	1.557	1317	1.65	2.60	0.659	0.32	175
0.392	194	1.557	1330	1.22	2.32	0.596	0.213	102
0.707	320	1.628	1411	1.17	2.02	0.367	0.265	180
0.612	325	1.648	1444	1.29	1.77	0.350	0.226	152
0.646		1.780	1610	1.36	2.06	0.289	0.250	198
0.612	455	1.784	1610	1.16	1.75	0.294	0.234	160
0.646	527	1.791	1627	1.23	1.71	0.224	0.213	171
0.680	468	1.799	1634	1.22	1.70	0.290	0.261	180
0.612	549	1.803	1643	1.47	1.90	0.309	0.250	188
0.314	314	1.844	1685	1.29	2.36	0.659	0.290	107
0.544	570	1.850	1708	0.99	1.37	0.331	0.256	120
0.544	550	1.875	1743	1.11	1.64	0.285	0.238	143
0.612	580	1.884	1752	1.04	1.42	0.267	0.245	145
0.680	703	1.883	1755	1.09	1.59	0.244	0.195	176
0.157	351	1.987	1893	0.97	2.19	0.732	0.204	49

Table A.2 Experimental results for the vibrational relaxation of pure C_2H_2.

P_o	P_D	U_o	T_e	t_{min} & t_{max}		τ^*	$P\tau'$	Zt
torr	torr	mm/μsec.	K	μsec.		μsec.	μsec.atm.	
0.612	92	1.146	613	1.74	2.59	0.341	0.0411	142
0.476	98	1.185	634	1.28	1.89	0.388	0.0426	88
1.18	116	1.206	642	1.43	1.90	0.327	0.0940	238
0.471	92	1.209	642	1.52	2.36	0.392	0.0455	109
1.02	94	1.256	666	1.33	2.03	0.448	0.127	219
0.628	101	1.254	669	1.42	2.15	0.302	0.0525	143
1.14	105	1.278	681	1.44	1.88	0.438	0.148	250
1.18	101	1.284	684	1.59	1.90	0.222	0.0785	274
1.02	94	1.296	693	1.63	1.81	0.244	0.0767	237
0.903	92	1.301	696	1.31	1.87	0.300	0.0850	194
0.903	92	1.322	705	1.42	1.96	0.266	0.0790	211
0.612	111	1.319	707	1.68	1.95	0.285	0.0590	158
0.628	90	1.322	708	1.28	1.84	0.309	0.0641	136
0.581	120	1.332	713	1.55	2.03	0.296	0.0588	148
0.550	87	1.374	726	1.33	1.83	0.286	0.0592	128
0.785	94	1.366	729	1.22	1.62	0.301	0.0870	162
0.785	111	1.369	731	1.21	1.69	0.292	0.0858	166
0.92	120	1.362	731	1.51	2.17	0.335	0.112	246
0.864	105	1.368	731	1.23	1.63	0.337	0.108	180
0.785	103	1.382	737	1.29	1.70	0.231	0.0689	174
0.746	92	1.377	737	1.33	1.73	0.270	0.0766	168
0.762	92	1.379	740	1.34	1.71	0.240	0.0698	172
0.471	92	1.397	740	1.54	1.80	0.329	0.0616	118
0.707	101	1.406	749	1.14	1.55	0.273	0.0781	144
0.455	98	1.412	752	1.38	1.95	0.293	0.0546	115
0.589	92	1.412	752	1.29	1.74	0.310	0.0746	136
0.393	125	1.410	755	1.42	1.78	0.275	0.0442	95
"	"	"	"	1.78	2.04	0.328	0.0527	114
0.628	101	1.408	755	1.24	1.47	0.270	0.0697	128
0.430	92	1.408	755	1.45	1.80	0.286	0.0508	105
0.612	92	1.424	761	1.16	1.67	0.250	0.646	134
0.628	98	1.422	761	1.30	1.66	0.347	0.0914	143
0.628	103	1.427	764	1.34	1.59	0.275	0.0739	142
0.628	114	1.445	770	1.15	2.00	0.289	0.0803	157
0.589	103	1.440	770	1.14	1.63	0.258	0.0663	128
0.550	92	1.437	770	1.28	1.79	0.246	0.0591	132
0.353	87	1.430	770	1.36	2.05	0.384	0.0578	92
0.628	92	1.434	772	1.31	1.64	0.293	0.0797	144
0.628	98	1.445	773	1.17	1.73	0.208	0.0578	144
0.353	92	1.457	782	1.06	1.85	0.311	0.0503	82
0.432	90	1.468	793	1.26	1.83	0.280	0.0567	107
0.476	92	1.467	796	1.15	1.77	0.236	0.0527	112
0.432	92	1.486	802	1.26	1.67	0.282	0.0592	104
0.392	96	1.494	796	1.19	1.75	0.274	0.0531	96

Table A.2 Continued

P_o	P_D	U_o	T_e	t_{min} & t_{max}		τ^*	$P\tau'$	Zt
torr	torr	mm/μsec.	K	μsec.		μsec.	μsec.atm.	
0.408	90	1.528	826	1.12	1.93	0.295	0.0645	107
0.573	142	1.528	829	1.34	2.29	0.454	0.139	178
0.314	92	1.525	829	1.34	1.99	0.391	0.0653	89
0.476	105	1.516	826	1.24	1.70	0.248	0.0616	119
0.204	89	1.519	829	1.05	1.91	0.375	0.0400	50
0.471	111	1.522	829	1.39	1.89	0.188	0.0616	132
0.314	103	1.541	835	1.04	1.85	0.366	0.0633	78
0.329	101	1.542	838	1.18	1.80	0.316	0.0574	84
0.338	101	1.553	844	1.12	1.74	0.283	0.0555	86
0.442	168	1.555	846	1.31	1.71	0.242	0.0602	117
0.353	103	1.565	855	1.12	1.56	0.284	0.0584	83
0.694	101	1.565	855	1.35	1.86	0.181	0.0727	197
0.314	96	1.577	866	1.35	1.63	0.333	0.0627	84
0.544	151	1.575	864	1.36	1.66	0.171	0.0554	147
0.550	146	1.585	867	1.08	1.37	0.168	0.0560	122
0.298	101	1.597	879	1.29	1.62	0.314	0.0586	79
0.377	149	1.653	912	1.21	1.62	0.235	0.0618	102
0.680	184	1.650	915	1.09	1.42	0.203	0.0955	163
0.510	166	1.664	923	1.21	1.41	0.235	0.0850	130
0.235	116	1.674	926	0.89	1.53	0.306	0.0522	55
0.251	134	1.680	932	1.09	1.26	0.214	0.0394	57
"	"	"	"	1.37	1.67	0.280	0.0515	75
0.550	240	1.724	965	1.17	1.27	0.145	0.0636	137
0.306	148	1.752	983	1.07	1.55	0.219	0.0504	75
0.471	360	1.785	1000	0.97	1.40	0.141	0.0588	120
0.628	310	1.790	1003	0.88	0.98	0.087	0.0491	127
0.455	249	1.830	1032	0.94	1.18	0.160	0.0699	109
0.707	140	1.850	1051	1.35	1.64	0.250	0.176	238
0.272	175	1.871	1063	0.98	1.51	0.210	0.0586	77
0.374	322	1.933	1096	0.89	1.08	0.137	0.0581	89
0.314	249	1.926	1098	0.10	1.50	0.193	0.0685	93
0.235	258	1.928	1101	0.93	1.23	0.164	0.0436	60
0.510	415	1.940	1110	0.89	0.99	0.164	0.0962	115
0.353	323	1.976	1134	1.01	1.40	0.174	0.0752	105
0.272	286	1.990	1140	1.14	1.40	0.153	0.0521	86
0.314	330	1.993	1144	0.91	1.26	0.150	0.0595	86
0.365	341	1.999	1148	0.99	1.19	0.185	0.0860	100
0.338	378	2.033	1175	0.82	1.13	0.168	0.0760	85
0.314	323	2.042	1184	0.82	1.24	0.175	0.079	84

Table A.3. Experimental results for the vibrational relaxation of 50.5% C_2H_2-Ar mixture.

P_o	P_D	U_o	T_e	t_{min} & t_{max}		τ^*	$P\tau$	zt
torr	torr	mm/μsec	K	μsec		μsec	μsec·atm	
0.879		0.929	659	2.19	2.34	0.184	0.0156	148
0.510		1.028	739	1.79	3.08	0.523	0.0359	106
1.73		1.100	798	1.60	2.00	0.292	0.0841	296
1.02		1.160	848	1.55	2.12	0.342	0.0683	192
1.04		1.170	860	1.72	2.18	0.360	0.0616	211
1.20		1.185	872	1.48	2.31	0.313	0.0788	241
0.644		1.255	934	1.49	1.85	0.169	0.0272	124
0.793		1.273	951	1.50	1.99	0.304	0.0629	162
0.785		1.288	969	1.53	1.95	0.300	0.0642	163
0.982		1.302	978	1.64	2.00	0.314	0.0863	217
0.565		1.307	984	1.52	2.13	0.323	0.0519	125
1.18		1.344	1019	1.47	1.87	0.242	0.0884	251
0.550		1.355	1031	1.55	2.20	0.304	0.0532	132
0.589		1.376	1049	1.35	2.21	0.333	0.0655	136
0.628		1.380	1055	1.31	2.07	0.355	0.0751	138
0.612		1.387	1064	1.45	1.86	0.336	0.700	133
0.462		1.388	1064	1.24	2.41	0.572	0.0908	110
0.471		1.395	1067	1.55	2.01	0.342	0.0561	111
0.62		1.392	1076	1.29	2.04	0.314	0.0688	138
0.448		1.402	1079	1.28	2.19	0.410	0.0649	103
1.14		1.402	1079	1.33	1.65	0.208	0.0841	229
0.864		1.412	1084	1.46	2.28	0.266	0.0836	220
1.141		1.416	1090	1.39	1.70	0.255	0.106	241
0.510		1.422	1093	1.25	1.94	0.287	0.0543	111
0.443		1.422	1093	1.17	1.77	0.400	0.0661	89
0.683		1.426	1099	1.36	1.85	0.262	0.0669	151
0.628	95	1.465	1141	1.23	1.55	0.274	0.0698	125
0.746	90	1.467	1141	1.39	1.84	0.225	0.0685	173
0.526		1.447	1123	1.24	1.89	0.333	0.0686	114
0.785	90	1.477	1155	1.25	1.75	0.222	0.0728	171
0.903		1.500	1182	1.23	1.69	0.222	0.0879	195
0.824	90	1.522	1203	1.15	1.66	0.206	0.0778	174
0.516	130	1.554	1241	1.31	1.85	0.262	0.0653	125
0.487		1.553	1241	1.27	1.60	0.300	0.0710	109
"		"	"	1.67	1.91	0.390	0.0930	135
0.392		1.557	1241	1.16	1.61	0.290	0.0565	82
0.628	123	1.560	1244	1.20	1.55	0.240	0.0744	135
1.26		1.564	1250	1.33	1.69	0.221	0.138	300
0.589		1.596	1280	1.36	1.83	0.289	0.0897	151
0.942	170	1.609	1300	0.58	0.79	0.129	0.0661	106
0.683	130	1.616	1303	1.27	1.42	0.195	0.0730	152
"	"	"	"	1.45	1.67	0.311	0.116	175
0.824		1.657	1350	1.09	1.49	0.181	0.0877	181
0.330		1.662	1359	1.05	1.67	0.323	0.0636	75

Table A.3 Continued

P_o	P_D	U_o	T_e	t_{min} & t_{max}		τ^*	$P\tau'$	Zt
torr	torr	mm/μsec.	K	μsec.		μsec.	μsec.atm.	
0.942		1.685	1380	1.23	1.63	0.273	0.159	234
0.330		1.692	1389	1.26	1.59	0.187	0.0387	82
0.549		1.705	1404	1.08	1.44	0.244	0.0859	120
0.785	130	1.711	1410	1.09	1.36	0.203	0.103	170
0.448		1.711	1410	1.04	1.45	0.233	0.0675	98
0.510		1.776	1477	1.11	1.53	0.260	0.0947	124
0.707		1.810	1525	1.09	1.28	0.155	0.0833	160
0.440		1.839	1563	1.05	1.59	0.191	0.0672	113
0.550		1.846	1569	1.07	1.37	0.178	0.0790	131
0.393		1.844	1569	1.09	1.53	0.208	0.0658	100
0.353		1.864	1596	1.02	1.41	0.228	0.0670	84

Table A.4 Experimental results for vibrational relaxation of 23.61% C_2H_2-Ar mixture.

P_o	P_D	U_o	T_e	t_{min} & t_{max}		τ^*	$P\tau'$	Zt
torr	torr	mm/μsec.	K	μsec.		μsec.	μsec.atm.	
2.43		1.044	926	1.56	2.19	0.411	0.103	351
2.12		1.050	944	1.63	1.81	0.383	0.0872	285
"		"	"	1.81	2.21	0.441	0.100	335
1.53		1.127	1035	1.51	2.24	0.425	0.0854	246
1.02		1.197	1124	1.35	1.69	0.415	0.0661	141
"		"	"	1.69	2.20	0.520	0.0828	184
1.18		1.240	1180	1.44	1.62	0.362	0.0740	175
"		"	"	1.62	1.77	0.421	0.0860	195
"		"	"	1.77	2.05	0.571	0.116	221
0.903		1.260	1209	1.42	1.59	0.362	0.0595	135
"		"	"	1.59	1.86	0.428	0.0700	155
"		"	"	1.86	2.17	0.484	0.0790	182
0.942		1.269	1221	1.31	2.05	0.374	0.0653	158
0.903		1.283	1239	1.42	1.64	0.464	0.0800	138
"		"	"	1.64	1.92	0.548	0.0940	162
"		"	"	1.92	2.19	0.680	0.120	188
0.746		1.314	1283	1.17	2.01	0.364	0.0556	124
0.674		1.341	1322	1.32	1.51	0.354	0.0512	101
"		"	"	1.51	1.95	0.451	0.0654	125
0.612		1.358	1348	1.24	1.66	0.428	0.0590	96
"		"	"	1.66	2.29	0.650	0.0900	133
1.37		1.397	1407	1.23	1.95	0.324	0.108	250
0.589		1.399	1410	1.17	1.46	0.337	0.0486	85
"		"	"	1.46	1.98	0.440	0.0634	115
1.33		1.447	1481	1.15	1.93	0.362	0.130	248
0.824	95	1.452	1490	1.24	1.87	0.375	0.0838	153
0.942		1.481	1534	1.26	1.72	0.298	0.0804	172
0.785		1.503	1569	1.24	1.78	0.326	0.0761	148
0.785	95	1.508	1578	1.21	1.52	0.308	0.0725	134
"	"	"	"	1.52	1.90	0.392	0.0923	169
0.416		1.512	1584	1.04	1.38	0.360	0.0450	60
"		"	"	1.46	1.90	0.457	0.0574	85
0.903	105	1.519	1596	1.17	1.87	0.294	0.0824	174
0.589	93	1.550	1652	1.14	1.55	0.360	0.690	99
"	"	"	"	1.55	1.84	0.530	0.101	128
0.785		1.550	1652	1.20	1.95	0.340	0.0864	161
2.04	225	1.555	1655	1.24	1.47	0.250	0.167	363
0.609	95	1.573	1684	1.25	1.92	0.408	0.0841	128
0.455	95	1.583	1699	1.02	1.80	0.371	0.0581	82
0.510	90	1.587	1705	0.93	1.26	0.417	0.0737	70
"	"	"	"	1.26	1.47	0.480	0.0850	90
1.61		1.592	1714	1.10	1.45	0.262	0.147	279
1.29		1.612	1747	1.17	1.67	0.227	0.106	252
0.982		1.611	1747	1.14	1.65	0.274	0.0972	188
1.49	215	1.641	1796	1.15	1.53	0.192	0.109	282
1.06		1.649	1811	1.13	1.53	0.248	0.101	200

Table A.4 Continued

P_o	P_D	U_o	T_e	t_{min} & t_{max}		τ^*	$P\tau'$	z_t
torr	torr	mm/μsec.	K	μsec.		μsec.	μsec.atm.	
1.00		1.668	1844	1.23	1.53	0.240	0.0974	203
0.612	205	1.681	1873	1.08	1.79	0.271	0.0677	127
1.18	235	1.689	1880	1.26	1.66	0.220	0.107	253
0.785	190	1.718	1932	1.09	1.55	0.278	0.0938	153
0.667		1.720	1935	1.11	1.52	0.314	0.0903	128
0.475	150	1.746	1982	1.00	1.15	0.246	0.0520	73
"	"	"	"	1.15	1.41	0.303	0.0640	90
"	"	"	"	1.41	1.78	0.400	0.0840	114
0.644	190	1.749	1985	1.13	1.63	0.294	0.0853	134
0.628	190	1.752	1991	1.06	1.69	0.310	0.0883	131
0.667		1.757	2003	1.04	1.30	0.285	0.0869	117
"		"	"	1.37	1.67	0.354	0.108	155
0.667		1.793	2065	0.97	1.35	0.300	0.0966	120
0.605	215	1.798	2074	1.03	1.65	0.281	0.0826	127
0.597	212	1.835	2145	1.13	1.65	0.329	0.101	134
0.471	210	1.908	2295	0.86	1.62	0.294	0.0789	98
0.495	215	1.863	2201	0.93	1.55	0.343	0.0907	100

Table A.5 Experimental results for vibrational relaxation of 12.1% C_2H_2-Ar mixture.

P_o	P_D	U_o	T_e	t_{min} & t_{max}		τ^*	$P\tau'$	Zt
torr	torr	mm/μsec.	K	μsec.		μsec.	μsec.atm.	
4.98	116	0.919	888	2.01	2.51	0.388	0.112	666
4.79		0.935	912	1.92	2.53	0.560	0.163	646
4.16		0.968	956	1.93	2.54	0.414	0.115	592
2.63	98	1.000	999	1.84	2.13	0.733	0.141	344
2.83		1.010	1012	1.66	2.18	0.643	0.137	364
1.71	102	1.022	1029	1.65	2.34	0.586	0.0780	232
2.24	110	1.026	1033	1.66	2.43	0.700	0.124	313
2.59		1.032	1042	1.65	1.93	0.493	0.110	319
"	"	"	"	2.01	2.51	0.604	0.134	406
2.00	102	1.042	1054	1.61	2.50	0.640	0.105	285
1.61		1.152	1222	1.65	2.39	0.640	0.111	259
1.41	92	1.158	1233	1.75	2.36	0.644	0.0990	232
1.56	135	1.159	1236	1.98	2.46	0.600	0.0900	278
1.35	92	1.160	1236	1.85	2.54	0.687	0.102	238
1.33	102	1.197	1293	1.54	1.76	0.369	0.0640	181
"	"	"	"	1.93	2.71	0.622	0.110	259
1.22	102	1.211	1322	1.56	2.25	0.614	0.0930	196
2.51	185	1.231	1353	1.43	1.86	0.337	0.109	361
1.08	102	1.233	1358	1.63	2.30	0.600	0.0840	183
0.982		1.237	1362	1.29	1.53	0.320	0.041	118
"		"	"	1.58	2.20	0.600	0.0770	162
1.45	203	1.242	1373	1.74	2.28	0.633	0.121	255
1.02	96	1.272	1421	1.50	2.09	0.577	0.0833	165
2.00	185	1.290	1450	1.33	1.91	0.403	0.118	299
0.860		1.300	1468	1.43	2.27	0.582	0.0751	148
1.02	111	1.301	1471	1.38	2.25	0.778	0.119	170
1.62	176	1.303	1477	1.23	2.07	0.412	0.105	259
1.85	185	1.316	1498	1.30	2.06	0.350	0.0990	294
1.96	253	1.329	1524	1.47	1.83	0.311	0.0970	311
2.59	259	1.333	1530	1.39	1.87	0.341	0.141	383
2.75	268	1.336	1533	1.36	1.67	0.303	0.134	405
1.62	176	1.340	1545	1.20	1.77	0.392	0.103	233
1.53	176	1.354	1571	1.29	1.95	0.392	0.100	244
1.57	194	1.361	1581	1.40	1.87	0.486	0.129	253
1.61	277	1.378	1613	1.25	1.58	0.289	0.0810	227
0.820	185	1.377	1613	1.57	2.00	0.740	0.106	145
2.24		1.385	1625	1.25	1.71	0.254	0.100	336
1.34	181	1.389	1634	1.33	1.96	0.412	0.0980	223
3.26	379	1.405	1666	1.33	1.62	0.221	0.132	498
1.22	185	1.408	1669	1.30	1.74	0.380	0.0851	191
1.10	227	1.410	1672	1.20	1.67	0.289	0.0592	163
1.14	181	1.418	1687	1.32	2.03	0.467	0.0993	198
1.81		1.439	1726	1.19	1.50	0.267	0.0941	258
1.96	286	1.452	1752	1.23	1.44	0.333	0.131	282

Table A.5 Continued

P_o	P_D	U_o	T_e	t_{min} & t_{max}		τ^*	$P\tau'$	Z_t
torr	torr	mm/μsec.	K	μsec.		μsec.	μsec.atm.	
1.65	305	1.465	1776	1.21	1.49	0.291	0.0985	242
1.41	314	1.466	1779	1.10	1.86	0.308	0.089	227
1.65	268	1.471	1788	1.07	1.42	0.355	0.120	223
1.06	314	1.475	1800	1.18	1.70	0.312	0.0690	167
1.37	268	1.489	1823	1.12	1.53	0.290	0.0850	201
2.12	360	1.491	1826	1.12	1.49	0.270	0.123	308
0.824	185	1.515	1874	1.18	1.53	0.369	0.0679	124
1.96	351	1.514	1874	1.12	1.47	0.289	0.126	287
1.73	314	1.515	1874	1.08	1.52	0.338	0.130	254
0.860	198	1.516	1877	1.26	1.93	0.457	0.088	155
1.45		1.517	1879	1.14	1.64	0.317	0.103	228
0.722		1.522	1892	0.99	1.47	0.365	0.0605	99
1.10	261	1.558	1962	1.12	1.58	0.364	0.0961	173
1.10	360	1.561	1975	1.20	1.71	0.397	0.105	187
1.73	379	1.565	1981	1.06	1.53	0.310	0.130	263
1.39	342	1.569	1989	1.02	1.55	0.286	0.0972	210
1.81	416	1.577	2007	1.02	1.59	0.282	0.126	280
1.81	425	1.578	2011	0.99	1.83	0.282	0.126	303
1.73	397	1.586	2025	1.16	1.61	0.262	0.114	286
1.02	286	1.589	2031	1.16	1.86	0.373	0.0961	184
1.41	370	1.604	2060	0.91	1.31	0.236	0.0863	189
1.26	166	1.617	2090	1.08	1.63	0.343	0.114	207
0.710	301	1.620	2096	1.27	1.78	0.431	0.0811	130
1.22	342	1.630	2120	1.84	1.65	0.386	0.127	213
1.18	351	1.640	2137	1.01	1.28	0.233	0.0751	168
1.57	480	1.641	2140	1.11	1.36	0.333	0.143	242
0.860	333	1.683	2236	1.04	1.64	0.446	0.112	146
1.08	410	1.704	2277	0.94	1.55	0.296	0.0961	175
0.903	397	1.720	2312	1.13	1.82	0.365	0.101	175
0.667	333	1.748	2374	1.14	1.72	0.507	0.109	127
0.691	407	1.798	2489	1.03	1.42	0.333	0.0796	115
1.34	869	1.830	2566	1.11	1.39	0.371	0.178	237
0.630	481	1.866	2657	1.09	1.56	0.396	0.0945	120

Table A.6 Experimental results for vibrational relaxation of 5.0% C_2H_2-Ar mixture.

P_o	P_D	U_o	T_e	t_{min} & t_{max}		τ^*	$P\tau$	zt
torr	torr	mm/μsec.	K	μsec.		μsec.	μsec.atm.	
9.42	124	0.789	771	2.10	2.56	0.364	0.104	991
6.36		0.880	895	2.02	2.97	0.353	0.0921	828
4.79		0.939	984	1.96	2.88	0.390	0.0923	659
2.20		1.010	1096	1.69	2.10	0.607	0.0802	261
4.55		1.016	1105	1.79	2.77	0.427	0.119	657
3.18		1.017	1108	1.72	2.13	0.575	0.112	386
2.43		1.056	1173	1.54	2.42	0.538	0.0891	320
3.85		1.085	1226	1.69	2.52	0.414	0.116	556
4.12		1.118	1285	1.68	2.70	0.422	0.137	644
4.83	204	1.118	1285	1.67	2.13	0.443	0.168	653
2.75	130	1.120	1288	1.65	2.39	0.560	0.122	398
2.20		1.123	1294	1.46	1.75	0.362	0.0636	253
2.16	122	1.135	1315	1.55	2.29	0.600	0.106	302
2.00	111	1.136	1318	1.61	2.15	0.600	0.117	325
3.81		1.156	1353	1.58	2.34	0.373	0.122	557
1.65		1.175	1389	1.47	2.17	0.420	0.0628	228
2.51	178	1.175	1389	1.52	2.55	0.527	0.119	389
1.57	120	1.186	1407	1.25	1.50	0.187	0.0272	166
"	"	"	"	1.50	2.14	0.583	0.0841	219
1.73		1.190	1415	1.49	1.78	0.300	0.0485	218
3.30		1.190	1415	1.43	2.06	0.333	0.101	444
2.28	155	1.203	1439	1.59	2.14	0.500	0.108	332
2.12	139	1.204	1442	1.44	2.09	0.385	0.0781	293
3.22		1.207	1448	1.50	1.85	0.343	0.106	422
2.89	194	1.232	1495	1.47	2.10	0.431	0.124	412
2.20		1.233	1498	1.44	2.44	0.381	0.0846	343
1.30		1.236	1504	1.27	1.58	0.240	0.0315	149
"		"	"	1.81	2.18	0.615	0.0817	209
1.37		1.239	1510	1.36	1.64	0.292	0.0412	167
"		"	"	1.64	2.21	0.862	0.121	215
3.02	231	1.267	1566	1.44	1.97	0.352	0.114	429
2.39		1.277	1587	1.37	1.93	0.431	0.114	332
3.26	250	1.279	1593	1.38	2.37	0.410	0.148	515
3.85	278	1.281	1596	1.37	1.81	0.501	0.214	517
1.41	150	1.286	1604	1.47	1.83	0.620	0.0984	199
2.04		1.302	1640	1.53	1.86	0.475	0.112	298
3.10	278	1.306	1649	1.39	1.87	0.397	0.144	437
3.22		1.323	1684	1.33	1.77	0.415	0.159	438
2.89		1.327	1693	1.34	1.62	0.347	0.122	378
3.02	283	1.343	1726	1.33	1.96	0.388	0.147	444
1.63	190	1.376	1797	1.63	2.44	0.554	0.120	307
2.00	259	1.384	1826	1.45	1.90	0.567	0.134	312
2.75	314	1.396	1841	1.19	1.84	0.363	0.137	391
2.24	268	1.407	1864	1.34	1.83	0.486	0.151	336

Table A.6 Continued

P_o	P_D	U_o	T_e	t_{min} & t_{max}		τ^*	$P\tau'$	Zt
torr	torr	mm/μsec.	K	μsec.		μsec.	μsec.atm.	
2.12	278	1.420	1894	1.29	1.62	0.325	0.0991	296
2.12	283	1.447	1956	1.34	1.57	0.227	0.0722	303
3.30	416	1.448	1959	1.28	1.98	0.295	0.146	528
2.63		1.451	1965	1.37	1.77	0.275	0.109	405
1.61		1.474	2018	1.34	1.88	0.382	0.0966	260
2.65	394	1.475	2018	1.26	1.79	0.368	0.153	405
2.47	416	1.484	2039	1.15	2.19	0.417	0.165	417
2.83	486	1.532	2151	1.17	1.39	0.333	0.162	379
2.00		1.546	2184	1.22	1.58	0.461	0.163	297
1.29	342	1.563	2228	1.21	1.76	0.367	0.0853	205
2.06	427	1.571	2249	1.24	1.52	0.282	0.105	306
2.04	435	1.572	2252	1.21	2.02	0.306	0.114	355
1.18		1.580	2272	1.29	1.75	0.443	0.0962	195
1.96	431	1.582	2278	1.21	1.63	0.356	0.128	303
1.10	287	1.598	2322	0.67	0.92	0.385	0.0811	96
1.73	407	1.600	2328	1.12	1.49	0.291	0.0966	247
1.26	389	1.664	2488	1.19	1.59	0.309	0.0823	202

Table A.7 Experimental results for vibrational relaxation of 2.49% C_2H_2-Ar mixture.

P_o	P_D	U_o	T_e	t_{min} & t_{max}		τ^*	$P\tau'$	Zt
torr	torr	mm/μsec.	K	μsec.		μsec.	μsec.atm.	
2.04	111	1.121	1341	1.42	1.56	0.221	0.0322	210
1.96	111	1.133	1364	1.41	1.93	0.314	0.0453	229
1.84	124	1.152	1400	1.48	1.75	0.205	0.0289	213
1.87	129	1.165	1427	1.33	1.67	0.233	0.0343	203
1.59	120	1.203	1501	1.25	1.44	0.208	0.0281	161
"	"	"	"	1.44	2.04	0.388	0.0525	208
1.35	118	1.223	1539	1.48	1.86	0.347	0.0416	174
1.26	116	1.234	1563	1.36	1.72	0.235	0.0267	150
1.30	124	1.239	1575	1.42	1.65	0.217	0.0257	155
1.08		1.254	1604	1.30	1.54	0.233	0.0236	121
3.22	284	1.303	1702	1.38	2.29	0.393	0.131	490
2.81		1.342	1791	1.50	1.82	0.313	0.0974	401
2.52		1.397	1920	1.28	2.28	0.417	0.129	405
1.69	277	1.398	1923	1.35	1.62	0.202	0.0418	227
3.61	417	1.430	2004	1.31	1.61	0.263	0.123	491
1.85		1.441	2024	1.28	1.82	0.247	0.0600	268
1.69	277	1.470	2094	1.17	1.54	0.267	0.0621	219
2.88	472	1.491	2158	1.19	1.49	0.543	0.223	375
2.12	378	1.492	2158	1.25	1.57	0.313	0.0944	290
1.53	281	1.510	2195	1.17	1.57	0.236	0.0530	207
2.24	378	1.510	2201	1.17	1.78	0.237	0.0778	325
1.81	378	1.512	2201	1.30	1.81	0.327	0.0868	277
1.26	286	1.526	2239	1.28	1.60	0.277	0.0524	180
1.41	282	1.528	2245	1.39	1.62	0.316	0.0674	213
2.08	393	1.538	2272	1.09	1.36	0.255	0.0812	257
2.08	393	1.538	2272	1.36	1.70	0.410	0.131	321
2.47	526	1.552	2308	1.19	1.80	0.240	0.0928	375
2.26	437	1.552	2312	1.11	1.41	0.311	0.110	290
1.78	387	1.560	2332	1.15	1.43	0.282	0.0796	235
1.26		1.564	2333	1.16	1.41	0.213	0.0425	166
1.87	411	1.573	2364	1.06	1.61	0.197	0.0593	258
1.73	428	1.616	2480	1.09	1.43	0.221	0.0656	232
1.44	526	1.655	2583	1.20	1.85	0.400	0.105	241
1.49	471	1.668	2621	1.22	1.50	0.294	0.0813	225

Table A.8 Experimental results for vibrational relaxation of 1% C_2H_2-Ar mixture.

P_o	P_D	U_o	T_e	t_{min} & t_{max}		τ^*	$P\tau'$	Zt
torr	torr	mm/μsec.	K	μsec.		μsec.	μsec.atm.	
1.65	102	1.132	1386	1.35	1.98	0.364	0.0410	189
1.73	102	1.147	1418	1.44	1.56	0.222	0.0271	180
1.92		1.162	1449	1.41	1.65	0.186	0.0261	208
2.75	266	1.332	1817	1.39	2.16	0.560	0.156	407
3.42		1.340	1841	1.33	1.70	0.644	0.226	433
2.98		1.341	1841	1.24	1.73	0.400	0.123	371
2.08	289	1.346	1854	1.15	1.27	0.135	0.0292	212
"	"	"	"	1.27	1.51	0.277	0.0600	243
2.98		1.351	1866	1.40	1.98	0.304	0.0952	427
2.63	287	1.389	1959	1.18	1.33	0.271	0.0798	288
"	"	"	"	1.33	2.02	0.491	0.145	385
2.39	278	1.396	1974	1.09	1.25	0.127	0.0343	246
"	"	"	"	1.25	1.60	0.403	0.109	299
2.33		1.416	2027	1.28	1.53	0.231	0.0632	294
2.36		1.420	2039	1.18	1.57	0.275	0.0764	290
2.04		1.431	2064	1.28	1.73	0.341	0.0837	279
1.95		1.440	2086	1.21	1.44	0.187	0.0443	234
2.08	287	1.445	2094	1.08	1.34	0.293	0.0749	230
2.87	444	1.448	2109	1.30	1.62	0.333	0.118	384
2.03	287	1.450	2110	1.11	1.23	0.198	0.0495	218
"	"	"	"	1.30	1.91	0.406	0.102	299
1.98	287	1.464	2145	1.13	1.31	0.210	0.0526	224
"	"	"	"	1.31	1.87	0.433	0.108	293
2.49	370	1.475	2168	1.20	1.91	0.308	0.0985	363
1.73		1.483	2196	1.17	1.34	0.154	0.0346	204
2.75	438	1.502	2245	1.20	1.48	0.289	0.106	351
2.52	444	1.529	2304	1.07	1.87	0.475	0.166	361
2.12	413	1.550	2394	1.03	1.29	0.186	0.0564	241
1.26	296	1.560	2396	1.30	1.49	0.185	0.0341	176
1.36	278	1.564	2407	1.09	1.27	0.0905	0.0180	160
2.39	463	1.566	2436	1.04	1.40	0.163	0.0573	291
1.85	398	1.581	2480	1.14	1.32	0.173	0.0481	229
2.25	463	1.585	2489	1.02	1.48	0.261	0.0889	284
1.41	453	1.607	2518	1.00	1.27	0.194	0.0427	166
1.85	463	1.615	2546	1.03	1.41	0.178	0.0518	234
1.81	500	1.633	2597	1.03	1.26	0.173	0.0505	217
2.08	500	1.622	2593	1.05	1.27	0.188	0.0623	250
1.56	453	1.651	2645	1.12	1.51	0.292	0.0755	218

Table A.9 The reciprocal of vibrational relaxation time $(\mu sec.atm)^{-1}$ for C_2H_2-Ar mixtures as a function of % C_2H_2 and collisional number at T = 1000-1100 K.

Zt / % C_2H_2	50	100	150	200	250	300	350	400	450	T (K)	T (K)
100.0		13.3	8.62	6.62						1032-1184	1114 ±45
50.5		20.0	13.5	11.4	10.9					1019-1099	1069 ±23
23.6					12.3	10.9	9.71			926-1035	962 ±49
12.1					11.2	8.77	7.57			999-1054	1030 ±19
5.0					13.3	10.8	9.52	9.43		984-1108	1073 ±60

Table A.10 The Reciprocal of the vibrational relaxation time $(\mu sec.atm)^{-1}$ for C_2H_2-Ar mixtures as a function of % C_2H_2 and collisional number at T = 1200-1400 K.

Zt / % C_2H_2	50	100	150	200	250	300	350	400	450	T (K)	T (K)
50.5		15.9	11.5	9.00	7.35					1241-1596	1376 ±123
23.6		17.2	14.9	10.4						1124-1348	1234 ±70
12.1				13.1	9.80					1222-1293	1252 ±32
5.0				19.6	13.0	10.5	9.43	8.85	8.40	1285-1448	1368 ±61

Table A.11 The reciprocal of the vibrational relaxation times (μsec.atm)$^{-1}$ for C_2H_2-Ar mixtures as a function of % C_2H_2 and collisional number at T = 1300-1500 K.

% C_2H_2 \ Zt	50	100	150	200	250	300	350	400	450	T (K)	T (K)
50.5		15.9	11.5	9.00	7.35					1241-1596	1376 ±123
23.6	25.0	17.2	12.5	10.2	8.47					1407-1596	1471 ±65
12.1			14.5	10.0	8.92	8.85	8.85			1322-1477	1402 +57
5.0				19.6	13.0	10.52	9.43	8.85	8.40	1285-1448	1368 ±61
2.5			38.5	31.3	23.8	17.2	13.3			1341-1791	1526 +134

Table A.12 The reciprocal of the vibrational relaxation times (μsec.atm)$^{-1}$ for C_2H_2-Ar mixtures as a function of % C_2H_2 and collisional number at T = 1400-1600 K.

% C_2H_2 \ Zt	50	100	150	200	250	300	350	400	450	T (K)	T (K)
50.5		15.9	11.5	9.00	7.35					1241-1596	1376 ±123
23.6	25.0	17.2	12.5	10.2	8.47					1407-1596	1471 ±65
12.1			25	11.8	9.34	8.77	8.77			1498-1826	1662 ±105
5.0			33.3	13.5	10.3	9.26	8.47			1495-1604	1542 ±46
2.5			38.5	31.3	23.8	17.2	13.3			1341-1791	1526 ±134

Table A.13 The reciprocal of the vibrational relaxation times (μsec.atm)$^{-1}$ for C_2H_2-Ar mixtures as a function of % C_2H_2 and collisional number at T = 1600-1800 K.

% C_2H_2 \ Zt	50	100	150	200	250	300	350	400	450	T (K)	T (K)
23.6		13.3	10.3	8.77	8.00	7.41				1652-1747	1686 ±33
12.1			25.0	11.8	9.34	8.77	8.77			1498-1826	1662 ±105
5.0				11.0	9.09	7.87	7.19	6.80		1640-2488	2012 ±244
2.5			38.5	31.3	23.8	17.2	13.3			1341-1791	1526 ±134
1.0				31.3	18.9	12.8	9.43			1386-2039	1817 ±219

Table A.14 The reciprocal of the vibrational relaxation times (μsec.atm)$^{-1}$ for C_2H_2-Ar mixtures as a function of % C_2H_2 and collisional number at T = 1800-2000 K.

% C_2H_2 \ Zt	50	100	150	200	250	300	350	400	450	T (K)	T (K)
23.6		13.3	9.61							1932-2295	2029 ±99
12.1		18.2	12.6	10.2	8.69					1874-2060	1954 ±68
5.0				11.0	9.09	7.87	7.19	6.80		1640-2488	2012 ±244
2.5				27.8	19.6	14.3	11.5			1920-2024	1968 ±54
1.0				31.3	18.9	12.8	9.43			1386-2039	1817 ±219

Table A.15 The reciprocal of the vibrational relaxation times $(\mu sec.atm)^{-1}$ for C_2H_2-Ar mixtures as a function of % C_2H_2 and collisional number at T = 2000-2200 K.

% C_2H_2 \ Zt	50	100	150	200	250	300	350	400	450	T (K)	T (K)
23.6		13.3	9.61							1932-2295	2029 ±99
12.1		13.9	9.61	7.46	6.17					2090-2657	2291 ±194
5.0				11.0	9.09	7.87	7.19	6.80		1640-2488	2012 ±244
2.5				20.0	14.1	10.7				2094-2201	2168 ±41
1.0			45.5	23.8	15.4	10.9	8.47			2064-2645	2316 ±196

Table A.16 The reciprocal of the vibrational relaxation times $(\mu sec.atm)^{-1}$ for C_2H_2-Ar mixtures as a function of % C_2H_2 and collisional number at T = 2200-2600 K.

% C_2H_2 \ Zt	50	100	150	200	250	300	350	400	450	T (K)	T (K)
12.1		13.9	9.61	7.46	6.17					2090-2657	2291 ±194
5.0				11.0	9.09	7.87	7.19	6.80		1640-2488	2012 ±244
2.5			26.3	17.2	12.6	9.80	7.94			2239-2621	2363 ±129
1.0			45.5	23.8	15.4	10.9	8.47			2064-2645	2316 ±196

Figure B.1 Variation of the density with shock wave velocity for pure N_2O.

Appendix B.

Figures

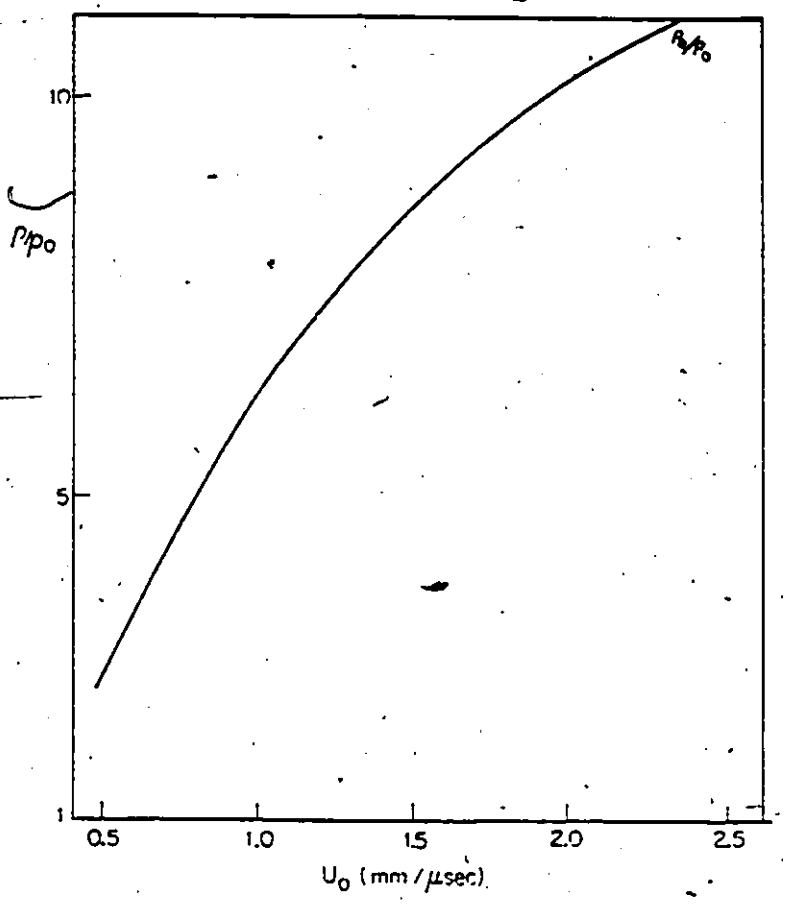

Figure B.2 Variation of the pressure with shock wave velocity for pure N_2O.

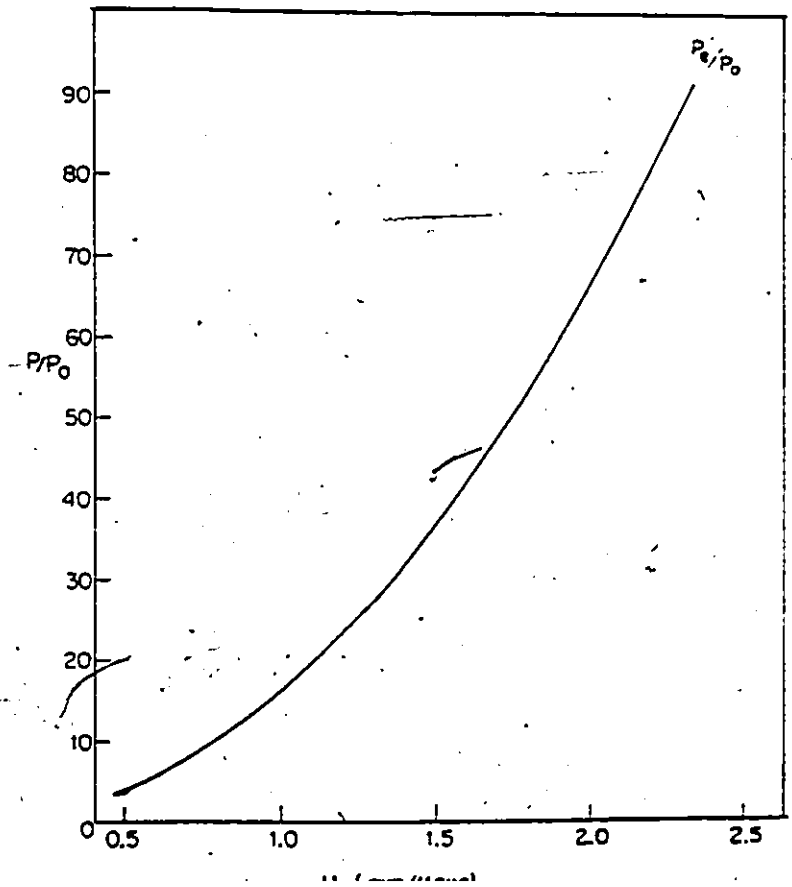

Figure B.3. Variation of the temperature with shock wave velocity for pure N_2O.

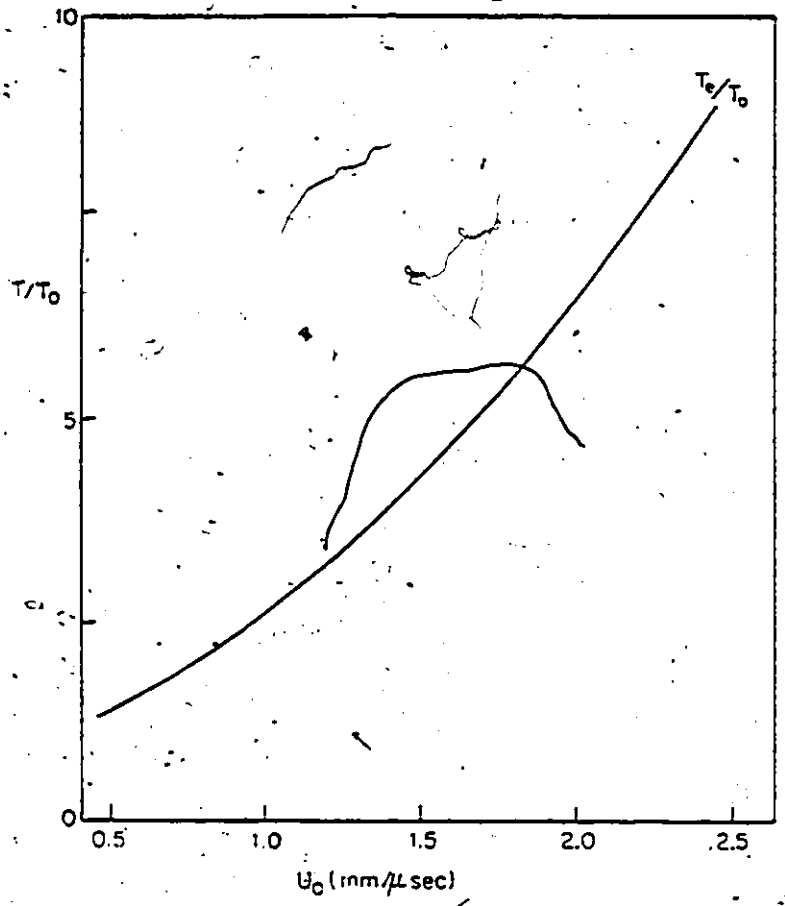

Figure B.4 Variation of $C_p/(C_p-C_{vib})$ with temperature for pure N_2O.

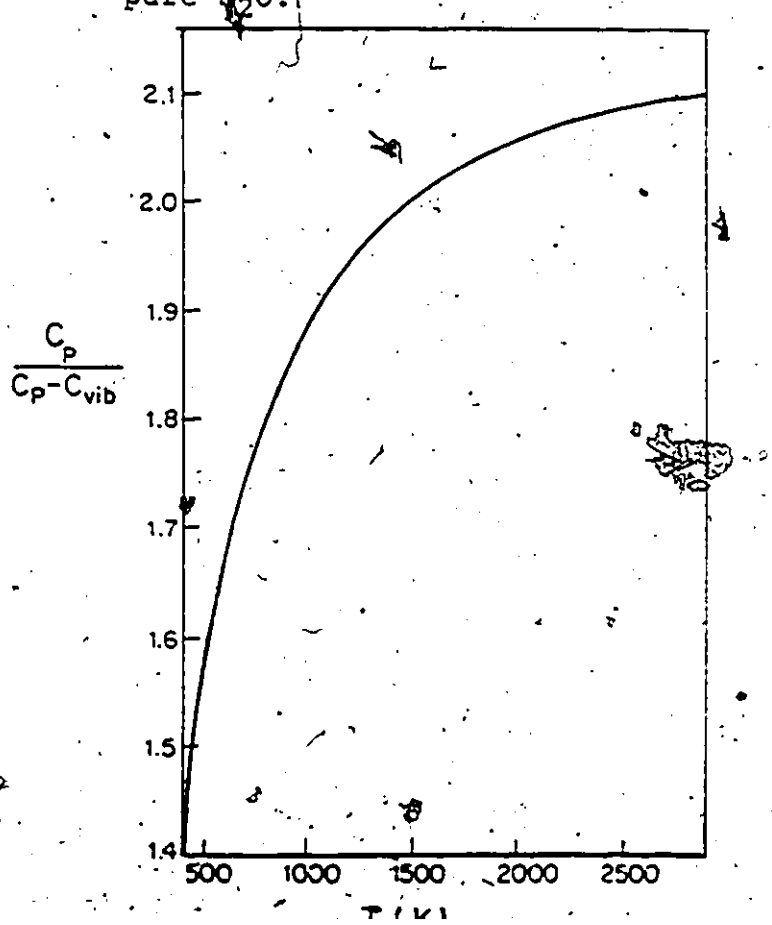

Figure B.5 Variation of the density with shock wave velocity for pure C_2H_2.

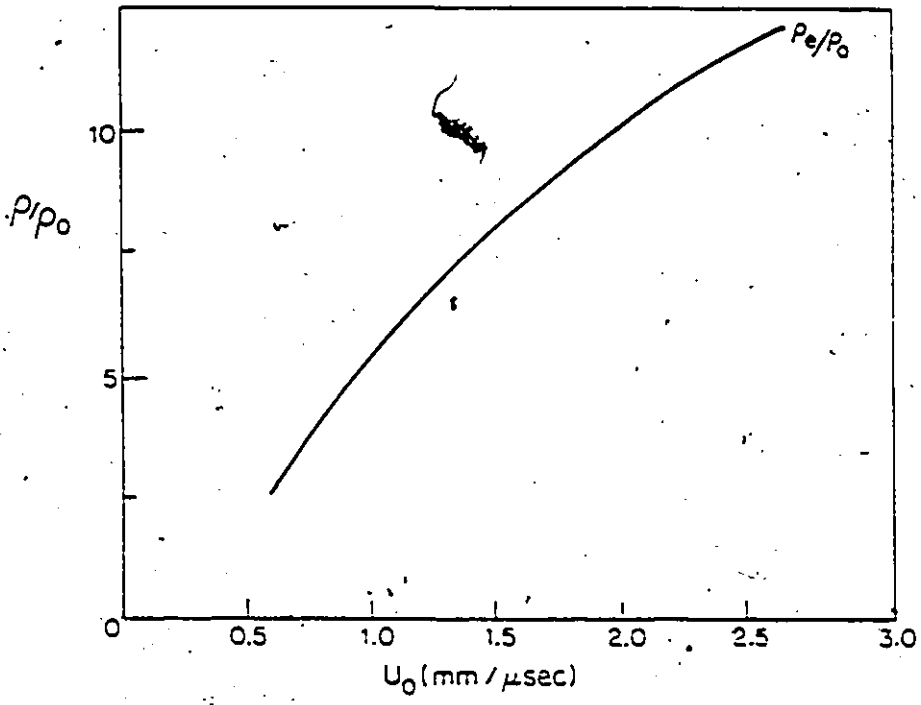

Figure B.6 Variation of the pressure with shock wave velocity for pure C_2H_2.

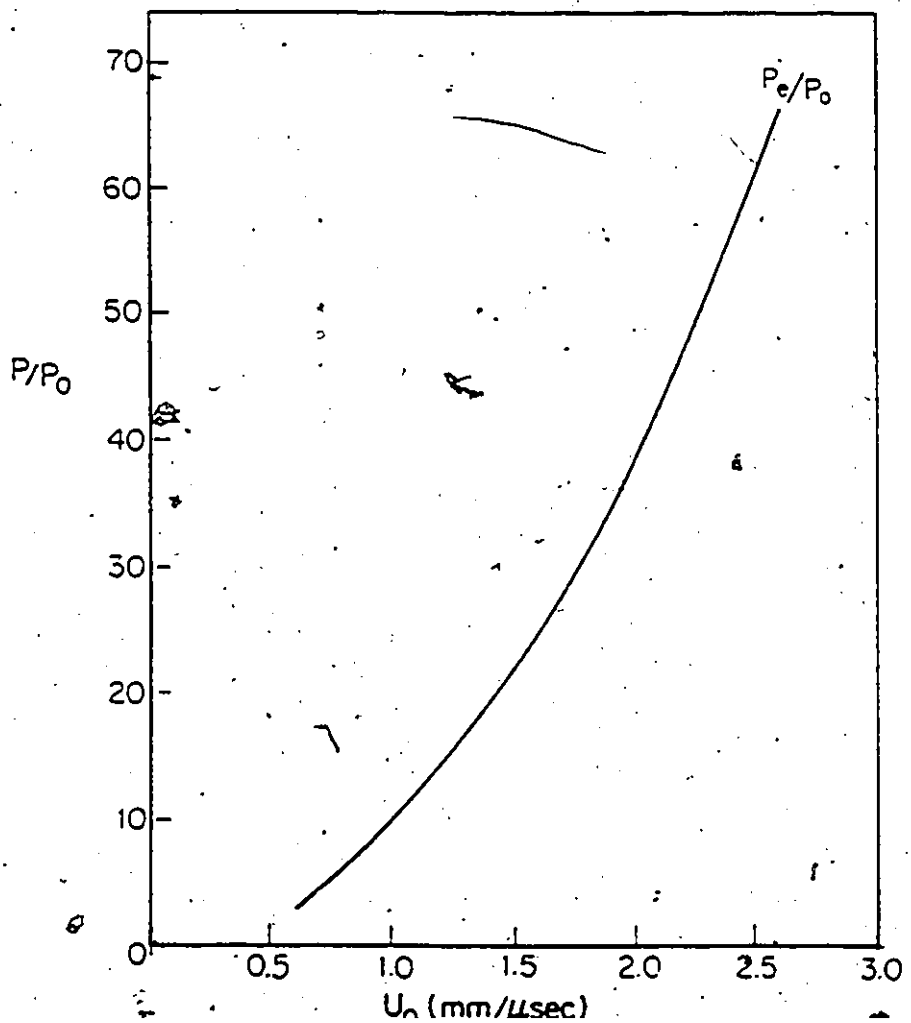

Figure B.7 Variation of the temperature with shock wave velocity for pure C_2H_2.

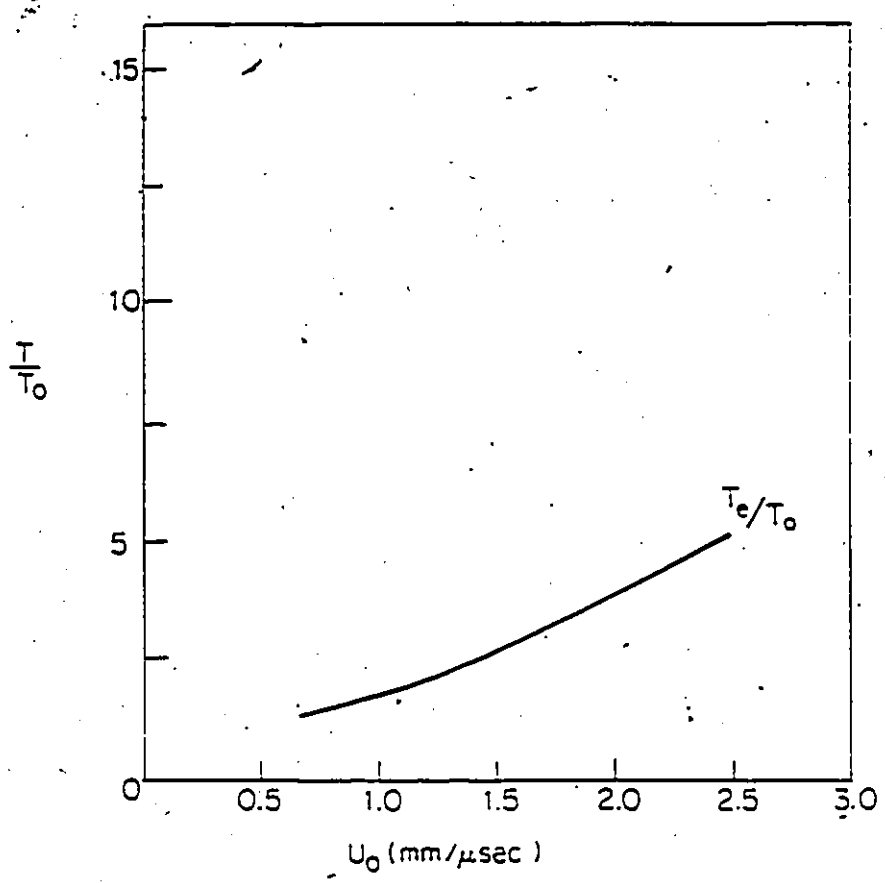

Figure B.8 Variation of $C_p/(C_p-C_{vib})$ with temperature for pure C_2H_2.

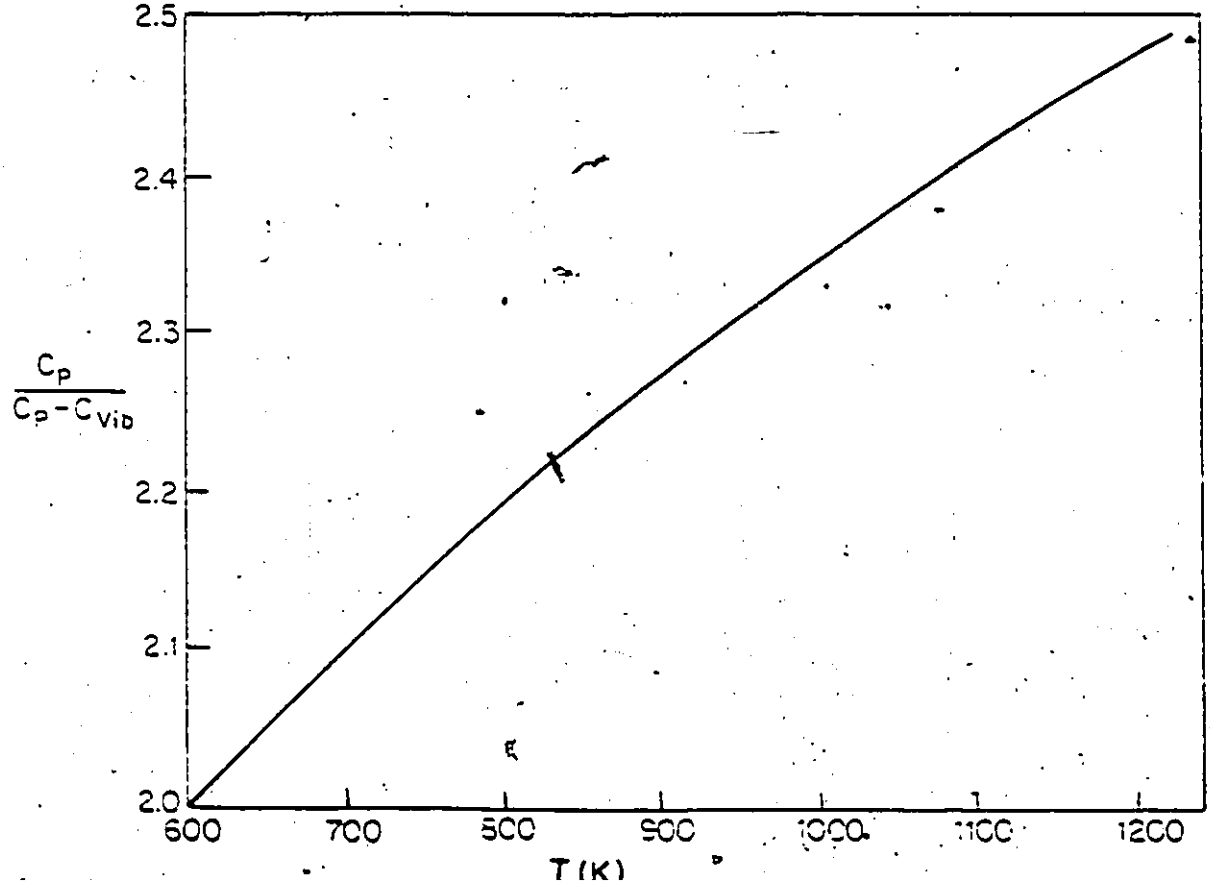

Appendix C. Computer program for the simulation of vibrational relaxation time

```
      IMPLICIT REAL*8 (A-H,O-Z)
      INTEGER N ,METH ,MITER ,INDEX ,IWK(94) ,IER ,K
      DIMENSION Y(100) , YPRIME(100) ,WK(9870) ,ENR(100),
     1IEG(100),Y8(100)
      EXTERNAL FCN
      COMMON /PARAM/ALAMA,Y8,ENR,FX,ALAMX,PHI,GAMMA,ALAMVV
      WRITE (6,23)
   23 FORMAT (///,' ',' N.B =
     1                              ',///)
      WRITE (6,19)
   19 FORMAT (' ',' N    X                    TOL        TH
     1H     ME MI IN',//)
      READ (5,1) N,X,TOL,TH,H,METH,MITER,INDEX
    1 FORMAT (I2,E12.7,F10.7,F9.3,F10.8,3I3)
      WRITE (6,21) N,X,TOL,TH,H,METH,MITER,INDEX
   21 FORMAT (' ',I2,5X,E12.7,5X,F10.7,5X,F5.1,5X,F10.8,3I3//)
      READ (5,24) FX,T,ALAMA,ALAMX,ALAMVV,PHI,GAMMA
   24 FORMAT(F10.9,F10.1,4F10.8,F18.4)
      WRITE (6,25)
   25 FORMAT (//' ',' FX      TEMP      ALAMA     ALAMX     ALAMVV
     1PHI      GAMMA',//)
      WRITE(6,26) FX,T,ALAMA,ALAMX,ALAMVV,PHI,GAMMA
   26 FORMAT(' ',F6.4,5X,F6.1,4(4X,F6.4),5X,F6.2//)
      READ (5,2) (ENR(I),IEG(I),I=1,N)
    2 FORMAT  (F9.3,I3)
      ALPHA=DEXP(-TH*1.439/T)
C
C     Calculation of Relative Population.
C
      SY =0.0
      DO 11  I=1,N
      Y(I) =IEG(I)*DEXP(-ENR(I)*1.439/295.0)
   11 SY =SY +Y(I)
      DO 12  I=1,N
   12 Y(I) = Y(I)/SY
      SY8 = 0.0
      DO 13 I=1,N
      Y8(I) = IEG(I)*DEXP(-ENR(I)*1.439/T)
   13 SY8 = SY8 +Y8(I)
      DO 14 I=1,N
   14 Y8(I) =Y8(I)/SY8
C
C     End of Calculation.
C
      WRITE (6,8)
    8 FORMAT (' ',2X,' ENERG  DEGENERECY  NV/N AT T=295  NV/N AT T ',/)
      WRITE (6,44) ( ENR(I), IEG(I), Y(I), Y8(I) ,I=1,N)
   44 FORMAT (F9.2,4X,I3,10X,F7.5,6X,F7.5)
      WRITE (6,5) T
    5 FORMAT(///,2X,' REDUCED RELAXATION TIME AS A FUNCTION OF OF REDUCED
     1 TIME AT  TEMPERATURE = ',F7.0,///)
      WRITE (6,4)
    4 FORMAT(' ',' X          T/TAU          Y              DY/DX
     1      ENR       DE/DX     TAUP/TAU  T/TAUP   SUMY   SUMDY/DX',//)
```

```
      E8=0.00
      DO 40 I=1,N
   40 E8=ENR(I)*Y8(I)+E8
      DO 101 KK=1,20,1
      XEND=FLOAT(KK)/10
      CALL FCN (N,X,Y,YPRIME)
      E=0.0
      DEDX=0.0
      SIGMY =0.0
      SIGMDY = 0.0
      DO 301 I=1,N
      SIGMY = SIGMY+Y(I)
      SIGMDY = SIGMDY +YPRIME(I)
      E=ENR(I)*Y(I)+E
  301 DEDX=ENR(I)*YPRIME(I)+DEDX
      TTAU=X*(1.0-ALPHA)
      TPTAU=(E8-E)*(1.0-ALPHA)/DEDX
      TTAUP=TTAU/TPTAU
      WRITE (6,66) X,TTAU,Y(1),YPRIME(1),E,DEDX,TPTAU,TTAUP,SIGMY,SIGMDY
   66 FORMAT (2E13.5,2E17.7,2F10.3,F10.5,E14.5,2E12.5)
      WRITE (6,77) (Y(I),YPRIME(I),I=2,N)
   77 FORMAT (28X,2E15.7)
      CALL DGEAR (N,FCN,FCNJ,X,H,Y,XEND,TOL,METH,MITER,INDEX,IWK,WK,IER)
      IF (IER.GT.128.) GO TO 20
  101 CONTINUE
      DO 10 K=3,60
      XEND=FLOAT(K)
      CALL FCN (N,X,Y,YPRIME)
      E=0.0
      DEDX=0.0
      SIGMY =0.0
      SIGMDY = 0.0
      DO 30 I=1,N
      SIGMY = SIGMY+Y(I)
      SIGMDY = SIGMDY +YPRIME(I)
      E=ENR(I)*Y(I)+E
   30 DEDX=ENR(I)*YPRIME(I)+DEDX
      TTAU=X*(1.0-ALPHA)
      TPTAU=(E8-E)*(1.0-ALPHA)/DEDX
      TTAUP=TTAU/TPTAU
      WRITE (6,6) X,TTAU,Y(1),YPRIME(1),E,DEDX,TPTAU,TTAUP,SIGMY,SIGMDY
    6 FORMAT (2E13.5,2E17.7,2F10.3,F10.5,E14.5,2E12.5)
      WRITE (6,7) (Y(I),YPRIME(I),I=2,N)
    7 FORMAT (28X,2E15.7)
      CALL DGEAR (N,FCN,FCNJ,X,H,Y,XEND,TOL,METH,MITER,INDEX,IWK,WK,IER)
      IF (IER.GT.128.) GO TO 20
   10 CONTINUE
      STOP
   20 WRITE (6,3) TOL ,N ,(Y(I),I=1,N) , XEND ,H ,X ,METH ,MITER ,INDEX
    3 FORMAT (F10.7 ,I3 ,94E15.7,3F10.7 ,3I3 )
      STOP
      END
C
C     Subroutine FCN required by DGEAR.
```

```
C
      SUBROUTINE FCN (N,X,Y,YPRIME)
      IMPLICIT REAL*8 (A-H,O-Z)
      DIMENSION Y(100),YPRIME(100),Y8(100) ,ENR(100)
      COMMON /PARAM/ALAMA,Y8,ENR,FX,ALAMX,PHI,GAMMA,ALAMVV
C
C     DY/DT
C
      DO 9 I=1,N
      A = 0.0
      B = 0.0
      IF (I.EQ.N) GO TO 18
      II = I+1
C
C     ( J > I  IE. J = I+1 TO  N )
C
      DO 15 J=II,N
      C = DABS(ENR(J)-ENR(I))
      IF (C.GT.616.) GO TO 17
C
C     ( i.e. stop adding)
C
   15 A = A + (Y(J)-Y(I)*Y8(J)/Y8(I))*DEXP(ALAMA*(588.0-C))*
     1(0.0+ENR(J)/588.0)*(1.0-FX)*PHI
     1+(Y(J)-Y(I)*Y8(J)/Y8(I))*DEXP(ALAMX*(588.0-C))*
     1(0.0+ENR(J)/588.0)*FX
   17 IF (I.EQ.1) GO TO 19
   18 III = I-1
      DO 16 J=1,III
C
C     ( J < I , IE. J = 1 TO I-1 )
C
      D = DABS(ENR(J)-ENR(I))
      IF (D.GT.616.) GO TO 16
C
C     (i.e. stop adding)
C
      B = B+(Y(J)*Y8(I)/Y8(J)-Y(I))*DEXP(ALAMA*(588.0-D))*
     1(0.0+ENR(I)/588.0)*(1.0-FX)*PHI
     1+(Y(J)*Y8(I)/Y8(J)-Y(I))*DEXP(ALAMX*(588.0-D))
     1*(0.0+ENR(I)/588.0)*FX
   16 CONTINUE
   19 Q = A+B
C
C     V-V effect.
C
      S=0.0
      DO 1 J=1,N
      DO 1 K=1,N
      DO 1 L=1,N
      IF (J.EQ.I) GO TO 1
      R = DABS(ENR(J)+ENR(L)-ENR(I)-ENR(K))
      IF (R.GT.616.) GO TO 1
      R1=DABS(ENR(J)-ENR(I))
```

```
      R2=DABS(ENR(L)-ENR(K))
      IF (R1.GT.616.0) GO TO 1
      IF (R2.GT.616.0) GO TO 1
      IF (K.EQ.L) GO TO 1
      E1 = DMAX1(ENR(J),ENR(I))
      E2 = DMAX1(ENR(K),ENR(L))
      IF (J.LT.I) GO TO 2
      T=(Y(J)*Y(L)-Y(I)*Y(K)*Y8(J)*Y8(L)/Y8(I)/Y8(K))*
     1GAMMA*(0.0+E1/588.0)*(0.0+E2/588.0)
     1*DEXP(-ALAMVV*R)*FX
      S = S+T
      GO TO 1
 2    U= (-Y(I)*Y(K)+Y(J)*Y(L)*Y8(I)*Y8(K)/Y8(J)/Y8(L))
     1*GAMMA*(0.0+E1/588.0)*(0.0+E2/588.0)
     1*DEXP(-ALAMVV*R)*FX
      S =S+U
   1  CONTINUE
      YPRIME(I)=Q*S
C
C     End of V-V effect.
C
   9  CONTINUE
C
C     End of DY/DT
C
      RETURN
      END
C
C     Dummy subroutine FCNJ required by DGEAR.
C
      SUBROUTINE FCNJ (N ,X ,Y ,PD)
      IMPLICIT REAL*8 (A-H,O-Z)
      INTEGER N
      REAL Y(N) ,PD(N,N) ,X
      RETURN
      END
```

References

1. B. Stevens, "Collisional Deactivation in Gases", Pergamon Press, Oxford (1967).
2. G.M. Burnett, A.M. North, "Transfer and Storage of Energy by Molecules", Volume 2, Wiley-Interscience (1969).
3. A.J. Grimley, P.L. Houston, J. Chem. Phys. 68, 3366 (1978).
4. H.A. Bethe, E. Teller, Ballistic Research Laboratories, Rept. X-117 (1941).
5. L. Landau, E. Teller, Phys. Z. Sowjetunion, 10, 34, (1936).
6. T.L. Cottrell, J.C. McCoubrey, "Molecular Energy Transfer in Gases", Butterworths, London (1961).
7. J.T. Yardley, "Introduction to Molecular Energy Transfer", Academic Press (1980).
8. D. Rapp, J. Chem. Phys., 32, 735 (1960).
9. J.G. Parker, Phys. Fluids, 2, 449 (1959).
10. K. Takayanagi, Progr. Theor. Phys. Suppl. (Kyoto), 25, 1, (1963).
11. J.D. Kelly, M. Wolfsberg, J. Chem. Phys., 44, 324 (1966).
12. R.E. Turner, D.J. Rapp, J. Chem. Phys., 35, 1076 (1961).
13. H. Teitelbaum, Ph.D. Thesis, University of Toronto (1974).
14. D. Rapp, T. Kassal, Chem. Rev., 69, 61 (1969).
15. T.E. Sharp, D. Rapp, J. Chem. Phys., 43, 1233 (1965).
16. J.D. Jackson, N.F. Mott, Proc. Roy. Soc., A137, 703 (1932).
17. J.D. Lambert, "Vibrational and Rotational Relaxation in Gases", Clarendon Press, Oxford (1977).
18. J.D. Lambert, D.G. Parks-Smith, J.L. Stretton, Trans. Faraday Soc., 66, 2720 (1970).
19. F.W. Wette, Z.I. Slawsky, Physica, 20, 1169 (1954).
20. R.N. Schwartz, K.F. Herzfeld, J. Chem. Phys, 22, 767 (1954).
21. F.I. Tanczos, J. Chem. Phys., 25, 439 (1956).
22. C.B. Moore, R.E. Wood, B.L.B. Hu, J.T. Yardley, J. Chem. Phys, 46, 4222 (1967).

23. R.L. Taylor, M. Camac, R.M. Feinberg, in 11th Symposium on Combustion, Berkeley, California p. 49 (1966).

24. R.D. Sharma, C.A. Brau, Phys, Rev. Lett., 19, 1273 (1967).

25. R.D. Sharma, C.A. Brau, J. Chem. Phys., 50, 924 (1969).

26. J.D. Lambert, R. Salter, Proc. R. Soc., A253, 277 (1959).

27. J.D. Lambert, J. Chem. Soc., Faraday II, 68, 364 (1972).

27a J.S. Rowlinson, Trans. Faraday Soc., 45, 980 (1949).

28. J.C. Polanyi, K.B. Woodall, J. Chem. Phys., 56, 1563 (1972).

28a R.D. Levine, Ann. Rev. Phys. Chem. 29, 59(1978).

28b I. Procaccia and R.D. Levine, J. Chem. Phys. 64, 808 (1976).

28c A.M.G. Ding and J.C. Polanyi, Chem. Phys. 10, 39 (1975).

28d N.C. Lang, J.C. Polanyi, and J. Wanner, Chem. Phys. 24, 219 (1977).

28e B.A. Esche, R.E. Kutina, N.C. Lang, J.C. Polanyi and A.M. Rulis, ibid. 41, 183 (1979).

28f J.C. Polanyi, N. Sathyamurthy, and J.L. Schreiber, Chem. Phys. 24, 105 (1977).

28g J.C. Polanyi, N. Sathyamurthy, ibid. 29, 9 (1978).

28h J.C. Polanyi and N. Sathyamurthy, J. Phys. Chem. 83, 978 (1979).

28i T.A. Brunner, R.D. Driver, N. Smith, and D.E. Pritchard, J. Chem. Phys. 70, 4155 (1979).

28j D.E. Pritchard, N. Smith, R.D. Driver, and T.A. Brunner, J. Chem. Phys. 70, 2115 (1979).

28k T. Brunner and D.E. Pritchard, Advances in Chemical Physics (Wiley, London, 1982), Vol. 50.

28l D.F. Heller, Chem. Phys. Lett. 45, 64 (1977).

28m Y. Alhassid and R.D. Levine, Phys. Rev. A18, 89 (1978).

28n B.C. Sanctuary, Chem. Phys. Lett. 62, 378 (1978).

28o G.C. Berend and R.L. Thommarson, J. Chem. Phys. 58 3203 (1973).

28p R.K. Lengel, D.R. Crosley, Chem. Phys. letters, 32, 261 (1975).

28q H. Ulrich and P. Hess, Chem. Phys. 29, 445 (1980).

28r H. Ulrich and P. Hess, Chem. Phys. 47, 381 (1980).

28s G. Jolicard, M-Y. Perrin, Chem. Phys. 81, 135 (1983).

29. H. Teitelbaum, Can. J. Chem., 61, 1267 (1983).

30. R.R. Stephens, T.A. Cool, J. Chem. Phys., 56, 5863 (1972).

31. G.W. Flynn. In State-to-State Chemistry, P.R. Brooks, E.F. Huages (eds.) ACS Symposium Series V. 56, Washington (1977).

32. W. Griffith, D. Brickl, V. Blackman, Phys. Rev., 102, 1209 (1956).

33. J.K. Bhangu, J. Fluid Mech., 25, 817 (1966).

34. C.J.S.M. Simpson, K.B. Bridgman, and T.R.D. Chandler, J. Chem Phys, 49, 509 (1968).

35. M.G. Foster, C.J.S.M. Simpson, J. Chem. Soc., Faraday Trans. II, 75, 509 (1979).

36. C.J.S.M. Simpson, P.D. Gait, T.J. Price, M.G. Foster, Chem. Phys., 68, 293 (1982).

37. J.E. Dove, W.S. Nip, H. Teitelbaum, Proceedings of the 15th Symposium (International) on Combustion (the Combustion Institute, Pittsburgh, 1975). p. 903 (1975).

38. A. Kantrowitz, J. Chem. Phys., 14, 150 (1946).

39. W. Griffith, J. Appl. Phys., 21, 1319 (1950).

40. M. Huetz, P. Chevalier, B. Sanson, Astronautica Acta, 17, 645 (1972).

41. M. Huetz-Aubert, R. Lenormand, H. Manceau, Advances in Molecular Relaxation Processes, 6, 153 (1974).

42. K.F. Herzfeld, T.A. Litovitz, "Absorption and Dispersion of Ultrasonic Waves", Academic Press, N.Y. and London (1959).

43. A. Eucken, H. Jaacks, Z. Phys. Chem., B30, 85 (1935).

44. A. Eucken, E. Numann, Z. Phys. Chem., B36, 163 (1937).

45. J.W. Arnold, J.C. McCoubrey, A.R. Ubelohde, Proc. Roy. Soc., A248, 445 (1958).

46. R. Holmes, H.D. Parbrook, W. Tempest, Acustica, 10, 155 (1960).

47. J.V. Martinez, J.G. Strauch, Jr. and J.C. Decius, J. Chem. Phys., 40, 186 (1964).

48. T.L. Cottrell, I.M. Macfarlane, A.W. Read, A.H. Young, Trans. Faraday Soc., 62, 2655 (1966).

49. A.W. Read, Advan. Mol. Relaxation Processes, 1, 257 (1967-68).

50. T.L. Cottrell, I.M. Macfarlane, A.W. Read, Trans. Faraday Soc., 63, 2093 (1967).

51. P.V. Slobodskaya, N.F. Tkachenko, Opt. Spektrosk., 23, 480 (1967).

52. M. Rebelo Da Silva, M.H. De Vasconcelos, Physica, 106C, 142 (1981).

53. J.T. Yardley, J. Chem. Phys., 49, 2816 (1968).

54. J.T. Yardley, C.B. Moore, J. Chem Phys, 46, 4491 (1967).

55. R.D. Bates, G.W. Flynn, A.M. Ronn, J. Chem. Phys., 49, 1432 (1968).

56. L.O. Hocker, M.A. Kovacs, C.K. Rhodes, G.W. Flynn, A. Javan, Phys. Rev. Lett, 17, 233 (1966).

57. C.B. Moore, R.E. Wood, B.L. Hu, J.T. Yardley, J. Chem. Phys., 46, 4222 (1967).

58. I. Arditi, M. Margottin-Maclou, H. Gueguen, L. Doyennette, C.R. Acad. Sc., 270B, 477 (1970).

59. M. Margottin-Maclou, L. Doyennette, L. Henry, Applied Optics, 10, 1768 (1971).

60. H. Gueguen, A. Carion, M. Margottin-Maclou, L. Doyennette, C.R. Acad. Sc., 274B, 482 (1972).

61. L. Doyennette, M. Margottin-Maclou, H. Gueguen, A. Carion, L. Henry, J. Chem. Phys., 60, 697 (1974).

62. H. Gueguen, I Arditi, M. Margottin-Maclou, L. Doyennette, L. Henry, C.R. Acad. Sc., 272B, 1139 (1971).

63. M. Margottin-Maclou, H. Gueguen, L. Doyennette, L. Henry, C.R. Acad. Sc., 274B, 1414 (1972).

64. H. Gueguen, F. Yzambart, A. Chakroun, M. Margottin-Maclou, L. Doyennette, L. Henry, Chem. Phys. Lett., 35, 198 (1975).

65. J.C. Stephenson, C.B. Moore, J. Chem. Kin., 56, 1295 (1972).

66. J. K. Hancock, D.F. Starr, W.H. Green, J. Chem. Phys., 61, 3017 (1974).

67. D.F. Starr, J.K. Hancock, J. Chem. Phys., 62, 3747 (1975).

68. C. Alamichel, A. Picard-Bersellini, Chem. Phys., 35, 381 (1978).

69. R.T. V. Kung, J. Chem. Phys., 63, 5305 (1975).

70. R.T. V. Kung, J. Chem. Phys., 63, 5313 (1975).

71. P.D. Edmonds, J. Lamb, Proc. Phys. Soc., London, 72, 940 (1958).

72. J.D. Lambert, R. Salter, Proc. Roy. Soc., London, A253, 277 (1959).

73. J.L. Stretton, Trans. Faraday Soc., 61, 1053 (1965).

74. J.C.F. Wang, G.S. Springer, J. Chem. Phys., 59, 6556 (1973).

75. J. Hager, W. Krieger, T. Ruegg, H. Walther, J. Chem. Phys., 72, 4286 (1980).

76. J. Hager, W. Krieger, J. Pfab, J. Chem. Soc., Faraday Tans. 2, 77, 469 (1981).

77. D.L.S. McElwain, H.O. Pritchard, J. Am. Chem. Soc., 92, 5027 (1970).

78. C. Carruthers, H. Teitelbaum, Can. J. Chem 63, 381 (1985).

79. E.W. Schlag, W.G.Valance, J. Chem. Phys., 49, 605 (1968).

80. J. Troe, Ber. Bunsenges. Phys. Chem., 84, 829 (1980).

81. J.E. Dove, S. Raynor, J. Phys. Chem., 83, 127 (1979).

82. J.E. Dove, S. Halperin, S. Raynor, J. Chem. Phys., 81, 799 (1984).

83. H. Teitelbaum, Proceedings of the 13th International Symposium on Shock Tubes and Waves, C.E. Treanor (editor), Niagara Falls, 560 (1981).

84. Y.V. Chalapati Rao., B.V. Mallu, Chem. Phys., 74, 43 (1983).

85. R.G. Agrawal, Y.V. Chalapati Rao., Chem. Phys. Lett., 89, 59 (1982).

86. D.G. Jones, J.D. Lambet, J.L. Stretton, Proc. Phys. Soc., 86, 857 (1965).

87. J.K. Hancock, A.W. Saunders Jr., J. Chem. Phys., 65, 1277 (1976).

88. J.K. Hancock, W.H. Green, J. Chem. Phys., 57, 4515 (1972).

89. J.T. Knudtson, G.W. Flynn, J. Chem. Phys., 58, 1467 (1973).

90. U.E. Schnaus, J. Acoustic Soc. Am., 37, 1 (1965).

91. P. Hess, C.B. Moore, J. Chem. Phys., 65, 2339 (1976).

92. F.D. Shields, J. Chem. Phys., 46, 1063 (1967).

93. V.S. Rao, G.B. Skinner, J. Chem. Phys., 81, 775 (1984).

94. J.E. Dove, H. Teitelbaum, Chem. Phys., 6, 431 (1974).

95. P.M. Borrell, P. Borrell, R. Gutteridge, J. Chem. Soc. Faraday Trans. II, 71, 571 (1975).

96. W.D. Breshears, P.F. Bird, J. Chem. Phys., 55, 4017 (1971).

97. H.L. Chen, J. Chem. Phys., 55, 5551 (1971).

98. R.G. Miller, J.K. Hancock, J. Chem. Phys., 66, 5150 (1977).

99. K. Glanzer, Chem. Phys., 22, 367 (1977).

100. A. Hariri, C. Wittig, J. Chem. Phys., 68, 2109 (1978).

101. J. Finzi, F.E. Hovis, V.N. Panfilou, P. Hess, C.B. Moore, J. Chem. Phys., 67, 4053 (1977).

102. J.D. Lambert, P.G. Rarks-Smith, J.L. Stretton, Proc. Roy. Soc., A282, 380 (1964).

103. P. Borrell, G.E. Millward, J. Chem. Soc. Faraday Trans. II, 69, 1060 (1973).

104. V.A. Apkarian, E. Weitz, J. Chem. Phys., 71, 4349 (1979).

105. Z. Baalbaki, H. Teitelbaum, J.E. Dove, W.S. Nip, Sub to Chem. Phys., in press (1985).

106. A.G. Gaydon, I.R. Hurle, "The Shock Tube in High-Temperature Chemical Physics", Chapman and Hall Ltd., London (1963).

107. H. Teitelbaum, M. Sc. Thesis, University of Toronto (1971).

108. JANAF Thermochemical Tables, 2nd ed., NSRDS-NBS 37, NBS, Washington (1971).

109. J.H. Kiefer, R.W. Lutz, J. Chem. Phys. 44, 658 (1966).

110. F.J. Weinberg, "Optics of Flames", Butterworths, London (1963).

111. J.R. Partington, "An Advanced Treatise on Physical Chemistry", Vol. 4, Longmans, Green and Co., London, pages 9-20 (1953).

112. V. Blackman, J. Fluid Mech., 1, 61 (1956).

113. J.O. Hirschfelder, C.F. Curtiss, R.B. Bird, "Molecular Theory of Gases and Liquids", Wiley, N.Y. (1964).

114. G.W. Gear, Comm. ACM 14, 176 (1971).

115. F.J.S.M. Simpson, Private Communication.

116. H. Teitelbaum, Can. J. Chem., 61, 1253 (1983).